Cell Journal (Yakhteh)

Guide for Authors

Aims and Scope: The "Cell Journal (Yakhteh)" is a peer review and monthly English publication of Royan Institute of Iran. The aim of the journal is to disseminate information through publishing the most recent scientific research studies on exclusively Cellular, Molecular and other related topics. **Cell J**, has been certified by the Ministry of Culture and Islamic Guidance since 1999 and also accredited as a scientific and research journal by HBI (Health and Biomedical Information) Journal Accreditation Commission since 2000 which is an open access journal. **This journal holds the membership of the Committee on Publication Ethics (COPE).**

1. Types of articles

The articles in the field of Cellular and Molecular can be considered for publications in **Cell J.** These articles are as below:

A. Original articles Original articles are scientific reports of the original research studies. The article consists of English Abstract (structured), Introduction, Materials and Methods, Results, Discussion, Conclusion, Acknowledgements, Author's Contributions, and References **(Up to 40).**

B. Review articles Review articles are the articles written by well experienced authors and those who have excellence in the related fields. The corresponding author of the review article must be one of the authors of at least three published articles appearing in the references. The review article consists of English Abstract (unstructured), Introduction, Conclusion, Author's Contributions, and References **(Up to 70).**

C. Systematic Reviews

Systematic reviews are a type of literature review that collect and critically analyzes multiple research studies or papers. The Systematic reviews consist of English Abstract (unstructured), Introduction, Materials and Methods, Results, Discussion, Conclusion, Acknowledgements, Author's Contributions, and References **(Up to 70).**

D. Short communications: Short communications are articles containing new findings. Submissions should be brief reports of ongoing researches. The short communication consists of English Abstract (unstructured), the body of the manuscript (should not hold heading or subheading), Acknowledgements, Author's Contributions, and References **(Up to 30).**

E. Case reports: Case reports are short discussions of a case or case series with unique features not previously described which make an important teaching point or scientific observation. They may describe novel techniques or use equipment, or new information on diseases of importance. It consists of English Abstracts (Unstructured), Introduction, Case Report, Discussion, Acknowledgements, Author's Contributions, and References **(Up to 30).**

F. Editorial: Editorial should be written by either the editor in chief or the editorial board.

G. Imaging in biology: Images in biology should focus on a single case with an interesting illustration such as a photograph, histological specimen or investigation. Color images are welcomed. The text should be brief and informative.

H. Letter to the editors: Letter to editors are welcome in response to previously published **Cell J** articles, and may also include interesting cases that do not meet the requirement of being truly exceptional, as well as other brief technical or clinical notes of general interest.

I. Debate.

2. Submission process

It is recommended to see the guidelines for reporting different kinds of manuscripts here. This guide explains how to prepare the manuscript for submission. Before submitting, we suggest authors to familiarize themselves with **Cell J** format and content by reading the journal via the website (www.celljournal.com). The corresponding author ensures that all authors are included in the author list and agree with its order, and they must be aware of the manuscript submission.

A. Author contributions statements

It is essential for authors to include a statement of responsibility in the manuscript that specifies the contribution of every one of them. This participation must include conception and design of the manuscript, data acquisition or data analysis and interpretation, drafting of the manuscript and/or revising it for critically important intellectual content, revision and final approval of the manuscript and statistical analysis, obtaining funding, administrative, technical, or material support, or supervision. Authors who do not meet the above criteria should be acknowledged in the **Acknowledgments section.**

B. Cover letter and copyright

Each manuscript should be accompanied by a cover letter, signed by all authors specifying the following statement: "The

manuscript has been seen and approved by all authors and is not under active consideration for publication. It has neither been accepted for publication nor published in another journal fully or partially (except in abstract form). Also, no manuscript would be accepted in case it has been pre-printed or submitted to other websites I hereby assign the copyright of the enclosed manuscript to **Cell J."** Corresponding author must confirm the proof of the manuscript before online publishing. Also, is it needed to suggest three peer reviewers in the field of their manuscript.

C. Manuscript preparation

Authors whose first language is not English encouraged to consult a native English speaker in order to confirm his manuscripts to American or British (not a mixture) English usage and grammar. It is necessary to mention that we will check the plagiarism of your manuscript by iThenticate Software. The manuscript should be prepared in accordance with the "International Committee of Medical Journal Editors (ICMJE)". Please send your manuscript in two formats Word and Pdf (including: title, name of all the authors with their degree, abstract, full text, references, tables and figures) and also send tables and figures separately in the site. The abstract and text pages should have consecutive line numbers in the left margin beginning with the title page and continuing through the last page of the written text. Each abbreviation must be defined in the abstract and text when they are mentioned for the first time. Avoid using abbreviation in the title. Please use the international and standard abbreviations and symbols

It should be added that an essential step toward the integration and linking of scientific information reported in published literature is using standardized nomenclature in all fields of science and medicine. Species names must be italicized (*e.g., Homo sapiens*) and also the full genus and species written out in full, both in the title of the manuscript and at the first mention of an organism in a paper.

It is necessary to mention that genes, mutations, genotypes, and alleles must be indicated in italics. Please use the recommended name by consulting the appropriate genetic nomenclature database, e.g., HUGO for human genes. In another words; if it is a human gene, you must write all the letters in capital and italic (*e.g., OCT4, c-MYC*). If not, only write the first letter in capital and italic (*e.g., Oct4, c-Myc*). **In addition, protein designations are the same as the gene symbol but are not italicized.**

Of note, Cell J will only consider publishing genetic association study papers that are novel and statistically robust. Authors are advised to adhere to the recommendations outlined in the STREGA statement (http://www.strega-statement.org). The following criteria must be met for all submissions:

1. Hardy-Weinberg Equilibrium (HWE) calculations must be carried out and reported along with the P-values if applicable [see Namipashaki et al. 2015 (Cell J, Vol 17, N 2, Pages: 187-192) for a discussion].

2. Linkage disequilibrium (LD) structure between SNPs (if multiple SNPs are reported) must be presented.

3. Appropriate multiple testing correction (if multiple independent SNPs are reported) must be included.

Submissions that fail to meet the above criteria will be rejected before being sent out for review.

Each of the following manuscript components should begin in the following sequence:

Authors' names and order of them must be carefully considered (full name(s), highest awarded academic degree(s), email(s), and institutional affiliation(s) of all the authors in English. Also, you must send mobile number and full postal address of the corresponding author).

Changes to Authorship such as addition, deletion or rearrangement of author names must be made only before the manuscript has been accepted in the case of approving by the journal editor. In this case, the corresponding author must explain the reason of changing and confirm them (which has been signed by all authors of the manuscript). If the manuscript has already been published in an online issue, an erratum is needed.

Title is providing the full title of the research (do not use abbreviations in title).

Running title is providing a maximum of 7 words (no more than 50 characters).

Abstract must include Objective, Materials and Methods, Results, and Conclusion (no more than 300 words).

Keywords, three to five, must be supplied by the authors at the foot of the abstract chosen from the Medical Subject Heading (MeSH). Therefore; they must be specific and relevant to the paper.

The following components should be identified after the abstract:

Introduction: The Introduction should provide a brief background to the subject of the paper, explain the importance of the study, and state a precise study question or purpose.

Materials and Methods: It includes the exact methods or observations of experiments. If an apparatus is used, its manufacturer's name and address should be stipulated in parenthesis. If the method is established, give reference but if the

method is new, give enough information so that another author can perform it. If a drug is used, its generic name, dose, and route of administration must be given. Standard units of measurements and chemical symbols of elements do not need to be defined.

Statistical analysis: Type of study and statistical methods should be mentioned and specified by any general computer program used.

Ethical considerations*:* Please state that informed consent was obtained from all human adult participants and from the parents or legal guardians of minors and include the name of the appropriate institutional review board that approved the project. It is necessary to indicate in the text that the maintenance and care of experimental animals complies with National Institutes of Health guidelines for the humane use of laboratory animals, or those of your Institute or agency.

Clinical trial registration: All of the Clinical Trials performing in Iran must be registered in Iranian Registry of Clinical Trials (www.irct.ir). The clinical trials performed abroad, could be considered for publication if they register in a registration site approved by WHO or www.clinicaltrials.gov. If you are reporting phase II or phase III randomized controlled trials, you must refer to the CONSORT Statement for recommendations to facilitate the complete and transparent reporting of trial findings. Reports that do not conform to the CONSORT guidelines may need to be revised before peer-reviewing.

Results: They must be presented in the form of text, tables, and figures. Take care that the text does not repeat data that are presented in tables and/or figures. Only emphasize and summarize the essential features of the main results. Tables and figures must be numbered consecutively as appeared in the text and should be organized in separate pages at the end of the manuscript while their location should be mentioned in the main text.

Tables and figures: If the result of your manuscript is too short, it is better to use the text instead of tables & figures. Tables should have a short descriptive heading above them and also any footnotes. Figure's legend should contain a brief title for the whole figure and continue with a short explanation of each part and also the symbols used (no more than 100 words). All figures must be prepared based on cell journal's guideline in color (no more than 6 Figures and Tables) and also in GIF or JPEG format.

Of Note: Please put the tables & figures of the result in the results section not any other section of the manuscript.

Supplementary materials would be published on the online version of the journal. This material is important to the understanding and interpretation of the report and should not repeat material within the print article. The amount of supplementary material should be limited. Supplementary material should be original and not previously published and will undergo editorial and peer review with the main manuscript. Also, they must be cited in the manuscript text in parentheses, in a similar way as when citing a figure or a table. Provide a legend for each supplementary material submitted.

Discussion: It should emphasize the present findings and the variations or similarities with other researches done by other researchers. The detailed results should not be repeated in the discussion again. It must emphasize the new and important aspects of the study.

Conclusion: It emphasizes the new and important aspects of the study. All conclusions are justified by the results of the study.

Acknowledgements: This part includes a statement thanking those who contributed substantially with work relevant to the study but does not have authorship criteria. It includes those who provided technical help, writing assistance and name of departments that provided only general support. You must mention financial support in the study. Otherwise; write this sentence "There is no financial support in this study".

Conflict of interest: Any conflict of interest (financial or otherwise) and sources of financial support must be listed in the Acknowledgements. It includes providers of supplies and services from a commercial organization. Any commercial affiliation must be disclosed, regardless of providing the funding or not.

References: The references must be written based on the Vancouver style. Thus the references are cited numerically in the text and listed in the bibliography by the order of their appearance. The titles of journals must be abbreviated according to the style used in the list of Journals Indexed in PubMed. Write surname and initials of all authors when there are six or less. In the case of seven or more authors, the names of the first six authors followed by "et al." must be listed. You can download Endnote file for Journal references style: endnote file

The reference of information must be based on the following order:

Article:

Surname(s) and first letter of name &middle name(s) of author(s) .Manuscript title. Journal title (abbr).publication date (year); Volume & Issue: Page number.

Example: Manicardi GC, Bianchi PG, Pantano S, Azzoni P, Bizzaro D, Bianchi U, et al. Presence of endogenous nicks in DNA of ejaculated human spermatozoa and its relationship to chromomycin A3 accessibility. Biol Reprod. 1995; 52(4): 864-867.

Book:

Surname(s) and first letter of name & middle name(s) of author(s).Book title. Edition. Publication place: publisher name; publication date (year); Page number.

Example: Edelman CL, Mandle CL. Health promotion throughout the lifespan. 2nd ed. ST Louis: Mosby; 1998; 145-163.

Chapter of book:

Surname(s) and first letter of name & middle name(s) of author(s).Chapter title. In: Surname(s) and first letter of name & middle name(s) of editor(s), editors. Book title. Edition. Publication place: publisher name; publication date (year); Page number.

Example: Phillips SJ, Whisnant JP. Hypertension and stroke. In: Laragh JH, Brenner BM, editors. Hypertension: pathophysiology, diagnosis, and management. 2nd ed. New York: Raven Press; 1995; 465-478.

Abstract book:

Example: Amini rad O.The antioxidant effect of pomegranate juice on sperm parameters and fertility potential in mice. Cell J. 2008;10 Suppl 1:38.

Thesis:

Name of author. Thesis title. Degree. City name. University. Publication date (year).

Example: Eftekhari Yazdi P. Comparison of fragment removal and co-culture with Vero cell monolayers on development of human fragmented embryos. Presented for the Ph.D., Tehran. Tarbiyat Modarres University. 2004.

Internet references

Article:

Example: Jahanshahi A, Mirnajafi-Zadeh J, Javan M, Mohammad-Zadeh M, Rohani M. Effect of low-frequency stimulation on adenosineA1 and A2A receptors gene expression in dentate gyrus of perforant path kindled rats. Cell J. 2008; 10 (2): 87-92. Available from: http://www.celljournal.org. (20 Oct 2008).

Book:

Example: Anderson SC, Poulsen KB. Anderson's electronic atlas of hematology.[CD-ROM]. Philadelphia: Lippincott Williams & Wilkins; 2002.

D. Proofs are sent by email as PDF files and should be checked and returned within 72 hours of receipt. It is the authors' responsibility to check that all the text and data as contained in the page proofs are correct and suitable for publication. **We are requested to pay particular attention to author's names and affiliations as it is essential that these details be accurate when the article is published.**

E. Pay for publication: Publishing an article in Cell J requires Article Processing Charges (APC) that will be billed to the submitting author following the acceptance of an article for publication. For more information please see www.celljournal.org.

F. Ethics of scientific publication: Manuscripts that have been published elsewhere with the same intellectual material will refer to duplicate publication. If authors have used their own previously published work or work that is currently under review, as the basis for a submitted manuscript, they are required to cite the previous work and indicate how their submitted manuscript offers novel contributions beyond those of the previous work. Research and publication misconduct is considered a serious breach of ethics.

The Journal systematically employs iThenticate, plagiarism detection and prevention software designed to ensure the originality of written work before publication. Plagiarism of text from a previously published manuscript by the same or another author is a serious publication offence. Some parts of text may be used, only where the source of the quoted material is clearly acknowledged.

3. General information

A. You can send your manuscript via online submission system which is available on our website. If the manuscript is not prepared according to the format of **Cell J**, it will be returned to authors.

B. The order of article appearance in the Journal is not demonstrating the scientific characters of the authors.

C. Cell J has authority to accept or reject the manuscript.

D. The received manuscript will be evaluated by associate editor. **Cell J** uses a single-blind peer review system and if the manuscript suits the journal criteria, we select the reviewers. If three reviewers pass their judgments on the manuscript,

it will be presented to the editorial board of **Cell J.** If the editorial board has a positive judgment about the manuscript, reviewers' comments will be presented to the corresponding author (the identification of the reviewers will not be revealed). The executive member of journal will contact the corresponding author directly within 3-4 weeks by email. If authors do not receive any reply from journal office after the specified time, they can contact journal office. Finally, executive manager will respond promptly to authors' request.

The Final Checklist

The authors must ensure that before submitting the manuscript for publication, they have to consider the following parts:

1. Title page should contain title, name of the author/coauthors, their academic qualifications, designation & institutions they are affiliated with, mailing address for future correspondence, email address, phone, and fax number.

2. Text of manuscript and References prepared as stated in the "guide for authors" section.

3. Tables should be on a separate page. Figures must be sent in color and also in JPEG (Jpg) format.

4. Cover Letter should be uploaded with the signature of all authors.

5. An ethical committee letter should be inserted at the end of the cover letter.

The Editor-in-Chief: Ahmad Hosseini, Ph.D.

Cell Journal *(Yakhteh)*

P.O. Box: 16635-148, Iran

Tel/Fax: + 98-21-22510895

Emails: Celljournal@royaninstitute.org

info@celljournal.org

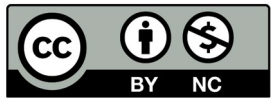

Dr. Saeed Kazemi Ashtiani

IN THE NAME OF GOD

Gone But not Forgotten

In the memory of the late Director of Royan Institute, Founder of Stem Cells Research in Iran and Chairman of ***Cell Journal*** *(Yakhteh)*. May he rest in peace.

PUBLISHED & SPONSORED BY:
Publication of Royan Institute (ACECR)

Indexed in:
1. Thomson Reuters (ISI)
2. PubMed
3. PubMed Central (PMC)
4. National Library Medicine (NLM)
5. Biosis Preview
6. Index Medicus for the Eastern Mediterranean Region (IMEMR)
7. Regional Information Center for Sciences and Technology (RICeST)
8. Index Copernicus International
9. Cambridge Scientific Abstract (CSA)
10. EMBASE
11. Scopus
12. Cinahl Database
13. Google Scholar
14. Chemical Abstract Service (CAS)
15. Proquest
16. Directory of Open Access Journals (DOAJ)
17. Open Academic Journals Index (OAJI)
18. Directory of Research Journals Indexing (DRJI)
19. Scientific Information Database (SID)
20. Iranmedex
21. Islamic World Science Citation Center (ISC)
22. Magiran
23. Science Library Index
24. Biological Abstracts
25. Essential Science Indicators
26. EuroPub

ACECR

Editorial Office Address (Dr. Ahmad Hosseini):
Royan Institute, P.O.Box: 16635-148,
Tehran, Iran
Tel & Fax: (+9821)22510895
Website: www.celljournal.org
Emails: info@celljournal.org
celljournal@royaninstitute.org

Printing Company:
Naghshe e Johar Co.
No. 103, Fajr alley, Tehranpars Street,
Tehran, Iran.

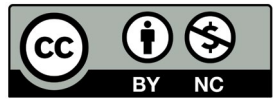

Cell Journal$_{(Yakhteh)}$, Vol 23, No 2, July 2021, Serial Number: 90, Pages: 145-250

CONTENTS

Original Articles

Letter to The Editor

Original Article

Xeno-Free Human Wharton's Jelly Mesenchymal Stromal Cells Maintain Their Characteristic Properties after Long-Term Cryopreservation

Caroline Mathen, Ph.D.*, Wilfrid Dsouza, M.Sc.

OCT Therapies and Research, Pvt. Ltd., Mumbai, India

***Corresponding Address: OCT Therapies and Research, Pvt, Ltd.3, Nimbkar Society, Malabar Hill Road, Mulund Colony, Mumbai 400082, India**
Email: caroline@octtherapies.com*

Received: 2/September/2019, Accepted: 22/December/2019

Abstract

Objective: The past decade has witnessed a rapid growth in harnessing the potential of adult stem cells for regenerative medicine. An investigational new drug (IND) or a regenerative medicine advanced therapy (RMAT) product must fulfil many requirements, such as stability studies, after cryopreservation. Such studies are important to ascertain the utility of off-the-shelf allogeneic cells for clinical applications. The present work describes a complete characterisation of xeno-free human Wharton's Jelly mesenchymal stromal cells (hWJ-MSCs) before and up to 28 months post-cryopreservation.

Materials and Methods: In this experimental study, culture methods that involved plasma derived human serum and recombinant trypsin were used to develop clinical grade cells. Complete cell characterisation involved flow cytometry studies for viability, positive and negative markers, colony forming unit (CFU) potential, population doubling time (PDT), soft agar assay to evaluate *in vitro* tumourigenicity, karyotype analysis and differentiation studies which were performed before and at 6, 12, 18 and 28 months post-cryopreservation.

Results: Our data showed consistency in the flow cytometry, CFU assay, PDT, soft agar assay, karyotyping and differentiation studies.

Conclusion: Using our protocols for extended xeno-free culture and cryopreservation of hWJ-MSCs, we could establish the shelf life of the cell-based product for up to 28 months.

Keywords: Mesenchymal Stromal Cells, Stability, Umbilical Cord, Wharton's Jelly

Cell Journal(Yakhteh), Vol 23, No 2, July 2021, Pages: 145-153

Citation: **Mathen C, Dsouza W. Xeno-free human wharton's jelly mesenchymal stromal cells maintain their characteristic properties after long-term cryopreservation. Cell J. 2021; 23(2): 145-153. doi: 10.22074/cellj.2021.7131.**

Introduction

Mesenchymal stromal cells (MSCs) are adult multipotent cells characterized by self-renewal as well as differentiation into various fibroblastic lineages, including transdifferentiation into other lineages. These cells were initially studied by Owen and Friedenstein (1) who recognized their differentiation potential across various lineages. Although these cells are implicated in various intrinsic healing mechanisms, the process may be slow, absent or compromised in certain clinical conditions. The human body retains contingent reserves of stem cells in various organs to replace diseased or damaged tissues when needed. Since this process is time-consuming *in vivo*, these cells can be expanded *in vitro* in the laboratory and be used to facilitate the body's innate self-healing mechanisms. More than two decades ago, McElreavey et al. (2) isolated MSCs from the umbilical cord matrix, also known as Wharton's jelly (WJ), and these cells have been well-studied (3-5). Umbilical cord represents an abundant, young, non-invasive and non-controversial tissue source without any ethical implications if carried out within the confines of Institutional Ethics approval and accompanied by documented donor informed consent. Interestingly, apart from their differentiation capacities, MSCs also have inherent immunomodulatory properties (6), while being hypoimmune cells themselves. These cells are negative for class II major histocompatibility markers (7). Thus, human MSCs are non- antigenic and indiscernible to the recipient's immune system (8, 9).

Caplan (10) theorizes that perhaps the most vital role of MSCs is to evade immunosurveillance and promote a microenvironment that supports regeneration. Various groups that have used laboratory expanded bone marrow-derived MSCs in clinical settings, irrespective of autologous or allogeneic sources, have not reported any adverse events. This proves that isolation and *in vitro* expansion is safe and translates to clinical benefit following intravenous delivery of human MSCs (11). Apart from healing and regenerative properties for various indications (12, 13), MSCs have also been implicated in immune-modulated remediation for graft versus host disease (GvHD) and type one diabetes (14, 15).

Stem cells from adults, foetal and other sources are widely used to regenerate tissues in humans after they have suffered damages due to diseases or injuries. For this purpose, cells must be grown *in vitro* for different periods of time using defined media, an important component of which is animal serum. Fetal bovine serum (FBS) or calf serum, a derivative of the meat industry, is a commonly

used additive in cell culture as it contains factors that the cells need for attachment, proliferation and differentiation (16). For clinical applications, cells are cultured in media that contain animal sera, human allogeneic serum or a cocktail of growth factors from xeno (animal) or recombinant sources. Nevertheless, there are scientific, safety and ethical issues regarding the use of animal serum (17). Additionally, when the aim is cell-based therapeutics or clinical applications, there are limitations and risks while using these methods, given the chance for transmission of pathogens (18) or prions (19) from animal sources to the cells that may eventually end up in humans during transplantation. Consequently, during translational research, it is preferable to have a cell-based product, which is free from any animal products or xeno-free. In this study, we have analysed xeno-free human WJ-MSCs (hWJ-MSCs) at different time points over 28 months after cryopreservation.

Materials and Methods

In this experimental study, human umbilical cords from elective caesarean deliveries were collected after obtaining written informed consent from the potential donors and relevant Ethics approvals in compliance with the National Guidelines for Stem Cell Research (NGSCR). Approvals were obtained from the Institutional Committee for Stem Cell Research of the Company (ICSCR/OCT/UID/002) and Hospital (ISCC/04/14) as well as the hospital's Institutional Ethics Committee (IEC/38/14).

All reagents were procured from Sigma (UK) or Gibco (Life Technologies, Denmark). Other chemicals were from Qualigens and were of analytical grade. Differentiation media, alizarin red S, oil red O and alcian blue stains were from HiMedia (India). Consumables were either from Nunc Thermo Fisher Scientific or Tarsons. The culture media used to isolate MSCs was Dulbecco's modified eagle medium (DMEM) supplemented with 1 mM sodium pyruvate, 4 mM L-glutamine, 10% human serum, 1% penicillin/streptomycin and 2.5 mg/mL amphotericin B. The human serum was recovered from plasma using modified protocols as described elsewhere (20). Briefly, pooled plasma lots were treated with 9% of 0.1 M calcium chloride, allowed to clot, and the recovered serum was heat inactivated at 56˚C for 30 minutes. The serum was further processed to neutralise viruses, bacteria and mycoplasma (21). Cold sterilization was carried out using 0.1% peracetic acid.

Human umbilical cords were collected after a three-tier donor-screening protocol, which consisted of documented informed consent, medical history and infectious disease screening that included, but was not limited to: human immunodeficiency viruses (HIV), syphilis, hepatitis B and hepatitis C as per the NGSCR. The umbilical cords were coded to protect donor identities and were processed according to good manufacturing practice (GMP) compliant conditions.

Isolation of the hWJ-MSCs was carried out as previously described (22) with some modifications. Briefly, the donor tissue was transported to the laboratory tissue processing facility under cold conditions (<20˚C) in cold Dulbecco's phosphate buffered saline (DPBS), supplemented with 10X amphotericin B and penicillin-streptomycin using previously validated protocols. The tissue was quarantined at 2-8˚C and processed within 48 hours. Each umbilical cord was cut into 5 cm pieces. The tissue sample was washed 2-3 times with DPBS supplemented with 2X antibiotic. The cord was cut lengthwise and the blood vessels excised. The remaining soft tissue was cut into 4-8 mm pieces and plated in 90 mm petri dishes. The petri dishes were incubated at 37˚C and 5% CO_2. Media change was carried out every three days until the MSCs were 80% confluent. Cells were subcultured using TrypLE™ Select and further culturing was carried out in T-75 or triple flasks up to the second passage, which comprised the master cell bank and up to the sixth passage, which comprised the working cell bank. Cells were cryopreserved in 90% serum and 10% dimethyl sulphoxide (DMSO) using a frosty in a -80˚C freezer overnight, after which they were transferred to liquid nitrogen for extended storage.

Passage 2 (P-2) and passage 6 (P-6) MSCs from five lots (5 donors) were subjected to the following characterisation and analyses pre- and post-cryopreservation at 0, 6, 12, 18 and 28 months. Characterisation was carried out in accordance with the International Society for Cellular Therapy (ISCT) guidelines (23) and included the following:

Morphological evaluation

The cells were observed under an inverted microscope for confirmation of fibroblastic morphology and adherence to plastic.

Flow cytometry

This analysis was carried out to confirm that the cells were MSCs. All antibodies were procured from Biolegend. 0.5×10^6 cells of each sample were used for flow cytometry. Viability was assessed using Zombie Violet™ dye (0.092%, cat. no. 423113). The cells were analysed for FITC conjugated CD90 (0.5% concentration, cat. no. 328107), PE conjugated CD105 (0.5% concentration, cat. no. 323205) and PerCP conjugated CD34 (0.2% concentration, cat. no. 343519), CD45 (0.2% concentration, cat. no. 304025) and HLA-DR (0.3% concentration, cat. no. 307627). Onecomp EBeads (EBioscience cat. no. 01-1111-41) were used to prepare single colour controls for the fluorescent labelled antibodies and the cells were used to prepare a single colour control for Zombie Violet. At least 20000 events were recorded on an Attune Acoustic flow cytometer (Thermo Fisher) and FlowJo software v7.6.5 was used for data analysis. One sample of P-6 at 12 months was lost; however, this did not affect the overall analysis.

Colony forming unit

For this assay, cells were seeded at a concentration of 1×10^4 in 60 mm petri dishes for approximately 10 days

and terminated when discrete colonies that comprised at least 50 cells per colony were visible. After termination, the cells were stained with 0.4% Sulforhodamine B (SRB) in 1% acetic acid dye for visualisation (24) and counted under an inverted microscope. Each experiment was carried out in triplicate for three lots of the early and late passages and at different time points.

Population doubling time

A total of 8×10^3 cells/cm^2 were seeded and the population doubling time (PDT) was calculated as per the formula recommended by the American Type Culture Collection

(ATCC):

DT=T ln2/ln(Xe/Xb)

Where:

T is the incubation time in hours.
Xb is the cell number at the beginning of the incubation time.
Xe is the cell number at the end of the incubation time.
The experiments were carried out for five lots from passages 2 to 6.

Soft agar assay

This is an *in vitro* tumorigenic assay. A 2% base of agar mixed with 2X medium (final concentration: 1% agar and 1X medium) was plated onto 60 mm petri dishes followed by 1% agar mixed with 2X medium that contained a 1×10^5 cell suspension (final concentration: 0.5% agar and 1X medium). A positive control was concurrently run using MCF7, a breast cancer cell line. Growth was observed over 21 days. The experiments were carried out in duplicate for each passage and time points for all lots.

Karyotype analysis

This was carried out according to a modified protocol described by Moorehead et al. (25). In brief, cells were arrested in the log phase of growth by the addition of 1×10^{-7} M colchicine (final volume) and incubated for up to three hours. Cells were enzymatically dispersed, washed and given hypotonic treatment at 37˚C with 0.075 M KCl for 15 minutes. The cells were repeatedly washed with fresh, chilled Carnoy's fixative and finally re-suspended in the same. The cells were fixed onto chilled glass slides, air-dried and stained for G-banding by trypsin with Giemsa (GTG banding). At least five spreads were captured and chromosomal analysis was carried out using Olympus microscopes BX-41 and BX-43, and Cytovision software from Leica.

Differentiation studies

Osteogenic, chondrogenic and adipogenic differentiation studies were carried out per the manufacturer's instructions. The experiments were carried out in triplicate and repeated twice for all five lots at passages 2 and 6 at all of the time points. Miniaturized experiments were carried out in 96-well plates. Each well was seeded with 5×10^4 cells and allowed to grow in normal growth medium. Differentiation media was added once 70% confluency was achieved. This media change was counted as the first day of differentiation. The spent media was replaced with fresh differentiation medium every 48-72 hours for up to 18-21 days. Osteogenic differentiation was confirmed by 2% alizarin red S staining while adipogenic staining of lipid vesicles was by 0.21% oil red O staining. The spent media was discarded, the cells were washed with PBS and fixed with 4% paraformaldehyde (PFA). After further washes with distilled water for alizarin red S and with 60% isopropyl alcohol (IPA) for oil red O, further incubation was carried out in the dark. The stain was washed away and cells were visualized under the microscope. Mineralized osteoblasts appeared bright orange-red in comparison with the control cells. Cells which have undergone adipogenic differentiation have red coloured lipid vesicles, which are not visible in control cells.

For chondrogenic differentiation, 1×10^6 cells in a centrifuge tube that contained medium were centrifuged at 1000 rpm for 10 minutes. The supernatant was carefully discarded without disturbing the pellet. Fresh media was added to the pellet, and the centrifuge tube with a loosened lid was incubated at 37˚C in a 5% CO_2 humidified incubator for 48 hours following which the growth medium was replaced with chondrogenic differentiation medium. The pellet was gently re-suspended and centrifuged at 1000 rpm for 10 minutes. Media change was carried out every 48 hours for 18-21 days, during which time the cells aggregated and formed spheroids. For the staining procedure, a PBS wash was given and the spheroids fixed with 1% PFA. After further washes, the spheroids were stained with 1% alcian blue for 30 minutes. Excess stain was removed by washing thrice with 0.1N HCl. Distilled water was added to neutralize the acidity.

Statistics

Unless otherwise mentioned, the data are written as mean ± SD. All data were subjected to two-way ANOVA using GraphPad Prism Version 6.01 for Windows (GraphPad Software, San Diego, USA) with $P<0.05$ considered as significant.

Results

All cells from all of the five lots/donors exhibited normal morphology with characteristic fibroblastic, spindle shaped morphology and plastic adherent properties (Fig.1).

Flow cytometry studies for mean cell viabilities, and for positive and negative markers across different lots, passages and time points did not reveal any difference between freshly isolated and cryopreserved cells (Fig.2A, B).

Figure 3A and B are representative flow cytometry images of one lot for cell viability and positive markers, respectively, across early and late passages at different time points. This data indicated the stringency of the cell manufacturing processes whereby cell specific markers and viabilities were unaffected, and demonstrated that extended cryopreservation did not negatively impact the quality of the cells.

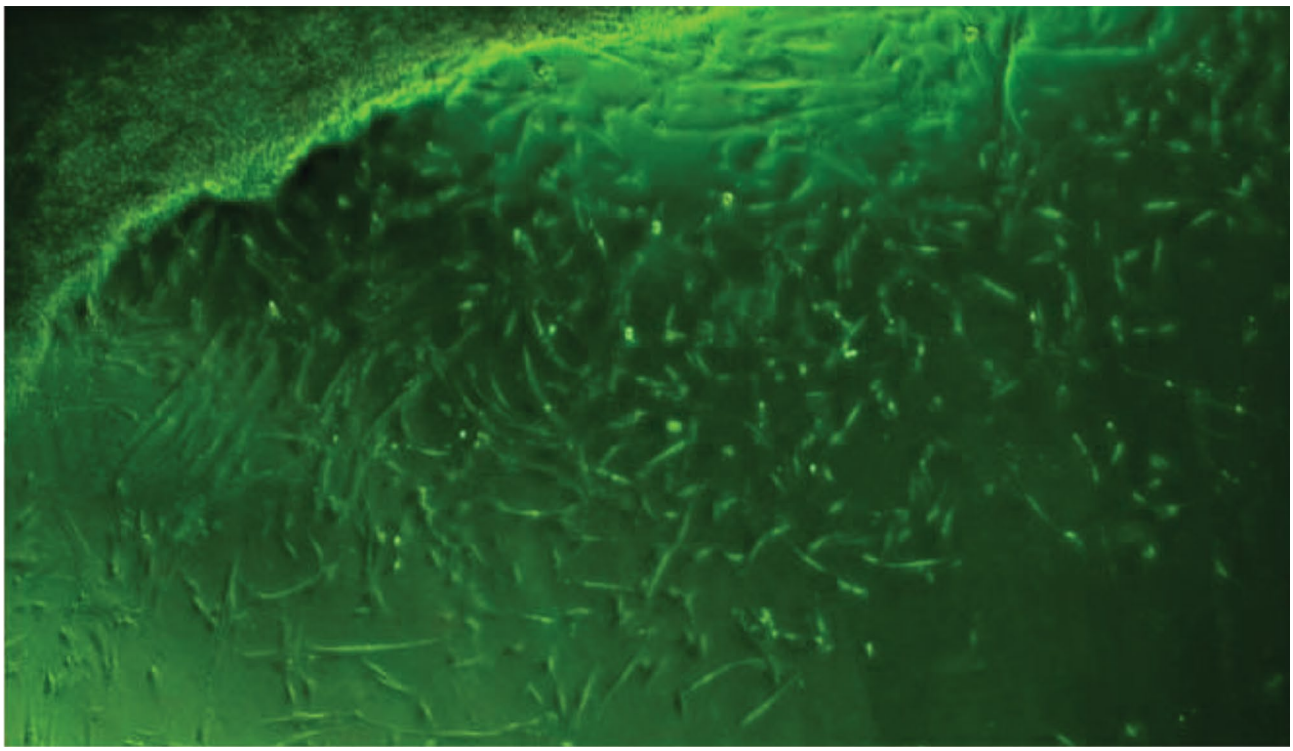

Fig.1: Human Wharton's jelly mesenchymal stromal cells (hWJ-MSCs) migrating after 7-10 days of explant culture as observed under an inverted microscope (phase contrast: X4). The adherent cells appear typically fibroblastic. The first cells to migrate out of the tissue are denoted as passage-0 cells.

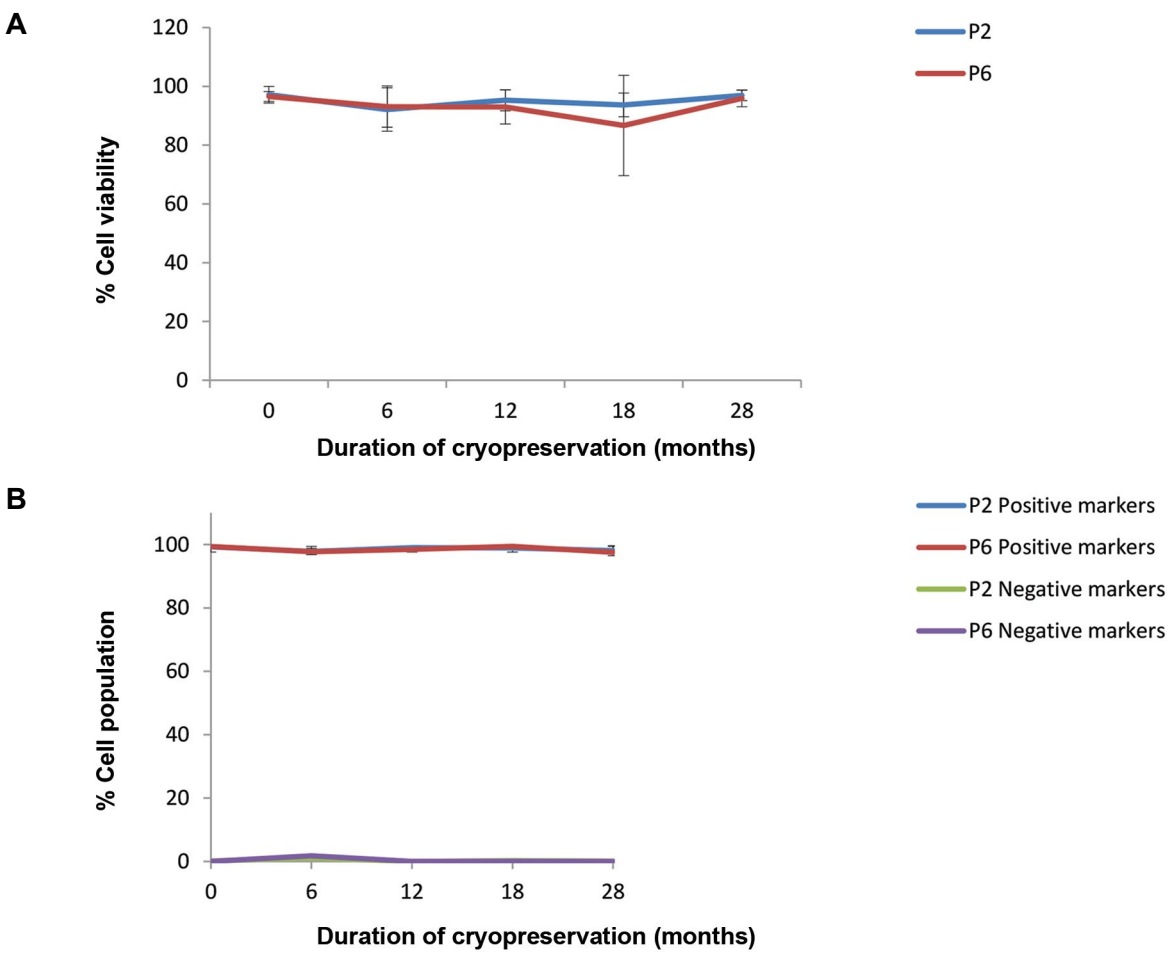

Fig.2: Flow cytometry studies for cell viability, and positive and negative markers. **A.** Mean cell viabilities and **B.** Haematopoietic and non-haematopoietic markers. The difference between the lots, passages and time points was not significant (data for five different lots; two-way ANOVA, P>0.05).

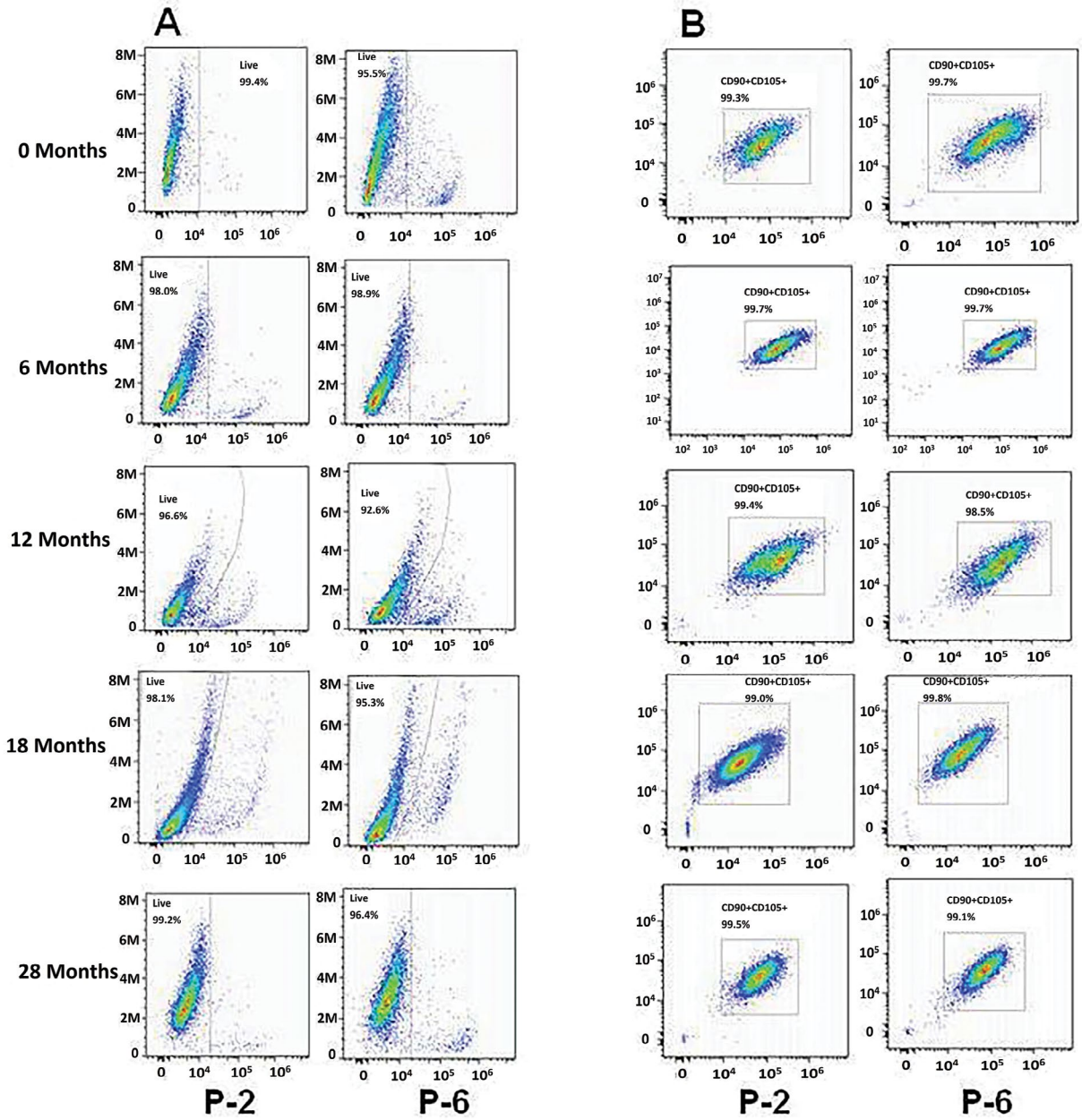

Fig.3: Representative images for flow cytometry studies across early and late passages, and at different time points. **A.** Cell viability remained unchanged, and **B.** Positive markers CD105 and CD90 were >95% in keeping with International Society for Cellular Therapy (ISCT) definitions for the mesenchymal stromal cells (MSCs).

Evaluation of the mean colony forming unit (CFU) potential revealed that the duration of cryopreservation and passage number had no effect on the number of colonies formed (Fig.4A). Although there was some lot-to-lot variability, this was anticipated due to the biological nature of the tissue. The efficiency of the CFU remained stable despite the passage number and cryopreservation, with an average of 66 ± 18 colonies at P-2 and 62 ± 12 colonies at P-6, and represents the quality and stemness of the MSCs.

The PDT indicates the age of the cells and maybe a better measurement of cell health than the passage number. The mean PDT was 45.01 ± 9.44 hours across all lots, passages and time points (Fig.4B).

After prolonged cell culture expansion and cryopreservation, the MSCs did not show any growth during the soft agar assay while the positive control clearly showed *in vitro* tumorigenic potential (Fig.5A).

Karyotype analysis revealed normal karyotype for all cells irrespective of lots, passages or duration of cryopreservation (Fig.5B).

Both the soft agar and karyotype data were important as cryopreservation, culture methods or reagents may contribute to genotypic instability; however, we did not see any evidence of the same in our studies.

The MSCs from all lots could be successfully differentiated into osteogenic, chondrogenic and adipogenic lineages at all passages and time-points post-cryopreservation (Fig.6A-C). The differentiation potential did not seem to vary. Since this was a qualitative analysis, quantification could not be carried out.

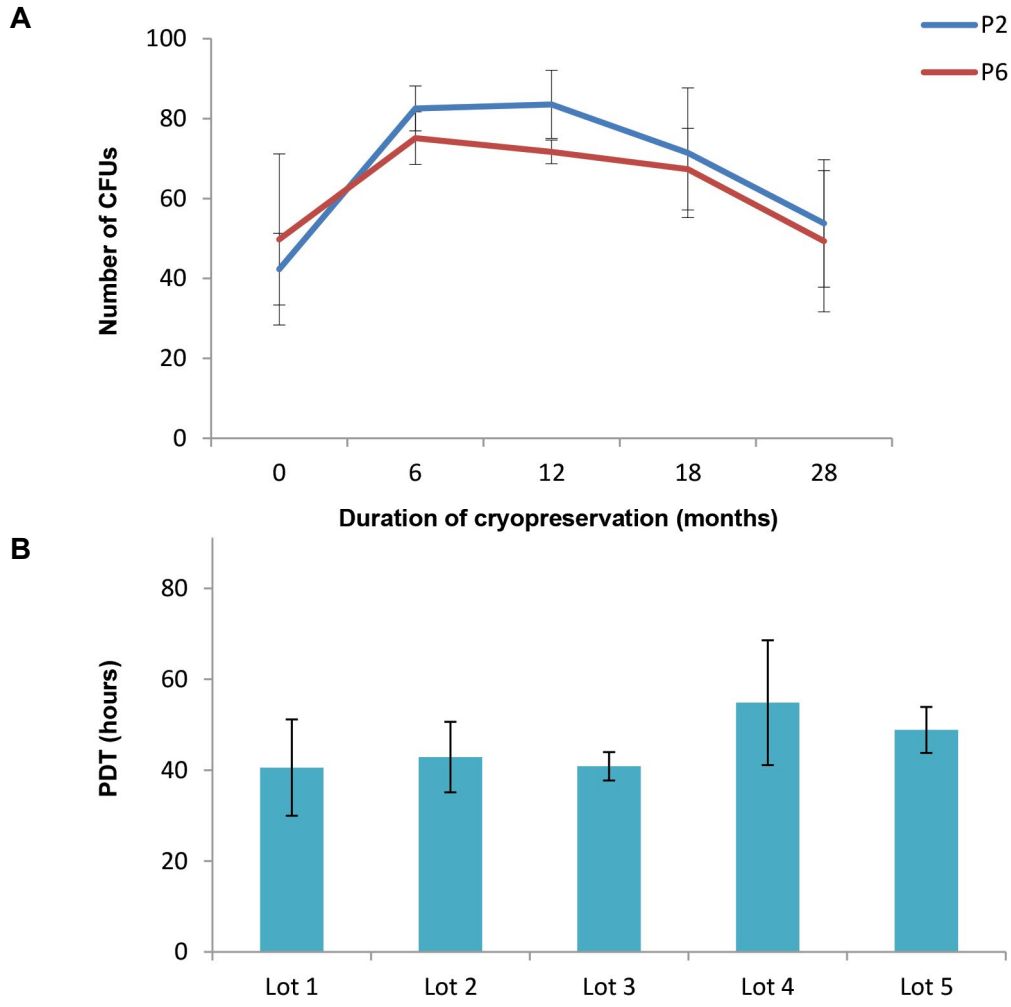

Fig.4: Colony forming unit (CFU) assay and population doubling time (PDT) were evaluated. **A.** The mean CFU potential at early and late passages, and at different time points (data for three different lots; two-way ANOVA, P>0.05). The stemness of the cells was retained despite cryopreservation. **B.** Depicts the mean PDT across five lots, at early and late passages and different time points, which remained largely unchanged except for the anticipated lot to lot variability.

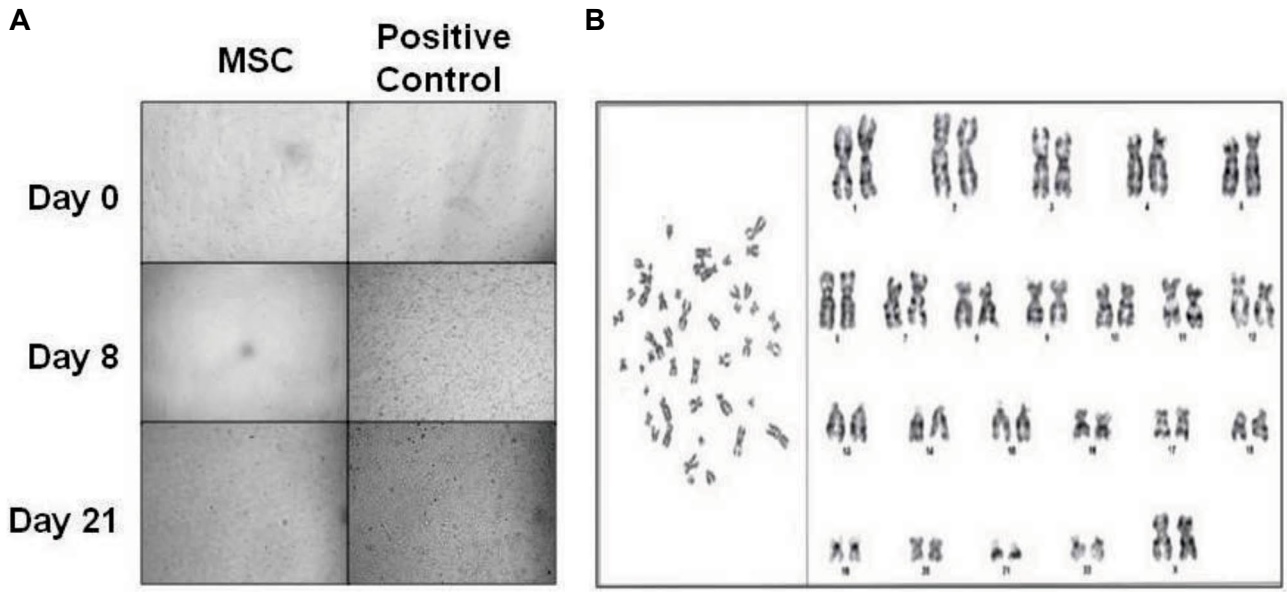

Fig.5: The soft agar assay was carried out to evaluate *in vitro* tumourigenicity. **A.** *In vitro* soft agar assay showed that after long-term culture and cryopreservation, the Wharton's jelly mesenchymal stromal cells (WJ-MSCs) did not exhibit altered growth characteristics of plastic adherence and could not grow in soft agar. However, the positive control, the MCF7 breast cancer cell line, showed vigorous growth in soft agar and was not anchorage dependent, and **B.** Representative karyotype (46, XX) of WJ-MSCs. Long-term culture and cryopreservation did not affect the karyotype.

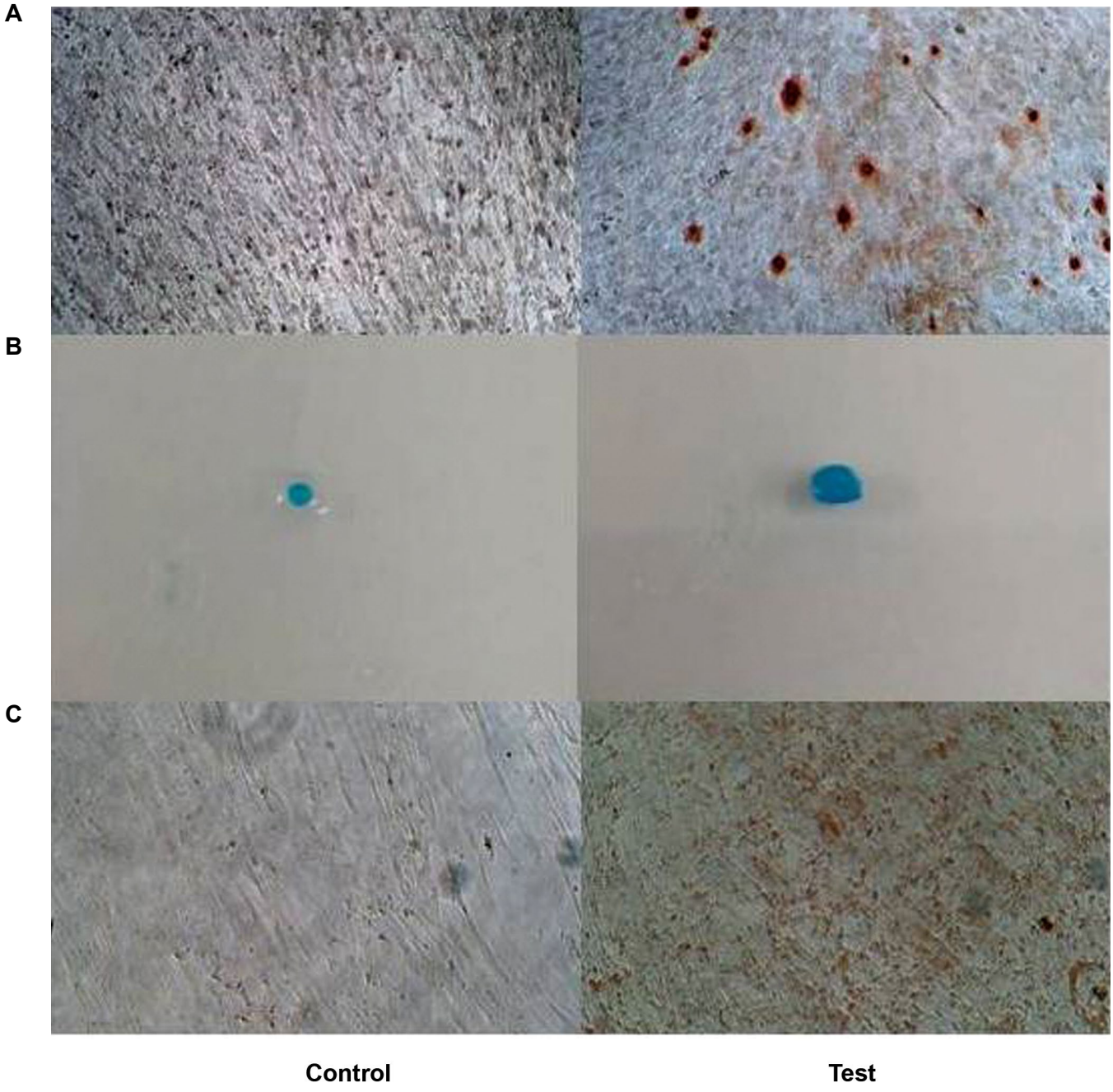

Fig.6: Representative images of differentiation studies of Wharton's jelly mesenchymal stromal cells (WJ-MSCs). **A.** Osteogenic, **B.** Chondrogenic, and **C.** Adipogenic lineages.

Discussion

Our study established the stability of cryopreserved WJ-derived MSCs and demonstrated the feasibility of large-scale working cell banks for clinical applications. The cells were well within the characterisation parameters that are globally recognized and accepted. Cell morphology, CD markers and differentiation capacities were consistent among different lots, passages and after 28 months of cryopreservation in liquid nitrogen. Moreover, there was no indication of chromosomal abnormalities in the karyotype studies, nor did the cells display any tumourigenic properties as evidenced in the soft agar assay. CFU studies revealed retained stemness and PDT showed largely unchanged growth patterns.

Other groups have carried out stability studies of MSCs from alternate sources like bone marrow (26) and recommended the use of bone marrow MSCs up to passage 4 after which signs of differentiation were observed. Stultz et al. (27) applied spectral karyotyping as a tool to study bone marrow MSCs and used FBS as a growth supplement to culture cells up to passage 7. Their studies indicated early passage abnormalities which decreased inversely with increasing passages. Blázquez-Prunera et al. (28) utilised a commercially available human plasma

fraction to develop xeno-free MSCs from adipose tissue, bone marrow and umbilical cord, and demonstrated the suitability of human plasma derived growth supplements for large scale expansions of stable cell populations. Patrikoski et al. (29) comparatively evaluated culture conditions of adipose derived MSCs using FBS, human serum and commercially available serum-free medium (STEMPRO). Although the results were comparable, they advocated chemically defined media in lieu of serum based media for better safety profiles during clinical applications. However, in our opinion, this greatly increases the cost of the final cell-based products. Many have reported the potential of human umbilical cord blood or cord tissue MSCs as the future of regenerative medicine due to numerous desirable traits that included availability, non-invasiveness, low immunogenicity and better proliferative and differentiation capacities (30, 31). There are emerging reports about translational work that used these cells for various applications (32-35). We have demonstrated that WJ-MSCs have the stability and requisite traits which are relevant for cell-based therapies.

Among other requirements, development of clinical grade cells for therapeutic use necessitates stability studies, especially if the intention is to create a large scale stem cell bank that involves expansion of cultured cells. This is required, not only for regulatory submissions, but to determine the shelf life of the cell-based product. We expanded the MSCs up to passage 6 without loss of critical parameters. These cells are normal diploid cells that follow the Hayflick limit (36) and can thus safely be used for cell-based therapies.

Conclusion

We were able to develop and study fully characterized WJ-derived MSCs of the master and working cell banks, both before and after cryopreservation. These studies were carried out in real time and demonstrate the stability, stemness and regenerative potential of the cell populations across various lots, early and late passages, and at different thawing time points without the loss of desirable characteristics up to 28 months. This validates the robustness of the cell expansion to establish a large scale cell bank that can be used for clinical applications. The risk of transplantation of these xeno-free MSCs is as much as or less than a blood transfusion and acceptable in terms of safety, and scientific and regulatory perspectives. Accordingly, we developed a method to derive human serum from plasma which, in addition to complement inactivation, was also subjected to cold viral inactivation and served as a safe, feasible and economical cell culture growth supplement. Further, we used recombinant trypsin in the disaggregation process and thus eliminated all possible sources of potential xeno contamination, which is in keeping with the global alignment towards xeno-free products. Establishment of a large scale cell bank involves various processes and multi-level validations that include procuring the umbilical cords, developing a master cell bank and finally establishing release criteria for the final cell-based product. We recommend that future studies evaluate the immune functions of MSCs; however, this study was a major step towards our goal of developing cell-based clinical applications.

Acknowledgments

This work was partially funded by a grant-in-aid from the Biotechnology Industry Research Assistance Council under the Biotechnology Ignition Grant (grant number C-CAMP/BIG/101K). We are deeply grateful to the Centre for Cellular and Molecular Platforms for support during the BIRAC-BIG funding. The authors gratefully acknowledge the encouragement and support of OCT Therapies and Research Pvt. Ltd. in carrying out the research work. We are indebted to Dr. Anjali Tilu and Dr. Y.S. Nandanwar, Professor and Head of the Department of Obstetrics and Gynecology, Lokmanya Tilak Municipal General Hospital and Lokmanya Tilak Municipal Medical College, Mumbai for providing the umbilical cords. We are grateful to Dr. Varsha Pancholi from Triumph Blood Bank, Thane for helping us with the human plasma procurement. We thank Dr. Pratiksha Alagh from the National Facility for Biopharmaceuticals, Mumbai and Dr. Hemant Agrawal for assistance with the flow cytometry studies. Dr. Caroline Mathen is the Director and Wilfrid Dsouza is an employee of OCT Therapies and Research Pvt., Ltd. This work is protected under patent number 1471/MUM/2014 and PCT application PCT/IN2018/050078.

Authors' Contributions

C.M.; Contributed to conception and study design, and obtained funding. C.M., W.D.; Contributed to all experimental work, data collection and evaluation, drafting and statistical analysis. All authors performed editing and approving the final version of this manuscript for submission, participated in the finalization of the manuscript and approved the final draft.

References

1. Owen M, Friedenstein AJ. Stromal stem cells: marrow-derived osteogenic precursors. Ciba Found Symp. 1988; 136: 42-60.
2. McElreavey KD, Irvine AI, Ennis KT, McLean WH. Isolation, culture and characterisation of fibroblast-like cells derived from the Wharton's jelly portion of human umbilical cord. Biochem Soc Trans. 1991; 19(1): 29S.
3. Koliakos I, Tsagias N, Karagiannis V. Mesenchymal cells isolation from Wharton's jelly, in perspective to clinical applications. J Bio Res-Thessaloniki. 2011; 16: 194-201.
4. Christodoulou I, Kolisis FN, Papaevangeliou D, Zoumpourlis V. Comparative evaluation of human mesenchymal stem cells of fetal (Wharton's Jelly) and Adult (adipose tissue) origin during prolonged in vitro expansion: Considerations for Cytotherapy. Stem Cells Int. 2013; 2013: 246134.
5. Kim DW, Staples M, Shinozuka K, Pantcheva P, Kang SD, Borlongan CV. Wharton's jelly-derived mesenchymal stem cells: phenotypic characterization and optimizing their therapeutic potential for clinical applications. Int J Mol Sci. 2013; 14(6): 11692-11712.
6. Hass R, Kasper C, Böhm S, Jacobs R. Different populations and sources of human mesenchymal stem cells (MSC): a comparison of adult and neonatal tissue-derived MSC. Cell Commun Signal. 2011; 9: 12.
7. Sorrell JM, Caplan AI. Topical delivery of mesenchymal stem cells

and their function in wounds. Stem Cell Res Ther. 2010; 1: 30.
8. Tse WT, Pendleton JD, Beyer WM, Egalka MC, Guinan EC. Suppression of allogeneic T-cell proliferation by human marrow stromal cells: implications in transplantation. Transplantation. 2003; 75(3): 389-397.
9. Krampera M, Glennie S, Dyson J, Scott D, Laylor R, Simpson E, et al. Bone marrow mesenchymal stem cells inhibit the response of naive and memory antigen-specific T cells to their cognate peptide. Blood. 2002; 101(9): 3722-3729.
10. Caplan AI. Why are MSCs therapeutic? New data: new insight. J Pathol. 2009; 217(2): 318-324.
11. Koç ON, Gerson SL, Cooper BW, Dyhouse SM, Haynesworth SE, Caplan AI, et al. Rapid hematopoietic recovery after coinfusion of autologous-blood stem cells and culture-expanded marrow mesenchymal stem cells in advanced breast cancer patients receiving high-dose chemotherapy. J Clin Oncol. 2000; 18(2): 307-316.
12. Trounson A, Thakar RG, Lomax G, Gibbons D. Clinical trials for stem cell therapies. BMC Med. 2011; 9: 52.
13. Wang S, Qu X, Zhao RC. Clinical applications of mesenchymal stem cells. J Hem Onco. 2012; 5: 19.
14. Lin Y, Hogan WJ. Clinical application of mesenchymal stem cells in the treatment and prevention of graft-versus-host disease. Adv Hematol. 2011; 2011: 427863.
15. Abdi R, Fiorina P, Adra CN, Atkinson M, Sayegh MH. Immunomodulation by mesenchymal stem cells a potential therapeutic strategy for type 1 diabetes. Diabetes. 2008; 57(7): 1759-1767.
16. Gstraunthaler G. Alternatives to the use of fetal bovine serum: serum-free cell culture. ALTEX. 2003; 20(4): 275-281.
17. Tekkatte C, Gunasingh GP, Cherian KM, Sankaranarayanan K. Humanized stem cell culture techniques: the animal serum controversy. Stem Cells Int. 2011; 2011: 504723
18. Erickson GA, Bolin SR, Landgraf JG. Viral contamination of fetal bovine serum used for tissue culture: risks and concerns. Dev Biol Stand. 1991; 75: 173-175.
19. Simonetti AB, Englert GE, Campos K, Mergener M, de David C, de Oliveira AP, et al. Nanobacteria-like particles: a threat to cell cultures. Brazil J Micro. 2007; 38(1): 153-158.
20. Stehlík D, Pytlík R, Rychtrmocová H, Kideryová L, Veselá R, Kopečný Z, et al. Xenogeneic protein-free cultivation of mesenchymal stromal cells-towards clinical applications. Folia Biol (Praha). 2012; 58(3): 106-114.
21. Wutzler P, Sprossig M, Peterseim H. Suitability of peracetic acid for sterilization of media for mycoplasma cultures. J Clin Microb. 1975; 1(3): 246-249.
22. Can A, Balci D. Isolation, culture, and characterization of human umbilical cord stroma-derived mesenchymal stem cells. Methods Mol Biol. 2011; 698: 51-62.
23. Dominici M, Le Blanc K, Mueller I, Slaper-Cortenbach I, Marini FC, Krause DS, et al. Minimal criteria for defining multipotent mesenchymal stromal cells. The International Society for Cellular Therapy position statement. Cytotherapy. 2006; 8(4): 315-317.
24. Mathen C, Hardikar BP. A method for photomicrography of cytotoxicity in 96-well plates. Asia J Biotech. 2010; 2: 232-238.
25. Moorehead PS, Nowell PC, Mellman WJ, Battips DM, Hungerford DA. Chromosome preparations of leukocytes cultured from human peripheral blood. Exp Cell Res. 1960; 20: 613-616.
26. Binato R, de Souza Fernandez T, Lazzarotto-Silva C, Du Rocher B, Mencalha A, Pizzatti L, et al. Stability of human mesenchymal stem cells during in vitro culture: considerations for cell therapy. Cell Prolif. 2013; 46(1): 10-22.
27. Stultz BG, McGinnis K, Thompson EE, Surdo JLL, Bauer SR, Hursh DA. Chromosomal stability of mesenchymal stromal cells during in vitro culture. Cytotherapy. 2016; 18(3): 336-343.
28. Blázquez-Prunera A, Díez JM, Gajardo R, Grancha S. Human mesenchymal stem cells maintain their phenotype, multipotentiality, and genetic stability when cultured using a defined xeno-free human plasma fraction. Stem Cell Res Ther. 2017; 8: 103.
29. Patrikoski M, Juntunen M, Boucher S, Campbell A, Vemuri MC, Mannerström B, et al. Development of fully defined xeno-free culture system for the preparation and propagation of cell therapy-compliant human adipose stem cells. Stem Cell Res Ther. 2013; 4(2): 27.
30. Watson N, Divers R, Kedar R, Mehindru A, Mehindru A, Borlongan MC, et al. Discarded Wharton jelly of the human umbilical cord: a viable source for mesenchymal stromal cells. Cytotherapy. 2015; 17(1): 18-24.
31. Olson AL, McNiece IK. Novel clinical uses for cord blood derived mesenchymal stromal cells. Cytotherapy. 2015; 17(6): 796-802.
32. Chang YS, Ahn SY, Yoo HS, Sung SI, Choi SJ, Oh WI, et al. Mesenchymal stem cells for bronchopulmonary dysplasia: phase 1 dose-escalation clinical trial. J Pediatr. 2014; 164(5): 966-972.
33. Wang L, Li J, Liu H, Li Y, Fu J, Sun Y, et al. Pilot study of umbilical cord-derived mesenchymal stem cell transfusion in patients with primary biliary cirrhosis. J Gastroenterol Hepatol. 2013; 28 Suppl 1: 85-92.
34. Zhang Z, Lin H, Shi M, Xu R, Fu J, Lv J, et al. Human umbilical cord mesenchymal stem cells improve liver function and ascites in decompensated liver cirrhosis patients. J Gastroenterol Hepatol. 2012; 27 Suppl 2: 112-120.
35. Pang X, Yang H, Peng B. Human umbilical cord mesenchymal stem cell transplantation for the treatment of chronic discogenic low back pain. Pain Physician. 2014; 17(4): E525-530.
36. Hayflick L. The limited in vitro lifetime of human diploid cell strains. Exp Cell Res. 1965; 37(3): 614-636.

Original Article

In Vitro Implantation Model Using Human Endometrial SUSD2+ Mesenchymal Stem Cells and Myometrial Smooth Muscle Cells

Marzieh Rahimipour, Ph.D.[1], Mina Jafarabadi, M.D.[2], Mojdeh Salehnia, Ph.D.[1]*

1. Department of Anatomy, Faculty of Medical Sciences, Tarbiat Modares University, Tehran, Iran
2. Reproductive Health Research Centre, Tehran University of Medical Sciences, Tehran, Iran

Corresponding Address: P.O.Box: 14115-111, Department of Anatomy, Faculty of Medical Sciences, Tarbiat Modares University, Tehran, Iran
Email: salehnim@modares.ac.ir

Received: 29/May/2019, Accepted: 10/December/2019

Abstract

Objective: This study evaluated a novel *in vitro* implantation model using human endometrial mesenchymal stem cells (EMSCs), SUSD2+, and myometrial smooth muscle cells (SMCs) that were co-cultured with mouse blastocysts as the surrogate embryo.

Materials and Methods: In this experimental study, SUSD2+ MSCs were isolated from human endometrial cell suspensions (ECS) at the fourth passage by magnetic-activated cell sorting. The ECS and SUSD2+ cells were separately co-cultured with human myometrial muscle cells for five days. After collection of mouse blastocysts, the embryos were placed on top of the co-cultured cells for 48 hours. The interaction between the embryo and the cultured cells was assessed morphologically at the histological and ultrastructural levels, and by expression profiles of genes related to implantation.

Results: Photomicrographs showed that trophoblastic cells grew around the embryonic cells and attached to theECS and SUSD2+ cells. Ultrastructural observations revealed pinopode and microvilli-like structures on the surfaces of both the ECS and SUSD2+ cells. Morphologically, the embryos developed to the egg-cylinder stage in both groups. Gene expression analysis showed no significant differences between the two groups in the presence of an embryo, but an increased expression of *αV* was detected in SUSD2+ cells compared to ECS cells in the absence of an embryo.

Conclusion: This study showed that SUSD2+ cells co-cultured with SMCs could interact with mouse embryos. The co-cultured cells could potentially be used as an implantation model.

Keywords: Embryo Implantation, Endometrium, Epithelial Differentiation, Mesenchymal Stem Cells, SUSD2+ Cells

Cell Journal(Yakhteh), Vol 23, No 2, July 2021, Pages: 154-163

Citation: Rahimipour M, Jafarabadi M, Salehnia M. In vitro implantation model using human endometrial SUSD2+ mesenchymal stem cells and myometrial smooth muscle cells. Cell J. 2021; 23(2): 154-163. doi: 10.22074/cellj.2021.6979.

Introduction

Implantation results from successful interactions between the embryo and endometrial epithelium during the mid-secretory phase of the menstrual cycle when the endometrium is receptive. At this so-called "window of implantation", ultrastructural alterations occur on the surface of endometrial epithelial cells and serve as important implantation markers of the receptive endometrium (1, 2).

Human implantation proceeds through three main stages: apposition, adhesion, and invasion. During the apposition stage, the blastocyst interacts with the apical surface of the luminal epithelium through two-way molecular communication. During the receptive phase, the luminal epithelial surface changes from a non-adhesive to adhesive surface, which results in the appearance of pinopodes and reduction of lateral junctional complexes. During attachment, the embryo initiates a physical connection with the apical surface of the endometrial epithelium; however, during invasion, the trophoblast cells penetrate between the epithelial cells, migrates to and invades the blood vessels (3).

Impairment of implantation is considered a major cause of human pregnancy loss and infertility in assisted reproductive technologies (ART) (4, 5). Improving ART outcomes and preventing early pregnancy loss requires a better understanding of the mechanisms of interactions between the embryo and the endometrium during the implantation process. Since the *in vivo* study of human embryo implantation is unethical and has limitations, and the results of studies performed in animal models are not always applicable in humans, *in vitro* implantation models using human cells provide an alternative approach (6).

In vitro implantation models are categorized into several types (6). One mainly focuses on the interaction between endometrial epithelial cells and the embryo to evaluate the early stages of implantation (6-8). In another group of implantation models, late stages of implantation are studied through two-dimensional culture of endometrial stromal cells with an embryo (6, 9). In more complex models, endometrial epithelial and stromal cells are co-cultured with an embryo in a three-dimensional culture system, allowing the study of both early and late stages of implantation (6, 10-12). Because of limited access to human embryos, a number of studies have used surrogate embryos in designing implantation models (6). Several have employed mouse blastocysts (13, 14),

while most have used trophoblast spheroids derived from trophoblastic cell lines (15, 16).

The human endometrium is a dynamic tissue that undergoes cyclical shedding and regeneration during each reproductive cycle. The identification of rare populations of adult stem cells in both the stratum functionalis and basalis suggest that they may play a critical role in endometrial regenerative activities (17-19). Endometrial stem/progenitor cells have adult stem cell characteristics of clonogenicity, high proliferative potential and multilineage differentiation potential (17, 20). They comprise epithelial, mesenchymal, and endothelial stem/progenitor cells. Endometrial mesenchymal stem cells (EMSCs) are located ina perivascular region, and include pericytes and perivascular cells (21). They are identified by specific markers, such as co-expression of CD146 and PDGF-Rβ and a single marker, SUSD2 (W5C5) (17, 18, 22-26).

EMSCs have the potential to differentiate into several cell types *in vitro* (18, 26); thus, they may have extensive applications in cell therapy, tissue reconstruction, and regenerative medicine (27, 28). There are limited reports regarding the differentiation of endometrial stem/progenitor cells into endometrial glands and epitheliaupon transplantation under the kidney capsules of immunodeficient mice (29). Recently, we showed that $CD146^+$ cells isolated from human endometrium differentiated into endometrial epithelial-like cells during co-culture with myometrial smooth muscle cells (SMCs) (30). Campo et al. (31) demonstrated that transplantation of cultured human endometrial side population (SP) cells, which were comprised of stromal and epithelial cells, to a decellularised porcine uterus resulted in some recellularisation with human vimentin positive stromal cells and rare cytokeratin positive epithelial cells. Recently, López-Pérez et al. (28) reported that injection of a human endometrial SP under kidney capsules induced reformation of human endometrium, which was confirmed by the presence of typical endometrial markers. They concluded that these cells had the optimum capacity to regenerate endometrial-like tissue.

Despite the differentiation potential of adult stem cells to endometrial-like cells, and according to our knowledge, few studies have designed an *in vitro* implantation model by using these cell types. Thus, the aim of the present study was to evaluate a novel *in vitro* implantation model that mimics the *in vivo* condition by using human EMSCs co-cultured with human myometrial SMCs to assess implantation with mouse blastocysts as the surrogate embryo.

Materials and Methods

All reagents were purchased from Sigma Aldrich (Germany) unless otherwise indicated.

Human tissue collection

For this experimental study, human endometrial (n=10) and myometrial (n=10) tissues were obtained from healthy fertile women (aged 25-40 years) during the proliferative phase, and who were undergoing hysterectomies for non-pathological conditions. The women had not taken any exogenous hormones for three months before surgery (Table S1, See Supplementary Online Information at www.celljournal.org). Samples were transported to the laboratory in equilibrated and pre-warmed Leibovitz'sL-15 medium supplemented with 10 mg/ml human serum albumin, 100 IU/ml penicillin and 100 µg/ml streptomycin within 1-2 hours.

The Ethics Committee of the Medical Faculty of Tarbiat Modares University (Tehran, Iran, no.1394.137) approved this experimental study and written informed consent was received from all patients.

Experimental design

Figure S1 (See Supplementary Online Information at www.celljournal.org) shows the experimental design. Human endometrial cells were isolated mechanically and enzymatically from endometrial tissues and cultured up to the fourth passage. Then, the $SUSD2^+$ cells were sorted by magnetic activated cell sorting (MACS) and their characteristics were confirmed by immunohistochemistry. The endometrial cell suspensions (ECS) and sorted $SUSD2^+$ cells were separately co-cultured with myometrial smooth muscle for five days, after which the cultivation period was extended for an extra 48 hours in the presence or absence of mouse blastocysts in order to establish two *in vitro* embryo implantation models. At the end of the culture periods, the endometrial (ECS and $SUSD2^+$ cells) and embryonic cell interactions were assessed by morphological, ultrastructural and molecular studies.

Morphological evaluations of endometrial and myometrial samples

Ten samples each of endometrial and myometrial tissue were separately fixed in Bouin's solution, processed, embedded in paraffin wax and sectioned into 7 µm thicknesses. After hematoxyline and eosin (H&E) staining, the sections were observed with a light microscope and their normal morphology was evaluated (32).

Isolation of human endometrial cells

Human endometrial cells were isolated from tissues as per the Chan et al. (33) method. Briefly, human endometrial tissue was washed in phosphate-buffered saline (PBS) and then cut into small 1×1 mm pieces within Dulbecco's modified Eagle's Medium/Hams F-12 (DMEM/F-12) that contained 100 mg/ml penicillin G sodium and 100 mg/ml streptomycin sulphate B. The tissue fragments were separated into single cells using collagenase type 1 (300 µg/ml) and deoxyribonuclease type I (40 µg/ml) for 90 minutes together with a mechanical method. To eliminate glandular and epithelial components, the cell suspension was passed sequentially through sieves of mesh at sizes of 100 and 40 µm (SPL Life Sciences

Co., Korea), respectively (34). Endometrial stromal cells in the supernatant were cultured using DMEM/F-12 that contained antibiotics and 10% fetal bovine serum (FBS, all from Invitrogen, UK) and incubated at 37˚C in 5% CO_2. The cells were cultured up to passaged when they reached to 80-100% confluency, used for the following assessments.

Confirmation of endometrial mesenchymal cells using flow cytometry

A number of the passage-4 endometrial cells were evaluated for mesenchymal (CD90, CD73 and CD44) and hematopoietic markers (CD45 and CD34) by flow cytometric analysis. A total of 1×10^5 endometrial cells were suspended in 50 µl of PBS and incubated with direct fluorescein isothiocyanate (FITC)-conjugated antibodies (anti-human CD90, CD44, and CD45, 1:50 dilutions) and direct phycoerythrin (PE)-conjugated antibodies (anti-human CD73 and CD34; 1:50 dilutions) at 4˚C for 45 minutes. Finally, 200 µl of PBS was added and the cells were examined with a FACSCaliburcytometer (Becton Dickinson, Germany). The flow cytometric analysis was repeated three times.

SUSD2+ cell isolation by magnetic-activated cell sorting

After the fourth passage, the cultured human endometrial cells were washed, resuspended (up to 1×10^7cells/100 µl) in cold PBS and incubated with mouse anti-SUSD2 monoclonal antibody (327401, 8:200, Biolegend, UK) at 4˚C for 30 minutes. The cells were washed with MACS separation buffer (130-091-221, Miltenyi Biotec, Germany), then they were incubated with goat anti-mouse IgG Microbeads antibody (130047102, 20:100, Miltenyi Biotec, Germany) at 4˚C for 20 minutes. The cell suspensions were washed and run through the MACS column, followed by washing the column for three times with 500 µl MACS separation buffer. Magnetically labelled cells ($SUSD2^+$) were mostly retained on the column and the unlabelled cells ($SUSD2^-$) were eluted. Trypan blue staining (0.4%) was performed to determine $SUSD2^+$ cell viability following MACS sorting. All experiments were repeated three times.

Immunocytochemistry of sorted endometrial SUSD2+ cells

The purity of the magnetic bead-sorted human endometrial ($SUSD2^+$) cells was assessed by immunocytochemistry (n=3 samples). These cells were incubated with mouse anti-SUSD2 monoclonal antibody (327401, 8:200, Biolegend, UK) at 4˚C for 30 minutes. After washing the cells with PBS, they were incubated with secondary goat anti-mouse polyclonal antibody conjugated with Alexa Fluor® 488 (405319, 1:100 in PBS, Biolegend, UK) for 2 hours at 37˚C and washed three times with PBS. Nuclei were counterstained with 4', 6-diamidino-2-phenylindole (DAPI, D9542, Sigma, Germany) for 30 seconds. For negative controls, the cells were treated with the 10% unimmunized mouse serum in PBS instead of primary antibody. All experiments were repeated three times.

In vitro culture of human myometrial cells

After dissection, the tissue fragments of the myometrium were cultured according to the explant method as reported by Fayazi et al. (30). Briefly, the human myometrial tissues (n=10) were washed with PBS and then cut into 1×1 mm pieces in DMEM/F-12 that contained 100 mg/ml penicillin G sodium and 100 mg/ml streptomycin sulphate B. Finally, the fragments were placed in each well and the emerging cells were allowed to grow in complete DMEM/F-12 supplemented with 10% FBS to confluency at 37˚C and 5% CO_2 for three weeks. The medium was changed every two days. The characteristics of isolated myometrial cells were confirmed by immunocytochemical analysis.

Immunocytochemistry of myometrial cultured cells

Passage-2 trypsiniszed myometrial cells (n=3 samples) were cultured on cover slips. After attachment, the cultured cells were washed three times with PBS, fixed with 4% paraformaldehyde at 4˚C for 20 minutes, and permeabilised with 0.3% TritonX-100 for 45 minutes. Non-specific binding was blocked with 10% normal goat serum in PBS. Cells were separately incubated with the SMC markers, mouse anti-vimentin monoclonal antibody (V6389, 3:100 in PBS, Sigma-Aldrich, Germany) and rabbit anti-alpha smooth muscle actin polyclonal antibody (ab5694, 1:100 in PBS, Abcam, UK) at 4˚C overnight. The cells were washed in PBS three times, and incubated with secondary antibodies rabbit anti-mouse polyclonal antibody conjugated with Texas red (315-075-003, 3:100 in PBS, Biolegend, UK) and goat anti-rabbit IgG conjugated with FITC (ab6717, 1:1000 in PBS, Abcam, UK) at 37˚C for 2 hours. For negative controls, 10% unimmunized mouse serum in PBS was used instead of primary antibody. The immunocytochemistry analysis was repeated three times.

Collection of mouse blastocysts

Adult, 8-10 week-old female (n=40) and 8-12 week-old male (n=10) National Medical Research Institute (NMRI) mice were housed and used under standard conditions for laboratory animals at Tarbiat Modares University (Iran). The Committee for Animal Research of the University approved all of the experimental procedures. Adult female mice were super ovulated with an intraperitoneal (i.p.) injection of 7.5 IU pregnant mare serum gonadotropin (PMSG, Folligon, Intervet, Australia) and then by an i.p. injection of 10 IU human chorionic gonadotropin hormone (hCG, Pregnyl, Netherlands) 48 hours later. After the second injection, the mice were individually mated with fertile males. On the morning of the fifth day of pregnancy, blastocysts were flushed from the uterine horns and the hatched blastocysts were used for the experiments.

Implantation models using SUSD2$^+$ cells and endometrial cell suspensions

The SUSD2$^+$ cells (group 1) and ECS (group 2) were separately co-cultured with myometrial cells as two experimental groups. In each group, 10^4 SUSD2$^+$ or ECS cells were cultured in 48-well plates with 5×10^3 myometrial cells per well for five days. On the fifth day of culture, the mouse blastocysts were placed on the top of each well, with n=5 embryos in each well and a total of 45 embryos in each group for at least 9 repeats. The groups co-cultured in the absence of mouse blastocysts were considered to be the control groups. Then, these cells were cultured and monitored up to an additional 48 hours and evaluated morphologically by inverted microscope, live/dead staining, scanning electron microscope (SEM) and analysis of gene expressions related to implantation.

Live/dead staining

We assessed the viability of the embryos and cells at 48 hours after the embryo culture on the top of each of the co-culture experimental groups by using a live/dead viabilitykit (L-3224, Invitrogen, UK). For this purpose, the cells were incubated with calcein AM (green) and ethidium homodimer-1 (EthD-1, red) for intracellular esteraseactivity and plasma membrane integrity, respectively, according to the manufacturer's instructions. Then, the embryos and cells were observed under a fluorescent microscope (Nikon TE2000, Japan). This experiment was performed in triplicate.

Scanning electron microscope

After two days of co-culture of the experimental groups with embryos, we examined the ultrastructure and interaction of the implanted embryos with co-cultured cells by SEM and compared them with their respective controls (groups without embryos). The specimens were fixed in 2.5% glutaraldehyde and post-fixed with 1% osmium tetroxide in PBS for two hours. After dehydration in an ascending ethanol series, the specimens were dried in a freeze dryer (Snijders Scientific LY5FME, Netherlands), mounted and coated with gold particles (BalTec, Switzerland) and examined under SEM (Philips XL30, Netherland). These experiments were repeated three times.

Expression of implantation genes by real-time reverse transcription polymerase chain reaction

We evaluated the expressions of genes related to implantation: *αV* and *β3* integrin, interleukin-1 receptor (*IL-1R*), leukaemia inhibitory factor (*LIF*) and LIF receptor (*LIFR*). Total RNA was extracted from the collected cells after seven days of co-culture in both groups in the presence and absence of mouse embryos (5 embryosper well and, in total, 15 embryos per group with at least 3 replicates) using TRIzol (Invitrogen, UK). The concentration of isolated RNA was determined by a spectrophotometer, then cDNA was synthesized using a cDNA kit (Thermo Scientific, Lithuania, EU) in a total volume of 20 µl and the samples were stored at -80˚C until analysis. As shown in Table 1, the primers were designed based on human mRNA coding sequences using GenBank (http://www.ncbi.nlm.nih.gov) and synthesized at CinnaGen Company (Iran). The *β-actin* gene was used as an internal control.

Table 1: Characteristics of primers used for the real-time RT-PCR assay

Target gene	Primer pair sequences (5′-3′)	Accession number	Fragment size (bp)	Temp. (˚C)
αV	F: ATCTCAGAGGTGGAAACAGGA	NM_002210.4	21	58.09
	R: TGGAGCATACTCAACAGTCTTTG		23	58.68
β3	F: AGTAACCTGCGGATTGGCTTC	NM_000212.2	21	60.68
	R: GTCACCTCGTCAGTTAGCGT		20	59.76
LIF	F: CCAATGTGACGGACTTCCC	NM_002309.4	19	58.15
	R: TACACGACTATGCGGTACAGC		21	59.94
LIFR	F: TGTAACGACAGGGGTTCAGT	NM_001127671.1	20	58.58
	R: GAGTTGTGTTGTGGGTCACTAA		22	58.46
IL-1R	F: GGCACACCCTTATCCACCAT	NM_001261419.1	20	59.74
	R: GCGAAACCCACAGAGTTCTCA		21	60.54
β-actin	F: TCAGAGCAAGAGAGGCATCC	NM_001101.3	20	60.5
	R: GGTCATCTTCTCACGGTTGG		20	60.5

RT-PCR; Reverse transcription polymerase chain reaction.

After cDNA synthesis, real time reverse transcription polymerase chain reaction (RT-PCR) was performed by an Applied Biosystems real-time thermal cycler according to a QuantiTect SYBR Green RT-PCR kit (Applied Biosystems, UK). For each sample, the target genes and the reference gene were amplified in the same run and melting curve analysis was used to confirm the amplified product. Real-time thermal conditions included a holding step: 95˚C for 10 minutes and a cycling step: 95˚C 15 seconds and 60˚C 1 minute, followed by a melting curve step: 95˚C 15 seconds, 60˚C 1 minute and 95˚C 15 seconds. The Pfaffl method (35) was used to determine the relative quantification of target genes to the housekeeping gene. All experiments were repeated three times.

Statistical analysis

Quantitative variables were expressed as mean ± SD. The results of real-time RT-PCR were compared by the independent samples t test, one-way ANOVA and post hoc Turkey's tests. $P \leq 0.05$ were considered statistically significant. Statistical analysis was performed using SPSS software (V24, SPSS Inc., Chicago, IL, USA).

Results

Morphology of human endometrial and myometrial tissue

H&E stained sections of human endometrial tissue from the proliferative phase showed typical morphologies of the basalis and functionalis layers (Fig.1A, B). The glands were lined with simple columnar epithelium (arrow) and the stroma comprised fibroblast-like stromal cells. The normal morphology of SMCs in myometrial tissue after H&E staining are presented in Figure 1C and D.

The morphology of cultured endometrial cell suspensions, SUSD2+ and myometrial cells

Dissociation of the endometrial tissue yielded single cell suspensions of epithelial cells and stromal cells. At passage 4, cultured ECS showed a typical fibroblast morphology (Fig.2A). The morphology of cultured SUSD2-sorted cells under inverted microscope is shown in Figure 2B. Explant cultures of myometrium yielded stellate or triangular shaped cells (Fig.2C), which became confluent after three weeks of culturing. Their immunostaining with α-smooth muscle actin and vimentin are presented in Figure 2 D-F and G-I, respectively, which confirmed their smooth muscle identity.

Phenotypic analysis of cultured endometrial stromal cells

After the fourth passage, the endometrial cells showed the typical mesenchymal stem cell surface phenotype for markers CD73 (97.7 ± 1.5%), CD90 (87.3 ± 2.1%) and CD44 (69.1 ± 2%). They were negative for hematopoietic markers CD34 (1.99 ± 0.1%) and CD45 (1.03 ± 0.06%) as mentioned in our previous study (36).

Cell survival and the percent of SUSD2+cells after sorting

The survival rate of sorted SUSD2+ cells after MACS isolation was 91 ± 3.4%. The confirmation of the sorted cells by immunocytochemistry for the SUSD2 marker showed that 88 ± 2.7% of the nucleated cells were positive for the SUSD2 antibody (Fig.2J-L).

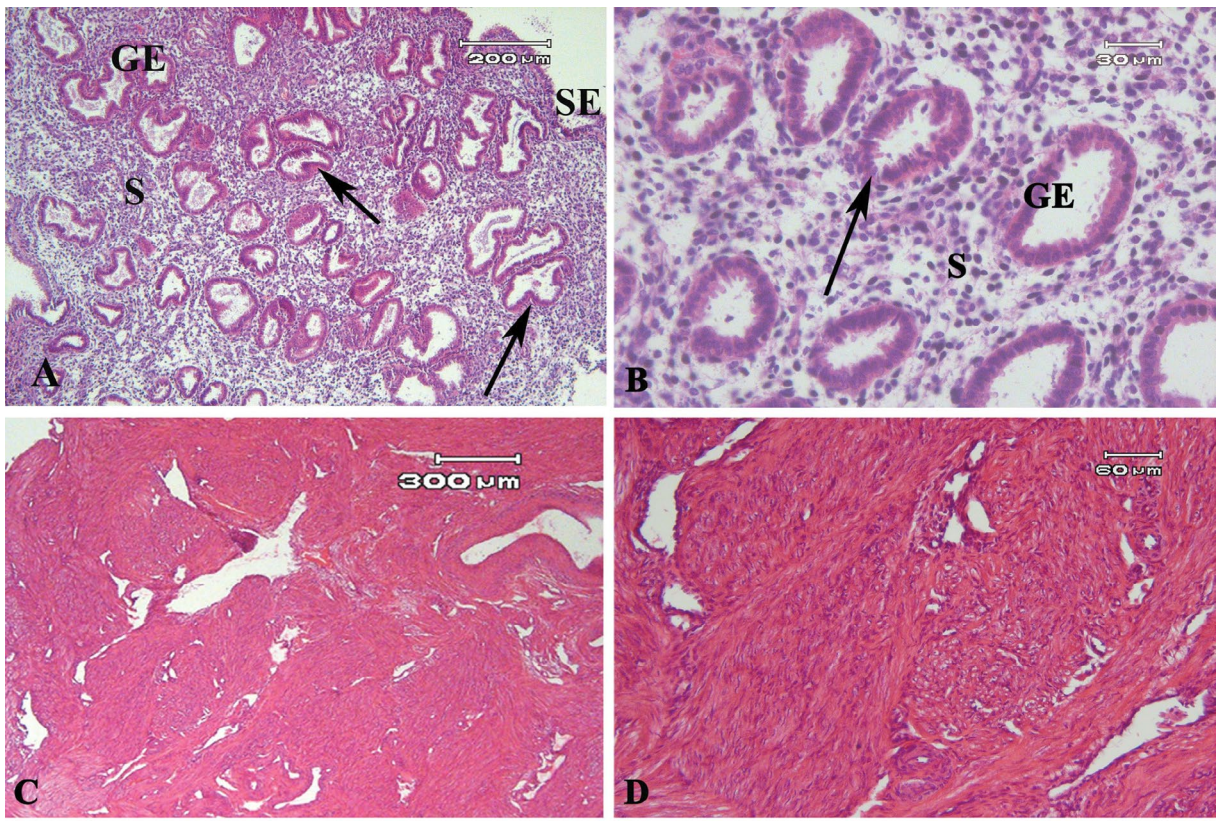

Fig.1: Light microscopic observation of hematoxyline and eosin (H&E) stained sections. **A, B.** Human endometrial tissue sections, **C, D.** Human myometrium tissue sections. GE; Glandular epithelium, SE; Surface epithelium, and S; Stroma, simple columnar epithelium of gland (black arrow).

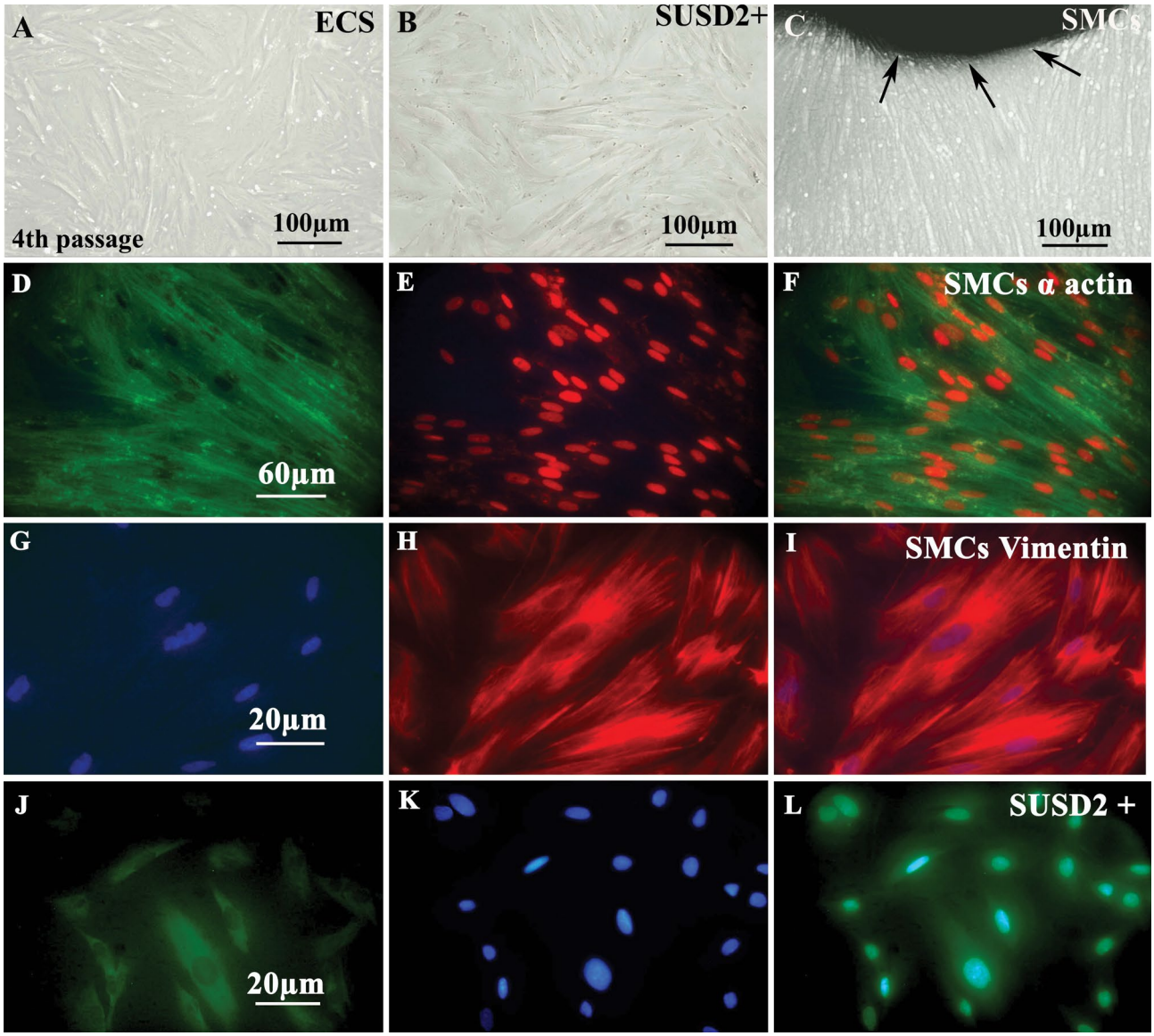

Fig.2: Phase contrast and immunohistochemistry of human cultured endometrial amd myometrial cells. **A.** Phase contrast imaging of cultured human endometrial cell suspension (ECS) at passage 4, **B.** SUSD2$^+$ cells after separation and sorting by magnetic-activated cell sorting and **C.** Human myometrial cultured smooth muscle cells (SMCs) 25 days after tissue culture. The black arrows show the border of tissue explant as a dark colour. **D-F.** Immunofluorescence staining of cultured myometrial cells with anti-alpha SMC actin antibodies. **D.** The cytoplasm is stained green with fluoresce in isothiocyanate (FITC)-conjugated secondary antibody, **E.** The nucleus is stained red with propidium iodide, and **F.** The merged image is presented in third column. **G-I.** Immunofluorescence staining of cultured myometrial cells with anti-vimentin antibodies. **G.** The cytoplasm is stained red with Texas red-conjugated secondary antibody, **H.** The nucleus is stained blue with 4', 6-diamidino-2-phenylindole (DAPI), and **I.** The merged image is presented in the third column. **J-L.** Immunocytochemistry of magnetic activated cell sorting (MACS)-sorted cells for SUSD2 is demonstrated. The sorted cells were shown in (J) that stained with nuclear staining by DAPI were demonstrated in (K) and the merged figure is shown in (L). The green colour shows the positive reaction for SUSD2 expression and blue colour is related to nuclear staining by DAPI.

Light microscopic observation of implantation models

Phase contrast imaging of implantation models using mouse blastocyst in studied groups were demonstrated in Figure 3A-F. The morphology of ECS and SUSD2$^+$ cells co-cultured with myometrial SMCs without embryos showed a flattened monolayer of spindle-shaped cells after the cultivation period (Fig.3, first column).

However, the implanted mouse embryos incubated with the co-cultures demonstrated similar morphological features between the ECS and SUSD2$^+$ groups. The trophoblastic cells migrated from the embryos and proliferated, and the embryonic cells spread on the endometrial/myometrial cell layer and were tightly attached (Fig.3, second column).

The vital live/dead staining of the embryos on the co-cultured cells shows that all of the mouse implanted embryos were viable after 48 hours of culture (Fig.3, third column).

Electron microscopic observation of implantation models

SEM evaluation of mouse blastocyst implantation

on top of the ECS co-cultured with myometrial SMCs and the SUSD2+ cells co-cultured with myometrial SMCs are shown in Figure 4A-E and F-J, respectively. Ultrastructural evaluation of the human ECS or SUSD2+ cells co-cultured with human myometrial cells demonstrated that both had similar flattened spindle-shaped and flattened cells attached to the plate (Fig.4A, F). Some surface apical projections were seen on the endometrial cells adjacent to the implanted embryos, and these projections were similar to pinopodes (red arrowhead, Fig.4D, I) and microvilli (yellow arrowhead, Fig.4D, I).

The images obtained from the SEM indicated vertical growth of the embryos and the formation of mouse egg-cylinders in both studied groups. However, two different morphologies related to implanted embryos were observed at the ultrastructural level in each group: one with the presence of polarized cells (epiblast cells) arranged radially around the lumen of the pro-amniotic cavity and the other without polarized cells. This observation showed embryonic development on these co-cultures.

Molecular analysis of implantation models

Figure 4K shows a comparison of the ratios of gene expressions related to implantation (*αV, β3, IL-1R, LIF* and *LIFR*) to *β-actin* in both implantation models to the expression of *β-actin* in both implantation models in the absence or presence of embryos.

In the absence of embryos, the ratios of the expression of genes to that of the housekeeping gene were 0.65 ± 0.01 (*αV*), 0.97 ± 0.18 (*β3*), 0.57 ± 0.01 (*IL-1R*), 0.81 ± 0.11 (*LIF*) and 0.95 ± 0.18 (*LIFR*). These ratios in SUSD2+ cells co-cultured with SMCs were 0.59 ± 0.005 (*αV*), 1.25 ± 0.21 (*β3*), 0.62 ± 0.08 (*IL-1R*), 1.02 ± 0.07 (*LIF*) and 0.99 ± 0.06 (*LIFR)*. The expression of *αV* significantly increased (P=0.003) in SUSD2+ cells compared to ECS. Expressions of the *β3, IL-1R, LIF* and *LIFR* genes were not significantly different between the two groups.

In SUSD2+ cells that were co-cultured with the embryo had the following ratios of expression: *αV* (0.61 ± 0.03*), β3* (1.10 ± 0.25)*, IL-1R* (0.59 ± 0.02)*, LIF* (0.79 ± 0.04) and *LIFR* (1.42 ± 0.60) compared to *β-actin*. In the ECS cells, these rates were: 0.57 ± 0.02 (*αV*), 1.34 ± 0.51 (*β3*), 0.59 ± 0.04 (*IL-1R*), 0.77 ± 0.04 (*LIF*) and 1.30 ± 0.37 (*LIFR*). There was no significant difference between the two groups.

The expression of genes related to implantation was not significantly different between the groups in the presence and absence of mouse embryos.

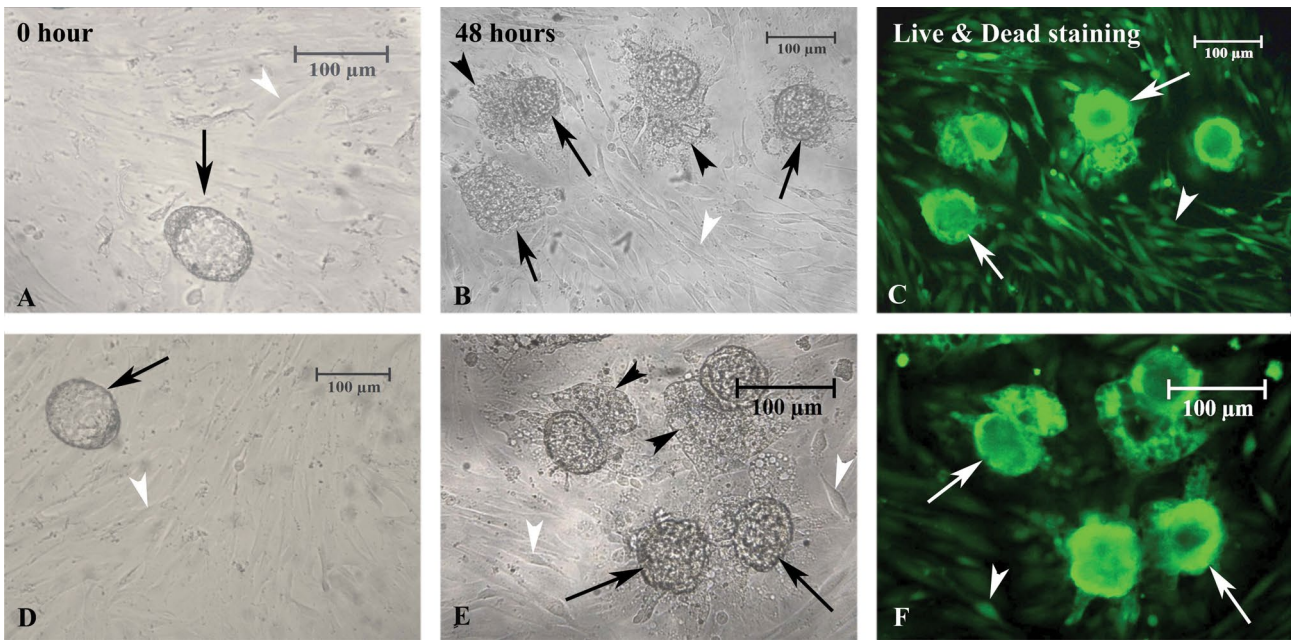

Fig.3: Phase contrast imaging of implantation models using mouse blastocyst in studied groups. **A-C.** The implantation of mouse embryo on top of the human endometrial cell suspension (ECS) and **D-F.** The embryo implanted on top of SUSD2+ cells co-cultured with myometrial smooth muscle cells (SMCs). First column showed the figures at the start (0 hours) of co-culture and in the second column showed after 48 hours of co-culture. The black arrows indicate the mouse blastocysts during the co-culture period, the black arrowheads indicate the expanded trophoblastic cells, and the white arrowheads indicate the human endometrial cells co-cultured with SMCs as the feeder layer. Fluorescence microscopy imaging of implanted mouse blastocyst in studied groups using a live/dead viability kit. **C.** ESC co-cultured with myometrial SMCs and **F.** The SUSD2+ cells co-cultured with myometrial SMCs. The white and black arrows indicate the mouse blastocysts and the white arrowheads demonstrate the feeder layer. Viable cells were stained green.

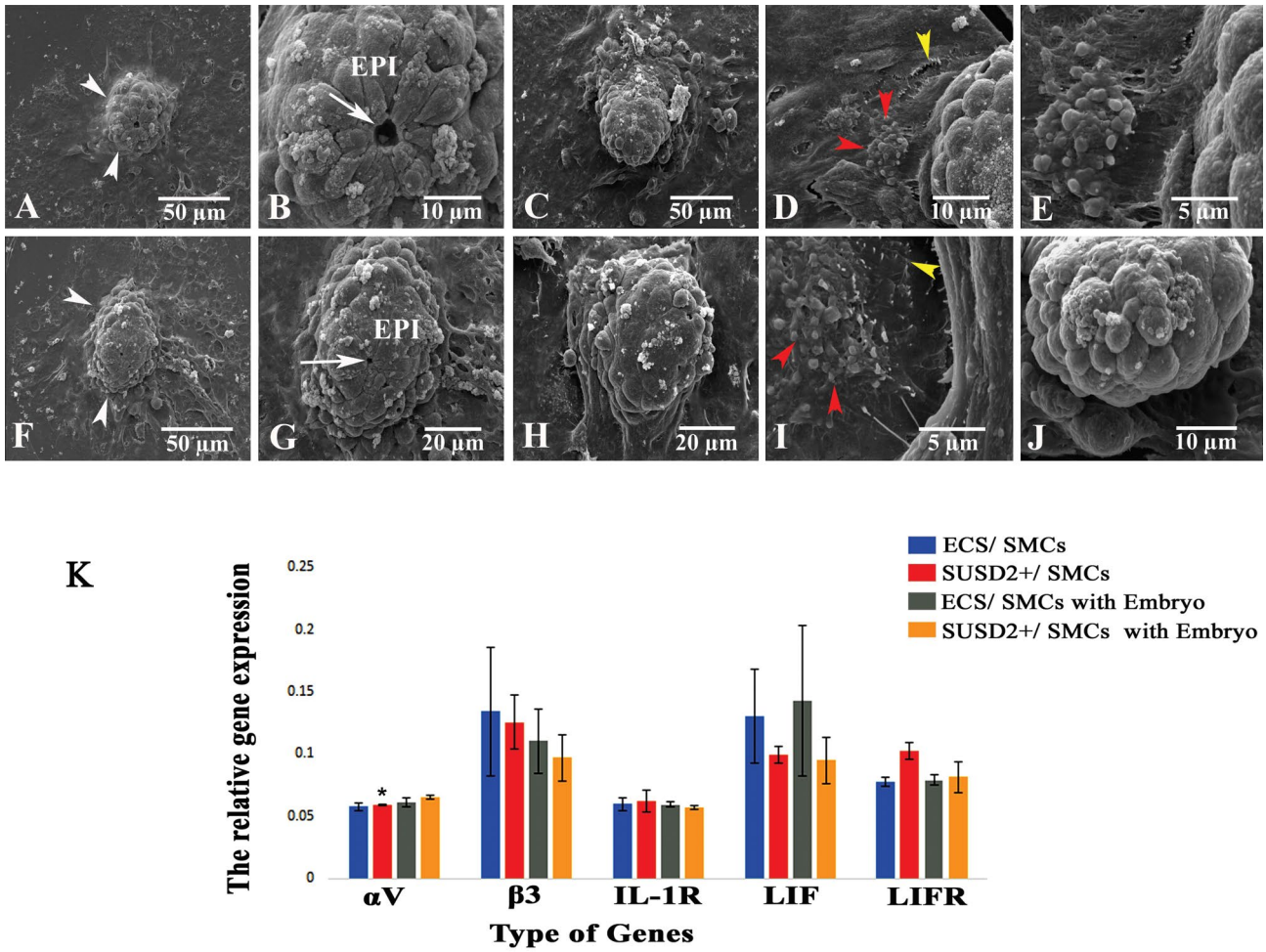

Fig.4: Scanning electron micrographs of studied implantation models. **A-E.** The micrographs of mouse blastocyst implantation on top of the endometrial cell suspension (ECS) co-cultured with myometrial smooth muscle cells (SMCs) with different magnifications, **F-J.** The figures of mouse embryo that implanted on the SUSD2$^+$ cells co-cultured with myometrial SMCs at different magnifications. Two types of morphology were seen in the mouse embryos. White arrowheads; Mouse embryo (egg-cylinder), White arrow; Lumen of the pro-amniotic cavity, Red arrowheads; Pinopode-like structures, Yellow arrowheads; Microvilli-like structures, and EPI; Pluripotent epiblast, and **K.** Comparison of expression profiles of genes related to implantation relative to *β-actin* as the housekeeping gene are presented in ECS and SUSD2$^+$ cells co-cultured with SMCs in the absence and in the presence of embryos. *; Significant differences with ECS/SMCs group (P=0.003), *IL-1R*; Interleukin-1 receptor, and *LIFR*; Leukaemia inhibitory factor receptor.

Discussion

Considering the differentiation potential of EMSCs, SUSD2$^+$ stem cells were used in the present study, for the first time, to create a new model of embryo implantation in comparison with an endometrial cell suspension that used mouse blastocysts as the surrogate embryo. For this purpose, SUSD2$^+$ mesenchymal stem cells were isolated and co-cultured with SMCs and mouse blastocysts. Our results at the morphological and ultrastructural levels showed that the mouse blastocysts could interact with ECS and SUSD2$^+$ cells and advance through the early stages of *in vitro* development within 48 hours. Moreover, electron micrographs indicated the ultrastructural changes in endometrial epithelial-like cells, including the appearance of pinopode-like and microvilli-like structures that are markers for early stages of implantation.

In another point of view, the ultrastructure of mouse embryos in the present study indicated the progression of their developmental stages and the formation of an egg-cylinder. This stage of *in vitro* development is observed before gastrulation in mouse embryos (37, 38).

Evaluation of the expression of genes related to implantation in ECS and SUSD2$^+$ cells after co-culture with SMCs indicated that these genes were expressed. Moreover, there was an increase in the expression of αV in SUSD2$^+$ cells compared to ECS. No significant differences were observed in the expressions of the other genes (*β3*, *IL-1R*, *LIF* and *LIFR*) between these groups. These data showed that SUSD2$^+$ EMSCs are multipotential cells that could differentiate to endometrial-like cells. Similarly, Fayazi et al. (30) revealed that CD146$^+$ endometrial cells could express genes related to implantation, including secreted phosphoprotein 1 and matrix metalloproteinase-2, after differentiation into epithelial-like cells. In agreement, Lü et al. (11) showed that, after co-culturing endometrial epithelial and stromal cells with SMCs, the reconstructed tissue expressed β3 integrin, heparin-binding epidermal growth factor-like growth factor, and HOXA-10.

Our results showed no significant differences between

the studied groups in the presence and absence of mouse embryos regarding the expression of genes related to implantation. It seems that epithelial-like cells derived from SUSD2+ stem cells and ECS in the presence of mouse embryo exhibit the same gene expression profile as that in the absence of an embryo. Thus so far, no evidence has been reported to evaluate the effects of embryos on the expression of genes related to implantation in cultured endometrial stem cells. In relation to this, Popovici et al. (39) have reported that co-culture of trophoblast with endometrial stromal cells reduces the expression of matrix metalloproteinase-11 and increases the expression of IL-1 receptors in these cells. It has been suggested that the difference in the species sources of embryo and cultured cells (human endometrial cells and mouse embryos) in our study can affect the expression pattern profile of genes related to implantation and/or the expression of these genes may be time-dependent. Considering that implantation has a wide genomic profile, gene expression analyses in this study were not timed according to their *in vivo* time of expression. Moreover, possibly during the expansion of SUSD2+ cells in culture, they undergo some changes depending on cell density, cell-cell contact, and Notch signalling (40). In the present study, the endometrial tissue samples were collected from a population between 25 and 40 years of age. It should be mentioned that the age of human samples as a source of the endometrial cells might affect embryo implantation and the expressions of genes related to implantation. Nevertheless, due to a limited sample size and some limitations to prepare more human tissue in this study, this should be considered in further investigations.

Conclusion

This study showed that SUSD2+ cells during co-culture with SMCs can interact with mouse embryos. These co-cultured cells have the potential to be used as an implantation model.

Acknowledgements

We express our appreciation to Professor Caroline Gargett for her scientific comments and for kindly editing this manuscript. This research was financially supported by Tarbiat Modares University as part of a Ph.D. thesis and the Iranian Stem Cell Network. The authors have no conflict of interest.

Authors' Contributions

M.R.; Performed the experiments, analysed the data and contributed to writing the manuscript. M.S.; Supervised and designed the study and contributed to writing the manuscript and provided technical help. M.J.; Contributed to management of human patients and preparation of endometrial samples. All authors read and approved the final manuscript in this study.

References

1. Aplin JD, Ruane PT. Embryo-epithelium interactions during implantation at a glance. J Cell Sci. 2017; 130: 15-22.
2. Lopata A, Bentin-Ley U, Enders A. "Pinopodes" and implantation. Rev Endocr Metab Disord. 2002; 3: 77-86.
3. Su RW, Fazleabas AT. Implantation and establishment of pregnancy in human and nonhuman primates. Adv Anat Embryol Cell Biol. 2015; 216: 189-213.
4. Koot YE, Macklon NS. Embryo implantation: biology, evaluation, and enhancement. Curr Opin Obstet Gynecol. 2013; 25(4): 274-279.
5. Pawa, S, Hantak AM, Bagchi IC, Bagchi MK. Minireview: steroid-regulated paracrine mechanisms controlling implantation. Mol Endocrinol. 2014; 28(9): 1408-1422.
6. Weimar CH, Post Uiterweer ED, Teklenburg, G, Heijnen CJ, Macklon NS. Reprint of: in-vitro model systems for the study of human embryo-endometrium interactions. Reprod Biomed Online. 2013; 27(6): 673-688.
7. Tiwari R, Mehrotra PK, Srivastava A. Implantation in vitro: co-culture of rat blastocyst and epithelial cell vesicles. Cell Tissue Res. 2004; 315(2): 271-227.
8. Galán A, O'Connor JE, Valbuena D, Herrer R, Remohí J, Pampfer S, et al. The human blastocyst regulates endometrial epithelial apoptosis in embryonic adhesion. Biol Reprod. 2000; 63(2): 430-439.
9. Grewal S, Carver JG, Ridley AJ, Mardon HJ. Implantation of the human embryo requires Rac1-dependent endometrial stromal cell migration. Proc Natl Acad Sci USA. 2008; 105(42): 16189-16694.
10. Islam MR, Ikeguchi Y, Yamagami K, El-Sharawy M, Yamauchi N. Development of an in vitro model to study uterine functions and early implantation using rat uterine explants. Cell Tissue Res. 2017; 370(3): 501-512.
11. Lü SH, Wang HB, Liu H, Wang HP, Lin QX, Li DX, et al. Reconstruction of engineered uterine tissues containing smooth muscle layer in collagen/matrigel scaffold in vitro. Tissue Eng Part A. 2009; 15(7): 1611-1618.
12. Yang H, Han S, Kim H, Choi YM, Hwang KJ, Kwo HC, et al. Expression of integrins, cyclooxygenases and matrix metalloproteinases in three-dimensional human endometrial cell culture system. Exp Mol Med. 2002; 34(1): 75-82.
13. Cervero A, Domínguez F, Horcajadas JA, Quiñonero A, Pellicer A, Simón C. Embryonic adhesion is not affected by endometrial leptin receptor gene silencing. Fertil Steril. 2007; 88: 1086-1092.
14. Singh H, Nardo L, Kimber SJ, Aplin JD. Early stages of implantation as revealed by an in vitro model. Reproduction. 2010; 139(5): 905-914.
15. Weimar CH, Kavelaars A, Brosens JJ, Gellersen B, de Vreeden-Elbertse JM, Heijnen CJ, et al. Endometrial stromal cells of women with recurrent miscarriage fail to discriminate between high and low quality human embryos. PLoS One. 2012; 7(7): e41424.
16. Holmberg JC, Haddad S, Wünsche V, Yang Y, Aldo PB, Gnainsky Y, et al. An in vitro model for the study of human implantation. Am J Reprod Immunol. 2012; 67(2): 169-178.
17. Gargett CE, Schwab KE, Zillwood RM, Nguyen HP, Wu D. Isolation and culture of epithelial progenitors and mesenchymal stem cells from human endometrium. Biol Reprod. 2009; 80(6): 1136-1145.
18. Gargett CE, Masuda H. Adult stem cells in the endometrium. Mol Hum Reprod. 2010; 16(11): 818-834.
19. Ghobadi F, Mehrabani D, Mehrabani G. Regenerative potential of endometrial stem cells: a mini review. World J Plast Surg. 2015; 4(1): 3-8.
20. Gurung S, Deane JA, Masuda H, Maruyama T, Gargett CE. Stem cells in endometrial physiology. Semin Reprod Med. 2015; 33(5): 326-332.
21. Cousins FL, O DF, Gargett CE. Endometrial stem/progenitor cells and their role in the pathogenesis of endometriosis. Best Pract Res Clin Obstet Gynaecol. 2018; 50: 27-38.
22. Masuda H, Anwar SS, Bühring HJ, Rao JR, Gargett CE. A novel marker of human endometrial mesenchymal stem-like cells. Cell Transplant. 2012; 21(10): 2201-2214.
23. Indumathi S, Harikrishnan R, Rajkumar JS, Sudarsanam D, Dhanasekaran M. Prospective biomarkers of stem cells of human endometrium and fallopian tube compared with bone marrow. Cell Tissue Res. 2013; 352(3): 537-549.
24. de Souza LE, Malta TM, Kashima Haddad S, Covas DT. Mesenchymal stem cells and pericytes: to what extent are they related? Stem Cells Dev. 2016; 25(24): 1843-1852.
25. Guimarães-Camboa N, Cattaneo P, Sun Y, Moore-Morris T, Gu Y, Dalton ND, et al. Pericytes of multiple organs do not behave as mesenchymal stem cells in vivo. Cell Stem Cell. 2017; 20(3): 345-359.
26. Fayazi M, Salehnia M, Ziaei S. Differentiation of human CD146-

positive endometrial stem cells to adipogenic-, osteogenic-, neural progenitor-, and glial-like cells. In Vitro Cell Dev Biol Anim. 2015; 51(4): 408-414.
27. Gargett CE, Schwab KE, Deane JA. Endometrial stem/progenitor cells: the first 10 years. Hum Reprod Update. 2016; 22(2): 137-163.
28. López-Pérez N, Gil-Sanchis C, Ferrero H, Faus A, Díaz A, Pellicer A, et al. Human endometrial reconstitution from somatic stem cells: the importance of niche-like cells. Reprod Sci. 2019; 26(1): 77-87.
29. Masuda H, Maruyama T, Hiratsu E, Yamane J, Iwanami A, Nagashima T, et al. Noninvasive and real-time assessment of reconstructed functional human endometrium in NOD/SCID/γcnullimmunodeficient mice. Proc Natl Acad Sci USA. 2007; 104: 1925-1930.
30. Fayazi M, Salehnia M, Ziaei S. In vitro construction of endometrial-like epithelium using CD146+ mesenchymal derived from human endometrium. Reprod Biomed Online. 2017; 35(3): 241-252.
31. Campo H, Baptista PM, López-Pérez N, Faus A, Cervelló I, Simón C. De- and recellularization of the pig uterus: a bioengineering pilot study. Biol Reprod. 2017; 96(1): 34-45.
32. Noyes RW, Hertig AT, Rock J. Dating the endometrial biopsy. Am J Obstet Gynecol. 1975; 122(2): 262-263.
33. Chan RW, Schwab KE, Gargett CE. Clonogenicity of human endometrial epithelial and stromal cells. Biol Reprod. 2004; 70(6): 1738-1750.
34. Kao AP, Wang KH, Chang CC, Lee JN, Long CY, Chen HS, et al. Comparative study of human eutopic and ectopic endometrial mesenchymal stem cells and the development of an in vivo endometriotic invasion model. Fertil Steril. 2011; 95(4): 1308-1315.
35. Pfaffl MW. A new mathematical model for relative quantification in real-time RT-PCR. Nucleic Acids Res. 2001; 29(9): e45.
36. Rahimipour M, Salehnia M, Jafarabadi M. Morphological, ultrastructural, and molecular aspects of in vitro mouse embryo implantation on human endometrial mesenchymal stromal cells in the presence of steroid hormones as an implantation model. Cell J. 2018; 20(3): 369-376.
37. Bedzhov I, Leung CY, Bialecka M, Zernicka-Goetz M. In vitro culture of mouse blastocysts beyond the implantation stages. Nat Protoc. 2014; 9(12): 2732-2739.
38. Srinivas S. Imaging cell movements in egg-cylinder stage mouse embryos. Cold Spring Harb Protoc. 2010; (12): pdb.prot5539.
39. Popovici RM, Betzler NK, Krause MS, Luo M, Jauckus J, Germeyer A, et al. Gene expression profiling of human endometrial-trophoblast interaction in a coculture model. Endocrinology. 2006; 147(12): 5662-5675.
40. Murakami K, Lee YH, Lucas ES, Chan YW, Durairaj RP, Takeda S, et al. Decidualization induces a secretome switch in perivascular niche cells of the human endometrium. Endocrinology. 2014; 155(11): 4542-4553.

Original Article

Alpha-Lipoic Acid Can Overcome The Reduced Developmental Competency Induced by Alcohol Toxicity during Ovine Oocyte Maturation

Ali Moghimi Khorasgani, B.Sc.[1, 2], Reza Moradi, M.Sc.[1], Farnoosh Jafarpour, D.V.M., Ph.D.[1*], Faezeh Ghazvinizadehgan, M.Sc.[1], Somayyeh Ostadhosseini, D.V.M.[1], Alireza Heydarnezhad, D.V.M.[1], Ali Akbar Fouladi-Nashta, Ph.D.[3], Mohammad Hossein Nasr-Esfahani, Ph.D.[1*]

1. Department of Reproductive Biotechnology, Reproductive Biomedicine Research Center, Royan Institute for Biotechnology, ACECR, Isfahan, Iran
2. Department of Agricultural Biotechnology, College of Agriculture, Isfahan University of Technology, Isfahan, Iran
3. Reproduction Genes and Development Group, Department of Veterinary Basic Sciences, The Royal Veterinary College, HawksheadLane Hatfield, Herts AL97TA, UK

Corresponding Address: P.O.Box: 8165131378, Department of Reproductive Biotechnology, Reproductive Biomedicine Research Center, Royan Institute for Biotechnology, ACECR, Isfahan, Iran
Emails: Jafarpour.farnoosh@gmail.com, mh.nasr-esfahani@royaninstitute.org

Received: 27/July/2019, Accepted: 8/December/2019

Abstract

Objective: Alpha-lipoic acid (ALA) as a strong antioxidant has a protective effect. This study was designed to assess whether supplementation of maturation medium with ALA during *in vitro* maturation (IVM) can attenuate the toxic effect of ethanol.

Materials and Methods: In this experimental study, to assess the antioxidant capacity of ALA challenged by 1% ethanol during *in vitro* maturation, immature ovine oocytes were exposed to 1% alcohol in the presence or absence of 25 μM ALA during oocyte maturation. The cumulus expansion index, intracellular reactive oxygen species (ROS), and thiol content levels were assessed in matured oocytes of various treatment groups. Consequently, the blastocyst formation rate of matured oocytes in various treatment groups were assessed. In addition, total cell number (TCN), cell allocation, DNA fragmentation, and relative gene expression of interested genes were assessed in resultant blastocysts.

Results: The results revealed that alcohol significantly reduced cumulus cells (CCs) expansion index and blastocyst yield and rate of apoptosis in resultant embryos. Addition of 25 μM ALA to 1% ethanol during oocyte maturation decreased ROS level and elevated Thiolcontent. Furthermore, supplementation of maturation medium with ALA attenuated the effect of 1% ethanol and significantly increased the blastocyst formation and hatching rate as compared to control and ethanol groups. In addition, the quality of blastocysts produced in ALA+ethanol was improved based on the low number of TUNEL positive cells, the increased expression level of mRNA for pluripotency, and anti-oxidant markers, and decreased expression of apoptotic genes.

Conclusion: The current findings demonstrate that ALA can diminish the effect of ethanol, possibly by decreasing the ROS level and increasing Thiolcontent during oocyte maturation. Using the ALA supplement may have implications in protecting oocytes from alcohol toxicity in affected patients.

Keywords: Alcohol, Alpha-Lipoic Acid, Oocyte Maturation, Reactive Oxygen Species, Thiol

Cell Journal(Yakhteh), Vol 23, No 2, July 2021, Pages: 164-173

Citation: **Moghimi Khorasgani A, Moradi R, Jafarpour F, Ghazvinizadehgan F, Ostadhosseini S, Heydarnezhad A, Fouladi-Nashta AA, Nasr-Esfahani MH. Alpha-lipoic acid can overcome thereduced developmental competency induced by alcohol toxicity during ovine oocyte maturation. Cell J. 2021; 23(2): 164-173. doi: 10.22074/cellj.2021.7071.**

Introduction

Ethanol can be used as a cryoprotectant (1) and also a chemical activator for artificial activation of oocytes and reconstructed oocytes (2). However, high concentrations of alcoholcan not only influence the biological nature of somatic cells but also adversely affect the germ cell ofspermatogenesis. While there are limited studies addressing the effect of ethanol on gametogenesis and preimplantation embryos (3), many studies have shown that ethanol at high concentrations can be a teratogen for developing embryos after implantation. The molecular pathway through which it induces fetal teratogenicity is well studied and has led to public awareness to avoid alcohol consumption throughout pregnancy (4).

Alcohol use and heavy drinking are common during adolescence, and its prevalence escalates into late adolescence and early adulthood, which have a devastating effect on an individual's health (5) and may lead to abortion, birth defects, and developmental disabilities (6). In a recent study using porcine embryos, Larivière et al. (3) showed that the presence of physiological doses for several days is toxic for porcine pre-implantation embryos and leads to mitochondrial impairment. These authors attribute this effect to vulnerability of embryos during differentiation of the inner cell mass (ICM) and trophectoderm (TE) cells which requires massive reorganization at genomic, epigenomic and mitochondrial level. Similar results were reported by Maier et al. (7)

who showed that alcohol toxicity at blastocyst stage cases alteration at transcriptomic level, resembling when neurons are exposed to alcohol.

Despite numerous studies on the effect of oxidative stressors on early embryos (7), to our knowledge, there are few studies thataddressed the impact of alcohol toxicity during oocyte maturation on the competency of oocytes to process the sperm genome during fertilization. Inthis regard (8), have shown that ingestion of 10% ethanol for 15 days can cause a significant reduction in the ratio of blastocyst expansion and hatching, and also impair trophoblast invasion. Furthermore (9), have revealed that treating porcine oocytes with 1 and 3% ethanol during *in vitro* maturation promotes the generation of reactive oxygen species (ROS) and diminish glutathione (GSH) level in treated oocytes.These oocytes had significantly lower cleavage rate and produced less blastocyst following *in vitro* fertilization (IVF).

Alpha-lipoic acid (ALA), as a disulfide derivative of octanoic acid, is well-known for its antioxidant capacity in various biological processes and also scavenging ROS (8). It has been proposed that ALA is a potential therapeutic agent in the treatment or prevention of different pathologies that may be related to an imbalance of oxidative cellular status (9). It has been well studied that ALA could be effective in preventing ethanol-induced neurotoxicity in the clonal hippocampal cell line HT22 (10). Furthermore, ALA inhibited toxicant-induced inflammation and ROS generation in hepatic stellate cell activation and liver fibrosis (11). In addition, many studies suggest ALA for thetreatment of diabetic peripheral neuropathy (12).

For the investigation of the possible effect of ALA to rescue the development of oocytes exposed to ethanol during oocyte maturation, this study was designed to assess whether supplementation of maturation medium with ALA during *in vitro* maturation (IVM) can attenuate the toxic effect of ethanol.

Materials and Methods

Media and chemicals

In this experimental study, all media and chemical reagents were obtained from Gibco (Grand Island, NY, USA) and Sigma Chemical Co. (St. Louis, MO, USA), respectively, unless otherwise specified.

All animal experiments were approved by the Institutional Review Board and Institutional Ethical Committee of the Royan Institute (95000229).

Cumulus-oocyte complexes recovery and *in vitro* maturation

Abattoir-derived ovaries from ovine were used as the source of oocytes. Ovaries were transported to the laboratory within the minimum possible time (2-3 hours) in saline solution (0.90% w/v NaCl) at 15-20˚C. After trimming and washing, they were stored for 12 hours at 15˚C (13). Cumulus-oocyte complexes (COCs) were aspirated from the antral follicle (2-6 mm diameter) with the aid of a 20-G needle attached to a vacuum pump (80 mm Hg). Thereafter, the best quality COCs with at least threelayers of cumulus cells (CCs) and, intact and evenly granulated cytoplasm were randomly allocated into one of three experimental groups (Fig.1A). COCs were matured in tissue culture medium 199 (TCM199) containing 10% fetal bovine serum (FBS), follicle-stimulating hormone(FSH, 10 µg/mL), luteinizing hormone(LH, 10 µg/mL), estradiol-17b (1 µg/mL), cysteamine (0.1 mM) (maturation medium: MM) at 38.8˚C, 5% CO_2 and humidified air for 22 hours (14).

Cumulus expansion index

Cumulus expansion index of COCs was scored 24 hours after maturation based on Vanderhyden et al. (15). Expansion was scored 0-4: Score 0: no expansion in CCs (Fig.1B_1); score 1: no expansion in CCs but cells appear as spherical (Fig.1B_2); score 2: only the outermost layers of CCs expanded (Fig.1B_3); score 3: all layers of cells expanded except the corona radiate (Fig.1B_4); and score 4: expansion occurred in all layers of cell (Fig.1B_5).This experiment was done in triplicate, and in each replicate, at least 30 matured COCs were assessed.

Measurement of thiol content

Cell Tracker™ Blue CMF2HC (4-chloromethyl-6, 8-difluoro-7-hydroxycoumarin) (C12881, Molecular Probes), a membrane-permeable fluorescence probe was used as a sensitive and specific probe to evaluate intracellular thiol content, especially GSH (16-18). Following the maturation of COCs in various treatment groups, matured COCs were denuded by vortexing for 3-5 minutes in HEPES-buffered TCM199 (H-TCM199) supplemented with 300 IU/ml hyaluronidase. Subsequently, denuded matured oocytes were exposed to 20 µM Cell Tracker Blue CMF2HC for 20 minutes at 38.5˚Cin the dark and then washed three times with phosphate buffer solution without calcium and magnesium (PBS^-) containing 1 mg/ml polyvinyl alcohol (PVA). The oocytes were then placed into 10 µl droplets of PBS+PVA and observed using an inverted fluorescent microscope (Olympus, IX71, Japan). Immediately after exposure, a digital image of each matured oocyte was taken with a highly sensitive camera (DP-72, Olympus, Japan) operated on DP2-BSW software. The fluorescence intensity of oocytes was analyzed using ImageJ software (National Institutes of Health, Bethesda, MD). Assessing oocyte thiol content was done in three replications, and at least 30 matured COCs were used in each replication.

Measurement of reactive oxygen species

The procedure for ROS measurement was as described previously (16, 17). In brief, after the preparation of matured oocytes similar to the previous section (the measurement of thiol content), oocytes were exposed to 10 µM DCHFDA (2, 7-dichloro dihydrofloureseindiacetate, Sigma, D6883) for 30 minutes at 38.5˚C in the dark and

then washed extensively in PBS. For themeasurement of ROS levels, matured oocytes were exposed to UV light of a fluorescent microscope (Olympus, IX71, Japan) and observed using filter sets (excitation wavelength: 450-490 nm, emission wavelength: 515-565 nm). Taking digital images and quantification of fluorescent intensity was exactly the same as the previous section. The measurement of ROS level was done in three replications and using at least 30 matured COCs in each replicate.

In vitro fertilization

Fresh ram semen was washed and centrifuged two times and resulted pellet was re-suspended with fertilization medium containing 2 mg/ml BSA (18, 19). Matured COCs from various treatment groups were washed separately in fertilization medium, and groups of 10 matured COCs were transferred into 50 µl droplets of fertilization medium containing 2×10^6/ml motile sperm under mineral oil as previously described (20). The inseminated COCs were incubated for 20 hours in 5% CO_2 in humidified air at 38.5˚C. Thereafter, presumptive zygotes mechanically denuded via pipetting and then cultured in groups of five to seven in modified synthetic oviductal fluid (mSOF) (21) under mineral oil at 38.5˚C, 5% CO_2, 5% O_2 and humidified air for seven days in 20 µl droplets. The cleavage, blastocyst, and hatching rates were evaluated on days 3, 7, and 8 post-fertilization, respectively. The number of replications and matured oocytes in each group is depicted in Table 1.

Differential staining

In order to determine the number of ICM and TE, differential staining was carried out as described previously (22). In brief, hatched blastocysts onday 8 from various treatment groups were used for staining. Thereafter, blastocysts were washed in PBS+PVA and permeabilized with 0.5% triton-X-100 in H-TCM199 containing 5 mg/ml BSA for 30 seconds. Then, blastocysts were stained with 30 µg/ml propidium iodide (PI) for 10 seconds. Subsequently, blastocysts were transferred to 10 mg/ml Hoechst at 4˚C for 15 minutes. Finally, blastocysts were mounted in mounting fluid and observed under a fluorescence microscope. ICM and TE were recognized based on their blue and red colors, respectively. Finally, the total cell number (TCN: ICM+TE) was also assessed. Totally 30 blastocysts were used for differential staining in at least three replications.

DNA fragmentation

To determine the apoptotic cells in blastocysts from various treatment groups, in situ cell death detection kit (Promega Diagnostic Corporation, Germany), known as TUNEL (TdT-mediated dUTP-digoxigenin nick end labeling) (20). Initially, hatched blastocysts onday 8 were fixed with 4% freshly prepared paraformaldehyde for 60 minutesatroom temperature (RT). After washing the blastocysts with PBS+PVA, they were permeabilized with 0.5% triton-X-100 for 30 minutes in RT. Subsequently, blastocysts were equilibrated in equilibration buffer (EQ) in RT for 10 minutes and after that incubated in rTdT Incubation Buffer (EQ 45 µl+5 µl nucleotide mix+1 µl rTdT enzyme) for 60 minutes in 37˚C in darkness and humid environment. Immediately the reaction was inhibited by incubating the blastocysts in 2X SSC buffer for 15 minutes in RT. Finally, the blastocysts were counterstained with 10 µg/ml for 5 minutes, and after washing, they were mounted on microscopic slides and observed under a fluorescence microscope (Olympus, Japan). Total nuclei were counted by PI, and cells were considered as TUNEL positive if their nuclei showed light green. Totally 30 blastocysts were used for TUNEL assay in at least three replications.

Gene expression analysis

Pools of expanded blastocysts in day 7 (5 in each pool) in three independent replicates were used for RNA extraction using the RNeasy Micro Kit (QIAGEN, Cat. No.74004, Germany). Reverse transcription was immediately performed using a QµantiTect Reverse Transcription (RT) Kit (QIAGEN, Cat. No.205311, Germany). The cDNA was stored at -70˚C until analysis by quantitative polymerase chain reaction (qPCR) using standard conditions. Ct values used for calculating relative expression were normalized against the reference gene *(β-ACTIN)*. Three technical replicates were done in each PCR reaction that wasrepeated three times. ΔΔCT method was used to estimate fold changes between genes of interest. The primer sequences, annealing temperature, and product size are listed in Table 2.

Table 1: Development of preimplantation ovine embryos after treatment of immature COCs with 1% ethanol or 25 µM ALA+1% ethanol compared to the control group

Treatment	Number of oocyte	Number of cleavage (%)	Number of blastocyst (%)	Number of hatching
Control	1106	982 (86.9 ± 2.57)[a]	430 (34.19 ± 4.67)[b]	107 (27.77 ± 3.84)[a]
Ethanol	1415	1091 (75.47 ± 2.37)[b]	194 (18.19 ± 2.81)[c]	47 (16.66 ± 4.85)[b]
ALA+ethanol	1621	1522 (98.65 ± 0.37)[a]	651 (49.76 ± 1.98)[a]	136 (33.33 ± 3.61)[a]

Data are presented as mean ± SEM. Different letters in each column indicates statistically significant differences (P<0.05). COCs; Cumulus oocyte complexes and ALA; Alpha-lipoic acid.

Table 2: Primer sequence

Gene name	Primer sequences (5´-3´)	Annealing temp. (˚C)	Accession number
β- ACTIN	F: CCATCGGCAATGAGCGGT	58	NM_001009784.2
	R: CGTGTTGGCGTAGAGGTC		
BCL2	F: AGCATCACGGAGGAGGTAGAC	62	XM_012103831.2
	R: CTGGATGAGGGGGTGTCTTC		
BAX	F: AGCGAGTGTTCTGAAGCG	60	XM_015100639.1
	R: CCCAGTTGAAGTTGCCGT		
CASPASE3	F: GCTACAAGGTCCGTTATGCC	59	XM_015104559.1
	R: GATGCTGCCGTATTCGTTCTC		
GPX4	F: TCAATCACTTCCTCACTCAGACTG	57	XM_015096017.1
	R: GTGTGCTGGGCGACTGTATC		
SOD1	F: TGGCAGAGATGATACAGAGG	55	NM_001145185.1
	R: GAACTACAGCGGAGGTAAAC		
OCT4	F: AGCGAGTGTTCTGAAGCG	50	XM_004018968.3
	R: CCCAGTTGAAGTTGCCGT		
NANOG	F: ATCACCATCTTCCAGGAGCGA	54	XM_004006901.3
	R: TTCTCCATGGTGGTGAAGACG		

Experimental design

As is demonstrated in Figure 1A, the experimental groups included: i. Control group; COCs were cultured in MM, ii. ALA+ethanol group; COCs were cultured in MM in the presence of 25 μM ALA (23) which was diluted in ethanol and final concentration of ethanol in MM reached to 1% (v/v) (24). The concentration of ALA was chosen based on the literature in farm animal species (21), iii. Ethanol group COCs were cultured in MM in the presence of 1% ethanol (v/v) based on the concentration of Ethanol which was used for dilution of ALA. 1% alcohol was used based on the legal limit of intoxication in human serum or 0.8% in the blood as the concentration of alcohol in human serum (25). In addition, we should mention that while the solvent of ALA is ethanol, we can't have a separate ALA group.

Data analysis

Wherever possible, data were presented as mean ± SEM. All percentage data were analyzed by SPSS16.0 statistical software (IBM Corporation, Somers, NY, USA). The normality of data and equality of variances were checked using Kolmogorov-Smirnov and Levene tests, respectively. Cumulus expansion index (CEI) was analyzed using a nonparametric Kruskal-Wallis test. Furthermore, because CEI is a nonparametric data, they were presented as only mean without any SEM. Other data were analyzed using a one-way ANOVA followed by LSD test. The differences were considered significant at $P<0.05$.

Results

The effect of ethanol and alpha-lipoic acid on cumulus expansion was investigated in matured oocytes. As shown in Figure1C, D, the analysis of CEI data revealed a significant reduction in the expansion of CCs in ethanol group (1.1) as compared to control (3.1) and ALA+ethanol (3.37) ($P<0.05$). The CEI was similar between control and ALA+ethanol group ($P>0.05$).

Following staining with Cell Tracker Blue CMF2HC to assess thiol content in matured oocytes, the CMF2HC intensity in ALA+ethanol group (129.1 ± 2.11) was significantly higher than control (100) and ethanol (98.2 ± 1.54) groups ($P<0.05$, Fig.2A, B).

The level of intracellular ROS was assessed following staining with DCHFDA by measuring fluorescent intensity in matured oocytes. As it is depicted in Figure 2C and 2D, treatment of COCs with 25 μM ALA in the presence of 1% ethanol decreased the DCHFDA intensity (76.4 ± 1.47) as compared to ethanol (118.1 ± 1.78) and control group (100 ± 2.21) groups ($P<0.05$). However, there was no significant difference between control and ethanol groups ($P>0.05$).

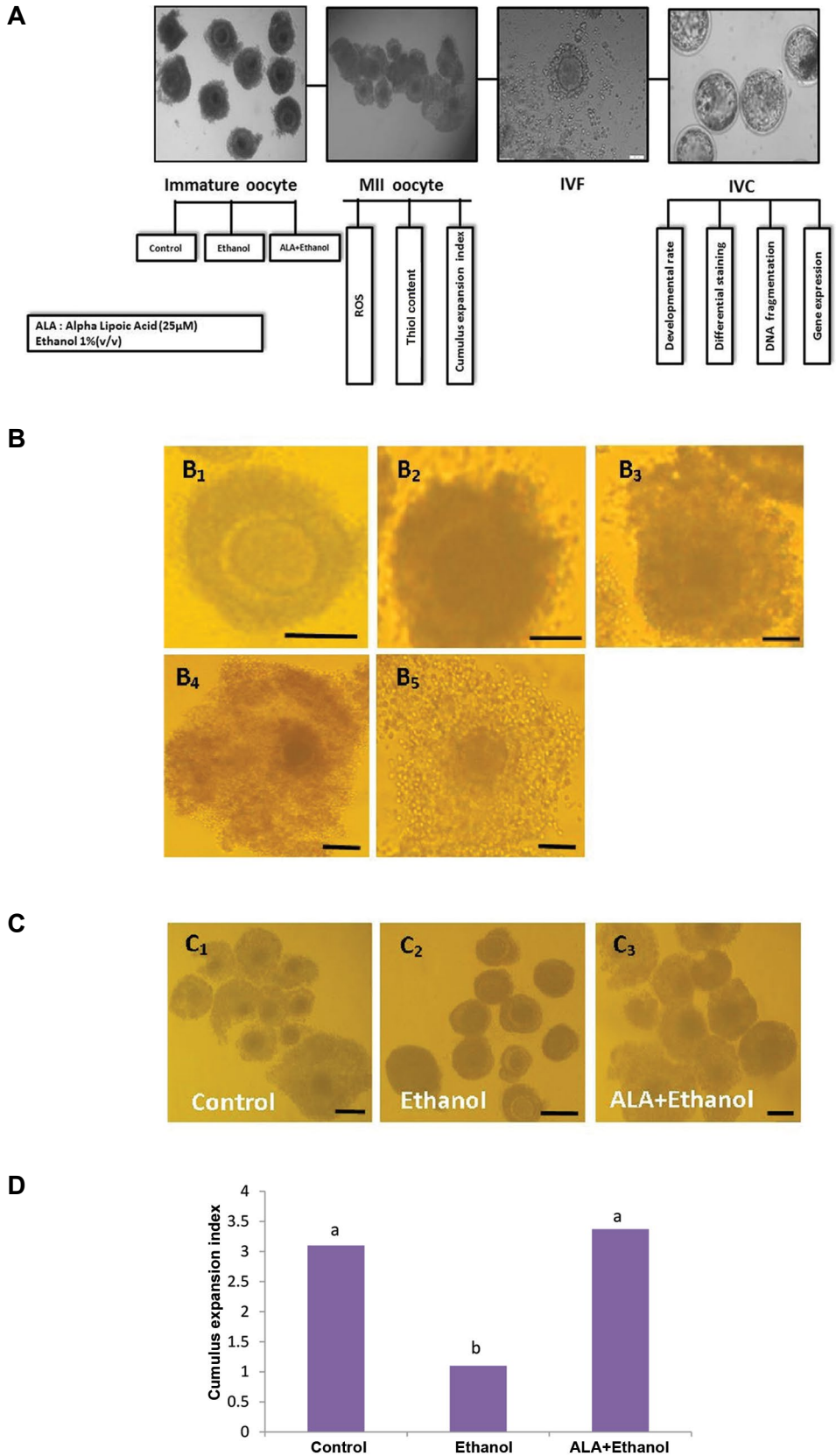

Fig.1: The schematic presentation of experimental design. **A.** Experimental design. According to our experiment abattoir-derived ovaries from ovine were used as the source of oocytes. Experimental groups included control, 1% ethanol and 25 µM ALA+1% ethanol groups. 22 hours after maturation of COCs in various treatment groups the cumulus expansion index was scored. Subsequently, matured COCs were stained for ROS and thiol content. Then matured COCs were transferred into droplets of fertilization medium and after the injection of sperm transferred into IVC medium. Then developmental rate, relative gene expression, DNA fragmentation, and differential staining of embryos were carried out. **B.** Morphology of COCs in different treatment groups scored 22 hours post IVM. B_1**.** Score 0, no expansion, B_2**.** Score 1, no expansion but cells appear as spherical, B_3**.** Score 2, only the outermost layers of cumulus cells have expanded, B_4**.** Score 3, all cell layers have expanded except the corona radiate, and B_5**.** Score 4, expansion has occurred in all cell layers including the corona radiate. Morphology of expansion in C_1**.** Control,C_2**.** Ethanol and C_3**.**ALA+ethanol groups. **D.** Expansion index of COCs in various treatment groups. Columns with different letters are considered as significant ($P<0.05$) (scale bars represent 200 µm).
COCs; Cumulus oocyte complexes, ALA; Alpha-lipoic acid, IVC; *In vitro* culture, IVF; *In vitro* fertilization, IVM; *In vitro* maturation, and ROS; Reactive oxygen species.

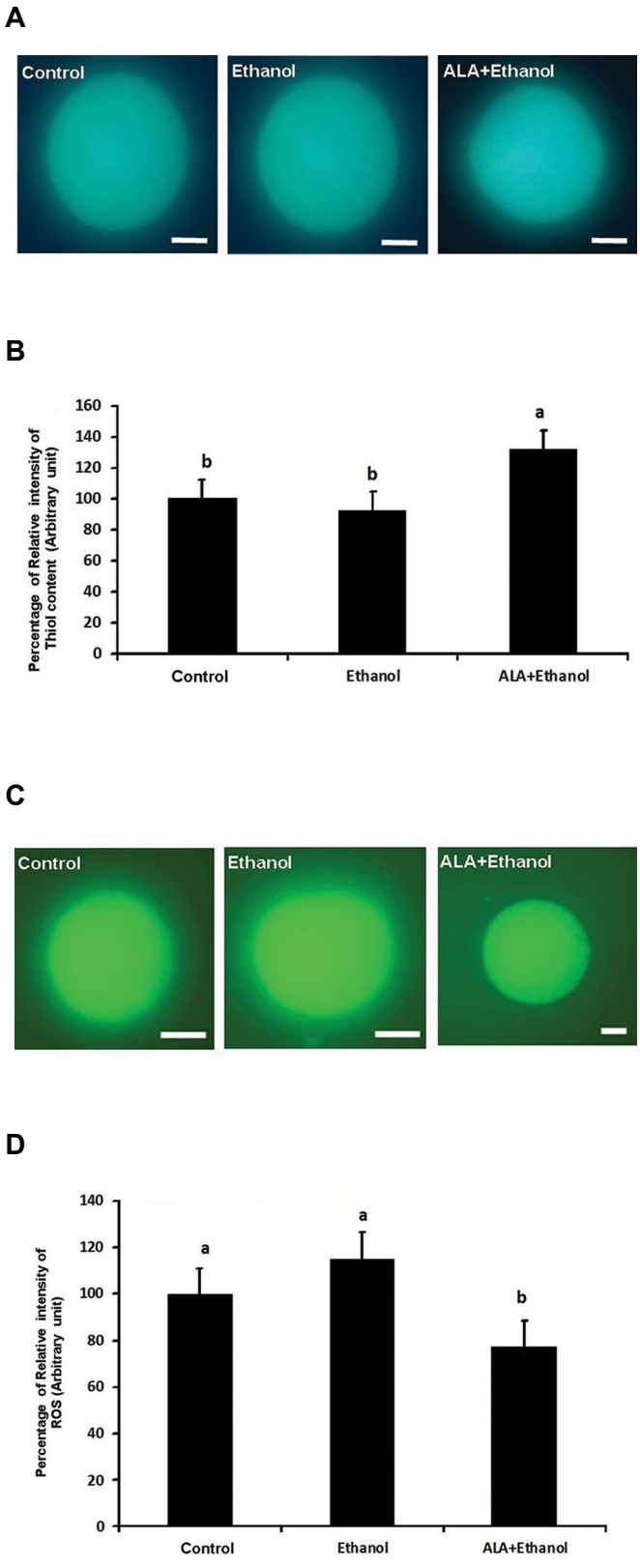

Fig.2: The effect of ethanol and ALA on relative ROS and thiol content of matured ovine oocytes. **A.** Representative fluorescence images of MII-oocytes for thiol content in different treatment groups groups, **B.** Percentage of relative intensity of thiol content in different treatment groups. Columns with different letters are considered as significant (P<0.05). **C.** Representative fluorescence images of MII-oocytes for ROS in different treatment groups, and **D.** Percentage of relative intensity of ROS level in different treatment groups. Columns with different letters are considered as significant (P<0.05, scale bars represent 50 µm). ALA; Alpha-lipoic acid and ROS; Reactive oxygen species.

In order to assess if ethanol and its combination with 25 µM ALA have any effect on the developmental competence of matured oocytes in terms of cleavage and blastocyst rates, IVF was carried out for various treatment groups. As depicted in Table 1, exposure to 1% ethanol during maturation significantly decreased the cleavage rate (75.47 ± 2.37) compared to control (86.9 ± 2.57) and ALA+ethanol group (98.65 ± 0.37, P<0.05). Furthermore, the addition of 25 µM ALA attenuated the effect of 1% ethanol and significantly increased blastocyst formation in ALA+ethanol group (49.76 ± 1.98) as compared to control (34.19 ± 4.67) and ethanol groups (18.19 ± 2.81, P<0.05). In addition, the blastocyst rate was significantly lower in the ethanol group compared to the control group (P<0.05). Finally, blastocysts hatching rate was significantly lower in the ethanol group (16.66 ± 4.85) compared to control (27.77 ± 3.84) and ALA+ethanol group (33.33 ± 3.61, P<0.05, Table 1).

In order to assess the quality of the blastocysts from various treatment groups, differential staining was done to determine ICM, TE, TCN, and ICM:TE ratio. As it is presented in Figure 3A, the number of TE and TCN were significantly higher in ALA+ethanol group as compared to control and ethanol group (P<0.05). In addition, the number of TE and TCNsweresignificantly lower in the ethanol group compared to the control group (P<0.05). Besides, the quality of hatched blastocysts in terms of ICM and ICM:TE was similar between control and ethanol groups (P>0.05). However, hatched blastocysts from ALA+ethanol group had significantly higher ICM and ICM:TE as compared to other groups (P<0.05, Fig.3A).

Furthermore, the effect of ethanol in the presence or absence of ALA was investigated on DNA fragmentation by TUNEL assay. As depicted in Figure 3B, the number of tunnel positive cells in the ethanol group (21.7 ± 2.41) was significantly higher than control (15.3 ± 2.12) and ALA+ethanol (6.4 ± 1.54) groups (P<0.05).

Finally, the quality of derived blastocysts was assessed in terms of expression of genes thatare related to the apoptosis pathway, antioxidant capacity, and pluripotency factors. As demonstrated in Figure 4, the expression of *BAX* was significantly lower in theALA+ethanol group compared to the ethanol group (P<0.05). However, the expression of this gene was significantly lower in the control group than the ethanol group (P<0.05). The expression of *BCL-2* as an anti-apoptotic factor was significantly higher in ALA+ethanol compared to control and ethanol groups (P<0.05).

The next gene which was assessed was *CASPASE3*, which showed significantly lower expression in ALA+ethanol COCs as compared to control and ethanol groups (P<0.05).

The anti-oxidant capacity of blastocysts derived in various treatment groups was assessed in terms of expression of *GPX4* and *SOD1*. Expression of both *GPX4* and *SOD1*was significantly higher in ALA+ethanol group as compared to control and ethanol groups (P<0.05). The expression of *OCT4* and *NANOG* was lower in the ethanol group in comparison to the control group, which was reached to a significant level for *NANOG* (P<0.05) but not for *OCT4*. However, the expression of these two pluripotency markers in theALA+ethanol group was similar to the control group.

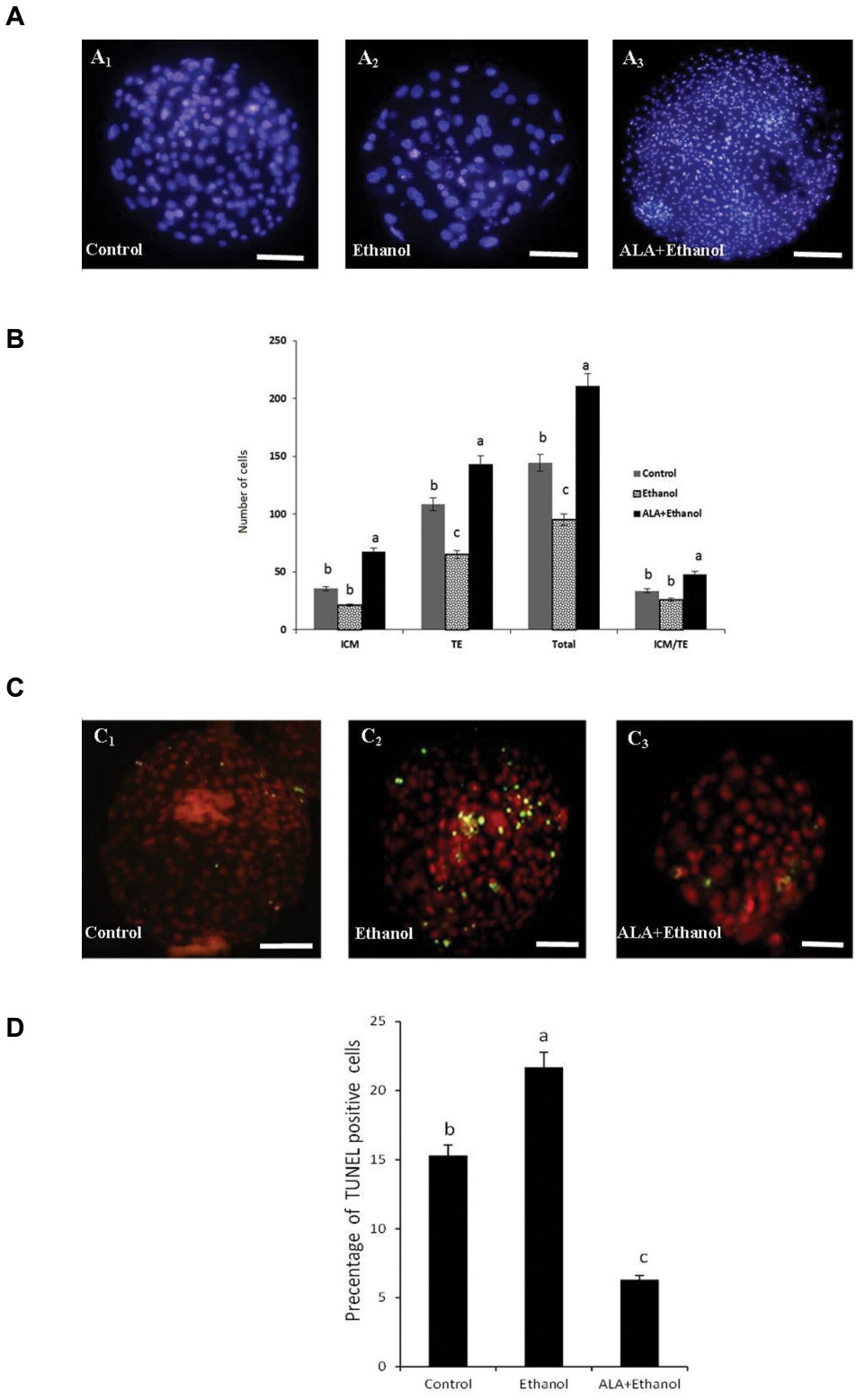

Fig.3: Cell number, trophectoderm and inner cell mass allocation and DNA fragmentation of cultured ovine blastocysts. **A, B.** Quality of ovine expanded blastocysts in terms of total cell number or allocation in different treatment groups (scale bars represent 100 µm). **C, D.** Quality of ovine expanded blastocysts in terms of DNA fragmentation assessed by TUNEL kit in different treatment groups (scale bars represent 50 µm). Columns with different letters are considered as significant (P<0.05).

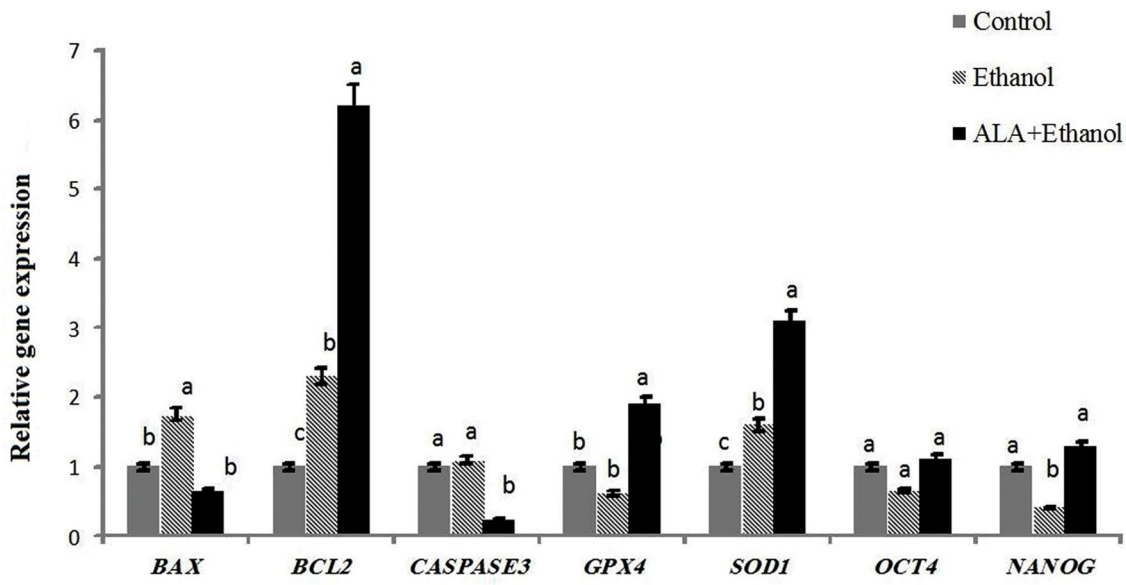

Fig.4: Relative gene expression of interested genes. Quality of ovine expanded blastocysts in terms of expression of genes related to apoptosis, antioxidant capacity and pluripotency in different treatment groups. Columns with different letters are considered as significant (P<0.05).

Discussion

Our results revealed that exposure to 1% ethanol significantly reduced the cumulus expansion and blastocyst yield. The quality of blastocysts was also reduced based on the assessment of ICM, TE, and total cell counts.

Although there are many studies in rodents that have demonstrated the effect of alcohol ingestion on sperm parameters and IVF results, there are very limited studies regarding the effect of alcohol abuse on oocytes and embryos (26). Regarding the effect of alcohol on the male reproductive system, it has been shown that alcohol drinking can alter spermatogenesis and induce morphological changes in spermatozoon (26), which may be due to alteration of the endocrine system in the male reproductive system (27).

Therefore, to assess this effect, ovine COCs were exposed to 1% alcohol during the period of maturation. To further enhance our knowledge regarding the alcohol toxicity, we assessed the degree of ROS production and GSH-antioxidant capacity of alcohol-treated oocytes. Interestingly, we found that the values of ROS and thiol content were not significantly different from control, indicating the production of ROS or reduction of antioxidant capacity does not account for the observed alcohol toxicity during oocyte maturation. One explanation for the unaltered level of thiol content may be related to the specificity of CMF2HC dye, which cannot detect other oxidized thiols and GSSG (18).

To evaluate whether apoptosis has been executed in the blastocysts derived from COCs exposed to alcohol, DNA fragmentation as the late apoptotic marker was assessed, and the results revealed a higher percentage of TUNEL positive cells in ethanol group compared to control group. Analysis of expression of *BAX*, *BCL2*, and *CASPASE3* as other apoptotic markers (28) and,*OCT4* and *NANOG* as pluripotent markers (29) were also assessed in the blastocyst derived from COCs treated with alcohol. Unlike *caspase3*, both *BAX* and *BCL2* were significantly altered. As expected, based on the TUNEL result, the expression of *BAX*, as a pro-apoptotic marker, was significantly higher in the alcohol group, further verifying the higher degree of apoptosis in this group. In contrary to our expectation, the expression of *BCL2*, as an anti-apoptotic marker, was also higher in the alcohol group. These data suggest that embryos thathave been able to reach blastocyst may express a higher degree of *BCL2* to overcome alcohol intoxication. The situation might have been completely different in embryos that were not competent to reach this stage, and therefore, inevitably, they were not included in our assessment.

Assessment of expression of genes related to antioxidant capacity, GPX4, and SOD1 (30, 31) revealed significantly higher expression of both SOD1 and GPX4 in the ALA+ethanol group. An increase in the expression of SOD may be related to a higher capacity of blastocysts to convert superoxide to less toxic ROS, the H_2O_2. Furthermore, higher expression of GPX4 in ALA+ethanol treated group may lead to a higher reduction of hydroperoxide groups on phospholipids, lipoproteins, and cholesteryl esters (32). In summary, the ethanol-exposed group treated with ALA demonstrated a higher anti-oxidant capacity in derived blastocysts.

In the next experiment, we evaluated how antioxidants, such as ALA, can overcome the toxic effects of alcohol. In our results, ALA overcomes the inhibitory effects of ethanol on the cumulus expansion index. It was also interesting to note that ALA improved the GSH-antioxidant capacity of the *in vitro* matured oocyte (33) and

concomitantly reduced the ROS level of ALA+ethanol-treated oocytes compared to both control and ethanol groups. Interestingly, both blastocyst yield and quality of blastocysts were improved which was further verified upon assessment of TUNEL assay, mRNA expression of apoptotic markers (27, 28), pluripotent markers and anti-oxidant markers These results indicate that ALA not only can detoxify the toxicity effects of alcohol but on its own has beneficial effect on the quality of *in vitro* matured oocytes. This observation is consistent with a previous report indicating ALA+ethanol can improve the quality of oocyte during maturation (26, 27). These observed effects can be attributed to several characteristics of ALA, which are rarely observed for other antioxidants, including (33): i. Small size, ii. Both water and fat-soluble nature with rapid absorption rate, iii. Metal chelating ability, iv. ROS scavenging activity, v. Rescuing or recycling the antioxidant capacity of vitamin E and C, vi. Improving intracellular GSH level, vii. Modulator of several signaling transduction pathways like suppressing tumor necrosis factor (TNF)-alpha-induced ROS generation,and 6-hydroxydopamine induced ROSgeneration, acting as co-activator in electron chain reaction in mitochondria and thereby increasing ATP production (28) and reducing electron leakage, and viii. Acting as a coenzyme of pyruvatedehydrogenase complex and improving consumption of pyruvate especially in ovarian folliclesand in oocytes (22).

It has been shown that ALA can inhibit oxidative stress induced by arsenic or thinner and improve the quantity and quality of sperms in rats (34). In a clinical trial, the effects of ALA supplement on the spermatogram and seminal oxidative stress in infertile men wereinvestigated, and it has been revealed that total sperm count, sperm concentration, and motility levels were significantly increased in the ALA group compared with baseline values. In addition, ALA supplementation improved total antioxidant capacity compared with the placebo group (28, 34).

Our results in this study areconsistent with the previous report of Zhang et al. (22) which showed that addition of ALA at 25 μM during maturation protects oocytes from manipulation and chemical stressor and results in the improved blastocyst and a significant increase in oocyte GSH level and reduction in apoptosis rate in blastocysts (24). The positive effect of ALA also has been shown in thesomatic cell nuclear transfer (SCNT) procedure,and researchers (22, 31) have shown that the efficiency of ALA to improve SCNT in porcine is 400 times more than vitamin C.

In the nervous system (35) and blastocyst (36), ethanol activates ROS production, and protection is acquired by activation of TGFß1 and P53 pathways. Indeed, TGFß1 limits the long term damages in the brain induced by alcohol toxicity, and *in vitro*, it improves embryos quality (36). This effect is believed to be mediated by overexpression of clusterin, which is observed both in the brain and the blastocyst exposed. In this study, we did not observe the overproduction of ROS following alcohol treatment; therefore it is likely that alcohol-induced cytotoxicity during IVM is mediated through other pathways, which requires further research.Despite this, ALA may partially alleviate the alcohol toxicity, through its antioxidant nature as observed by reduced ROS and improved thiol content. Improved developmental competency following ALA treatment during IVM may be related to other properties of ALA, like modulation ofsome signaling transduction pathways such as lowering inflammation reactions (e.g., NF-KB) (37) and increasing the endogenous cellular antioxidants (e.g., GSH) (22, 38), which needs future studies.

Conclusion

Taken together, our results in this study suggest that ALA not only overcomes the negative effect of alcohol toxicity during oocyte maturation but also improves blastocyst yield and quality of resultant embryos. Therefore, ALA, as a good supplement, or as a chemical highly available in green vegetables, is recommended for lowering ROS level and increasing the endogenous cellular antioxidants under oxidative stress conditions in the fertilization process.

Acknowledgments

A part of this study was funded by the Royan Institute of Tehran, Iran. The authors would like to thank the staff of the Royan Institute for their support. All the authors declare no conflict of interest.

Authors' Contributions

M.H.N.-E.; Conceived and designed the study. M.H.N.-E., S.O.; Conducted the research. A.M.Kh., R.M., S.O., A.H.; Participated in study design, data collection and evaluation. F.G.; Conducted molecular experiments and RT-qPCR analysis. A.M.Kh., F.J.; Analyzed the data. F.J., A.A.F.-N., M.H.N.-E.; Drafted the manuscript. A.A.F.-N., M.H.N.-E.; Discussed the reslts. All authors performed approving the final version of this paper for submission, also participated in the finalization of the manuscript and approved the final draft.

References

1. Farley C, Douglas HJ. Efficient cryoprotection of macromolecular crystals using vapor diffusion of volatile alcohols. J Struct Biol. 2014; 188(2): 102-106.
2. Jurkiewicz J. Factors inducing the activation of reconstructed oocytes of farm animals in somatic cloning procedures. J Anim Feed Sci. 2004;13(3): 373-388.
3. Larivière FP, Campagna C, Sirard MA. Mechanisms involved in porcine early embryo survival following ethanol exposure. Toxicol Sci.2017; 156(1): 289-299.
4. Streissguth AP, Landesman-Dwyer S, Martin, JC, Smith DW. Teratogenic effects of alcohol in humans and laboratory animals. Science. 1980; 209(4454): 353-361.
5. Hingson RW, Zha W, Weitzman ER. Magnitude of and trends in alcohol-related mortality and morbidity among U.S. college students ages 18-24, 1998-2005. J Stud Alcohol Drugs Suppl. 2009; 16: 12-20.
6. Wechsler H, Davenport A, Dowdall G, Moeykens B, Castillo S. Health and behavioral consequences of binge drinking in college a national survey of students at 140 campuses. JAMA. 1994;

272(21): 1672-1677.
7. Maier SE, Miller JA, Blackwell JM, West JR. Fetal alcohol exposure and temporal vulnerability regional differences in cell loss as a function of the timing of binge like alcohol exposure during brain development. Alcohol Clin Exp Res. 1999; 23(4): 726-734.
8. Rochette L, Ghibu S, Richard C, Zeller M, Cottin Y, Vergely C. Direct and indirect antioxidant properties of alpha-lipoic acid and therapeutic potential. Mol Nutr Food Res. 2013; 57(1): 114-125.
9. Lee S, Kim E, Hyun SH. Toxicity evaluation of ethanol treatment during in vitro maturation of porcine oocytes and subsequent embryonic development following parthenogenetic activation and in vitro fertilization. Int J Mol Med. 2014; 34(5): 1372-1380.
10. Ibrahim S, Osman Kh, Das S, Othman AM, Majid NA, Rahman MP. A study of the antioxidant effect of alpha lipoic acids on sperm quality. Clinics (Sao Paulo). 2008; 63(4): 545-550.
11. Pirlich M, Kiok K, Sandig G, Lochs H, Grune T. Alpha-lipoic acid prevents ethanol-induced protein oxidation in mouse hippocampal HT22 cells. Neurosci Lett. 2002; 328(2): 93-96.
12. Foo NP, Lin SH, Lee YH, Wu MJ, Wang YJ. α-lipoic acid inhibits liver fibrosis through the attenuation of ROS-triggered signaling in hepatic stellate cells activated by PDGF and TGF-β. Toxicology. 2011; 282(1-2): 39-46.
13. McIlduff CE, Rutkove SB. Critical appraisal of the use of alpha lipoic acid (thioctic acid) in the treatment of symptomatic diabetic polyneuropathy. Therclin Risk manag. 2011; 7: 377-385.
14. Pezhman M, Hosseini SM, Ostadhosseini S, RouhollahiVarnosfaderani S, Sefid F, Nasr Esfahani MH. Cathepsin B inhibitor improves developmental competency and cryo-tolerance of in vitro ovine embryos. BMC Dev Biol. 2017; 17(1): 10.
15. Vanderhyden BC, Caron PJ, Buccione R, Eppig JJ. Developmental pattern of the secretion of cumulus expansion-enabling factor by mouse oocytes and the role of oocytes in promoting granulosa cell differentiation. Dev Biol.1990; 140(2): 307-317.
16. Soto-Heras S, RouraM, Catalá MG, Menéndez-Blanco I, Izquierdo D, Fouladi-Nashta AA, et al. Beneficial effects of melatonin on in vitro embryo production from juvenile goat oocytes. Reprod Fertil Dev. 2018; 30(2): 253-261.
17. Forouzanfar M, Abid A, Hosseini SM, Hajian M, Nasr-Esfahani MH. Supplementation of sperm cryopreservation media with cell permeable superoxide dismutase mimetic agent (MnTE) improves goat blastocyst formation. Cryobiol. 2013; 67(3): 394-397.
18. Gharibi SH, Hajian M, Ostadhosseini S, Hosseini SM, Forouzanfar M, Nasr-Esfahani MH. Effect of phosphodiesterase type 3 inhibitor on nuclear maturation and in vitro development of ovine oocytes. Theriogenology. 2013; 80(4): 302-312.
19. Asgari V, Hosseini SM, Forouzanfar M, Hajian M, Nasr-Esfahani MH. Vitrification of in vitro produced bovine embryos effect of embryonic block and developmental kinetics. Cryobiol. 2012; 65(3): 278-283.
20. Fouladi-Nashta AA, Alberio R, Kafi M, Nicholas B, Campbell KH, Webb R. Differential staining combined with TUNEL labelling to detect apoptosis in preimplantation bovine embryos. Reprod Biomed Online. 2005; 10(4): 497-502.
21. Kitagawa Y, Suzuki K, Yoneda A, Watanabe T. Effects of oxygen concentration and antioxidants on the in vitro developmental ability production of reactive oxygen species (ROS) in embryos. Theriogenology. 2004; 62(7): 1186-1197.
22. Zhang H, Wu B, Liu H, Qiu M, Liu J, Zhang Y, et al. Improving development of cloned goat embryos by supplementing a-lipoic acid to oocyte in vitro maturation medium. Theriogenology. 2013; 80(3): 228-233.
23. Winek CL, Murphy KL, Winek TA. The unreliability of using a urine ethanol concentration to predict a blood ethanol concentration. Forensic Sci Int. 1984; 25(4): 277-281.
24. Jurema MW, Nogueira D. In vitro maturation of human oocytes for assisted reproduction. Fertil Steril. 2006; 86(5): 1277-1291.
25. Jones KL. The effects of alcohol on fetal development. Birth Defects Res C Embryo Today. 2011; 93(1): 3-11.
26. Sánchez MC, Fontana VA, Galotto C, Cambiasso MY, Sobarzo CMA, Calvo L, et al. Murine sperm capacitation, oocyte penetration and decondensation following moderate alcohol intake. Reproduction. 2018; 155(6): 529-541.
27. Moura FA, De Andrade KQ, Dos Santos JC, Goulart MO. Lipoic acid: its antioxidant and anti-inflammatory role and clinical applications. Curr Top Med Chem. 2015; 15(5): 458-483.
28. Prathima P, Pavani R, Sukeerthi S, Sainath SB. α-Lipoic acid inhibits testicular and epididymal oxidative damage and improves fertility efficacy in arsenic-intoxicated rats. J Biochem Mol Toxicol. 2018; 32(2): 1-9.
29. Samardzija C, Quinn M, Findlay JK, Ahmed N. Attributes of Oct4 in stem cell biology perspectives on cancer stem cells of the ovary. J Ovarian Res. 2012; 5(1): 37-42.
30. Haghighian HK, Haidari F, Mohammadi-Asl J, Dadfar M. Randomized, triple-blind, placebo-controlled clinical trial examining the effects of alpha-lipoic acid supplement on the spermatogram and seminal oxidative stress in infertile men. Fertil Steril. 2015; 104(2): 318-324.
31. Huang Y, Tang X, Xie W, Zhou Y, Li D, Zhu J. Vitamin C enhance in vitro and in vivo development of porcine somatic cell nuclear transfer embryos. Biochem Biophys Res Commun. 2011; 411(2): 397-401
32. Perez-Tito L, Bevilacqua E, Cebral E. Peri-implantational in vivo and in vitro embryo-trophoblastic development after perigestational alcohol exposure in the CD-1 mouse. Drug Chem Toxicol. 2014; 37(2): 184-197.
33. Packer L, Witt EH, Tritschler HJ. Alpha-Lipoic acid as a biological antioxidant. Free Radic Biol Med. 1995; 19(2): 227-250.
34. Pınar N, Çakırca G, Özgür T, Kaplan M. The protective effects of alpha lipoic acid on methotrexate induced testis injury in rats. Biomed Pharmacother. 2018;97(1):1486-1492.
35. Zhang X, Sliwowska JH, Weinberg J. Prenatal alcohol exposure and fetal programming: effects on neuroendocrine and immune function. Exp Biol Med (Maywood). 2005; 230(6): 376-388.
36. Zhang D, Jing H, Dou C, Zhang L, Wu X, Wu Q, et al. Supplement of betaine into embryo culture medium can rescue injury effect of ethanol on mouse embryo development. Sci Rep. 2018;8(1):1761.
37. Byun CH, Koh JM, Kim DK, Park SI, Lee KU, Kim GS. Alpha lipoic acid inhibits TNF- induced apoptosis in human bone marrow stromal cells. J Bone Miner Res. 2005; 20(7): 1125-1135.
38. Weydert CJ, Cullen JJ. Measurement of superoxide dismutase catalase and glutathione peroxidase in cultured cells and tissue. Nat Protoc. 2010; 5(1): 51-66.

Original Article

Metformin Reduces Vascular Assembly in High Glucose-Treated Human Microvascular Endothelial Cells in An AMPK-Independent Manner

Carolina Silva, Ph.D.[1, 2], Ilda Rodrigues, M.Sc.[1], Sara Andrade, Ph.D.[1, 2, 3], Raquel Costa, Ph.D.[1, 2], Raquel Soares, Ph.D.[1, 2*]

1. Department of Biomedicine, Unit of Biochemistry, Faculty of Medicine, University of Porto, 4200-319 Porto, Portugal
2. i3S, Institute of Research and Innovation in Health, University of Porto, Porto, Portugal
3. IPATIMUP, Institute of Pathology and Molecular Immunology, University of Porto, Porto, Portugal

Corresponding Address: Department of Biomedicine, Unit of Biochemistry, Faculty of Medicine, University of Porto, Al Prof Hernâni Monteiro 4200-319 Porto, Portugal
Email: raqsoa@med.up.pt

Received: 19/October/2019, Accepted: 1/January/2020

Abstract

Objective: The aim is to examine the effect of metformin in human microvascular endothelial cells exposed to high glucose (HG) concentration and compare them with the effects of other 5' adenosine monophosphate-activated protein kinase (AMPK) modulators under the same condition.

Materials and Methods: In this experimental study, human microvascular endothelial cells (HMECs) were treated with 15 mM metformin, 1 mM 5-aminoimidazol-4-carboxamideribonucleotide (AICAR) and 10 mM compound C in the presence of 20 mM glucose (hyperglycemic condition). Migration, invasion and proliferation were evaluated as well as the capillary-like structures formation. Moreover, the expression of angiogenic genes was assessed.

Results: Metformin significantly inhibited vessel formation and migration, although it did not change HMECs proliferation and invasion. In addition, metformin significantly reduced collagen formation as evidenced by histological staining. Concomitantly, expression of several genes implicated in angiogenesis and fibrosis, namely *TGFß2, VEGFR2, ALK1, JAG1, TIMP2, SMAD5, SMAD6* and *SMAD7,* was slightly upregulated. Immunostaining for proteins involved in ALK5 receptor signaling, the alternative TGFß signaling pathway, revealed significant differences in SMAD2/3 expression.

Conclusion: Our data showed that metformin prevents vessel assembly in HMECs, probably through an AMPK-independent mechanism. Understanding the molecular mechanisms by which this pharmacological agent affects endothelial dysfunction is of paramount importance and paves the way to its particular use in preventing development of diabetic retinopathy and nephropathy, two processes where angiogenesis is exacerbated.

Keywords: AICAR, AMPK Signaling, Compound C, Endothelial Cells, Metformin

Cell Journal(Yakhteh), Vol 23, No 2, July 2021, Pages: 174-183

Citation: **Silva C, Rodrigues I, Andrade S, Costa R, Soares R. Metformin reduces vascular assembly in high glucose-treated human microvascular endothelial cells in an ampk-independent manner. Cell J. 2021; 23(2): 174-183. doi: 10.22074/cellj.2021.7212.**

Introduction

In recent years, the incidence of type 1 diabetes mellitus (T1DM) has increased worldwide, contributing to a significant increase in overall rates of diabetes morbidity and mortality (1). Vascular complications present in the vast majority of patients with T1DM, are responsible for a considerable part of morbidity rate (2). It is known that inflammatory changes in the blood vessel wall lead to a dysfunction in endothelial and smooth muscle cells resulting in vascular disease (3). Endothelial cells are particularly vulnerable to hyperglycemia (4). Thus, uncontrolled hyperglycemic state, common in diabetic patients, leads to increased release of factors that favor endothelial dysfunction (5). In turn, endothelial dysfunction is a potential contributor to the pathogenesis of vascular disease in DM (6), resulting in reduced bioavailability of nitric oxide (7). Studies performed in humans, animals and cells showed that endothelial dysfunction is maintained even after normal glycemia is achieved, a concept designated by metabolic memory (8). Therefore, as vascular complications are the major cause of morbidity in diabetic patients, understanding the molecular events that occur in endothelial dysfunction is mandatory.

Previous studies of our group revealed that endothelial cells isolated from T1DM mice kidney and heart exhibited a distinct gene expression profile involving AMPK pathway, a major cell energy regulator (9). AMPK pathway can be modulated by pharmacological agents like metformin. In agreement, several reports suggested that stimulating AMPK signaling leads to endothelial dysfunction improvement (10). Moreover, AMPK signaling activation improves insulin sensitivity and reduces the risk of T2DM (11).

Metformin, one of the most commonly used antihyperglycemic drugs against T2DM (12), is a known activator of AMPK and has also been studied

as an adjuvant for T1DM treatment. Metformin could activate AMPK indirectly, through inhibition of mitochondrial complex I and increment of the AMP/ATP ratio, or directly, by α subunit phosphorylation (13). Although the molecular mechanisms of metformin action are not completely elucidated, this compound can be therapeutically successful in other pathological conditions as well. In cancer, for instance, metformin exerts anti-proliferative effects as demonstrated *in vitro* and *in vivo* (11).

Metformin was shown to target angiogenesis as well, interfering with endothelial function and attenuating the production of proangiogenic and inflammatory factors like metalloproteinases (MMP's), adhesion molecules, namely intercellular adhesion molecule 1 (ICAM-1) and vascular cell adhesion molecule 1 (VCAM-1), tumor necrosis factor α (TNFα) and nuclear factor-κB (NF-κB) (14-18).

Given the wide use of metformin in diabetic patients, as well as the relevance of AMPK signaling pathway in diabetic complications, the present study aimed to elucidate how AMPK modulators affect HMECs. To address this, HMECs cells were cultured with AMPK agonists, metformin and AICAR, and an AMPK antagonist, compound C, in the presence of 5.5 mM (normoglycemic) or 20 mM (hyperglycemic) glucose, and cell proliferation, migration and assembly into capillary-like structures, as well as expression of angiogenic genes were examined.

Materials and Methods

Cell culture and *in vitro* treatments

Human microvascular endothelial cells (HMECs, ATCC, UK) were cultured in RPMI 1640 medium (Sigma-Aldrich, Portugal) supplemented with 10% fetal bovine serum (FBS, Sigma-Aldrich, Portugal), 1.176 g/L sodium bicarbonate (Merck, Germany), 4.76 g/L HEPES, 1% penicillin/streptomycin (Sigma-Aldrich, Portugal), 1 mg/L hydrocortisone >98% (Sigma-Aldrich, Portugal), and 10 µg/ml endothelial growth factor (EGF, Sigma-Aldrich, Portugal). Cells were kept at 37˚C in a humidified 5% CO_2 atmosphere and the experiments were accomplished between passages 3 and 6. Assays were performed in serum-free media supplemented with glucose at two different concentrations: 5.5 mM [low glucose (LG)] or 20 mM D-Glucose [high glucose (HG)] (Sigma-Aldrich, Portugal). Cells were maintained under these conditions for 24 hours before treatment incubation. Cells were then treated with15 mM metformin (Sigma-Aldrich, Portugal), 1 mM 5-aminoimidazol-4-carboxamideribonucleotide (AICAR, Sigma-Aldrich, Portugal) and 10 µM compound C (Sigma-Aldrich, Portugal).These concentrations were selected based on a preliminary viability assay using different concentrations of metformin (10, 20, 30, 40 and 50 mM), AICAR (0.2, 0.5, 0.75, 1.0, 1.25 and 1.5 mM) and compound C (5, 7.5, 10, 12.5 and 15 µM), done based on previously published reports (16, 19-21). AICAR and metformin were dissolved in ultrapure water, whereas compound C was solubilized in dimethyl sulfoxide (DMSO, Merck, Germany). The working solutions were prepared in PBS and then added to respective treatment media.

Ethical issues

This study was approved by Department of Biomedicine, Faculty of Medicine, University of Porto, Portugal.

Cell viability

Cell viability was examined by3-(4,5-dimethylthiazol-2-yl)-5-(3-carboxymethoxyphenyl)-2-(4-sulfophenyl)-2H-tetrazolium (MTS) assay (Cell Titer 961 Aqueous ONE Solution Reagent, Promega, Madison, EUA). HMECs (1×10^5 cells/mL) were incubated with glucose at two concentrations, for 24 hours. Next, the cells were incubated with metformin, AICAR and compound C for 24 hours. Cell cultures were then incubated with 20 µL MTS according to the manufacturer instructions. Color development was quantified at 492 nm. The concentration of compounds used in all subsequent experiments was defined based on the MTS results in order to exclude possible cytotoxic effects. These concentrations were identical to the ones described in the literature (16, 19-21). Results are expressed as percentage of the control.

Bromodeoxyuridine proliferation assay

HMECs (1×10^5 cells/mL) were cultured in serum-free media supplemented with glucose at two different concentrations, in 96-well microplates for 24 hours. Cells were then incubated with treatments in the presence of bromodeoxyuridine (BrdU) at a final concentration of 0.01 mM for another 24 hours. Cells were then fixed and incubated with anti-BrdU antibody for 90 minutes. Detection was performed using the colorimetric BrdU Proliferation Assay kit (Roche, Germany), according to the manufacturer's instructions. Optical density was measured at 450 and 650 nm and the results are expressed as percentage of the control.

Injury assay

Injury assay was performed as described by Liang et al. (22). Cells were plated, maintained at 37˚C in a humidified 5% CO_2 atmosphere until confluence and then, incubated with the two different concentrations of glucose for 24 hours. Cell cultures were then injured by the pipette tip, which left a void space.

The wells were photographed at 200X amplification, and the treatments were added to serum-free media and incubated for 24 hours. The wound closure was determined by subtracting the wounded area measured after 24 hours, from the initial void space (FIJI software, National Institutes of Health, USA).

Matrigel assay

Matrigel assay was performed in 96-well microplates coated with 50 µl of Matrigel Basement Membrane Matrix (BD Matrigel™, BD-Biosciences, Belgium) per well. HMECs, previously incubated with 5.5 or 20 mM glucose, were harvested in complete medium over the Matrigel layer. Two hours later, the medium was removed and the treatments were added. Cell growth was monitored for 18 hours. Tube formation was observed and quantification was performed by vessel counting in each well using a phase contrast microscope (Nikon, UK), at ×200 magnification.

Collagen synthesis evaluation in cell culture

Production of collagen by cells was analyzed by Sirius Red histologic assay, as described by Pinheiro et al. (23). Briefly, cells were cultured with low and high concentrations of glucose for 24 hours and then, incubated with compounds (metformin, AICAR and compound C) for an additional 24 hours. Subsequently, HMECs were fixed with 4% p-formaldehyde for 15 minutes at room temperature (RT), washed with distilled water and stained with Sirius Red solution for 1 hour. Wells were washed with acidified water (5%), and incubated with 0.1 N NaOH for 30 minutes, and color development was measured by reading the absorbance at 550 nm using a microplate reader.

Invasion assay

Invasion assay was accomplished in CorningBioCoat™ Matrigel Invasion Chamber (Transwells, Corning Inc., Corning, USA) according to the manufacturer's instructions. Basically, following 24 hours under hyperglycemic condition, HMECs (2.5×10^4 cells/mL) were harvested on inserts, initially hydrated with complete medium. The lower chambers were filled with RPMI medium containing 10% FBS. After 24 hours incubation with compounds, the non-invasive cells were detached by a cotton swap. Cells enclosed to the lower surface membrane insert were fixed, stained and counted under a microscope from sixteen randomly chosen fields in each well. The mean number of the cells per field was recorded.

Western blot

Proteins were extracted from homogenates of treated HMECs cultures and quantified by BCA protein assay kit (Thermo Scientific, USA). Then, 15 µg of total protein was separated by electrophoresis and transferred to nitrocellulose membrane (Biorad, USA). The membranes were the incubated with primary antibodies [phospho-SMAD5 (1:500); total SMAD5 (1:500); phospho-SMAD2/3 (1:500); total SMAD2/3 (1:1000) and TGFβR1 (1:500)], and then incubated with secondary horseradish-peroxidase (HRP)-coupled antibodies (1:5000, anti-rabbit, HRP NA934V or 1:5000, anti-mouse, HRP NA931V). Antibodies were dissolved in BSA solution, containing 4% of BSA in 0.1% TBS-T. Detection was performed using enhanced chemiluminescence (ECL) kit (Biorad, USA) and relative intensity of different proteins expression was calculated and normalized against intensity of stained-free gels (Biorad, USA).

Quantitative real-time polymerase chain reaction assays

Total RNA was extracted from HMECs after incubation with compounds for 24 hours, using NZYol® isolation reagent (NZYtech, Portugal). Briefly, the cells were harvested with 1 mL of the reagent, homogenized and incubated for 5 minutes at RT. For the phase separation, we added 200 µL of chloroform to the tubes, and the tube was incubated for 2-3 minutes at RT and centrifuged. The aqueous phase was transferred to a new tube and RNA precipitation was performed by adding 500 µl cold isopropanol. RNA pellet was washed with 75% ethanol, air dried for 10 minutes and resuspended in RNase-free water. RNA was quantified by NanoDrop.

The cDNA was synthesized by RevertAid H Minus First Strand cDNA Synthesis Kit (Thermo Scientific, USA), and then, 1.5 µL of cDNA sample was used for each polymerase chain reaction (PCR) assay. Gene amplification was performed as previously established (9) under the following conditions: pre-incubation (95˚C for 600 seconds), amplification (95˚C for 10 seconds; specific temperature of each primer; 72˚C for 10 seconds 45 cycles) and melting (95˚C for 10 seconds; (AT+10)˚C for 60 seconds and 97˚C for 1 second); primers used for human *ALK1*, *JAG1*, *SMAD5*, *SMAD6, SMAD7, TGFBR1,TIMP2*, *TGFβ2*, *VEGFR2* and *β-ACTIN* are shown in Table 1. Samples were analyzed by Light Cycler 96 thermal cycler (Roche, USA) and quantified by the ΔΔCT method. All genes expression values was normalized against *β-ACTIN* expression values, as a commonly used housekeeping gene.

Statistical analysis

GraphPad Prism 6.0 Software (GraphPad Software Inc., CA, USA) was used for data analysis and the results are expressed as mean ± SEM, with a confidence interval of 95% and $P<0.05$ considered significant. Experiments were performed in triplicate and analyzed by one-way ANOVA and Bonferroni post hoc test. Student t test was used for two group analyses with $P<0.05$ considered significant.

Results

Effect of AMPK modulators on HMECs viability

To examine the effect of AMPK pathway in endothelial cells, we first analyzed the effect of metformin, AICAR and compound C, three AMPK modulators, at different concentrations in HMECs exposed to low and high concentrations of glucose. The analysis showed a dose-dependent reduction in cell viability for these three agents under both glucose conditions. Incubation with 30 to 50 mM metformin led to a significant decrease in HMECs cell viability at both glucose concentrations, indicating a toxic effect of this agent at these concentrations (Fig.1A). Furthermore, incubation of 5.5 mM glucose-treated HMECs cells with 12.5 μM compound Cresulted in a cytotoxic effect. No significant difference was observed between the two glucose concentrations used for any of the treatments tested (Fig.1B). We, therefore, used the nontoxic concentrations of 1 mM AICAR, 15 mM metformin and 10 μM compound C in the following experiments; the selected concentrations were in agreement with the literature.

Table 1: Primer sequences used in HMECs cells exposed to medium containing either 5.5 or 20 mM of glucose, and incubated with AICAR, metformin or compound C

Genes	Primer sequence (5′-3′)
ALK1	F: CAACATCCTAGGCTTCATC
	R: TCTCTGCAGAAAGTCGTAG
β-ACTIN	F: AGAGCCTCGCCTTTGCCGAT
	R: CCATCACGCCCTGGTGCCT
JAG1	F: ACTACTACTATGGCTTTGGC
	R: ATAGCTCTGTTACATTCGGG
SMAD5	F: CCAGTCTTACCTCCAGTATTAG
	R: TCCTAAACTGAACCAGAAGG
SMAD6	F: CCCATAGAGACACAAAAATCTC
	R: GTAAGACAATGTGGAATCGG
SMAD7	F: CAGATTCCCAACTTCTTCTG
	R: CTCTTGTTGTCCGAATTGAG
TGFBR1 (ALK5)	F: AGACAATGGTACTTGGACTC
	R: GTACCAACAATCTCCATGTG
TGFB2	F: AGATTTGCAGGTATTGATGG
	R:ATTTCTAAAGCAATAGGCCG
TIMP2	F: GGCCTGAGAAGCATATAGAG
	R: CTTTCCTGCAATGAGATATTCC
VEGFR2	F: GCCATGTGGTCTCTCTGGTT
	R: GCCGTACTGGTAGGAATCCA

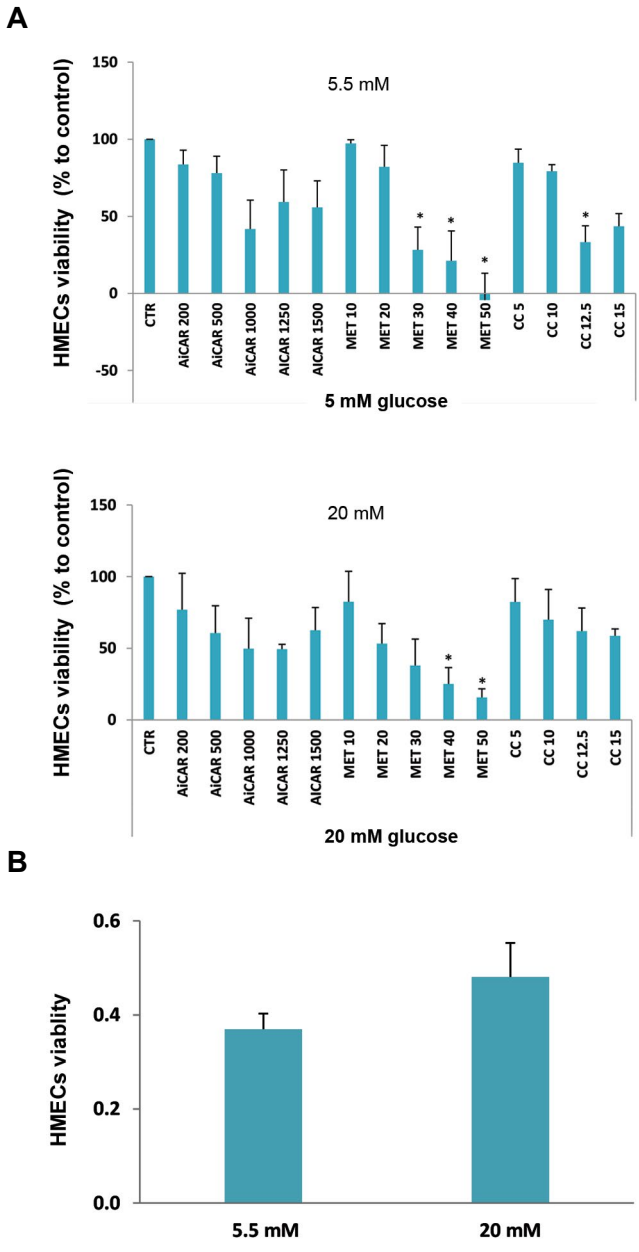

Fig.1: Cell viability evaluation in confluent HMECs cultures using MTS assay. **A.** No significant cytotoxicity was found following treatment with AICAR at a concentration range of 200-1500 μM, metformin (MET) at concentrations of 10-50 mM and compound C (CC) at concentrations of 5, 10 and 15 μM, in most of the doses tested. Results are expressed as percentage of control and are fold-increase relative to normoglycemic (5.5 mM) control cell cultures. Control bars (CTR) refer to cultures under the same conditions of glucose but without incubation with tested compounds. Three independent experiments were performed in triplicate with identical results. *P<0.05 vs. CTR under identical glucose conditions. **B.** Cytotoxicity evaluation in confluent HMECs cultures using MTS assay exposed to 5.5 (CTR5.5) and 20 mM (CTR20) of glucose. No significant difference in cell viability was found between the two concentrations.

Effect of treatment of HMECs with metformin, AICAR and compound C on HMECs proliferation, migration and invasion

In order to determine the effect of these compounds on HMECs proliferation, the BrdU assay was performed. As shown in Figure 2A, no difference in HMECs proliferation was observed between the two glucose concentrations.

Furthermore, incubation with 1 mM AICAR, 15 mM metformin or 10 μM compound C in the presence of high concentration of glucose (Fig.2A) did not significantly affect HMECs proliferation.

Moreover, upon incubation with metformin and compound C, a significant decrease in HMECs migration was verified in comparison with the control under the same glucose condition (Fig.2B). A minor reduction in cell invasion was found up on treatment with 1 mM of AICAR, though it did not reach statistical significance.

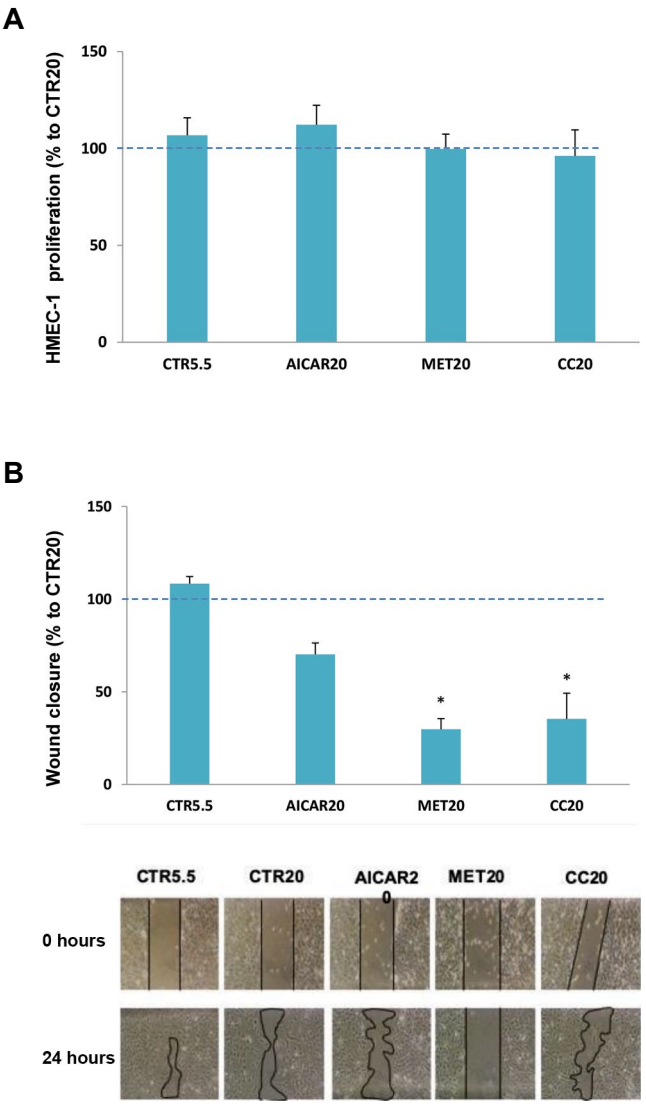

Fig.2: Proliferation and migration of HMECs were evaluated after incubation with AICAR, metformin (MET) or compound C (CC). **A.** Cell proliferation was assessed by BrdU incorporation assay. Cell proliferation was not significantly reduced by incubation with any of the compounds tested. Results are expressed as percentage of high glucose (HG) control. Three independent experiments were performed in triplicate with identical results. **B.** Cell migration was visualized by injury assay after 24 hours of incubation. A significant reduction of cell migration to the damaged areas was found after incubation with CC. Pictures are representative of three independent studies (magnification: ×200). CTR5.5 bar represents 5.5 mM glucose-incubated HMECs in the absence of compounds. *; P< 0.05 vs. CTR20.

Effect of AICAR, metformin and compound C incubation on vessels formation

To further examine the role of the three AMPK modulators in the development of capillary structures, we established HMECs cell cultures on a 3D basement membrane matrix and monitored the growth of vascular structures. Interestingly, hyperglycemic conditions slightly reduced the formation of capillary-like structures. Incubation of 20 mM glucose-treated cells with each AMPK modulator further reduced the capacity of HMECs to assemble into vessels; this decrease was statistically significant for 15 mM metformin and 10 μM of compound C (Fig.3A).

The assembly of endothelial cells within blood vessels tructures is strongly dependent on the formation of a basement membrane. Therefore, we next investigated whether the studied pharmacological agents influenced the formation of collagen under hyperglycemic conditions using Sirius Red staining. Treatment with HG resulted in a reduction of collagen formation (Fig.3B). When compared with the control at the same glucose concentration, the incubation with compound C (10 μM) and metformin (15 mM) resulted in a significant decrease of collagen formation by HMECs. However, incubation with 1 mM AICAR did not affect the collagen synthesis by HMECs. Only incubation with 10 μM compound C significantly affected the invasive behavior of HMECs as evidenced by transwells assay (Fig.3C).

Effect of AICAR, metformin and compound C on angiogenic-related genes

We next performed quantitative real time PCR in order to investigate whether AMPK modulators interfered with angiogenic gene expression in HMECs under HG conditions. Recent experiments of our group showed that *TGFβ2, SMAD5, ALK1, JAG1, VEGFR2* and *TIMP2* genes, which are known to play a role in angiogenesis and fibrosis, presented imbalanced expression in endothelial cells from T1DM mice (9). We, therefore, analyzed the expression of these transcripts in HMECs. Incubation with 20mM glucose did not result in significant differences in expression of these genes (Fig.4).

In general, incubation of cells with AMPK-modulating agents led to an increase in expression of these six genes analyzed in comparison to HG control (Fig.4A-F). Particularly, incubation with metformin resulted in a slight upregulation of *TGFβ2*, *TIMP2, ALK1, JAG1, SMAD5* and *VEGFR2*, although it did not reach statistical significance. Then, we examined the expression of specific genes of TGFβ signaling pathway like *SMAD6, SMAD7* and *TGFβR1*.Although metformin treatment led to a slight increase in expression of these transcripts, it was not statistically significant (Fig.5A).

To confirm these findings, we analyzed the protein expression of a TGFβ signaling downstream effector, SMAD5, through ALK1 receptor activity, as well as TGFβR1 and SMAD2/3, the TGFβ alternative pathway. Only treatment with compound C changed the expression of phosphorylated (active) SMAD5 and total SMAD2/3 (Fig.5B).

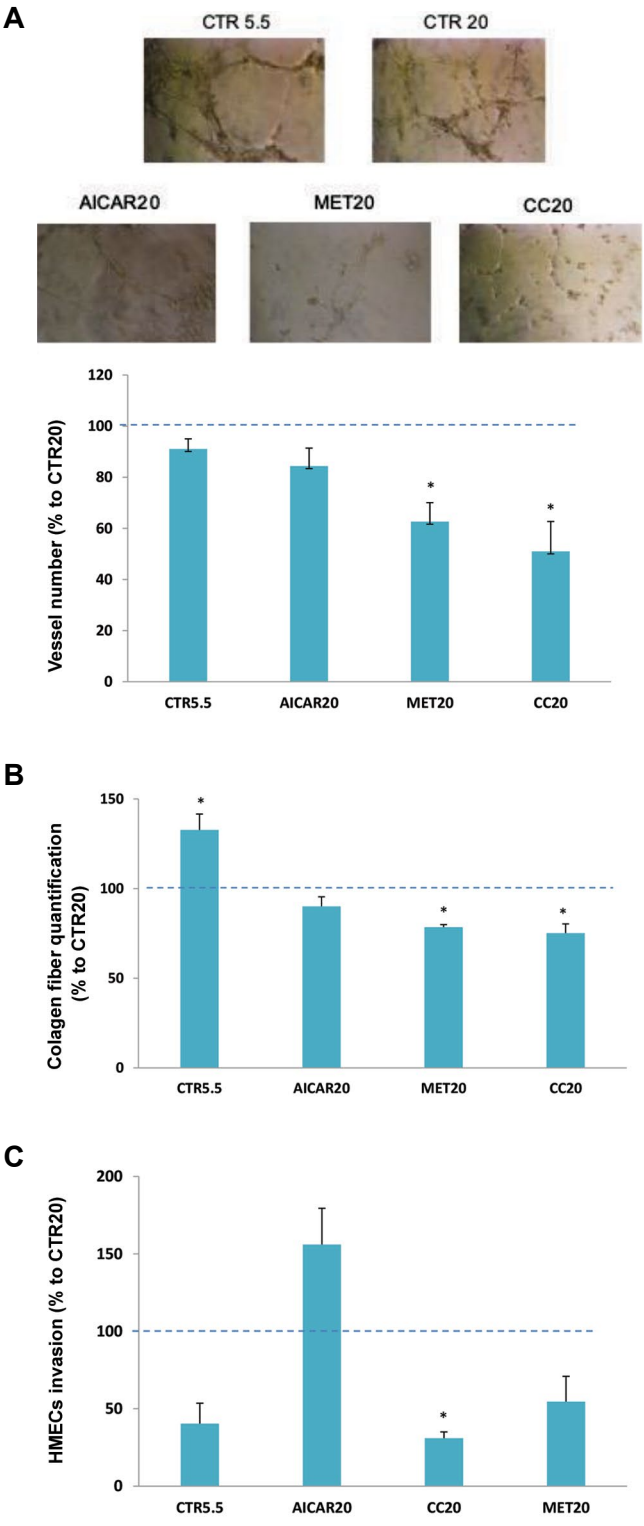

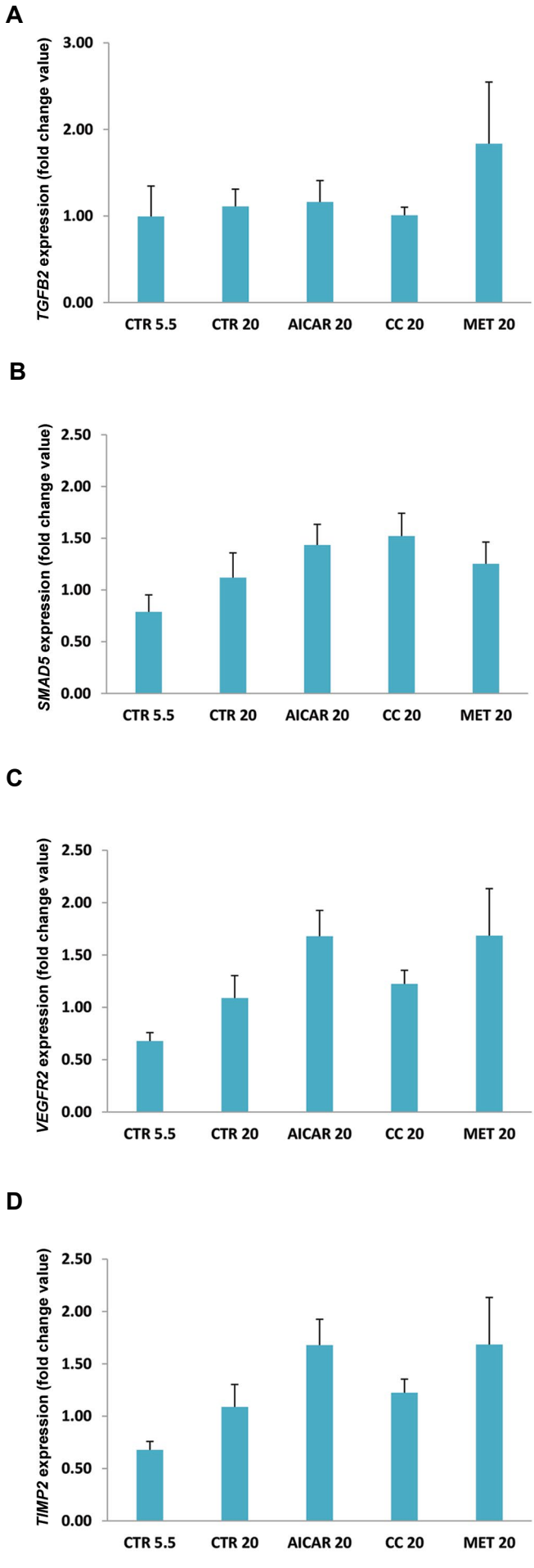

Fig.3: Analysis of vessel formation, cellular invasion and collagen fiber after treatments with compounds. **A.** Assembly of capillary-like structures after incubation with AICAR, metformin (MET) or compound C (CC). Results are expressed as percentage of CTR20 (dotted line); CTR5.5 bar represents 5.5 mM glucose-incubated HMECs left untreated. The number of cord structures was recorded on an inverted microscope. Vascular assembly was reduced in a significant manner after incubation with MET20 as compared to untreated cells (CTR20). *P<0.05 vs. CTR20. Pictures are representative of three independent studies. **B.** Quantification of histological staining for Sirius red in HMECs cells treated with AICAR, MET or CC in the presence of 20 mM glucose. **C.** Analysis of cellular invasion after treatments with AMPK modulators compounds by transwells assay. Significant reduction in HMECs treated with CC20 when compared to control at the same glucose concentration (CTR20, dotted line). Bars represent percentage of control (CTR20, dotted line, magnification: ×200).

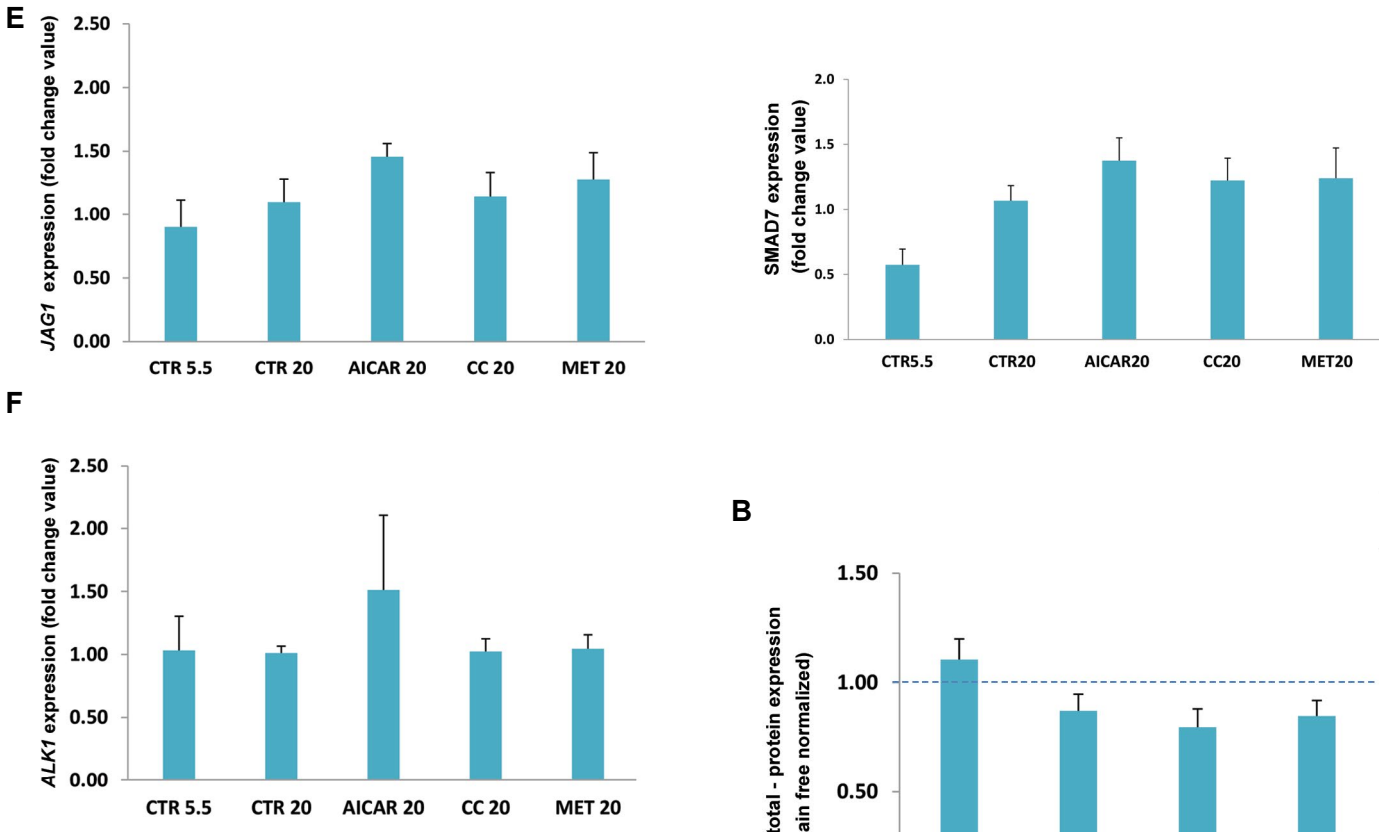

Fig.4: Expression analyses of genes associated with angiogenic process after treatments with compounds. Expression analyses of **A.** *TGFB2*, **B.** *SMAD5*, **C.** *VEGFR2*, **D.** *TIMP2*, **E.** *JAG1* and **F.** *ALK1* genes in HMECs after incubation with AICAR, metformin (MET) and compound C (CC) in 20 mM glucose for 24 hours. CTR5.5 and CTR20 bars represent gene expression of 5.5 and 20 mM glucose treated HMECs, respectively.

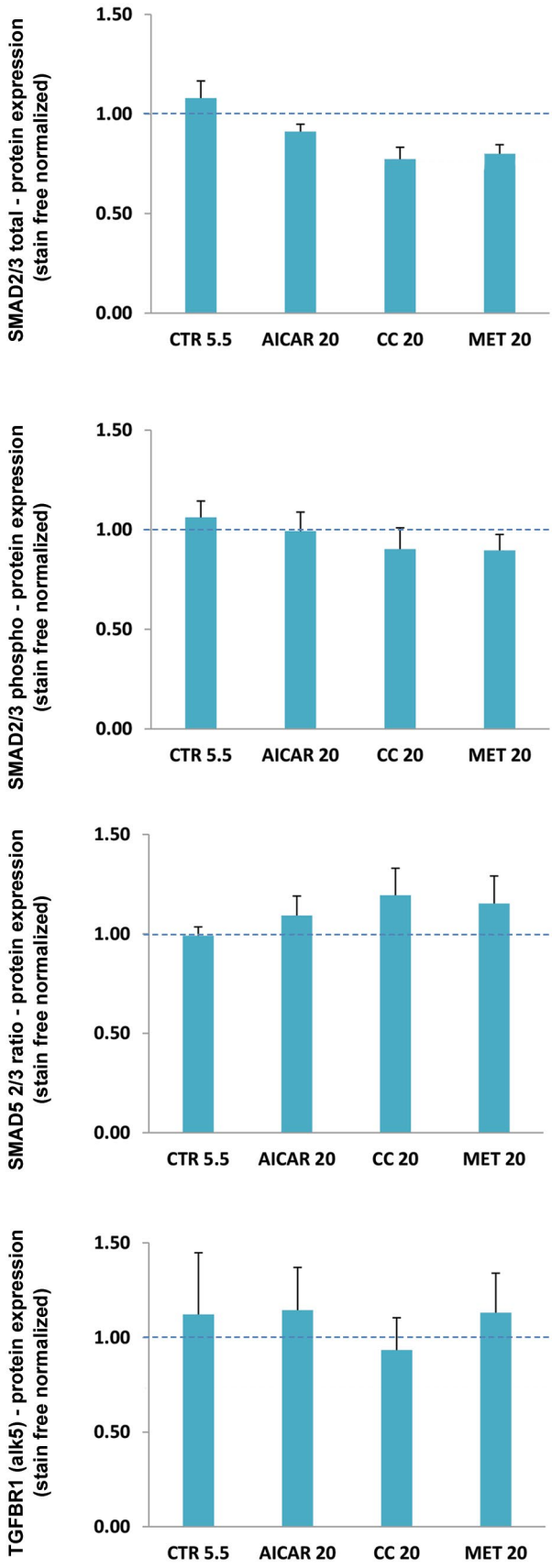

Fig.5: Gene and protein expression analyses in cells after treatment. **A.** Expression analyses of *TGFBR1*, *SMAD6* and *SMAD7* genes in HMECs after incubation with AICAR, metformin (MET) and compound C (CC) in 20 mM glucose for 24 hours. CTR5.5 and CTR20 bars represent gene expression of 5.5 and 20 mM glucose treated HMECs, respectively. **B.** Analysis of protein expression by Western Blot after treatments with AMPK modulators for 24 hours. None of the treatments significantly changed the active forms of proteins analyzed.

Discussion

Vascular complications are a major feature in diabetes. Metformin is largely used in diabetes treatment for its ability to control metabolism through AMPK. However, it is not well established whether modulating AMPK affects the angiogenic process within endothelial cells. Herein, we examined the effect of metformin on microvascular endothelial cell proliferation, invasion, migration and capillary-like structures formation, and compared this effect with two other AMPK modulators namely, AICAR and compound C. We were able to show that incubating HMECs with metformin under hyperglycemic conditions, leads to a significant reduction in the formation of capillary-like structures, as well as a significant reduction in migration and collagen production. Similar results were reported by Dallaglio et al. (12). By incubating HUVECs with different concentrations of metformin, these authors showed a significant dose- and time-dependent decline in the amount and length of segments of capillary-like structures. Metformin inhibitory effect was also reported in hepatic stellate cells (HSCs) activation, proliferation, migration and cell contraction (24).

Nevertheless, controversial findings have been described in the literature regarding the effect of metformin on cellular proliferation, apoptosis (21, 25) and angiogenesis under hyperglycemic conditions. Accordingly, metformin exhibited proangiogenic activity in experimental disease models like wound healing, cardiovascular disease and tumors (26, 27). In agreement, recent findings indicated that metformin improved angiogenesis and accelerated wound healing in diabetic mice, by promoting AMPK and eNOS signaling activity, often downregulated in diabetes. Cittadini et al. (26) investigated the effects of metformin in an experimental model of chronic heart failure, a common feature of diabetes, and observed a marked activation of AMPK with improved left ventricular remodeling, reduced perivascular fibrosis and minor cardiac lipid accumulation. Moreover, Bakhashab et al. (28) found that metformin can promote migration, inhibit apoptosis and increase the expression of VEGFA in HUVECs exposed to hyperglycemia-hypoxia condition.

Endothelial cells express two TβRI: ALK1 and ALK5, which present different affinities to both TGFβs and BMPs ligands. ALK1 binds with greater affinity to BMPs, whereas TGFβ preferentially binds to ALK5, enhancing angiogenesis. Since TGFβ expression was increased in diabetic kidney endothelial cells in previous studies of our group (29), and given the fact that metformin resulted in reduced angiogenesis, we next examined TGFβ/ALK5 signaling. Strikingly, ALK5 and SMAD2/3 expression was not affected by metformin. According to Iwata et al, metformin increased expression of SMAD6, an inhibitor of SMAD5 phosphorylation in human granulosa KGN cells (30). This inhibitory effect was further corroborated by the fact that Kdr did not significantly change after metformin treatment.

TGFβ plays an important role in collagen synthesis,

another process exacerbated during diabetes. TGFβ regulates the transcription of genes responsible for extracellular matrix components synthesis (31). Accordingly, in our experiment, a significant decrease in collagen synthesis was observed in metformin-treated HMEC under hyperglycemic conditions, which is in agreement with a putative inhibition of TGFβ signaling through SMAD6 upregulation by metformin.

To further analyze whether metformin effects were AMPK-dependent, we examined the action of AICAR, an AMPK agonist, and the AMPK inhibitor, compound C. AICAR is an adenosine analogue compound that has been extensively used to activate AMPK pathway *in vitro*. Its effects and efficacy vary according to the established cell culture conditions (32).

By stimulating AMPK activity, AICAR has been reported to prevent cell proliferation, migration, invasion and metastasis in several types of tumors both *in vivo* (33, 34) and *in vitro* (35-37). On the other hand, compound C, a pyrazolopyrimidine derivative, is a widely used potent inhibitor of AMPK. Nonetheless, it was shown to exert anti-proliferative effects and inhibit ICAM-1 and VCAM-1 expression in cell and animal models to a similar extent as metformin (38).

Despite AICAR and metformin are both AMPK agonists, in the current study, they exhibited distinct effects in terms of angiogenesis. AICAR did not change migration, invasion or vessel assembly in HMECs. In addition, compound C, the AMPK antagonist, resulted in effects similar to those of metformin. These findings suggest that the anti-angiogenic action of metformin is probably not mediated via AMPK signaling pathway. In fact, metformin is known to interfere with several other metabolic pathways and present AMPK independent effects. A recent study showed that metformin suppresses adipogenesis in C3H10T1/2 MSCs by inhibiting mTOR/p70S6k signaling pathway (39). According to Rena et al, metformin inhibits fructose-1,6-bisphosphatase, an enzyme implicated in glucose metabolism, through an AMPK-independent mechanism (40). These findings emphasize the hypothesis that the anti-angiogenic activity of metformin is AMPK independent.

Altogether, our findings suggest that the anti-angiogenic effects of metformin are AMPK-independent. Nevertheless, further studies are needed to confirm whether these activities involve the complex TGFβ signaling pathways.

Conclusion

The present study shows that metformin not only regulates metabolism, but also probably controls endothelial dysfunction, being important in preventing conditions where angiogenesis is exacerbated such as diabetic retinopathy or nephropathy.

Acknowledgements

This work was funded by CAPES (Sciences without Border - Full Doctorate Fellowship – Process 10010-13-0), and was supported by Norte Portugal Regional Programme (NORTE 2020), under the PORTUGAL 2020 Partnership Agreement, through the European Regional Development Fund (ERDF) – Bioengineered therapies for infectious disease and tissue regeneration (NORTE-01-0145-FEDER-0000012), and by FCT - *Fundação para a Ciência e Tecnologia* [UID/BIM/04293/2013]. There is no conflict of interests regarding the current paper.

Authors' Contributions

C.S., R.S.; Participated in conception and design. C.S., I.R., S.A., R.C.; Contributed to all experimental work and statistical analysis. All authors were responsible for interpretation of data. R.S.; Was responsible for overall supervision. C.S.; Drafted the manuscript, which was revised by S.A., R.C., R.S. All authors read and approved the final manuscript.

References

1. World Health Organization. Available from: https://www.who.int/en/news-room/fact-sheets/detail/diabetes.(8 Dec 2019).
2. DuganLL, Ali SS, Diamond-Stanic M, Miyamoto S, DeCleves AE, Andreyev A, et al. AMPK dysregulation promotes diabetes-related reduction of superoxide and mitochondrial function. J Clin Invest. 2013; 123(11): 4888-4899.
3. Costa PZ, Soares R. Neovascularization in diabetes and its complications. Unraveling the angiogenic paradox. Life Sci. 2013; 92(22): 1037-1045.
4. Funk SD, Yurdagul A Jr, Orr AW. Hyperglycemia and endothelial dysfunction in Atherosclerosis: lessons from type 1 diabetes. Int J Vasc Med. 2012; 2012: 569654.
5. Barrett EJ, Liu Z, Khamaisi M, King GL, Klein R, Klein BEK, et al. Diabetic microvascular disease: an endocrine society scientific statement. J Clin Endocrinol Metab. 2017; 102(12): 4343-4410.
6. Shi Y, Vanhoutte PM. Macro- and microvascular endothelial dysfunction in diabetes. J Diabetes. 2017; 9(5): 434-449.
7. Coco C, Sgarra L, Potenza MA, Nacci C, Pasculli B, Barbano R, et al. Can epigenetics of endothelial dysfunction represent the key to precision medicine in type 2 diabetes mellitus? Int J Mol Sci. 2019; 20(12): 2949.
8. Ceriello A. The emerging challenge in diabetes: the "metabolic memory." Vascul Pharmacol. 2012; 57(5-6): 133-138.
9. Silva C, Sampaio-Pinto V, Andrade S, Rodrigues I, Costa R, Guerreiro S, et al. Establishing a link between endotelial cell metabolism and vascular behaviour in a type 1 diabetes mouse model. Cell Physiol Biochem. 2019; 52(3): 503-516.
10. Dong Y, Zhang M, Wang S, Liang B, Zhao Z, Liu C, et al. Activation of AMP-activated protein kinase inhibits oxidized LDL-triggered endoplasmic reticulum stress in vivo. Diabetes. 2010; 59(6): 1386-1396.
11. LiuY, Hu X, Shan X, Chen K, Tang H. Rosiglitazone metformin adduct inhibits hepatocellular carcinoma proliferation via activation of AMPK/p21 pathway. Cancer Cell Int. 2019; 19: 13.
12. DallaglioK, Bruno A, Cantelmo AR, Esposito AL, Ruggiero L, Orecchioni S, et al. Paradoxic effects of metformin on endothelial cells and angiogenesis. Carcinogenesis. 2014; 35(5): 1055-1066.
13. Kazyken D, Magnuson B, Bodur C, Acosta-Jaquez HA, Zhang D, Tong X, et al. AMPK directly activates mTORC2 to promote cell survival during acute energetic stress. Sci Signal. 2019; 12(585): eaav3249.
14. Hirsch HA, Iliopoulos D, Struhl K. Metformin inhibits the inflammatory response associated with cellular transformation and cancer stem cell growth. Proc Natl Acad Sci. 2013; 110(3): 972-977.
15. Sun J, Huang N, Ma W, Zhou H, Lai K. Protective effects of metformin on lipopolysaccharide-induced airway epithelial cell injury via NF-κB signaling inhibition. Mol Med Rep. 2019; 19(3): 1817-1823.

16. Han J, Li Y, Liu X, Zhou T, Sun H, Edwards P, et al. Metformin suppresses retinal angiogenesis and inflammation in vitro and in vivo. PLoS One. 2018; 13(3): e0193031.
17. WangSQ, Cui SX, Qu XJ. Metformin inhibited colitis and colitis-associated cancer (CAC) through protecting mitochondrial structures of colorectal epithelial cells in mice. Cancer Biol Ther. 2019; 20(3): 338-348.
18. Pandey A, Verma S, Kumar VL. Metformin maintains mucosal integrity in experimental model of colitis by inhibiting oxidative stress and pro-inflammatory signaling. Biomed Pharmacother. 2017; 94: 1121-1128.
19. Xiao Z, Wu W, Poltoratsky V. Metformin suppressed CXCL8 expression and cell migration in HEK293/TLR4 cell line. Mediators Inflamm. 2017; 2017: 6589423.
20. Karnewar S, Neeli PK, Panuganti D, Kotagiri S, Mallappa S, Jain N, et al. Metformin regulates mitochondrial biogenesis and senescence through AMPK mediated H3K79 methylation: Relevance in age-associated vascular dysfunction. Biochim Biophys Acta Mol Basis Dis. 2018; 1864(4 Pt A): 1115-11128.
21. Han X, Wang B, Sun Y, Huang J, Wang X, Ma W, et al. Metformin modulates hight glucose- incubated human umbilical vein endothelial cells proliferation and apoptosis through AMPK/CREB/BDNF pathway. Front Pharmacol. 2018; 9: 1266.
22. Liang CC, Park AY, Guan JL. In vitro scratch assay: a convenient and inexpensive method for analysis of cell migration in vitro. Nat Protoc. 2007; 2(2): 329-333.
23. Pinheiro AR, Paramos-de-Carvalho D, Certal M, Costa MA, Costa C, Magalhães-Cardoso MT, et al. Histamine induces ATP release from human subcutaneous fibroblasts via pannexin-1 hemichannels leading to Ca2+ mobilization and cell proliferation. J Biol Chem. 2013; 288(38): 27571-27583.
24. LiZ, Ding Q, Ling LP, Wu Y, Meng DX, Li X, et al. Metformin attenuates motility, contraction, and fibrogenic response of hepatic stellate cells in vivo and in vitro by activating AMP-activated protein kinase. World J Gastroenterol. 2018; 24(7): 819-832.
25. Arunachalam G, Samuel SM, Marei I, Ding H, Triggle CR. Metformin modulates hyperglycemia-induced endothelail senescence and apoptosis through SIRT1. Br J Pharmacol. 2014; 171(2): 523-535.
26. Cittadini A, Napoli R, Monti MG, Rea D, LongobardiS, Netti PA, et al. Metformin prevents the development of chroni heart failure in the SHHF rat model. Diabetes. 2012; 61(4): 944-953.
27. Goggi JL, Haslop A, Boominathan R, Chan K, Soh V, Cheng P, et al. Imaging the proangiogenic effects of cardiovascular drugs in a diabetic model of limb ischemia. Contrast Media Mol Imaging. 2019; 2019: 2538909.
28. Bakhashab Sh, Ahmed F, Schulten HJ, Ahmed FW, Glanville M, Al-Qahtani MH, et al. Proangiogenic effect of metformin in endothelial cells is via upregulation of VEGFR1/2 and their signaling under hyperglycemia-hypoxia. Int J Mol Sci. 2018; 19(1): 293.
29. Hills C, Price GW, Wall MJ, Kaufmann TJ, Tang SCW, Yiu WH, et al. Transforming growth factor beta 1 drives a switch in connexin mediated cell-to-cell communication in tubular cells of the diabetic kidney. Cell Physiol Biochem. 2018; 45(6): 2369-2388.
30. Iwata N, Hasegawa T, Fujita S, Nagao S, Nakano Y, Nada T, et al. Effect of the interaction of metformin and bone morphogenetic proteins on ovarian steroidogenesis by human granulosa cells. Biochem Biophys Res Commun. 2018; 503(3): 1422-1427.
31. Li A, ZhangX, Shu M , Wu M, Wang J, Zhang J, et al. Arctigenin suppresses renal interstitial fibrosis in a rat model of obstructive nephropathy. Phytomedicine. 2017; 30: 28-41.
32. Dolinar K, Jan V, Pavlin M, Chibalin AV, Pirkmajer S. Nucleosides block AICAR-stimulated activation of AMPK in skeletal muscle and cancer cells. Am J Physiol Cell Physiol. 2018; 315(6): 803-817.
33. Faubert B, Boily G, Izreig S, Griss T, Samborska B, Dong Z, et al. AMPK is a negative regulator of the Warburg effect and suppresses tumor growth in vivo. Cell Metab. 2013; 17(1): 113-124.
34. Theodoropoulou S, Brodowska K, Kayama M, Morizane Y, Miller JW, Gragoudas ES, et al. Aminoimidazole carboxamide ribonucleotide (AICAR) inhibits the growth of retinoblastoma in vivo by decreasing angiogenesis and inducing apoptosis. PLoS One. 2013; 8(1): e52852.
35. Woodard J , Platanias LC . AMP-activated kinase (AMPK)-generated signals in malignant melanoma cell growth and survival. Biochem Biophys Res Commun. 2010; 398(1): 135-139.
36. Choi HJ, Kim TY, Chung N, Yim JH, Kim WG, Kim JA, et al.The influence of the BRAF V600E mutation in thyroid cancer cell lines on the anticancer effects of 5- aminoimidazole-4-carboxamide-ribonucleoside. J Endocrinol. 2011; 211(1): 79-85.
37. Liu J, Li M, Song B, Jia C, Zhang L, Bai X ,et al. Metformin inhibits renal cell carcinoma in vitro and in vivo xenograft. Urol Oncol. 2013; 31(2): 264-270.
38. Kim YM, Kim MY, Kim HJ, Roh GS, Ko GH, Seo HG, et al. Compound C independent of AMPK inhibits ICAM-1 and VCAM-1 expression in inflammatory stimulants-activated endothelial cells in vitro and in vivo. Atherosclerosis. 2011; 219(1): 57-64.
39. Chen SC, Brooks R, Houskeeper J, Bremner SK, Dunlop J, Viollet B, et al. Metformin suppresses adipogenesis through both AMP-activated protein kinase (AMPK)-dependent and AMPK-independent mechanisms. Mol Cell Endocrinol. 2017; 440: 57-68.
40. Rena G, Hardie DG. Pearson ER. The mechanisms of action of metformin. Diabetologia. 2017; 60(9): 1577-1585.

Original Article

Cardioprotective Effect of Quercetin against Ischemia/Reperfusion Injury Is Mediated Through NO System and Mitochondrial K-ATP Channels

Ying Liu, M.D., Yi Song, M.D., Siyuan Li, M.D., Li Mo, M.D.*

The Center of Gerontology and Geriatrics, West China Hospital, Sichuan University, Chengdu, Sichuan, China

Corresponding Address: The Center of Gerontology and Geriatrics, West China Hospital, Sichuan University, No. 37 Guoxue Lane, Chengdu, Sichuan, 610041, China
Email: molihxyy@sina.com

Received: 23/September/2019, Accepted: 30/October/2019

Abstract

Objective: Quercetin (Que) is a plant-derived polyphenolic compound, that was shown to possess anti-inflammatory activity in myocardial ischemia/reperfusion (I/R) models *in vivo;* however, detailed mechanisms of its anti-inflammatory effects remain unclear. This study aimed to examine the effects of quercetin postconditioning (QPC) on I/R-induced inflammatory response in a rat model and evaluate the role of the mitochondrial K-ATP (mitoK$_{ATP}$) channels and NO system in this regard.

Materials and Methods: In this experimental study, hearts of male Wistar rats (250 ± 20 g) perused by Langendorff apparatus, were subjected to 30 minutes of global ischemia followed by 55 minutes reperfusion, and Que was added to the perfusion solution immediately at the onset of reperfusion. Creatine kinase (CK) levels in the coronary effluent were measured by spectrophotometry. Interleukin-1 (IL-1β), IL-6, and tumor necrosis factor-alpha (TNF-α) levels were analyzed by an enzyme-linked immunosorbent assay (ELISA) rat specific kit to assess the inflammatory condition of the myocardial tissue.

Results: Our results showed that QPC significantly improved left ventricular developed pressure (LVDP) ($P<0.05$), and decreased the CK release into the coronary effluent vs. control group ($P<0.01$). The levels of IL-1β ($P<0.01$), TNF-α ($P<0.01$), and IL-6 ($P<0.05$) were significantly diminished in Que-treated groups when compared to the control group. Inhibiting mitoK$_{ATP}$ channels by 100 μM 5-hydroxydecanoate and blocking NO system by 100 μM L-NAME reversed the cardioprotective effects of Que.

Conclusion: The findings of this study suggested that QPC exerts cardioprotective effects on myocardial I/R injury (MIRI) through inhibition of inflammatory reactions and improvement of contractility potential. Also, mitoK$_{ATP}$ channels and NO system might be involved in this anti-inflammatory effect.

Keywords: Inflammation, Ischemia/Reperfusion, Myocardial Infarction, Nitric Oxide, Quercetin

Cell Journal(Yakhteh), Vol 23, No 2, July 2021, Pages: 184-190

Citation: Liu Y, Song Y, Li S, M.D., Mo L. Cardioprotective effect of quercetin against ischemia/reperfusion injury is mediated through no system and mitochondrial K-ATP channels. Cell J. 2021; 23(2): 184-190. doi: 10.22074/cellj.2021.7183.

Introduction

Acute myocardial infarction (AMI) caused as a result of coronary artery occlusion, is the most common leading cause of death and disability worldwide. At present, timely reperfusion is the major therapeutic strategy to treat myocardial ischemia; however, reperfusion itself further worsens the existent myocardial injury and may lead to extra complications such as diminished cardiac contractile function, arrhythmias, and necrosis of myocytes, a phenomenon termed "myocardial reperfusion injury" (1, 2). Therefore, in medical research, development of interventions capable of both preventing and treating ischemia/reperfusion (I/R) injuries is needed.

I/R is a complicated pathophysiological condition in which, inflammatory response, reactive oxygen-derived species (ROS) overproduction, Ca^{2+} overload, and apoptosis play central roles (3). Myocardial I/R injury (MIRI) is known to result in significant local and systemic inflammation. This inflammatory response which is triggered during ischemia, and greatly amplified during reperfusion, is characterized by increased levels of inflammatory and pro-inflammatory cytokines, including interleukin-1β (IL-1β), tumor necrosis factor-α (TNF-α), IL-6 and partially contributes to cardiac dysfunction and necrosis of cells (4-6). Increasing evidence suggests that inhibition of I/R-induced excessive inflammatory response can improve heart dysfunction caused by I/R injury (7, 8). Hence, understanding the precise mechanism of the inflammatory response is critical to improving clinical outcomes of I/R injury and designing effective therapies.

Mitochondria dysfunction is considered a major cause of cell death during I/R. Several studies demonstrated that a variety of cardioprotective strategies such as pre- and postconditioning, protects cardiomyocytes via the mitochondrial K-ATP (mitoK$_{ATP}$) channel. Activation of mitoK$_{ATP}$ channels maintains the mitochondrial membrane potential ($\Delta\Psi m$), inhibits mitochondrial permeability transition pore (mPTP) opening, and represses mitochondrial Ca^{2+} overload, overproduction of ROS, and necrotic/apoptotic cell death (9-12). The

linkage between mitoK_{ATP} channels opening and such a diverse number of the restorative processes, underscores its promising therapeutic potential in I/R injury; hence, a mitoK_{ATP} opener may improve mitochondrial function during I/R.

Nitric oxide (NO) is an important mediator in the cardiovascular system and I/R injury. Considerable evidence highlighted the beneficial roles of NO in the cardiovascular system and emphasized the link between NO and pathophysiological process of I/R injury in a way that effects of I/R injury are either mediated or antagonized by NO. Indeed, NO has both protective and detrimental role in I/R as I/R triggers a cascade involving increased NO production and leading to the excess formation of peroxynitrite ($ONOO^-$) and it is accompanied by increased production of ROS, which mediates the detrimental role of NO (13, 14). The cardioprotective function of NO during I/R is due to its anti-inflammatory and antioxidant effects; furthermore, protective role of NO may be mediated through activation of the mitoK_{ATP} channels (15, 16).

Quercetin (3,5,7,3',4'-pentahydroxy flavone, Que) is an important member of flavonoids with the highest concentrations being found in onions and apples. A broad range of biological activities has been attributed to Que including anti-inflammatory, antioxidant, and anti-cancer activity (17, 18). Also, Que possesses the capability to reduce blood pressure and protect the heart from I/R injury (19, 20). Several studies indicated that Que postconditioning (QPC) is an effective pharmacological strategy for achieving myocardial protection against I/R injuries; however, its protective mechanism remains unclear (21, 22).

In the present study, we investigated the cardioprotective and anti-inflammatory properties of Que and assumed that these effects were in part mediated through the NO system and mitoK_{ATP} channels.

Materials and Methods

In this experimental study, fifty-six 12-week-old male Wistar rats weighing 250 ± 20 g, were obtained from the animal center of Sichuan University. The rats were kept in an animal room with free access to food and water, at 25˚C on a 12 hours light/dark cycle. This study conformed to the Guidelines for the Care and Use of Laboratory Animals by the National Institutes of Health (NIH Publication No. 85-23, revised in 1985), and the experimental procedures were approved by the Institutional Animal Care and Use Committee (IACUC) of Sichuan University.

Isolated hearts and Langendorff perfusion setting

Animals were anesthetized intraperitoneally (i.p.) with pentobarbital sodium (60 mg/kg) and heparinized (500 U/kg) to protect the heart against microthrombi. The hearts were quickly removed via thoracotomy and immersed in ice-cold Krebs-Henseleit solution (K-H). Then, the hearts were cannulated via the aorta and perfused with K-H solution that contained (in mM): 4.8 KCl, 118 NaCl, 1.0 KH_2PO_4, 1.2 $MgSO_4$, 27.2 $NaHCO_3$, 10 glucose, and 1.25 $CaCl_2$. A mixture of 95% O_2 and 5% CO_2 was bubbled through the perfusate, and the perfusate pH was kept in the range of 7.35-7.45. Throughout the experiment, thermostatically controlled water circulator (Satchwell Sunvic, UK) maintained the perfusate and bath temperatures at 37˚C. For measurement of interventricular pressure changes, a saline-filled latex balloon was inserted into the left ventricle (LV) and the signals were delivered to the related transducer via a connecting pressure catheter. The left ventricular-developed pressure (LVDP) was considered a cardiac contractility index.

Induction of ischemia and reperfusion

Each experiment lasted 100 minutes in total. All groups of isolated rat hearts underwent a 15-minutes stabilization period. In all groups, after the stabilization period, the hearts were exposed to global ischemia for 30 minutes, followed by 55 minutes of reperfusion period with K-H solution at 37˚C. An immediate decline in CF at the onset of index ischemia and the recovery of the CF upon reperfusion served as evidence of effective coronary occlusion and reperfusion (23, 24).

Exclusion criteria

In the Langendorff apparatus, the isolated hearts were excluded from the test if their baseline coronary flow (CF) and LVDP were lower than 7.5 ml/minutes and 70 mmHg, respectively. Also, the hearts with weak contractions or with arrhythmias were excluded from the experiment and replaced with another one. The exclusion (and replacement) rate for groups was as follows: Sham=0; control=1 heart; EL-C receiving group=0; Que receiving groups=1 heart; 5-HD receiving group=2 hearts; Que plus 5-HD receiving group=1 heart; L-NAME receiving group=1 heart; and Que plus L-NAME receiving group=1 heart. The weak contraction or arrhythmias may be related to the failure in surgical procedure.

Experimental protocol

The fifty-six male Wistar rats were divided into eight groups (n=56, 7 per group, Fig.1):

i. Sham: in which the isolated hearts did not undergo ischemia, and were continuously perfused with a normal K-H buffer.

ii. Control: in which after the surgical preparation and 15 minutes stabilization, the isolated hearts were subjected to a 30 minutes ischemia and 55 minutes reperfusion with a normal K-H buffer.

iii. Cremophor-EL: in which the condition was similar to the control group except that the hearts were perfused with a K-H solution containing 0.1 % Cremophor-EL for 10 minutes at the onset of reperfusion.

iv. Quercetin: in which the condition was similar to control group except that the hearts were perfused with a K-H solution containing 100 nM Que for 10 minutes at

the onset of reperfusion.

v. 5-HD: in which the condition was similar to control group except that the hearts were perfused with a K-H solution containing 100 μM 5-hydroxydecanoate (5-HD, as a mitoK_{ATP} channel blocker) for 10 minutes at the onset of reperfusion.

vi. Quercetin plus 5-HD: in which the condition was similar to the control group except that the hearts were perfused with a K-H solution containing both 100 μM 5-HD and then, 100 nM Que, for 10 minutes at the onset of reperfusion.

vii. L-NAME: in which the condition was similar to the control group except that the hearts were perfused with a K-H solution containing 100 μM L-NAME (as a NO synthase blocker) for 10 minutes at the onset of reperfusion.

viii. Quercetin plus L-NAME: in which the condition was similar to the control group except that the hearts were perfused with a K-H solution containing both 100 μM L-NAME and then, 100 nM Que, for 10 minutes at the onset of reperfusion.

There were no significant differences between EL-C and control groups. Due to this reason we did not consider Cremophor-EL group in the analysis of results.

Creatine kinase release measurement

The coronary effluent was collected 10 minutes after the beginning of reperfusion, and samples were stored at -80˚C. Ischemic injury was measured based on the creatine kinase (CK-MB) activity. The CK-MB activity was determined spectrophotometrically by using commercial kits brought from Roche Diagnostic (Mannheim, Germany). The absorbance of CK-MB solution was read at 340 nm. The results were reported in Unit/l.

Preparation of tissue homogenates

At the end of each experiments, the hearts (LVs) were separated and the ischemic zones were sampled, immediately frozen in liquid nitrogen and stored at -80˚C. Approximately 0.5 g of ventricular tissue was cut into pieces in about 5 ml of ice-cold lysis buffer containing (mM/ml): 1.0 KH_2PO_4, 1.0 KCL, 50 Tris-HCl (pH=7.4), 1.0 EDTA, 1.0 NaF, 1.0 Na_3VO_4, and 1% Triton 100X and protease inhibitor cocktail (Sigma-Aldrich, USA) and then homogenized with a Polytron PT-10/ST homogenizer. The homogenates underwent centrifugation at 10,000 g for 10 minutes at 4˚C. The obtained supernatants were removed from the homogenates quickly frozen at -80˚C. The Bradford method was used for determination of the concentration of proteins and cytokine activity in supernatants.

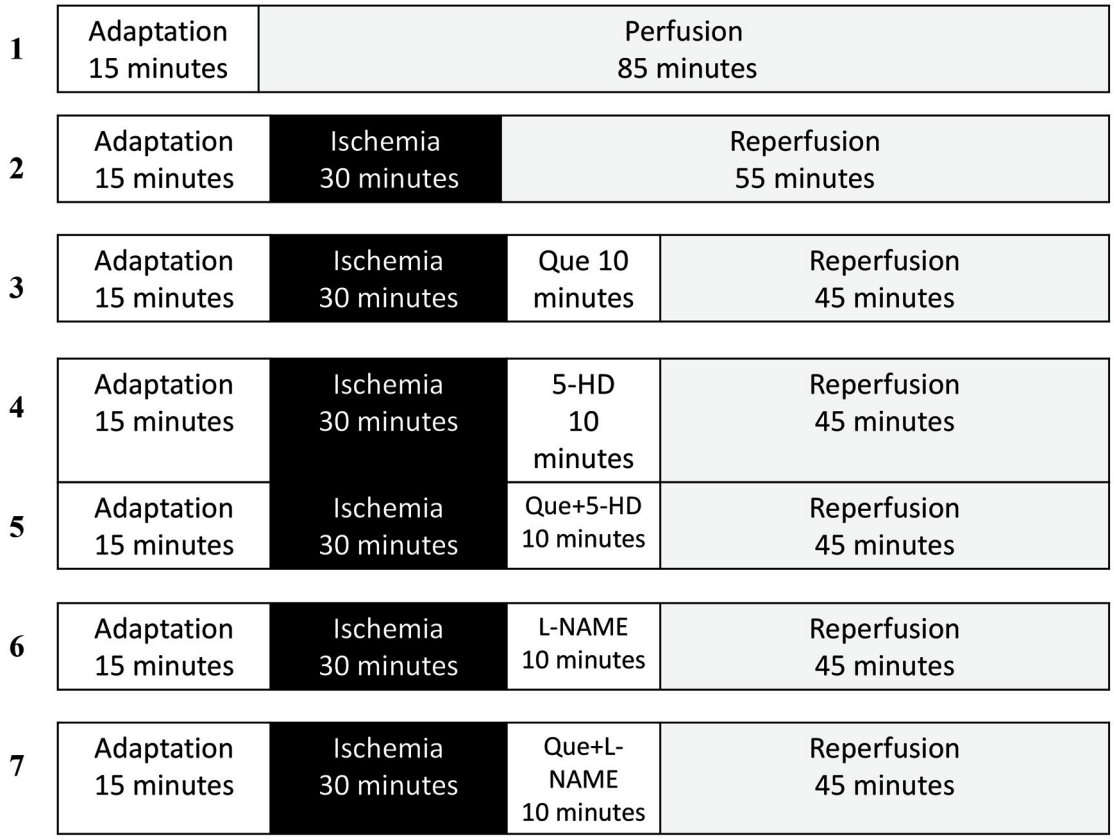

Fig.1: Experimental protocol. Except the Sham, which was perfused constantly for 85 minutes, the remaining hearts were subjected to 30 minutes of global ischemia followed by 55 minutes of reperfusion. 100 nM of Que was administered for 10 minutes at the onset of reperfusion. 5-HD (100 μM) or L-NAME (100 μM) was also administered for 10 minutes at the onset of reperfusion with Que absence or presence (n=7 per group). Que; Querctin, 5-HD (5-hydroxydecanoate); mitoK_{ATP} channel blocker, and L-NAME (L-nitro-arginine methyl ester); NO synthase blocker.

ELISA for measurement of tissue levels of cytokines

The supernatant levels of IL-1β, TNF-α, and IL-6 were determined using an enzyme-linked immunosorbent assay (ELISA) rat specific kit according to the manufacturer's protocol (Bender Medsystems, Austria). Pro-inflammatory cytokines concentrations were quantified relative to a standard curve. The optical density (OD) of each well was read at a wavelength of 450 nm. TNF-α, IL-1β, and IL-6 levels were expressed as picograms per milligram of total protein.

Statistical analysis

Data are presented as means ± standard deviation (SD). Statistical comparisons between experimental groups were made using ANOVA with Tukey multiple comparison test. A $P<0.05$ was considered statistically significant.

Results

Quercetin postconditioning improved cardiac contractility during myocardial ischemia/reperfusion

LVDP was applied to evaluate alterations in cardiac function. Induction of global ischemia for 30 minutes resulted in a significant decrease of LVDP in the experimental groups compared with ischemic values (Fig.2). In the 10th minute of reperfusion, the recovery of the cardiac function was increased after the administration of Que to the perfusion solution in the Que-treated group against rats that were not treated with Que (control or 5HD-treated, L-NAME treated, respectively). The LVDP was significantly higher in the Que-receiving group as compared with the control group ($P<0.05$). The recovery of myocardial function due to QPC was completely abolished by 5-HD. Similarly, administration of L-NAME eliminated the effects of QPC on LVDP.

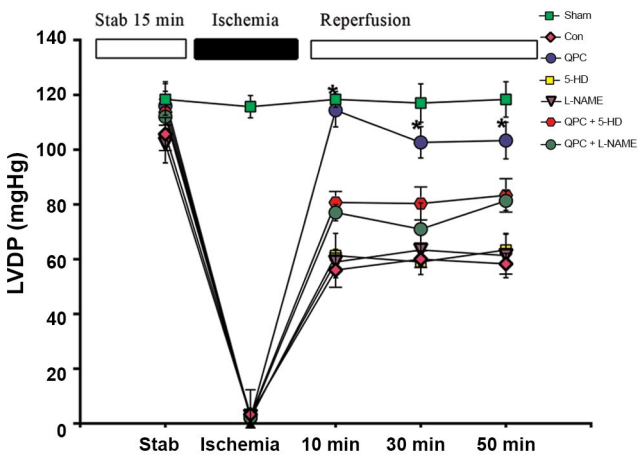

Fig.2: Left ventricular developed pressure (LVDP) changes in all experimental groups. The data were expressed as mean ± SD (n=7 per group). QPC; Quercetin postconditioning, *; $P<0.05$ QPC vs. control group, and min; Minutes.

Quercetin postconditioning decreased the release of creatine kinase during myocardial ischemia/reperfusion

The activities of CK were used to assess the injury of the myocardium. Levels of CK in the coronary effluent in I/R group were significantly increased compared with the sham group ($P<0.01$). The increased levels of CK were significantly attenuated by QPC ($P<0.01$, Fig.3). The effects of Que were abolished by the addition of the NO inhibitor, L-NAME, and the mitoK$_{ATP}$ channel blocker, 5-HD. However, there was no significant difference in CK level between the control, and 5-HD group and L-NAME group and 5-HD+QPC group, L-NAME+QPC group.

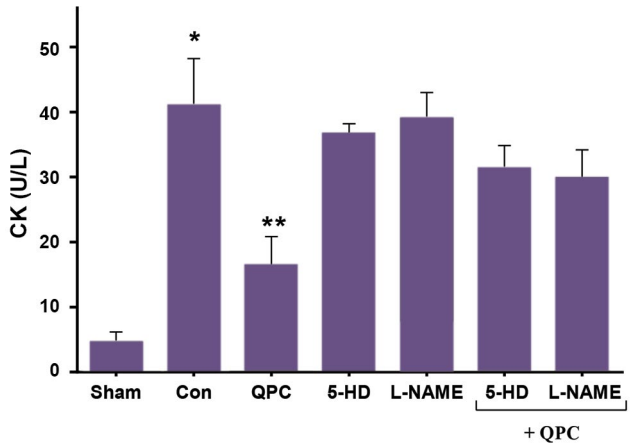

Fig.3: CK release during reperfusion 10 minutes in each experimental group. Data are presented as mean ± SEM (n=7 per group). *; $P<0.01$ vs. Sham group; **; $P<0.01$ vs. control, QPC; Quercitin postconditioning, 5-HD; mitoK$_{ATP}$ channel blocker, L-NAME; NO synthase blocke, CK; Creatine kinase, and Con; Control.

Quercetin postconditioning decreased tissue levels of tumor necrosis factor-alpha during myocardial ischemia/reperfusion

The results are shown in Figure 4. TNF-α level in the QPC group was significantly ($P<0.01$) decreased compared to the control group, and similar results were seen for 5-HD+QPC, L-NAME+QPC groups compared with the control group ($P<0.05$). Blocking the mitoK$_{ATP}$ channels using 5-HD and blocking the mitoK$_{ATP}$ channels using 5-HD, did not reverse the TNF-α-lowering influence of Que.

Quercetin postconditioning decreased tissue levels of IL-6 during myocardial ischemia/reperfusion

QPC caused a statically significant decrease in the IL-6 level in the Que-treated group vs. untreated control hearts ($P<0.05$, Fig.5). No significant difference was

observed between 5-HD+ QPC, L-NAME+QPC groups and untreated control hearts during reperfusion.

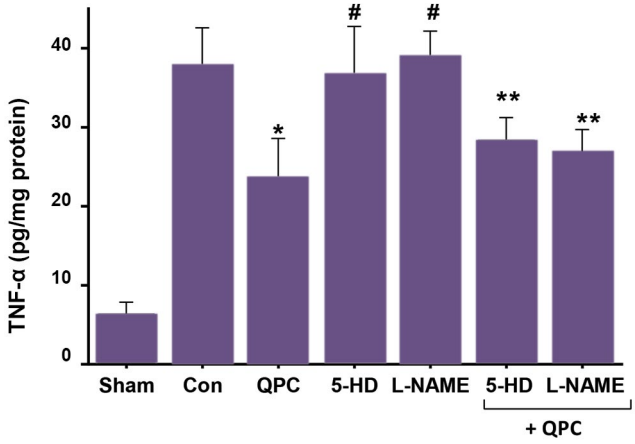

Fig.4: TNF-α level after reperfusion in each experimental group. Data are presented as mean ± SEM (n=7 per group). *; P<0.01 vs. control group, #; P<0.05 vs. QPC; **; P<0.05 vs. control group. QPC; Quercitin postconditioning, 5-HD; mitoK$_{ATP}$ channel blocker, L-NAME; NO synthase blocker, TNF-α; Tumor necrosis factor-alpha, and Con; Control.

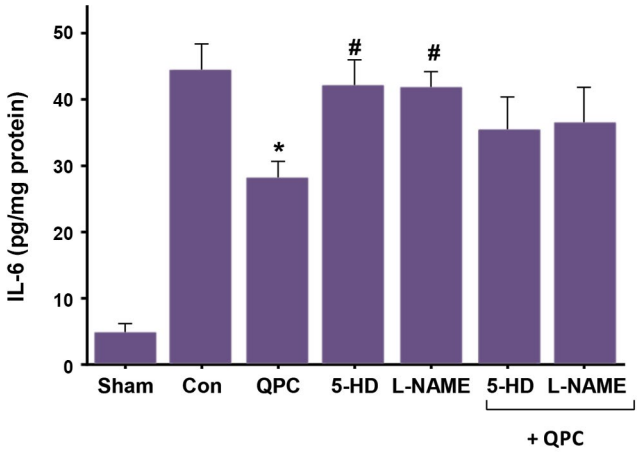

Fig.5: IL-6 level after reperfusion in each experimental group. Data are presented as mean ± SEM (n=7 per group).*; P<0.05 vs. control group, #; P<0.05 vs. QPC, QPC; Quercitin postconditioning, 5-HD; mitoK$_{ATP}$ channel blocker, L-NAME; NO synthase blocker, IL-6; Interleukin-6, and Con; Control.

Quercetin postconditioning decreased tissue levels of IL-1β during myocardial ischemia/reperfusion

QPC significantly reduced the IL-1β level in the treated group compared with control hearts that were not treated with Que (P<0.05, Fig.6). No significant difference was observed between 5-HD+QPC, L-NAME+QPC groups and untreated control hearts during reperfusion.

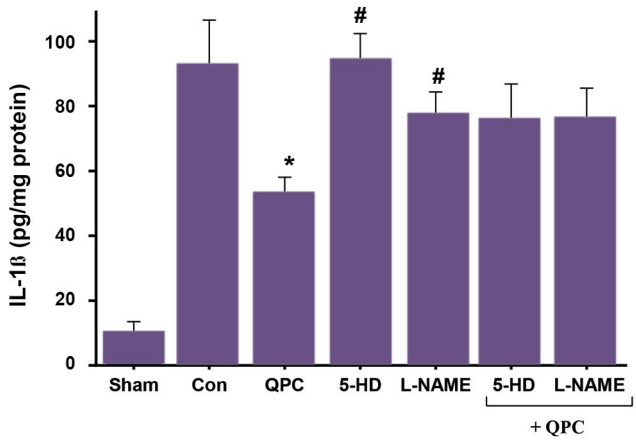

Fig.6: IL-1β level after reperfusion in each experimental group. Data are presented as mean ± SEM (n=7 per group). *; P<0.01 vs. control group, #; P<0.05 vs. QPC, QPC; Quercitin postconditioning, 5-HD; mitoK$_{ATP}$ channel blocker, L-NAME; NO synthase blocker, IL-1β; Interleukin-1β, and Con; Control.

Discussion

Previous studies documented a wide range of beneficial effects of Que on the cardiovascular system, such as blood pressure, left ventricular hypertrophy and myocardial I/R. In the present study, we used a rat model of MIRI to examine the protective effect of QPC against inflammatory response induced by I/R injury. We observed that QPC significantly improves decreased LVDP levels, and attenuates increased CK and pro-inflammatory cytokine levels induced by I/R injury. Importantly, the mitoK$_{ATP}$ channels inhibitor, 5-HD and NO inhibitor, L-NAME reversed the QPC protective effect on MIRI, indicating that mitoK$_{ATP}$ channel and NO activation could play a critical role in this regard.

In the present study, QPC significantly reduced IL-1, IL-6, and TNF-a levels compared with the untreated control group. Our results about anti-inflammatory properties of Que are consistent with a previous study done by Dong et al. (25) which indicated that Que attenuated inflammatory cytokines such as TNF-α, IL-6 and IL-1β in serum and cell supernatants in the rat heart model of I/R injury. Hong-Bo Jin showed that Que treatment inhibits inflammatory responses during MIRI through ameliorating the expression of both TNF-α and IL-10 and decreasing the levels of inflammatory cytokines in serum and cell supernatants (26). Liu et al. (19) indicated that pre-treatment with Que decreased the levels of C-reactive protein (CRP), IL-1β and TNF-α in a myocardial ischemia injury rat model. Thus, inhibitory effects of Que on the pro-inflammatory cytokines production may be a mechanism through which Que protects the heart against I/R injury.

Reperfusion of ischemic myocardium leads to an overproduction of ROS. I/R-mediated overproduction of ROS is also important for induction of inflammatory response in the infarcted myocardium (6, 27). Inflammatory reaction plays an important role in MIRI. Accumulating evidence indicated that the inflammatory response promotes the release of TNF-α from the ischemic tissue.

The secreted TNF-α further stimulates the release of pro-inflammatory cytokines from infiltrating neutrophils and macrophages and produces more pro-inflammatory cytokines, such as IL-6 and chemokines (21, 28). IL-6 contributes to the extent of infarct size in the early phase of myocardial I/R (29). Also, a high levels of pro-inflammatory cytokines, such as TNF-α and IL-1β during acute myocardial ischemia, lead to exaggerated cardiac functional depression and cardiomyocyte apoptosis (30). Reducing the levels of inflammatory cytokines (IL-6, IL-1β, and TNF-α) could protect hearts against MIRI (31). These results demonstrate that ischemia-induced inflammatory response leads to apoptosis in cardiomyocytes, and inhibition of inflammatory response protects hearts from ischemia injury. Therefore, strategies limiting the inflammatory response has become one of the useful therapeutic adjuncts in the clinical treatment of MIRI. It is important to reduce the production of ROS by natural antioxidants such as Que because elevated levels of ROS have been the focus of considerable attention as initiators of inflammatory response. Mitochondria are widely recognized as the main source of these ROS (32).

Several studies confirmed that conditioning strategy and pharmacological interventions mediate myocardial protection by attenuating mitochondrial dysfunction and ROS generation (9, 33). mitoK$_{ATP}$ channels have been reported to play a key role in conditioning mediating protection (10, 34). Opening these channels modulates the synthesis of ROS and prevents Ca^{2+} overload, mitochondrial dysfunction and cell death (9, 10). In addition, it was shown that oral administration of rats with a low dose of Que exerted cardioprotective effects in isolated rat heart models during I/R injury and these protective effects of Que may be mediated through improving mitochondrial function (35). Que is known to attenuate ROS generation and protect cardiomyocytes against I/R injury (36, 37). In this study, the anti-inflammatory effects of QPC were abolished by mitoK$_{ATP}$ channels blockade, which indicates that the anti-inflammatory effect of QPC is mediated, in part, by activation of mitoK$_{ATP}$ channels. Consequently, since mitochondrial ROS greatly induced inflammatory responses, inhibitory effects of Que on inflammatory response may be at least partly due to attenuation of mitochondrial ROS generation (essentially, through increasing the activation of mitoK$_{ATP}$ channels).

NO is another mediator that influences many aspects of physiological processes including inflammatory response, during MIRI (38). Although NO has been recognized as a potent biological active molecule for a variety of cardioprotective effects such as cardiac contractility and regulation of vasodilation, NO actually has both protective and detrimental role in myocardial I/R (13). In response to myocardial ischemia, enhanced amount of NO contributed to the formation of potent oxidative species peroxynitrite, the reaction product of NO with superoxide anions, which subsequently leads to significantly severe myocardial damage and mediated the detrimental role of NO (14). In contrast, NO is a reactive oxygen scavenger and by this action, increases antioxidant defenses; furthermore, NO plays a critical role in defense against MIRI through inhibition of respiratory chain. Inhibition of mitochondrial respiration by NO results in decreased oxygen-derived free radicals (16). Another mechanism that might be involved in the cardioprotective effects of NO during I/R injury is that NO increased the activity of the mitoK$_{ATP}$ channels (39, 40). Studies suggested that the activity of the mitoK$_{ATP}$ channel was increased directly by NO.

Independently, NO could activate GC/cGMP/PKG pathway and thereby leading to the mitoK$_{ATP}$ channel activation (16, 40). Based on the above, NO, with its role in producing ROS, may be involved in the induction of inflammatory response during I/R injury. Our results showed that blocking NO system reversed the anti-inflammatory effect of Que. The reason for the observed results could be that Que inhibits several enzymes that are involved in the generation of superoxide anions such as xanthine oxidase. Additionally, in rabbit hearts exposed to I/R injury, Que could reduce protein and mRNA expressions of NADPH oxidase 2 and inducible NO synthase (iNOS) (40). It was shown that Que modulated eNOS expression in rat isolated aorta and Que-supplemented diet modulated the expression and/or activity of specific proteins NOX, thereby leading to increased NO bioavailability in the heart of NO-deficient rats. Also, Que scavenges superoxide anion by scavenging superoxide radicals the bioavailability of NO improves. On the other hand, Que inhibits the expression of enzymes involved in ROS generation and by this action, prevents the superoxide-mediated NO inactivation. Therefore, Que increases the bioavailability of NO, thereby it may intensify the activation of mitoK$_{ATP}$ channels and ultimately leads to reduction of ROS generation. However, we did not detect the effect of mitoK$_{ATP}$ channel blockade with 5-HD and NO system blockade with L-NAME on the reducing effect of Que on TNF-α. We hypnotized that there were other possible molecular mechanisms involved in this event.

Conclusion

Our results showed that Que improved cardiac function in rats with cardiac I/R injury. The level of pro-inflammatory cytokines (TNF-α, IL-6, and IL-1) and the level of CK-MB were significantly decreased in the Que-treated group as compared with the control group. Reduction of the inflammatory response by Que is associated with its cardioprotective effects during I/R injury. The anti-inflammatory effects of Que are exerted partly through the mitoK$_{ATP}$ channels and NO system.

Acknowledgments

This study was supported by a grant from National Clinical Research Center of Geriatrics, West China Hospital (201700099.NCRCGH). There is no conflict of interest in this study.

Authors' Contributions

L.M.; Participated in study design, contributed extensively in interpretation of the data and the conclusion. Y.L., S.L.; Performed all experiments and drafting. Y.S.; Critical revision and statistical analysis. All authors performed editing and approving the final version of this manuscript for submission, also participated in the finalization of the manuscript and approved the final draft.

References

1. Garcia-Dorado D, Rodríguez-Sinovas A, Ruiz-Meana M, Inserte J. Protection against myocardial ischemia-reperfusion injury in clinical practice. Rev Esp Cardiol (Engl Ed). 2014; 67(5): 394-404.
2. Pasqualin RC, Auler Jr JOC. Myocardial protection by pre-and post-anesthetic conditioning. Rev Bras Anestesiol. 2008; 58(5): 512-519, 506-512.
3. Kalogeris T, Baines CP, Krenz M, Korthuis RJ. Ischemia/reperfusion. Compr Physiol. 2016; 7(1): 113-170.
4. Han J, Wang D, Ye L, Li P, Hao W, Chen X, et al. Rosmarinic acid protects against inflammation and cardiomyocyte apoptosis during myocardial ischemia/reperfusion injury by activating peroxisome proliferator-activated receptor gamma. Front Pharmacol. 2017; 8: 456.
5. Bakhta O, Blanchard S, Guihot AL, Tamareille S, Mirebeau-Prunier D, Jeannin P, et al. Cardioprotective role of colchicine against inflammatory injury in a rat model of acute myocardial infarction. J Cardiovasc Pharmacol Ther. 2018; 23(5): 446-455.
6. Frangogiannis NG. The inflammatory response in myocardial injury, repair, and remodelling. Nat Rev Cardiol. 2014; 11(5): 255-265.
7. Loubele STBG, Spek CA, Leenders P, van Oerle R, Aberson HL, Hamulyák K, et al. Activated protein C protects against myocardial ischemia/reperfusion injury via inhibition of apoptosis and inflammation. Arterioscler Thromb Vasc Biol. 2009; 29(7): 1087-1092.
8. Mohammadzadeh R, Baradaran B, Valizadeh H, Yousefi B, Zakeri-Milani P. Reduced ABCB1 expression and activity in the presence of acrylic copolymers. Adv Pharm Bull. 2014; 4(3): 219-224.
9. Jin C, Wu J, Watanabe M, Okada T, Iesaki T. Mitochondrial K+ channels are involved in ischemic postconditioning in rat hearts. J Physiol Sci. 2012; 62(4): 325-332.
10. McCully JD, Levitsky S. The mitochondrial K(ATP) channel and cardioprotection. Ann Thorac Surg. 2003; 75(2): S667-S673.
11. Halestrap AP, Clarke SJ, Khaliulin I. The role of mitochondria in protection of the heart by preconditioning. Biochim Biophys Acta. 2007; 1767(8): 1007-1031.
12. Mykytenko J, Reeves JG, Kin H, Wang NP, Zatta AJ, Jiang R, et al. Persistent beneficial effect of postconditioning against infarct size: role of mitochondrial K(ATP) channels during reperfusion. Basic Res Cardiol. 2008; 103(5): 472-484.
13. Yu X, Ge L, Niu L, Lian X, Ma H, Pang L. The dual role of inducible nitric oxide synthase in myocardial ischemia/reperfusion injury: friend or foe? Oxid Med Cell Longev. 2018; 2018: 8364848.
14. Liu P, Hock CE, Nagele R, Wong PY. Formation of nitric oxide, superoxide, and peroxynitrite in myocardial ischemia-reperfusion injury in rats. Am J Physiol. 1997; 272(5 Pt 2): H2327-H2336.
15. Walewska A, Szewczyk A, Koprowski P. Gas signaling molecules and mitochondrial potassium channels. Int J Mol Sci. 2018; 19(10): 3227.
16. Ferdinandy P, Schulz R. Nitric oxide, superoxide, and peroxynitrite in myocardial ischaemia-reperfusion injury and preconditioning. Br J Pharmacol. 2003; 138(4): 532-543.
17. Darband SG, Kaviani M, Yousefi B, Sadighparvar S, Pakdel FG, Attari JA, et al. Quercetin: a functional dietary flavonoid with potential chemo-preventive properties in colorectal cancer. J Cell Physiol. 2018; 233(9): 6544-6560.
18. Yousefi B, Abasi M, Mesgari Abbasi M, Jahanban-Esfahlan R. Antiproliferative properties of Cornus mass fruit in different human cancer cells. Asian Pac J Cancer Prev. 2015; 16(14): 5727-5731.
19. Liu H, Guo X, Chu Y, Lu S. Heart protective effects and mechanism of quercetin preconditioning on anti-myocardial ischemia reperfusion (IR) injuries in rats. Gene. 2014; 545(1): 149-155.
20. Perez-Vizcaino F, Duarte J, Jimenez R, Santos-Buelga C, Osuna A. Antihypertensive effects of the flavonoid quercetin. Pharmacol Rep. 2009; 61(1): 67-75.
21. Yousefi B, Samadi N, Ahmadi Y. Akt and p53R2, partners that dictate the progression and invasiveness of cancer. DNA Repair (Amst). 2014; 22: 24-29.
22. Montazami N, Kheir Andish M, Majidi J, Yousefi M, Yousefi B, Mohamadnejad L, et al. siRNA-mediated silencing of MDR1 reverses the resistance to oxaliplatin in SW480/OxR colon cancer cells. Cell Mol Biol (Noisy-le-grand). 2015; 61(2): 98-103.
23. Kim TH, Lee SM. The effects of ginseng total saponin, panaxadiol and panaxatriol on ischemia/reperfusion injury in isolated rat heart. Food Chem Toxicol. 2010; 48(6): 1516-1520.
24. Badalzadeh R, Mohammadi M, Najafi M, Ahmadiasl N, Farajnia S, Ebrahimi H. The additive effects of ischemic postconditioning and cyclosporine-A on nitric oxide activity and functions of diabetic myocardium injured by ischemia/reperfusion. J Cardiovasc Pharmacol Ther. 2012; 17(2): 181-189.
25. Dong LY, Chen F, Xu M, Yao LP, Zhang YJ, Zhuang Y. Quercetin attenuates myocardial ischemia-reperfusion injury via downregulation of the HMGB1-TLR4-NF-κB signaling pathway. Am J Transl Res. 2018; 10(5): 1273-1283.
26. Jin HB, Yang YB, Song YL, Zhang Yc, Li YR. Protective roles of quercetin in acute myocardial ischemia and reperfusion injury in rats. Mol Biol Rep. 2012; 39(12): 11005-11009.
27. Chandrasekar B, Smith JB, Freeman GL. Ischemia-reperfusion of rat myocardium activates nuclear factor-kappaB and induces neutrophil infiltration via lipopolysaccharide-induced CXC chemokine. Circulation. 2001; 103(18): 2296-2302.
28. Ahn J, Kim J. Mechanisms and consequences of inflammatory signaling in the myocardium. Curr Hypertens Rep. 2012; 14(6): 510-516.
29. Jong WMC, Ten Cate H, Linnenbank AC, de Boer OJ, Reitsma PH, de Winter RJ, et al. Reduced acute myocardial ischemia–reperfusion injury in IL-6-deficient mice employing a closed-chest model. Inflamm Res. 2016; 65(6): 489-499.
30. Rutschow S, Li J, Schultheiss HP, Pauschinger M. Myocardial proteases and matrix remodeling in inflammatory heart disease. Cardiovasc Res. 2006; 69(3): 646-656.
31. Xu T, Qin G, Jiang W, Zhao Y, Xu Y, Lv X. 6-Gingerol protects heart by suppressing myocardial ischemia/reperfusion induced inflammation via the PI3K/Akt-dependent mechanism in rats. Evid Based Complement Alternat Med. 2018; 2018: 6209679.
32. Muntean DM, Sturza A, Dănilă MD, Borza C, Duicu OM, Mornoș C. The role of mitochondrial reactive oxygen species in cardiovascular injury and protective strategies. Oxid Med Cell Longev. 2016; 2016: 8254942.
33. Zhou T, Prather ER, Garrison DE, Zuo L. Interplay between ROS and antioxidants during ischemia-reperfusion injuries in cardiac and skeletal muscle. Int J Mol Sci. 2018; 19(2): 417.
34. Schmidt MR, Smerup M, Konstantinov IE, Shimizu M, Li J, Cheung M, et al. Intermittent peripheral tissue ischemia during coronary ischemia reduces myocardial infarction through a KATP-dependent mechanism: first demonstration of remote ischemic perconditioning. Am J Physiol Heart Circ Physiol. 2007; 292(4): H1883-H1890.
35. Brookes PS, Digerness SB, Parks DA, Darley-Usmar V. Mitochondrial function in response to cardiac ischemia-reperfusion after oral treatment with quercetin. Free Radic Biol Med. 2002; 32(11): 1220-1228.
36. Annapurna A, Reddy CS, Akondi RB, Rao SRC. Cardioprotective actions of two bioflavonoids, quercetin and rutin, in experimental myocardial infarction in both normal and streptozotocin-induced type I diabetic rats. J Pharm Pharmacol. 2009; 61(10): 1365-1374.
37. Shao ZH, Vanden Hoek TL, Qin Y, Becker LB, Schumacker PT, Li CQ, et al. Baicalein attenuates oxidant stress in cardiomyocytes. Am J Physiol Heart Circ Physiol. 2002; 282(3): H999-H1006.
38. Qiao SG, Sun Y, Sun B, Wang A, Qiu J, Hong L, et al. Sevoflurane postconditioning protects against myocardial ischemia/reperfusion injury by restoring autophagic flux via an NO-dependent mechanism. Acta Pharmacol Sin. 2019; 40(1): 35-45.
39. Wang Y, Ahmad N, Kudo M, Ashraf M. Contribution of Akt and endothelial nitric oxide synthase to diazoxide-induced late preconditioning. Am J Physiol Heart Circ Physiol. 2004; 287(3): H1125-H1131.
40. Heusch G, Boengler K, Schulz R. Cardioprotection: nitric oxide, protein kinases, and mitochondria. Circulation. 2008; 118(19): 1915-1919.

Original Article

Anti-Atherosclerotic Effect of Afrocyclamin A against Vascular Smooth Muscle Cells Is Mediated via p38 MAPK Signaling Pathway

Yan Gu, M.M.[1*], Zhanzhan Xiao, B.Sc.[2], Jianlie Wu, M.M.[3], Mingjin Guo, M.D.[3], Ping Lv, B.Sc.[4], Ning Dou, M.M.[5]

1. Department of Vascular Surgery, Tianjin First Center Hospital, Tianjin, China
2. Department of Emergency Services, The Fourth People's Hospital of Jinan City, Jinan, Shandong Province, China
3. Department of Vascular Surgery, The Affiliated Hospital of Qingdao University, Qingdao City, China
4. Department of Hematology, The Fourth People's Hospital of Jinan City, Jinan, Shandong Province, China
5. Department of General Surgery, Shanghai Fourth People's Hospital Affiliated to Tongji University School of Medicine, Shanghai, China

Corresponding Address: Department of Vascular Surgery, Tianjin First Center Hospital, Tianjin, China
Email: 18291939982@sina.com

Received: 10/September/2019, Accepted: 19/July/2020

Abstract

Objective: Research suggests that fine particulate matter (PM2.5) contributes to the expansion and development of atherosclerosis. Infiltration and proliferation of vascular smooth muscle cells (VSMCs) from the blood vessel media into the intima, is an important step in the atherosclerosis pathophysiology. Afrocyclamin A, is an oleanane-type triterpene saponin, isolated from *Androsace umbellate*, which is commonly used in Chinese herbal medicine. In the study, we examined the effect of Afrocyclamin A on PM2.5-induced VSMCs proliferation and scrutinized possible mechanisms of action.

Materials and Methods: In the experimental study, counting Kit-8 (CCK-8) assay was used for estimation of VSMCs viability. BrdU immunofluorescence was used for estimation of VSMCs proliferation. The levels of antioxidant parameters such as malonaldehyde (MDA), superoxide dismutase (SOD), and glutathione (GSH); proinflammatory cytokines such as interleukin-1β (IL-1β), IL-6, tumor necrosis factor-α (TNF-α), nitric oxide (NO), endothelin-1 (ET-1), and vascular cell adhesion molecule-1 (VCAM-1), were estimated. The expression of proliferating cell nuclear antigen (PCNA) and phospho-p38 MAPK (p-p38 MAPK) was assessed.

Results: Compared to PM2.5-treated cells, in addition to reducing PM2.5-induced VSMCs proliferation, Afrocyclamin A reduced the expression of PCNA and p-p38 MAPK, down-regulated the level of TNF-α, IL-1β, IL-6, VCAM-1, MDA and ET-1, and up-regulated SOD, GSH and NO level. Furthermore, the anti-proliferative effect of Afrocyclamin A was considerably increased following co-incubation of Afrocyclamin A with SB203580 (p38 MAPK inhibitor) in comparison with Afrocyclamin A-treated cells.

Conclusion: Based on the results, we can conclude that Afrocyclamin A might reduce PM2.5-induced VSMCs proliferation via reduction of p38 MAPK signaling pathway.

Keywords: Afrocyclamin A, Cardioprotective, Pro-Inflammatory Cytokines, p38 Mitogen-Activated Protein Kinase

Cell Journal(Yakhteh), Vol 23, No 2, July 2021, Pages: 191-198

Citation: **Gu Y, Xiao Zh, Wu J, Guo M, Lv P, Dou N. Anti-atherosclerotic effect of afrocyclamin a against vascular smooth muscle cells is mediated via p38 mapk signaling pathway. Cell J. 2021; 23(2): 191-198. doi: 10.22074/cellj.2021.7148.**

Introduction

Previous researches suggested that the particulate matter less than 2.5 μm (PM2.5) air pollution exposure is related with overall cardiovascular mortality, cardiovascular disease (CVD) and mortality and long-term exposure of PM2.5 was found to be related to the risk of atherosclerosis, the underlying pathology of CVD (1). According to the American Heart Association, PM2.5 accelerates the expansion of atherosclerosis and ischemic disease (2). It was exhibited that exposure to PM2.5 for 1 year is positively concomitant with the carotid intima-media thickness in the general population, which is considered a significant index of subclinical atherosclerosis and contributes to the expansion of the atherosclerotic vascular disease (3). Furthermore, an *in vivo* study demonstrated that PM2.5 could induce systemic inflammation and oxidative stress and contributes to the expansion of atherosclerosis. Nevertheless, the underlying mechanisms of PM2.5-induced atherogenesis has not been fully explained.

Vascular smooth muscle cells (VSMCs) are considered the key constituent of the blood vessel wall and essential regulators of vascular function (4). Physiologically, VSMCs also help to regulate the blood flow, maintain the vascular tone, circulate the oxygen and equally distribute the nutrients. Moreover, during the arterial restenosis and atherogenesis, the biology of VSMCs is altered. VSMCs modify the contractile phenotype to the proliferate abnormally, synthetic phenotype and synthesize extracellular matrix proteins, which play a crucial role in the intimal hyperplasia and development of vascular injury.

Studies suggested that atherosclerosis pathogenesis and neo-intimal thickening post-angioplasty involve excessive proliferation and migration of smooth muscle

cells (SMCs) from media into the blood vessels (4, 5). It is well documented that enhanced expressions of various factors such as platelet-derived growth factor (PDGF) and basic fibroblast growth factor (bFGF) also take part in the formation of atheroma (6). The above discuss agonists activate the mitogen-activated protein kinase (MAPK) and phosphoinositide 3-kinases (PI-3) pathway and uphold proliferation and migration of VSMCs leading to their consequent deposition in the plaque. In the current experimental investigation, we scrutinized the anti-atherosclerotic effect of Afrocyclamin A on PM2.5-induced VSMCs proliferation and explored the underlying mechanism.

Materials and Methods

Afrocyclamin A was received as a gift sample. Bafilomycin A1, 3-Methyladenine (3-MA), ammonium chloride and chloroquine were purchased from the Sigma Aldrich, USA. Transforming growth factor beta 1 (TGF-β1) as purchased from Peprotech Inc. (Rocky Hill, NJ, USA). Pro-inflammatory cytokines such as tumor necrosis factor-α (TNF-α), interleukin-1β (IL-1β), IL-6 were purchased from the eBioscience (San Diego, CA, USA). Counting Kit-8 (CCK-8) (CK04) was purchased from Dojindo Molecular Technologies, Inc., USA; superoxide dismutase (SOD), glutathione (GSH), malonaldehyde (MDA), catalase (CAT) and nitric oxide (NO) were purchased from Jiancheng Bioengineering Institute (Nanjing, China). Collagen, type, α-actin, microtubule-associated protein 1light chain 3 (LC3), β-catenin and histone antibodies were purchased from Santa Cruz Biotechnology (Santa Cruz, CA). Antibodies for Beclin-1, Atg5 and osteocalcin were purchased from Epitomics (Burlingame, CA, USA).

In vitro study

Collection and preparation of PM2.5

PM2.5 samples were prepared based on a previously reported method with minor modifications (4). Briefly, Zefluor PTFE membrane filters were used for the collection of PM2.5 samples using the low volume particle samplers. PM2.5 samples were extracted from the filters by soaking for 30 minutes in ultra milli-Q water followed by sonication for 60 minutes. After that, arotary evaporator was used to concentrate the extracts which were then filtered through a Teflon membrane and kept in a dark place at -20ºC to maintain the chemical stability until assayed.

Cell culture

Human aortic VSMCs were purchased from Chinese Academy of Science Cell Bank (Shanghai, China). Dulbecco's Modified Eagle Medium (DMEM) supplemented with fetal bovine serum (FBS, 10%) and antibiotics (100 µg/ml streptomycin and 100 µg/ml of penicillin) was used for the culture of the VSMCs. In order to scrutinize VSMCs proliferation induced by PM2.5, the cells were treated with different concentration of Afrocyclamin A for 24 hours (7). To further scrutinize the effect and potential mechanism of Afrocyclamin A on PM2.5-induced VSMCs proliferation, cells were treated with different concentrations of Afrocyclamin A of p38 MAPK inhibitor for 1 hour and followed by the addition of PM2.5 for 24 hours.

Estimation of cell viability

The cells were seeded at a density of 1×10^4/well in 96-well plates and cultured at 37˚C in CO_2 (5%) incubator for 24 hours. After that, the medium was successfully replaced with the serum-free medium for the next 24 hours. After the above-discussed treatment, the medium was again replaced with the medium containing CCK-8 (10 µl) for 2 hours. Another one blank wells were performed with containing the CCK-8 (10 µL). Finally, the absorbance was read at 540 nm using nanodrop reader. Cell proliferation was estimated according to the following formula:

Cell viability=[A (PM2.5)−A (blank)]/[A (PBS)−A (blank)].

Biochemical and antioxidant parameters

The levels of MDA and SOD were estimated using colorimetric assay kits. The level of NO was estimated in the VSMCs culture supernatant using the nitrate reductase method according to the manufacturer's instructions. Radioimmunoassay technique was used for the estimation of ET-1 based on the manufacturer's instruction.

In vivo study

Animal

A total 30 Wistar rats (100-150 g) were used for the experimental study. The rats were received from the institute animal house. The rats were kept in the polyethylene cages under standard conditions (temperature 22 ± 3ºC; 60 ± 5 relative humidity) and they received standard diet and water ad libitum. The rats were acclimatized 7 days before the experimental study. The current experimental study was approved by the institutional animal Ethical Committee (202008-1006).

Cell culture and treatment

Wistar rats were sacrificed, the aorta was successfully removed and the VSMCs were isolated as previously reported (8, 9). The isolated VSMCs were cultured in the DMEM supplemented with FBS (10%) and maintained under CO_2 (5%) at 37˚C in a humidified atmosphere. The cells were cultured in the DMEM and the expression of known marker protein α-actin was assessed using an immunofluorescence assay. After that, the VSMCs were washed with phosphate buffered saline (PBS) and re-cultured in the serum-free medium for the next 24 hours, before stimulation by TGF-β. Various concentrations of afrocylamin A were used for further experiments.

Transfection of vascular smooth muscle cells

For the over-expressed the expression of β-catenin in VSMCs, cells were transferred with either empty vector or the same vector containing a cDNA encoding wild type β-catenin. Briefly, the cells were cultured in the plates and grown for 24 hours until they reached 50-60% confluence. Then VSMCs were transfected with WT β-catenin or empty vector using the transfection reagent based on the manufacturer's instructions.

Cell viability assay

MTT assay was used to assess cell viability. Here, 5×10^3 cells were seeded in the 96-well plates overnight. After that, the cells were treated with the test drug and incubated with 3-(4,5-dimethylthiazol-2-yl)-2,5-diphenyl tetrazolium bromide (MTT, 5 mg/ml) for 3 hours and subsequently, solubilized in dimethyl sulfoxide (DMSO, 200 µl). Finally, the absorbance was read at 570 nm using an enzyme-linked immunosorbent assay (ELISA) reader.

Calcification analysis

To estimate cell calcification, QuantiChromTM Calcium Assay Kit (Bioassay Systems, Hayward, CA) was used for the estimation of calcium content. The absorbance was read at 612 nm using an ELISA reader.

Nuclear and cytosolic fractionation

After culturing VSMCs, the cells were washed with ice-cold PBS. A previously reported method was used for the extraction of cytosolic and nuclear protein with minor modifications. Briefly, VSMCs were harvested in the hypotonic lysis buffer and incubated on the ice for 5 minutes. After that, the cell lysate was chilled for 10 minutes on ice and then, vigorously shaken in the presence of Nonidet P-40 for 10 minutes and centrifuged for separating the nuclear fraction. The supernatants containing the cytosolic protein were collected. For the collection of nuclear fractionation, the high salt buffer was added to the extract with continuous shaking and the extract was centrifuged for collection of the supernatants.

Statistical analysis

Data was analyzed by ANOVA, followed by Tukey's post hoc test, using the Graphpad Prism 7 version software (USA). Data is presented as means ± SEM. A value of $P<0.05$ was considered significant.

Results

Effect of Afrocyclamin A on PM2.5-induced proliferation in vascular smooth muscle cells

BrdU immunofluorescence and CCK-8 assay kits were used for estimation of cell proliferation. Figure 1A shows that the PM2.5 (200 mg/l) increased VSMCs cell viability. Figure 1B shows that PM2.5 (200 mg/l) exposure for 24 hours led to a considerable enhancement of VSMCs viability. Figure 1C demonstrates that Afrocyclamin A treatment (0~50 µM) for 24 hours compared to the untreated cells. Moreover, PM2.5 (200 mg/l)-treated cells pretreated with Afrocyclamin A (50 µM) were considered in subsequent experiments. PM2.5 considerably enhanced VSMCs viability as compared to the untreated cells, which was inverted by Afrocyclamin A in a dose-dependent manner. The anti-proliferative effect of Afrocyclamin A was increased via SB203580 as compared to Afrocyclamin A-treated cells (Fig.1D). The results showed that the pro-proliferative effect of PM2.5 on VSMCs, was reversed by Afrocyclamin A treatment. As shown by the BrdU immunofluorescence assay, PM2.5 (200 mg/l) considerably enhanced VSMCs proliferation as compared to the untreated cells (Fig.1E). Afrocyclamin A reduced PM2.5-induced proliferation of VSMCs, and the antiproliferative potential of Afrocyclamin A was increased by SB203580 administration as compared to Afrocyclamin A-treated cells.

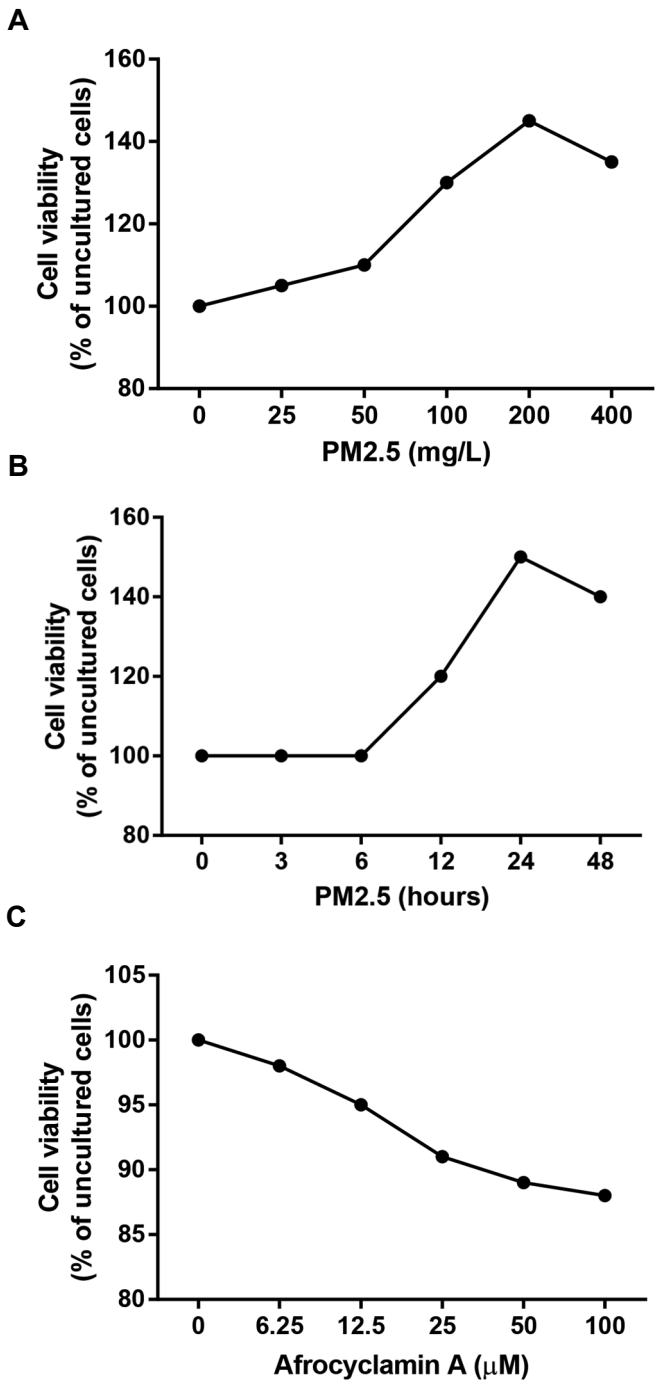

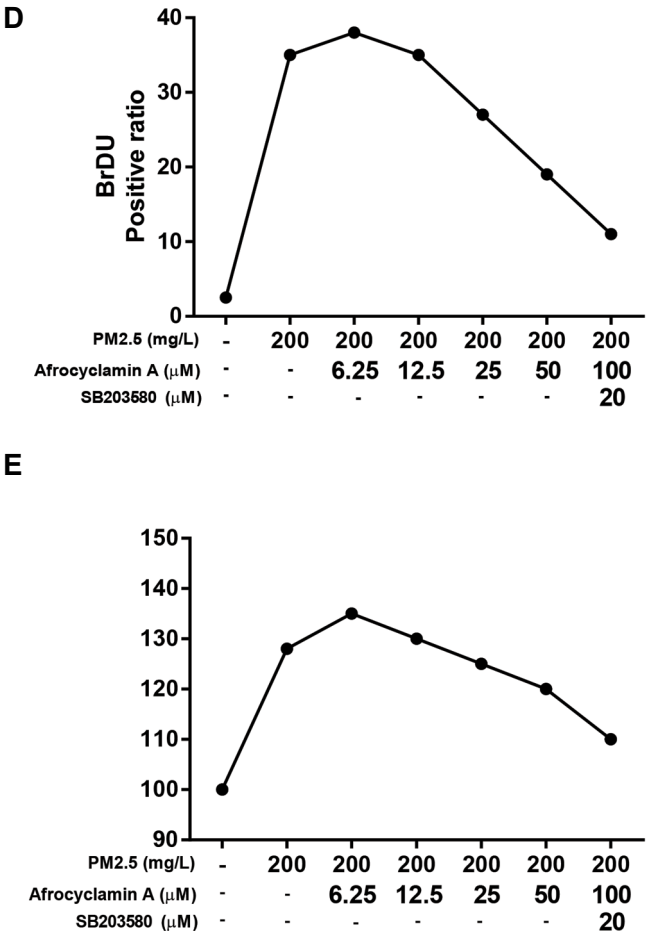

Fig.1: Effect of Afrocyclamin A on VSMCs proliferation. **A.** Cell were increased after 24 hours. **B.** Cells were stimulated with PM2.5 (200 mg/l) at different time intervals, **C.** Cells were treated with different concentrations of Afrocyclamin A (0, 6.25, 12.5, 25, 50 and 100 μM), **D.** Cells were treated with different concentrations of Afrocyclamin A and SB203580 (p38MAPK inhibitor) for 1 hour, followed by addition of PM2.5 (200 mg/l) for 24 hours, and **E.** Cells were treated with Afrocyclamin A and SB203580 (p38 MAPK inhibitor) for 1 hour, followed by addition of PM2.5 (200 mg/l). VSMCs; Vascular smooth muscle cells.

Effect of Afrocyclamin A on antioxidant parameters on vascular smooth muscle cells

Figure 2 shows the effect of Afrocyclamin A on the antioxidant parameters in VSMCs. PM2.5 (200 mg/l) increased the level of MDA as compared to control and treatment with Afrocyclamin A significantly (P<0.05) and dose-dependently reduced the level of MDA.

An opposite trend was observed in SOD and GSH levels. PM2.5 (200 mg/l) reduced the level of SOD and GSH and treatment with Afrocyclamin A dose-dependently increased their level almost near to the control group.

Effect of Afrocyclamin A on the level of endothelin-1, nitric oxide and vascular cell adhesion molecule-1 in vascular smooth muscle cells

Figure 3 exhibits the level of endothelin-1 (ET-1), NO and vascular cell adhesion molecule-1 (VCAM-1) in the treated and untreated cells. Compared to the untreated cells, PM2.5 considerably increased the level of ET-1, NO and VCAM-1 and treatment with Afrocyclamin A dose-dependently reduced the level of ET-1, NO and VCAM-1. These effects of Afrocyclamin A were increased by SB203580 as compared to the Afrocyclamin A-treated cell.

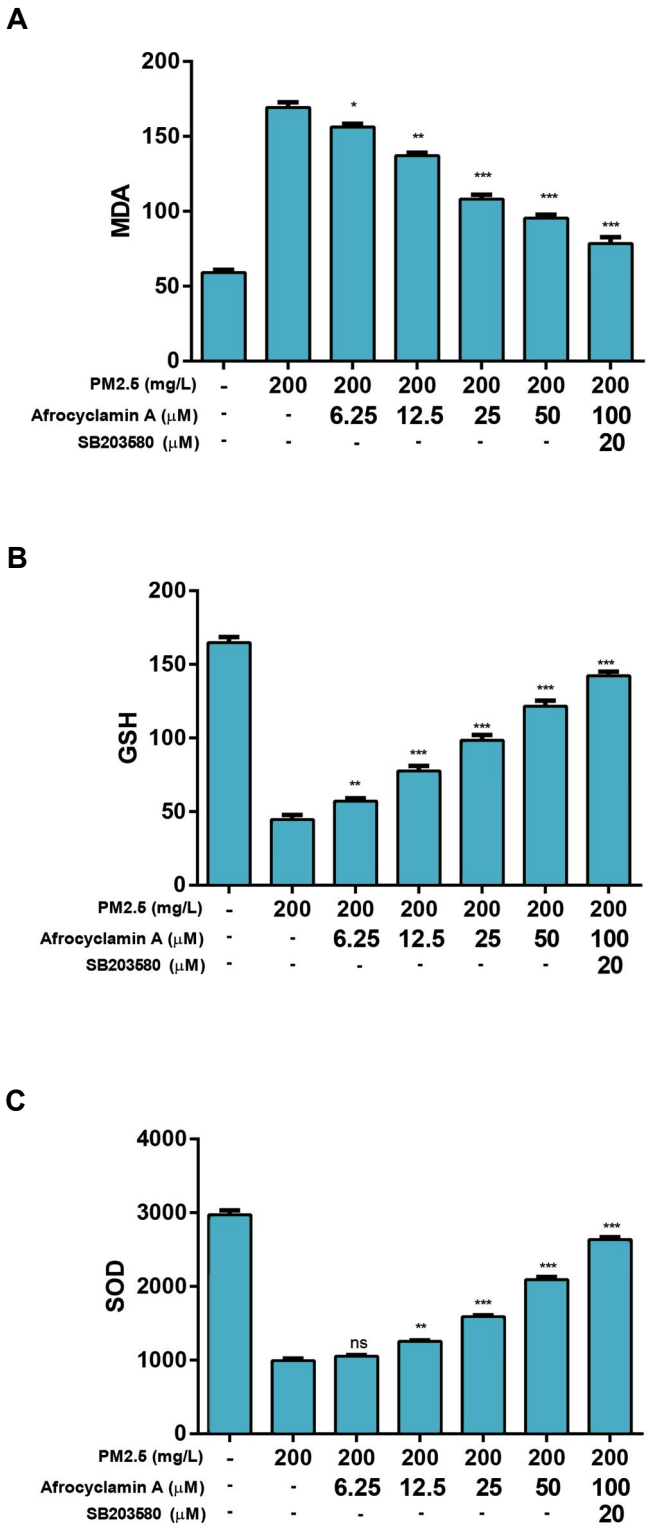

Fig.2: Effect of Afrocyclamin A on the antioxidant enzymes in VSMCs. **A.** Level of MDA, **B.** GSH, and **C.** SOD. The results are displayed as mean ± SEM (n=3). Compared to the PM2.5 (200 mg/l), *; P<0.05, **; P<0.01 and ***; P<0.01. VSMCs; Vascular smooth muscle cells, MDA; Malonaldehyde, GSH; Glutathione, SOD; Superoxide dismutase, and ns; Non significant.

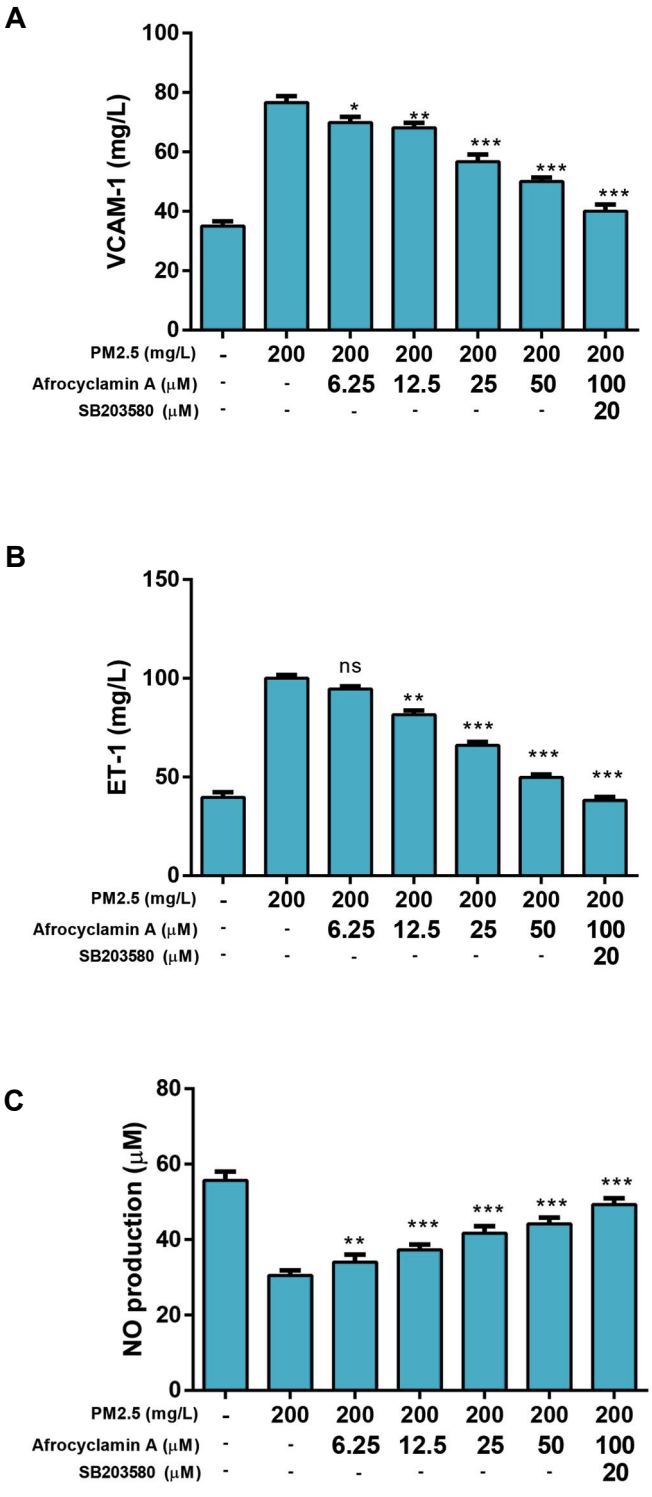

Fig.3: Effect of Afrocyclamin A on the antioxidant enzymes in VSMCs. **A.** Level of VCAM-1, **B.** ET-1 and **C.** NO. The results are displayed as mean ± SEM (n=3). Compared to the PM2.5 (200 mg/l), *; P<0.05, **; P<0.01 and ***; P<0.01. VSMC; Vascular smooth muscle cells, VCAM-1; Vascular cell adhesion molecule-1, ET-1; Endothelin-1, NO; Nitric oxide, and ns; Non significant.

Effect of Afrocyclamin A on the cytokines in vascular smooth muscle cells

Compared to the untreated cells, the levels of pro-inflammatory cytokines such as TNF-α, IL-1β and IL-6, were increased in the PM2.5-treated cells. Afrocyclamin A considerably decreased the level of cytokines such as TNF-α, IL-1β and IL-6 in a dose-dependent manner. These effects of Afrocyclamin A were enhanced by SB203580 as compared to the Afrocyclamin A-treated cell (Fig.4).

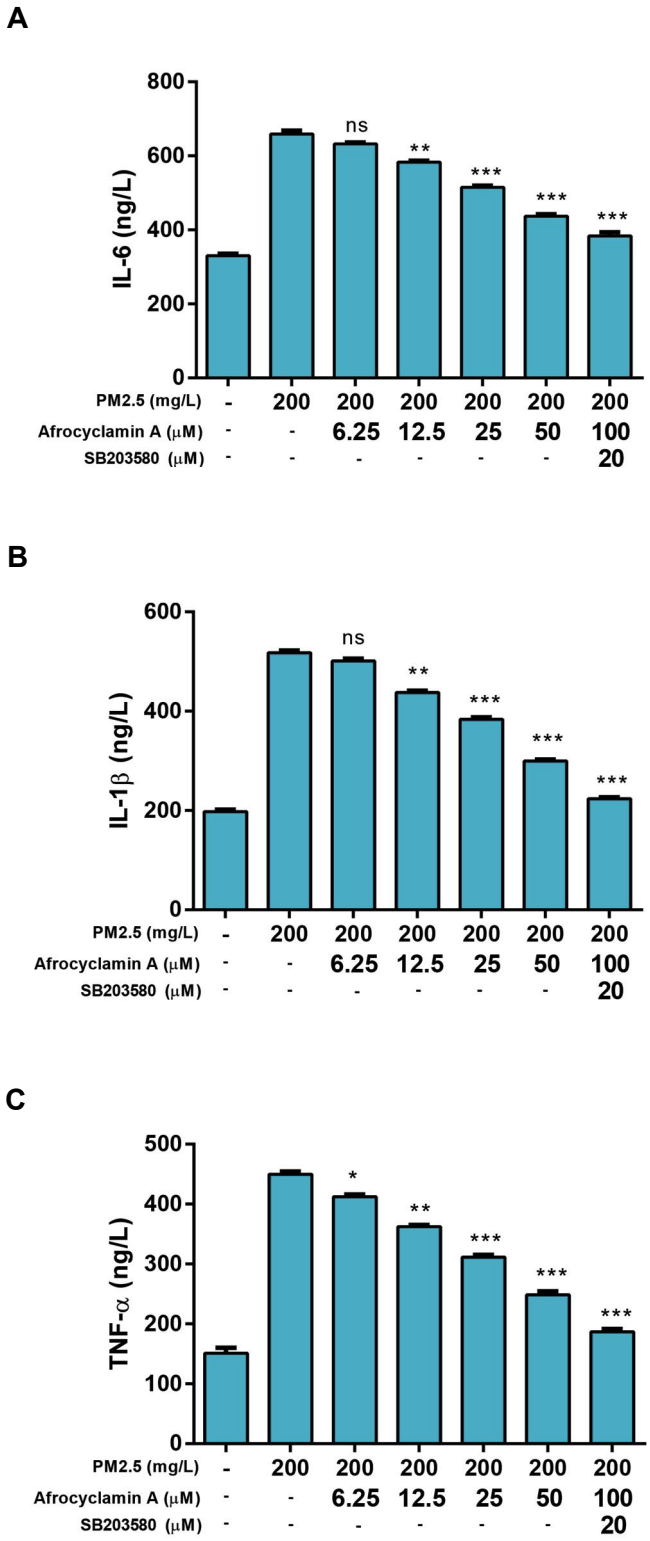

Fig.4: Effect of Afrocyclamin A on the pro-inflammatory cytokines in VSMCs. **A.** Level of IL-6, **B.** IL-1β, and **C.** TNF-α. The results are displayed as mean ± SEM (n=3). Compared to the PM2.5 (200 mg/l), *; P<0.05, **; P<0.01 and ***; P<0.01. VSMC; Vascular smooth muscle cells, IL-1β; Interleukin-1β, IL-6; Interleukin-6, TNF-α; Tumor necrosis factor-α, and ns; Non significant.

Effect of Afrocyclamin A on the expression of proliferating cell nuclear antigen and p-p38 MAPK in vascular smooth muscle cells

Figure 5 exhibits the effect of Afrocyclamin A on the expression of PCNA and p-p38 MAPK. Compared to the untreated cells, the PM2.5-treated cells demonstrated increased levels of PCNA and p-p-38 MAPK and Afrocyclamin A considerably decreased the level of PCNA and p-p38 MAPK in VSMCs. These effects of Afrocyclamin A were enhanced by SB203580 as compared to the Afrocyclamin A-treated cell.

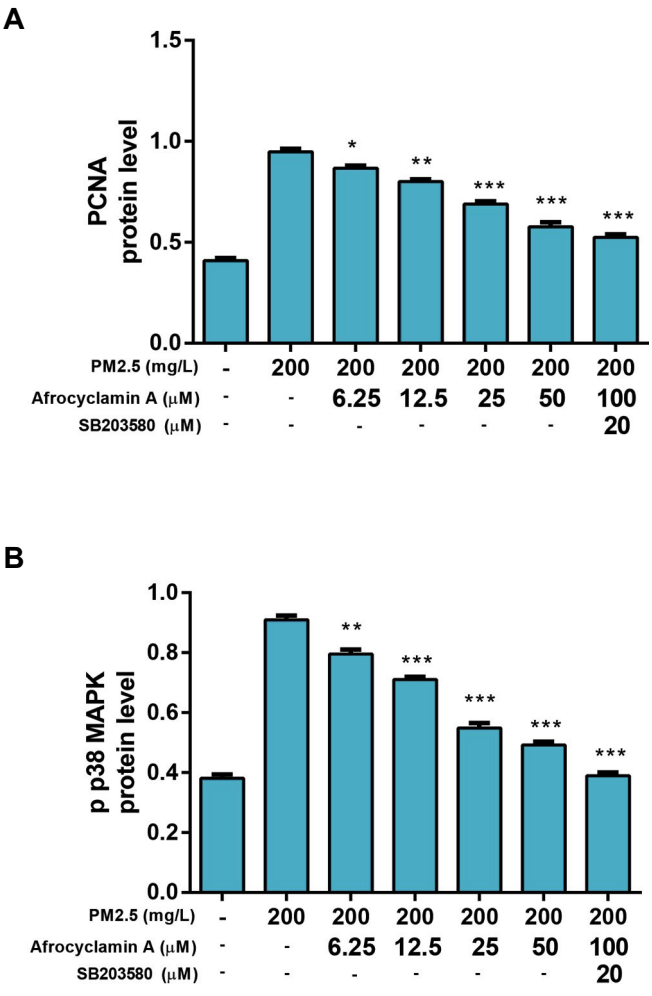

Fig.5: Showed the effect of Afrocyclamin A on the PCNA and p-p38MAPK in VSMCs. **A.** Showed the level of PCNA and **B.** p-p38 MAPK. Method described in the material and method section. The results are displayed as mean ± SEM (n=3). Compared to the PM2.5 (200 mg/L), *; P<0.05, **; P<0.01 and ***; P<0.01. VSMC; Vascular smooth muscle cells and PCNA; Proliferating cell nuclear antigen.

Discussion

Previous studies suggested that speedy industrialization and urbanization in China have led to a sharp boost in pollution emissions and energy consumption, especially in the metro city (10, 11). Due to urbanization, pollution is increased and coal consumption is increased during the winter season. According to the reports, only in Beijing, there is an increase in the concentration of PM2.5 particles due to continually increasing vehicle and coal use (12, 13).

Previous reports showed that the particulate matter is a combination of different chemical compositions such as elemental nitrate, carbon, ammonium ion, silicon, sulfate, sodium ion and organic carbon matter (14, 15). According to the aerodynamic diameter, particulate matter is divided according to the size of particles as follows: <0.1 μm (PM 0.1), <2.5 μm (PM2.5), <10 μm and thoracic particles (>10 μm) (16). PM2.5 is very minute in size, which allows it to easily threat the human health by entering via trachea and going into the alveoli, penetrating via pulmonary air blood barrier, diffusing into the capillaries and finally entering the blood circulation (17). Consequently, the above discussed points suggest that PM2.5 can affect CVD and increase the CVD-related mortality. Due to increasing pollution, there is an increase in the incidence of CVD (18, 19). CVDs including atherosclerosis are related to the endothelial dysfunction, and alteration of CVDs risk factor leads to increased vascular function (20, 21).

Previous researches suggested that the vascular calcification is a significant risk factor for cardiovascular mortality and morbidity and it is also predominant in the patients with atherosclerosis and diabetes (22, 23). Considering that the vascular calcification is related to the CVD risk factor, and various studies have attempted to interrupt the demonstration of disease. It was suggested that atherosclerosis is a progressive disease developed via deposition of fibrous plaque and lipids in the arteries (24, 25). The etiology of atherosclerosis is very complicated and its risk factors are hypertension, hyperlipidemia, smoking, lack of exercise and genetic defects (26). Various investigation suggested that PM2.5 may also take part in the expansion of CVD especially atherosclerosis (27, 28). It was shown that the endothelial dysfunction is considered a pathological condition, mostly produced by an imbalance between the vasoconstrictor and vasodilator substances, and this disproportion leads to damage of endothelium-dependent relaxation, which shows the functional characteristic of endothelial dysfunction (29, 30). All blood vessels play an important role in the switch of vascular tone partially via secretion of powerful vasodilators such as endothelium-derived hyperpolarizing factor (EDHF) and NO (31). The dysfunction of endothelial function is the 1st step towards the coronary arteriosclerosis disease, and long term exposure to PM2.5 was linked with the reduced level of NO-mediated endothelial function in a conduit artery independent of cardiovascular risk factors (31, 32). PM2.5 exposures resulted in increased level of inflammatory mediators and oxidative stress (33, 34). Currently, few studies suggest that plant-based drugs could decrease plasma calcification and arterial calcification concentration, but the underlying mechanism of action is still not clear. In the current experimental study, we scrutinized the antioxidant and anti-inflammatory effect of Afrocyclamin A against PM2.5-induced VSMCs.

During the expansion of atherosclerosis, the transformation of VSMCs from the inactive contractile phenotype towards the proliferative migratory phenotype into the plaque area to form a fibrous cap, is generally regarded as an important step in the formation of unstable atherosclerotic plaques (35). VSMCs drifted into the intima show an abnormally up-regulation in the production of extracellular matrix and proliferation, which further leads to the formation of the fibrous cap in atherosclerotic lesions. During atherosclerosis, the level of endothelial NO increased due to increase in the production of NO from the NO synthase (eNOS). Decreases in the level of NO, decrease the adhesion and aggregation of platelets and inflammatory cells. Decreased NO production plays a significant role in the expansion of leukocytes, which further increased the inflammation reaction and further increased the atherosclerotic plaque formation and instability (4, 35).

VCAM-1 (immunoglobulin-like glycoprotein), takes part in the adhesion of leukocytes to the endothelial cells and afterward, starts the transmigration into the arterial intima, and boosts the VSMCs proliferation via focal adhesion kinase pathway (36). It was shown that the pro-inflammatory cytokines such as IL-6, IL-1β and TNF-α, can induce VSMCs migration/proliferation and hypertrophic response, which can take part in the expansion of atherosclerosis (37). During atherosclerosis, the level of IL-6, IL-1β and TNF-α significantly increased and treatment with Afrocyclamin A dose-dependently reduced the level to almost near the control values. Oxidative stress plays a significant role in the development of atherosclerosis, and it is involved in the regulation of VSMCs migration/proliferation and differentiation (36). MDA (a marker of lipid peroxidation) acts as the endogenous lipid peroxidation and it is generated as the end product of lipid pre-oxidation (LPO). Other significant antioxidant enzymes such as SOD, play a role in the inhibition of neointima formation via attenuation of proliferation and migration of VSMCs. Other antioxidant enzymes like GSH, are reduced during atherosclerosis due to increased oxidative stress (38). Treatment with Afrocyclamin A significantly and dose-dependently altered the level of antioxidant enzymes.

It is well documented that endothelial cells, take part in the VSMCs hyperproliferation via MAPK-PI3K pathway (39). MAPKs are a group of signaling molecules that regulate apoptosis, proliferation, inflammatory reactions and differentiation via activating various downstream transcription factors. p38 MAPK is strongly activated in response to vascular damage, and signaling pathway of p38MAPK has been shown to affect VSMCs proliferation in response to proliferative factors via altering the progression of cell cycle linked proteins (40). According to their study, the effect of puerarin on the VSMCs proliferation is mediated via reduction of p38 MAPK signaling pathway. In our experimental study, Afrocyclamin A significantly inhibited the VSMCs proliferation via down-regulation of antioxidant and pro-inflammatory cytokines and down-regulated the p38 MAPK signaling pathway.

Conclusion

In this study, we observed that PM2.5 treatment significantly increased the VSMCs proliferation and increased the expression of p-p38MAPK, enhanced the level of IL-6, IL-1β, TNF-α, VCAM-1, MDA and reduced level of SOD, GSH and NO. The above-discussed results showed that PM2.5 might induce VSMCs proliferation through p38 MAPK signaling pathway activation. Afrocyclamin A significantly altered P38 MAPK and reduced the VSMCs proliferation.

Acknowledgements

This work was financially supported by the Affiliated Hospital of Qingdao University, China. The authors declare no conflict of interest.

Authors' Contribution

Y.G., Z.X., J.W.; Performed the experimental study. Y.G., Z.X., J.W., M.G., P.L.; Analyzed the biochemical data. M.G., P.L.; Write the draft of the manuscript. N.D.; Provide the necessary funding and design the experimental study. All the authors equally contributed to proof reading of the manuscript.

References

1. Brook RD, Rajagopalan S, Pope CA, Brook JR, Bhatnagar A, Diez-Roux A V, et al. Particulate matter air pollution and cardiovascular disease: an update to the scientific statement from the american heart association. Circulation. 2010; 121(21): 2331-2378.
2. Newman JD, Thurston GD, Cromar K, Guo Y, Rockman CB, Fisher EA, et al. Particulate air pollution and carotid artery stenosis. J Am Coll Cardiol. 2015; 65(11): 1150-1151.
3. Kälsch H, Hennig F, Moebus S, Möhlenkamp S, Dragano N, Jakobs H, et al. Are air pollution and traffic noise independently associated with atherosclerosis: The Heinz Nixdorf Recall Study. Eur Heart J. 2014; 35(13): 853-860.
4. Bennett MR, Sinha S, Owens GK. Vascular smooth muscle cells in atherosclerosis. Circ Res. 2016; 118(4): 692-702.
5. Haga JH, Li YSJ, Chien S. Molecular basis of the effects of mechanical stretch on vascular smooth muscle cells. J Biomech. 2007; 40(5): 947-960.
6. Leung DW, Cachianes G, Kuang WJ, Goeddel DV, Ferrara N. Vascular endothelial growth factor is a secreted angiogenic mitogen. Science. 1989; 246(4935): 1306-1309.
7. Qi YX, Jiang J, Jiang XH, Wang XD, Ji SY, Han Y, et al. PDGF-BB and TGF-β1 on cross-talk between endothelial and smooth muscle cells in vascular remodeling induced by low shear stress. Proc Natl Acad Sci. 2011; 108(5): 1908-1913.
8. Warditiani NK, Widjaja INK, Larasanty LPF, Noviyanti NWR, Gitarini NM, Juniari NPM, et al. Antiatherosclerosis effect of purified andrographis paniculata extract. Int J Pharm Clin Res. 2016; 8(5): 457-460.
9. Chang XY, Cui L, Wang XZ, Zhang L, Zhu D, Zhou XR, et al. Quercetin attenuates vascular calcification through suppressed oxidative stress in adenine-induced chronic renal failure rats. Biomed Res Int. 2017; 2017: 5716204.
10. Hou J, An Y, Song H, Chen J. The Impact of haze pollution on regional eco-economic treatment efficiency in China: an environmental regulation perspective. Int J Environ Res Public Health. 2019; 16(21): 4059.
11. Borup R, Meyers J, Pivovar B, Kim YS, Mukundan R, Garland N, et al. Scientific aspects of polymer electrolyte fuel cell durability and degradation. Chem Rev. 2007; 107(10): 3904-3951.
12. Xie W, Li G, Zhao D, Xie X, Wei Z, Wang W, et al. Relationship

between fine particulate air pollution and ischaemic heart disease morbidity and mortality. Heart. 2015; 101(4): 248-249.
13. Wang J, Zhao B, Wang S, Yang F, Xing J, Morawska L, et al. Particulate matter pollution over China and the effects of control policies. Sci Total Environ. 2017; 584: 426-447.
14. Kleeman MJ, Schauer JJ, Cass GR. Size and composition distribution of fine particulate matter emitted from wood burning, meat charbroiling, and cigarettes. Environ Sci Technol. 1999; 33(20): 3516-3523.
15. Dominici F, Wang Y, Correia AW, Ezzati M, Pope CA, Dockery DW. Chemical composition of fine particulate matter and life expectancy. Epidemiology. 2015; 26(4): 556-564.
16. Sun Q, Hong X, Wold LE. Cardiovascular effects of ambient particulate air pollution exposure. Circulation. 2010; 121(25): 2755-2765.
17. Barmpadimos I, Keller J, Oderbolz D, Hueglin C, Prévôt ASH. One decade of parallel fine (PM 2.5) and coarse (PM 10-PM 2.5) particulate matter measurements in Europe: trends and variability. Atmos Chem Phys. 2012; 12(7): 3189-3203.
18. Uthman OA, Hartley L, Rees K, Taylor F, Volmink J, Ebrahim S, et al. Multiple risk factor interventions for primary prevention of cardiovascular disease in low- and middle-income countries. Cochrane Database Syst Rev. 2014; 2015(8): CD011163.
19. Atzeni F, Turiel M, Caporali R, Cavagna L, Tomasoni L, Sitia S, et al. The effect of pharmacological therapy on the cardiovascular system of patients with systemic rheumatic diseases. Autoimmune Rev. 2010; 9(12): 835-839.
20. Salahuddin S, Prabhakaran D, Roy A. Pathophysiological mechanisms of tobacco-related CVD. Global Heart. 2012; 7(2): 113-120.
21. Yildiz O. Vascular smooth muscle and endothelial functions in aging. Ann N Y Acad Sci. 2007; 1100(1): 353-360.
22. Chen NX, Moe SM. Vascular calcification: pathophysiology and risk factors. Curr Hypertens Rep. 2012; 14(3): 228-237.
23. Stout RW. Diabetes and atherosclerosis. Biomed Pharmacother. 1993;47(1):1-2.
24. Bishop PD, Feiten LE, Ouriel K, Nassoiy SP, Pavkov ML, Clair DG, et al. Arterial calcification increases in distal arteries in patients with peripheral arterial disease. Ann Vasc Surg. 2008; 22(6): 799-805.
25. Gamble W. Atherosclerosis: The carbonic anhydrase, carbon dioxide, calcium concerted theory. J Theor Biol. 2006; 239(1): 16-21.
26. Glass CK, Olefsky JM. Inflammation and lipid signaling in the etiology of insulin resistance. Cell Metab. 2012: 15(5): 635-645.
27. Sun Q, Wang A, Jin X, Natanzon A, Duquaine D, Brook RD, et al. Long-term air pollution exposure and acceleration of atherosclerosis and vascular inflammation in an animal model. J Am Med Assoc. 2005; 294(23): 3003-3010.
28. Montiel-Dávalos A, Alfaro-Moreno E, López-Marure R. PM2.5 and PM10 induce the expression of adhesion molecules and the adhesion of monocytic cells to human umbilical vein endothelial cells. Inhal Toxicol. 2007; 19 Suppl 1. 91-98.
29. Goveia J, Stapor P, Carmeliet P. Principles of targeting endothelial cell metabolism to treat angiogenesis and endothelial cell dysfunction in disease. EMBO Mol Med. 2014; 6(9): 1105-1120.
30. Dinh QN, Drummond GR, Sobey CG, Chrissobolis S. Roles of inflammation, oxidative stress, and vascular dysfunction in hypertension. Biomed Res Int. 2014; 2014: 406960.
31. Komori K, Vanhoutte PM. Endothelium-derived hyperpolarizing factor. J Vasc Res. 1990; 27(2-5): 238-245.
32. Shimokawa H. Hydrogen peroxide as an e1105-1120ndothelium-derived hyperpolarizing factor. Pflugers Arch Eur J Physiol. 2010; 459(6): 915-922
33. Luksha L, Agewall S, Kublickiene K. Endothelium-derived hype. rpolarizing factor in vascular physiology and cardiovascular disease. Atherosclerosis. 2009; 202(2): 330-344.
34. Rubanyi GM. Endothelium-derived relaxing and contracting factors. J Cell Biochem. 1991; 39(4): 575-590.
35. Matthews C, Gorenne I, Scott S, Figg N, Kirkpatrick P, Ritchie A, et al. Vascular smooth muscle cells undergo telomere-based senescence in human atherosclerosis: effects of telomerase and oxidative stress. Circ Res. 2006; 99(2): 156-164.
36. Ley K, Huo Y. VCAM-1 is critical in atherosclerosis. J Clin Invest. 2001; 107(10): 1209-1210.
37. Haybar H, Shokuhian M, Bagheri M, Davari N, Saki N. Involvement of circulating inflammatory factors in prognosis and risk of cardiovascular disease. J Mol Cell Cardiol. 2019; 132: 110-119
38. Zakkar M, Van Der Heiden K, Luong LA, Chaudhury H, Cuhlmann S, Hamdulay SS, et al. Activation of Nrf2 in endothelial cells protects art eries from exhibiting a proinflammatory state. Arterioscler Thromb Vasc Biol. 2009; 29(11): 1851-1857.
39. Yue X, Wu M, Jiang H, Hao J, Zhao Q, Zhu Q, et al. Endothelial lipase is upregulated by interleukin-6 partly via the p38 MAPK and p65 NF-κB signaling pathways. Mol Med Rep. 2016; 14(3): 1979-1985.
40. Wan Q, Liu Z, Yang Y. Puerarin inhibits vascular smooth muscle cells proliferation induced by fine particulate matter via suppressing of the p38 MAPK signaling pathway. BMC Complement Altern Med. 2018; 18(1): 146.

Original Article

miR-373 Suppresses Cell Proliferation and Apoptosis via Regulation of SIRT1/PGC-1α/NRF2 Axis in Pancreatic Cancer

Qing-Hua Yin, M.D.[1], Yuan Zhou, M.D.[1], Zhi-Yuan Li, M.D.[2*]

1. Department of Hepatobiliary Surgery, The First Hospital of Changsha, Changsha 410000, P.R.China
2. Department of Gastrointestinal Surgery, The Central Hospital of Hengyang City, Hengyang 421001, P.R.China

Corresponding Address: Department of Gastrointestinal Surgery, The Central Hospital of Hengyang City, Hengyang 421001, P.R.China
Email: 183081297@qq.com

Received: 03/July/2019, Accepted: 9/December/2019

Abstract

Objective: Our study aimed to investigate function and mechanism of *miR-373* in proliferation and apoptosis of pancreatic cancer (PC) cells by regulating NAD+-dependent histone deacetylase sirtulin 1 (SIRT1).

Materials and Methods: This experimental study included two PC cell lines AsPC-1 and PANC-1 in which expression levels of *miR-373* and *SIRT1* were manipulated. The level of *miR-373* was detected by reverse transcription quantitative polymerase chain reaction (RT-qPCR) method. Expression levels of SIRT1, BCL-2, BAX, cleaved CASPASE-8/9/3, PARP, PGC-1α, NRF2, eNOS and iNOS were examined via RT-qPCR and western blotting, respectively. The binding sites of *miR-373* on the *SIRT1* were examined via dual-luciferase assay. Cell proliferation and apoptosis were examined by MTT assay, colony formation assay, Annexin-V/PI staining and TUNEL assay. The oxidative metabolic changes were monitored by reactive oxygen species (ROS), malondialdehyde (MDA) and superoxide dismutase (SOD) detection.

Results: *miR-373* could specifically target the 3'-UTR of *SIRT1* and reduce its expression in PC cells. Either elevated expression of *miR-373* or partial loss of SIRT1 inhibited cell proliferation and induced cell apoptosis. Accumulation of BAX and cleaved CASPASE-8/9/3, inhibition of PGC-1α/NRF2 pathway, increase oxidative stress and reduction of BCL-2 as well as uncleaved PARP were found in the presence of *miR-373* or the absence of *SIRT1*. Overexpression of *SIRT1* could reduce anti-proliferative and pro-apoptotic effects of *miR-373*.

Conclusion: Overall, this study concluded that *miR-373*-dependent *SIRT1* inhibition displays anti-proliferative and pro-apoptotic roles in PC cells via PGC-1α/NRF2 pathway, which highlights *miR-373* as a potential target for PC treatment.

Keywords: *miR-373*, Oxidative Stress, Pancreatic Cancer, PGC-1α/NRF2 Pathway, SIRT1

Cell Journal(Yakhteh), Vol 23, No 2, July 2021, Pages: 199-210

Citation: Yin QH, Zhou Y, Li ZhY. miR-373 suppresses cell proliferation and apoptosis via regulation of SIRT1/PGC-1α/NRF2 axis in pancreatic cancer. Cell J. 2021; 23(2): 199-210. doi: 10.22074/cellj.2021.7038.

Introduction

Pancreatic cancer (PC) is a notoriously fatal malignant tumor, characterized by a highly aggressive potential of invasion and metastasis (1, 2). At present, PC ranks the 4th cause of cancer related death, with statistics suggesting that it will eventually become the 2nd lethal cancer within the next decade (3). Owing to the lack of incipient symptom, PC patients are often diagnosed with a high-grade stage (4). Neo-adjuvant treatment in combination with radiotherapy/chemotherapy at present represents the best chance of increasing overall survival of patients (5). However, local recurrence and cancer metastasis to other organs suggest frequent issues faced during the treatment of PC (6). Therefore, it is urgent to explore new therapeutic strategies for PC treatment.

microRNAs (miRNAs), as a group of small non-coding RNAs, can bind to target genes and suppress their expressions (7, 8). Over the last decade, miRNAs have been highlighted due to their crucial roles in the molecular processes involved in the initiation and progression of various tumor types (9-12). For instance, *miR-373* was shown to be dramatically down-regulated in PC, and this decline of *miR-373* expression facilitated invasion of cancer cells by enhancing epithelial-mesenchymal transition (13). In line with this work, down-regulation of *miR-373* was also proved in the serum of PC patients, suggesting *miR-373* might serve as an independent predictor for early detection and prognosis of PC (14). It was reported that *miR-373* targeted Cycin D2 (CCND2) to promote the chemosensitivity of gemcitabine via cell cycle pathway in pancreatic carcinoma cells (15). *miR-373* could mediate qingyihuaji formula (QYHJ) effect on reversing gemcitabine-triggered resistant of human PC (16). However, the downstream regulatory mechanism of *miR-373*-mediated PC progression is still rarely reported.

Silent mating-type information regulation 2 homolog (SIRT1) is an NAD^+-dependent class III histone deacetylase, which has key roles in metabolic control (17). Increasing studies showed that SIRT1 was induced in PC and involved in the regulating proliferation and viability of PC cells. Recently, *miR-373* was proved as a potential therapeutic strategy for renal fibrosis by playing regulatory role in modulating SIRT1-mediated NF-κB/MMP-9 signaling (18). However, study of the relationship between *SIRT1* and *miR-373* in PC progression is yet unclear. SIRT1 participates in mitochondrial biogenesis

to maintain cellular redox homeostasis by deacetylation of PGC-1α, which is a peroxisome proliferator-activated metabolic regulator (19). The shear stress-induced SIRT1 could initiate PGC-1α production and activation, and thus it could enhance mitochondrial biogenesis (20). Nuclear factor E2-related factor 2 (NRF2), as an important cellular oxidative stress regulatory transcript factor, is an effective drug target for antioxidant therapy (21). NRF2 is transported to nucleus and induces production of downstream detoxification as well as antioxidant enzymes to produce an antioxidant effect in response to oxidative stresses (22, 23). SIRT1 was revealed to promote activity of NRF2 and increase expression levels of the NRF2 downstream genes (24). Hitherto, the role of *miR-373* on proliferation and apoptosis of PC cells via modulation of PGC-1α/NRF2 pathway is a mystery.

Presently, the study of *miR-373* regulated SIRT1 in PC is still lacking and the roles of this regulatory axis in the PC progression are unclear. Therefore, based the previous studies, the crucial objective of this study is to investigate *miR-373*-mediated SIRT1 regulation and its roles in the growth and progression of PC. Hopefully, this work can shed some light on finding alternative therapy method for PC and enrich the theoretical bases of PC treatment.

Materials and Methods

Cell culture

In this experimental study, PC cell lines AsPC-1 and PANC-1 were obtained from American Type Culture Collection (ATCC, USA). PC cells were cultured in Dulbecco's Modified Eagle's Medium (DMEM, Sigma-Aldrich, USA) supplemented with 10% fetal bovine serum and 100 U/mL penicillin/streptomycin (Thermo Fisher Scientific, USA) in a humidified 37˚C incubator with 5% CO_2. Further experiments were performed once cell confluence reached 70-80%.

Cell grouping and transfection

PC cells were trypsinized and inoculated into 24-well plates. After removing culture medium, the cells were classified into the following groups: i. *miR-373* negative control (NC) group (cells were treated with NC for *miR-373* mimics), ii. *miR-373* mimics group (cells were treated with *miR-373* mimics to elevate expression of *miR-373*), iii. shNC group (cells were treated with NC for shRNA as negative control), iv. sh*SIRT1* group (cells were treated with shRNA-*SIRT1* to knockdown *SIRT1*), v. *miR-373* mimics+pcDNA3.1-NC (cells were treated with *miR-373* mimics followed by the pcDNA3.1 empty vector), and vi. *miR-373* mimics+pcDNA3.1-*SIRT1* (cells were treated with *miR-373* mimics followed by pcDNA3.1-*SIRT1* vector). The cells were transfected for 48 hours as above indicated, according to the guidelines for the Lipofectamine™ 2000 (Invitrogen, USA). *miR-373* NC, *miR-373* mimics, shNC, sh*SIRT1*, pcDNA3.1-NC and pcDNA3.1-*SIRT1* were all purchased from GenePharma (Shanghai, China).

Dual-luciferase reporter gene assay

Binding sites between *miR-373* and *SIRT1* were predicted based on a bioinformatics prediction website (http://mirtarbase.mbc.nctu.edu.tw/php/index.php). The fragment sequences involved at the site of action were obtained. Dual-luciferase reporter gene assay was adopted to detect the relationship between *miR-373* and *SIRT1* and to identify whether *SIRT1* was indeed a direct target gene of *miR-373*. According to the binding sequences of 3′-UTR of *SIRT1*, both the wild type and mutation sequences were designed and synthesized accordingly from Sangon Biotech (Shanghai, China). *SIRT1* 3′-UTR was cloned into pGL4 luciferase reporter plasmid (Promega, USA). Cells were co-transfected with pGL4-*SIRT1* or control pGL4 reporter plasmid and *miR-373* mimics for 48 hours by Lipofectamine™ 2000 (Invitrogen, USA). Changes in the luciferase activity among the groups were detected using a dual-luciferase detection kit (D0010; Beijing Solarbio Science & Technology Co. Ltd., China). The fluorescence intensities were observed by GLomax20/20 Luminometer (E5311; Shaanxi Zhongmei Biotechnology Co., China).

MTT assay

MTT assay was performed to test cell proliferation. Transfected PC cells were seeded into 96-well plates and then incubated for 12 hours. 20 µl of MTT (Sigma-Aldrich, USA) was added into 96-well plates and incubated for 4 hours in a humidified 37˚C incubator with 5% CO_2. Then, medium was removed and 150 µl dimethyl sulfoxide (DMSO, Sigma-Aldrich, USA) was added into 96-well plates. Finally, following shaking at 25˚C for 15 minutes, the optical density was measured at 490 nm by microplate reader (Bio-Rad Laboratories Inc., USA).

Colony formation assay

PC cells were seeded in 6-well plates with 500 cells/well and cultured in a humidified 37˚C incubator with 5% CO_2 for 2 weeks. The cells were washed with phosphate buffer saline (PBS, Sigma-Aldrich, USA) and then fixed by 70% ethanol for 3 minutes after formation of clear colonies. The cells were then stained for 30 minutes with 1% crystal violet (Beyotime, China). The colony number was counted under the microscope.

Apoptosis assay

Apoptotic cells were observed via Annexin V-FITC Apoptosis Detection Kit (Sigma-Aldrich, USA) following the manufacturer's directions. Cells were collected and then washed with pre-cold PBS for twice and resuspended in 1× binding buffer. The cells were labeled with 5 µl Annexin V-FITC for 15 minutes and then 5 µl of PI for 10 minutes at 25˚C in dark. The cells were checked through a FACSCanto II flow cytometer (BD Biosciences, Germany).

TUNEL assay

Cleavage of genomic DNA during apoptosis was measured with In Situ Apoptosis Detection kit from

KeyGen BioTech Ltd. (Jiangsu, China). The samples were rinsed for 3 times with PBS solution. Then, 100 µl Proteinase K solution (9:1 mixture of PBS and Proteinase K) was added at 37˚C for 30 minutes and washed with PBS for 3 times. In the following step, 50 µl TdT enzyme solution was added into the cell samples and incubated at 37˚C for 60 minutes in dark. After washing with PBS for 3 times, the samples were supplemented with 5 µl Streptavidin-Fluorescein solution and 45 µl Labeling Buffer, and incubated at 37˚C for 30 minutes in dark. After washing with PBS and staining with 4',6-diamidino-2-phenylindole (DAPI, Sigma-Aldrich, USA) the cells were observed and photographed via fluorescence microscope.

Analysis of oxidative stress indicators

Cells were lysed with Tris-HCl (Beijing Biotopped Science & Technology Co., China) and treated with extraction buffer (150 mM NaCl, 1 mM Na_2EDTA, 1 mM EGTA, 2.5 mM sodium pyrophosphate and 1% NP-40) on ice. The cells were then centrifuged at 12,000 rpm at 4˚C for 10 minutes. The cell lysates were used for further reactive oxygen species (ROS), malondialdehyde (MDA) and superoxide dismutase (SOD) measurement. ROS, MDA and SOD values of PC cells were detected using the kits produced by Nanjing Jiangcheng Bioengineering Institute (China), and measurement was conducted according to the protocols provided by the manufacturer.

RNA extraction and reverse transcription quantitative polymerase chain reaction

Total RNA was extracted from PC cells using Trizol Kit (ThermoFisher Scientific, USA) based on the manufacturer's instruction, followed by measurement of RNA concentration. The primers were synthesized from TaKaRa Biotechnology Co. (China). Sequences of PCR primers were as follows:

miR-373-
F*:* 5′-GTAGCAGGATGGCCCTAGAC-3′
R: 5′-CGCCCTCTGAACCTTCTCTT-3′

SIRT1-
F: 5′-TAGCCTTGTCAGATAAGGAAGGA-3′
R: 5′-ACAGCTTCACAGTCAACTTTGT-3′

U6 snRNA-
F: 5′-AAAGCAAATCATCGGACGACC-3′
R: 5′-GTACAACACATTGTTTCCTCGGA-3′

GAPDH-
F*:* 5′-GTCGGAGTCAACGGATTTGG-3′
R: 5′-AAAAGCAGCCCTGGTGACC-3′

Reverse transcription was conducted by the PrimeScript RT reagent Kit (TaKaRa Biotechnology Co.). The obtained cDNA was diluted to 50 ng/µl to perform reverse transcription quantitative polymerase chain reaction (RT-qPCR) with SYBR Premix EX TaqTM kit (TaKaRa Biotechnology Co.) in an ABI 7500HT real time PCR system (Applied Biosystems, USA). Glyceraldehyde phosphate dehydrogenase (*GAPDH*) and *U6* snRNA were used as internal controls for mRNA and miRNA, respectively. Relative expression levels were measured by the $2^{-\Delta\Delta Cq}$ method.

Western blotting assay

The cells were harvested and lysed with RIPA buffer (Sigma-Aldrich, USA). Protein concentration of each sample was evaluated by bicinchoninic acid (BCA) protein assay kit (Yi Sheng Biotechnology Co., China). After separation by SDS-PAGE, the proteins were transferred onto polyvinylidenefluoride (PVDF) membranes, and sealed with 5% bovine serum albumin (BSA) at room temperature for 1 hour. The membranes were incubated with primary antibodies SIRT1, BAX, BCL-2, CASPASE-9, CASPASE-8, CASPASE-3, PARP, PGC-1α, NRF2, eNOS, iNOS and GAPDH for 12 hours at 4°C. Then, the membranes were washed three times with Tris-buffered saline containing 0.1% Tween 20 (TBST). Diluted horseradish peroxidase (HRP)-labeled goat anti-rabbit secondary antibody was added to the samples at 25˚C for 1 hour. The membranes were again washed three times with TBST, and the protein bands were visualized using Immobilon Western Chemiluminescent HRP substrate (Millipore, USA). Quantitative protein analysis was performed by ImageJ 1.48u software (National Institutes of Health, USA). GAPDH was served as the internal reference. The antibodies for western blotting were produced by Cell Signaling Technology (USA).

Statistical analysis

All experiments were performed at least for three times in triplicate. Data were expressed as mean ± standard deviation (SD). Data were analyzed with Prism 6.0 (GraphPad Software, USA). Statistical evaluation was performed via Student's t test between two groups and one-way analysis of variance (ANOVA) followed by Tukey's post hoc test for multiple comparisons. Value of $P<0.05$ was statistically considered significant.

Results

miR-373 negatively regulates SIRT1 expression level by binding to *SIRT1* 3′-UTR directly

The expression of *miR-373* was monitored by RT-qPCR and the results showed that in comparison with the *miR-373* NC treated group, level of the *miR-373* was boosted for about 3-4 times after *miR-373* mimics treatment in the both AsPC-1 and PANC-1 cells (Fig.1A). This result suggested successful introduction of *miR-373* mimics into the PC cells included in this study. To test whether *miR-373* can regulate *SIRT1* related to proliferation and apoptosis of PC cells, expression of SIRT1 was monitored upon the application of *miR-373* mimics. As indicated in Figure 1B, mRNA level of *SIRT1* was suppressed by overexpression of *miR-373* in the AsPC-1 and PANC-1 cells compared to *miR-373* NC treated group. Expression of SIRT1 was also monitored at protein level by western blotting. Result revealed that accumulation of SIRT1 protein in tested PC cell lines was decreased about 50% upon overexpression of *miR-373* (Fig.1C, D). These results suggested the *miR-*

373 suppressed expression of SIRT1 in PC cells.

As *miR-373* was able to down-regulate the expression of SIRT1, the potential target 3′-UTR sequence of *miR-373* in *SIRT1* was predicted (Fig.1E), and dual-luciferase reporter assay was employed to identify the potential interaction. As shown in Figure 1F, the relative luciferase activity was declined significantly in AsPC-1 and PANC-1 cells co-transfected with *miR-373* mimics and constructs harboring wild-type of *SIRT1* 3′-UTR. However, luciferase activity retained similar to control in the cells transfected with *miR-373* mimics and constructs harboring *SIRT1* 3′-UTR with mutation at the predicted seed binding sites (Fig.1F). According to these results, we concluded that *miR-373* was able to suppress SIRT1 expression by direct targeting.

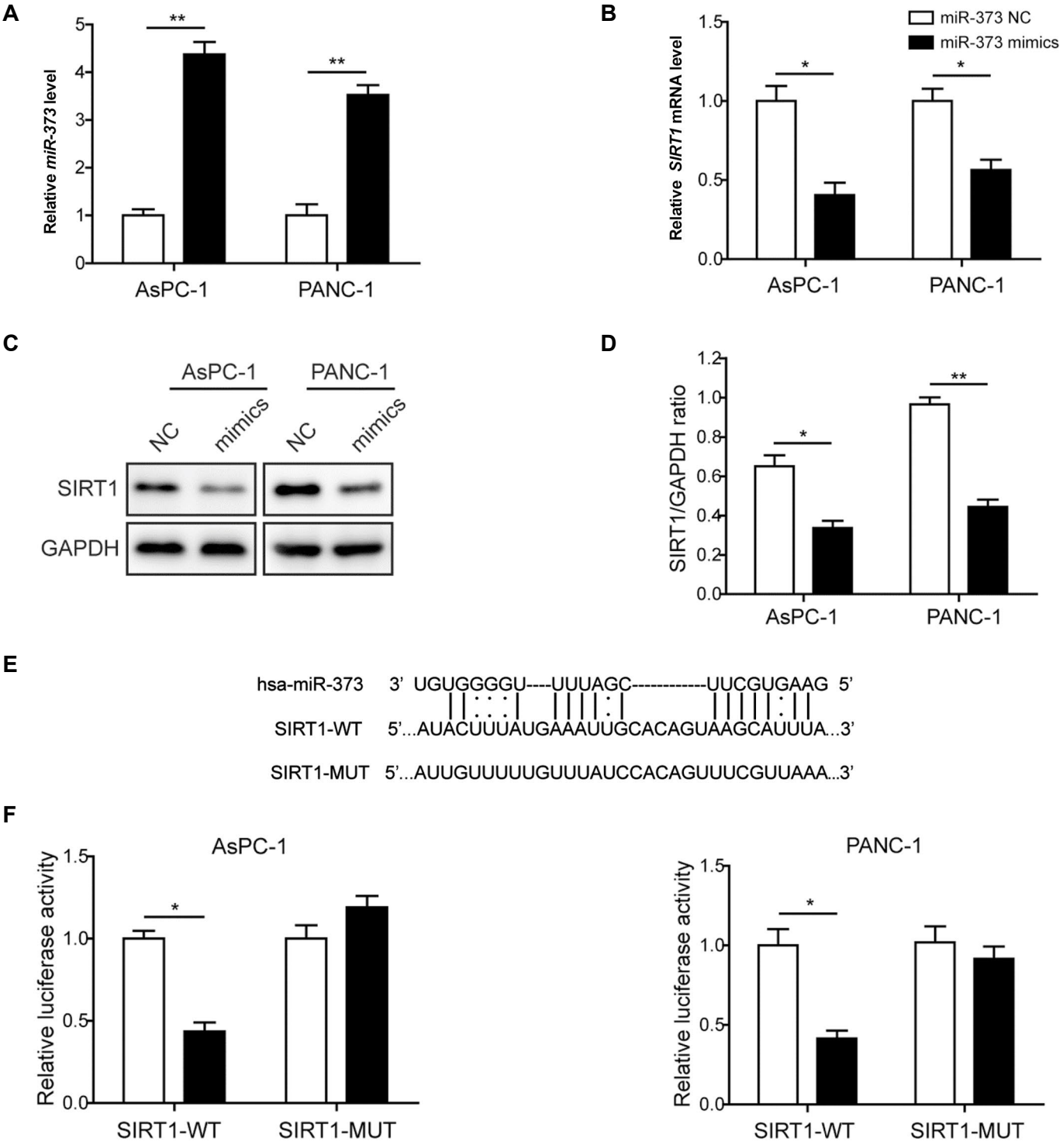

Fig.1: *miR-373* negatively regulates SIRT1 expression level by binding to *SIRT1* 3′-UTR directly. **A.** Relative expression level of *miR-373* in control and mimics-transfected PC cell lines. **B.** Expression of *SIRT1* evaluated by RT-qPCR under regulation of *miR-373*. **C.** Protein level of SIRT1 in *miR-373* mimics-transfected PC cell lines and control cells. **D.** Statistical analysis of the relative protein expression of SIRT1 in the presence of *miR-373* overexpression. **E.** The binding sequences between 3′-UTR of *SIRT1* and *miR-373*. **F.** Luciferase activity detection. PC; Pancreatic cancer, RT-PCR; Reverse transcription-polymerase chain reaction,*; P<0.05, and **; P<0.01.

Restoring *miR-373* or silencing *SIRT1* inhibits proliferation of pancreatic cancer cells

To study the regulatory functions of *miR-373* and *SIRT1* in proliferation of PC cells, MTT and colony formation assays were conducted. The results indicated that introduction of *miR-373* mimics and sh*SIRT1* were both able to hinder proliferation of PC cells (Fig.2A, B). Additionally, as presented in Figure 2C and 2D, transfection with *miR-373* mimics and sh*SIRT1* both impaired colony formation ability of the AsPC-1 and PANC-1 cells versus control group. These results indicated that overexpression of *miR-373* or knockdown of *SIRT1* could dispute proliferation of PC cells.

Restoring *miR-373* or silencing *SIRT1* facilitates apoptosis of pancreatic cancer cells

To explore the effects of *miR-373* and *SIRT1* on cell apoptosis, the PC cells transfected with *miR-373* mimics or sh*SIRT1* were analyzed. The data collected using flow cytometry revealed that the number of apoptotic PC cells in the both *miR-373* mimics-transfected cells was increased significantly in comparison with the control groups (Fig.3A). Similarly, transfection of sh*SIRT1* increased apoptosis ratio of PC cells in the two cell lines included in this study (Fig.3B). Furthermore, TUNEL staining consistently showed that introduction of either *miR-373* mimics or sh*SIRT1* could significantly promote the number of TUNEL$^+$ cells in the both AsPC-1 and PANC-1 cells (Fig.3C, D). All together, these findings indicated that overexpression of *miR-373* or silence of *SIRT1* enhanced apoptosis of PC cells.

Restoring *miR-373* or silencing *SIRT1* regulates apoptosis-related proteins in pancreatic cancer cells

To further study the cellular mechanisms of proliferation and apoptosis alteration in *miR-373* mimics and sh*SIRT1*-transfected PC cells, western blot was performed to examine the expression levels of apoptosis-associated proteins. Introduction of *miR-373* mimics significantly increased accumulation of BAX and cleaved CASPASE-8/9/3 in the two PC cell lines included in this work, while the expression levels of BCL-2 and uncleaved PARP were suppressed (Fig.4A, B). Likewise, silence of *SIRT1* also promoted expression of BAX and activated CASPASE-8/9/3 in studied PC cells, whereas the accumulation of BCL-2 and uncleaved PARP were declined (Fig.4C, D). These results indicated that *miR-373* and *SIRT1*-mediated cell apoptosis was mediated by activating CASPASE-8/9/3 signaling pathways in PC cells.

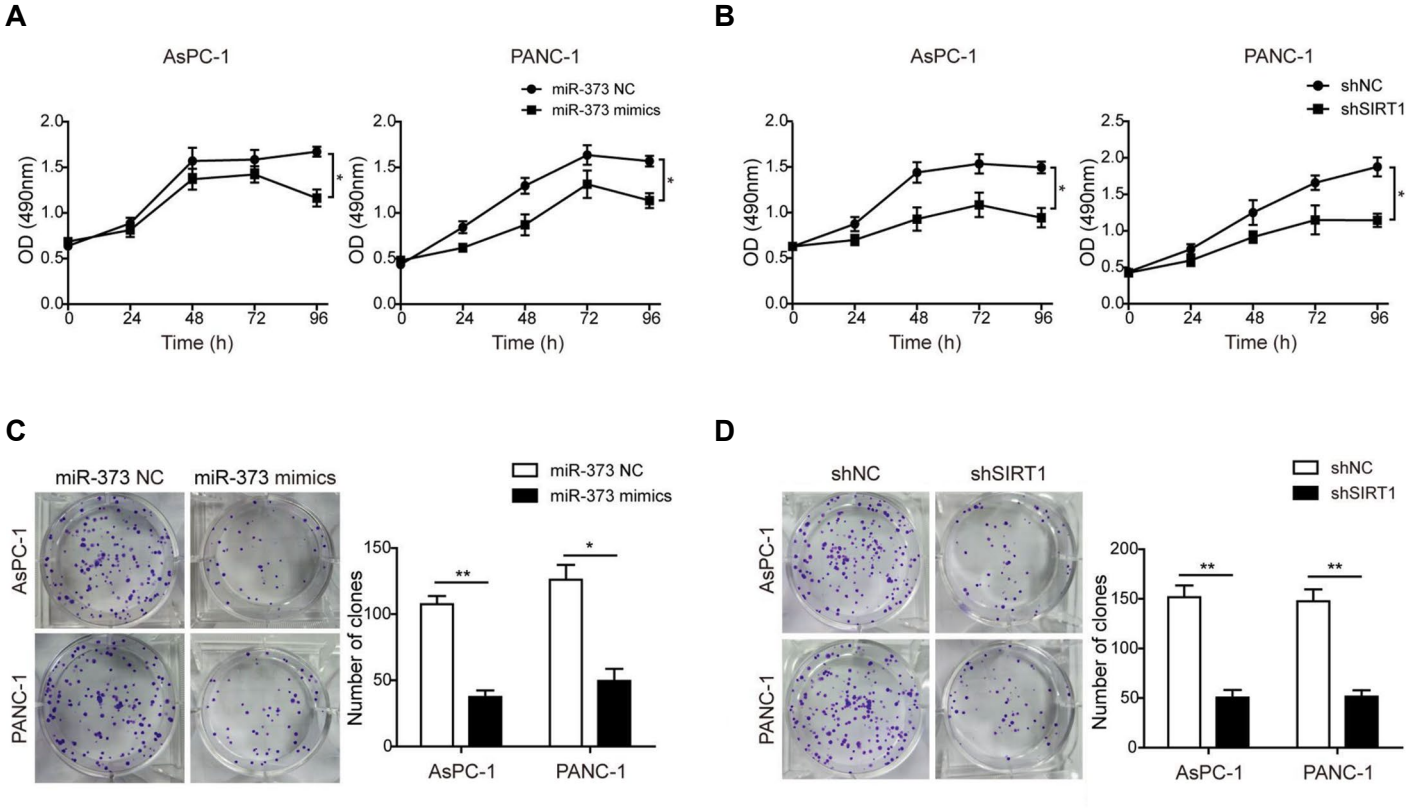

Fig 2: *miR-373* and *SIRT1* regulate proliferation of PC cells. Proliferation of the AsPC-1 and PANC-1 cells after transfection of **A.** *miR-373* mimics and **B.** sh*SIRT1* were examined by MTT assay. Colony formation of the AsPC-1 and PANC-1 cells after transfection of **C.** *miR-373* mimics and **D.** sh*SIRT1* were evaluated by colony formation analysis. PC; Pancreatic cancer, h; Hour, *; P<0.05, and **; P<0.01.

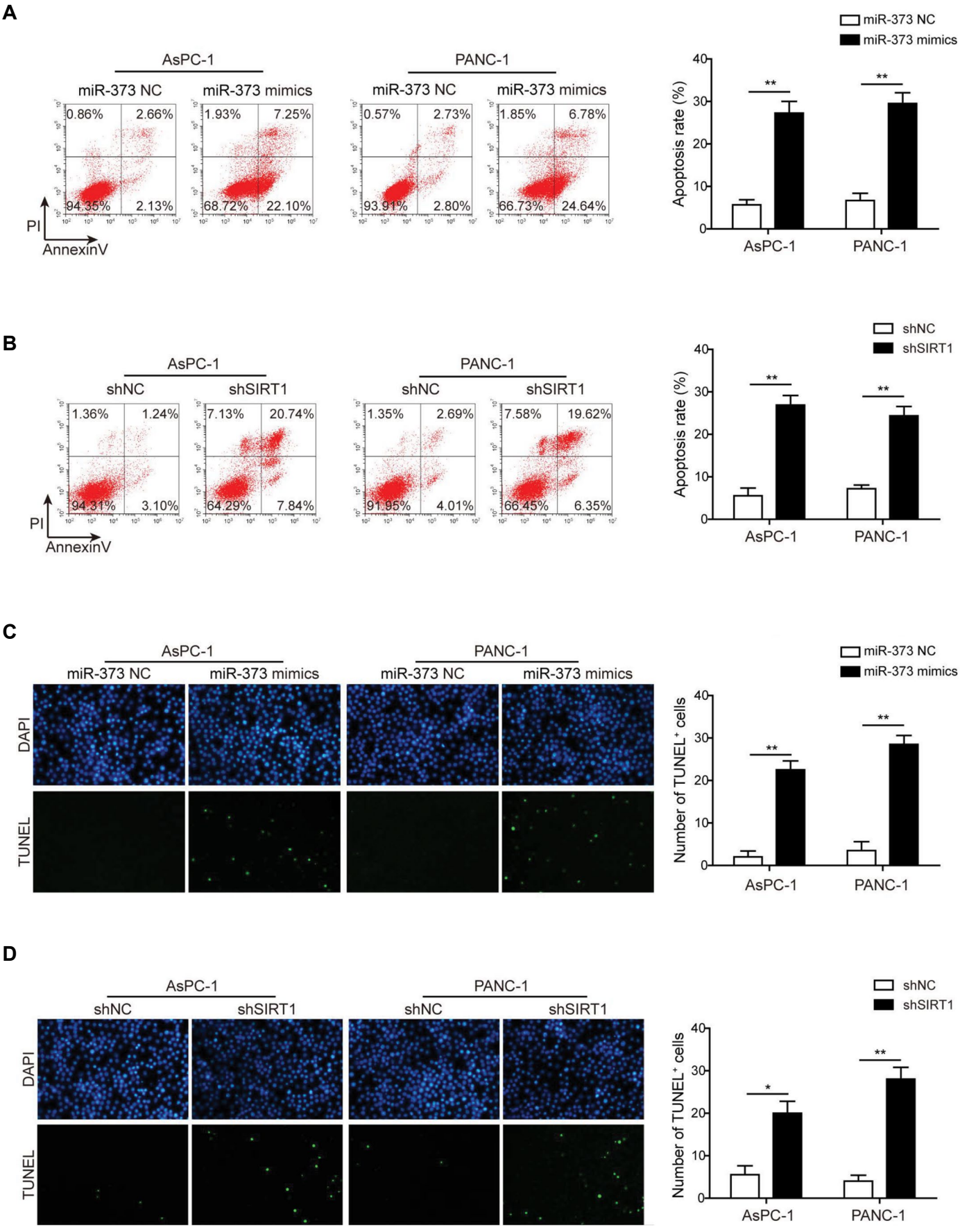

Fig.3: Effects *miR-373* and *SIRT1* on apoptosis of PC cells. **A.** Detection of cell apoptosis by flow cytometry in *miR-373* mimics-transfected AsPC-1 and PANC-1 cells. **B.** Detection of cell apoptosis by flow cytometry in AsPC-1 and PANC-1 cells after *SIRT1* knockdown. **C.** Representative pictures of apoptosis detection by TUNEL in *miR-373* mimics-transfected AsPC-1 and PANC-1 cells. **D.** Representative pictures of apoptosis detection by TUNEL assay in sh*SIRT1*-transfected AsPC-1 and PANC-1 cells. PC; Pancreatic cancer, *; P<0.05, and **; P<0.01.

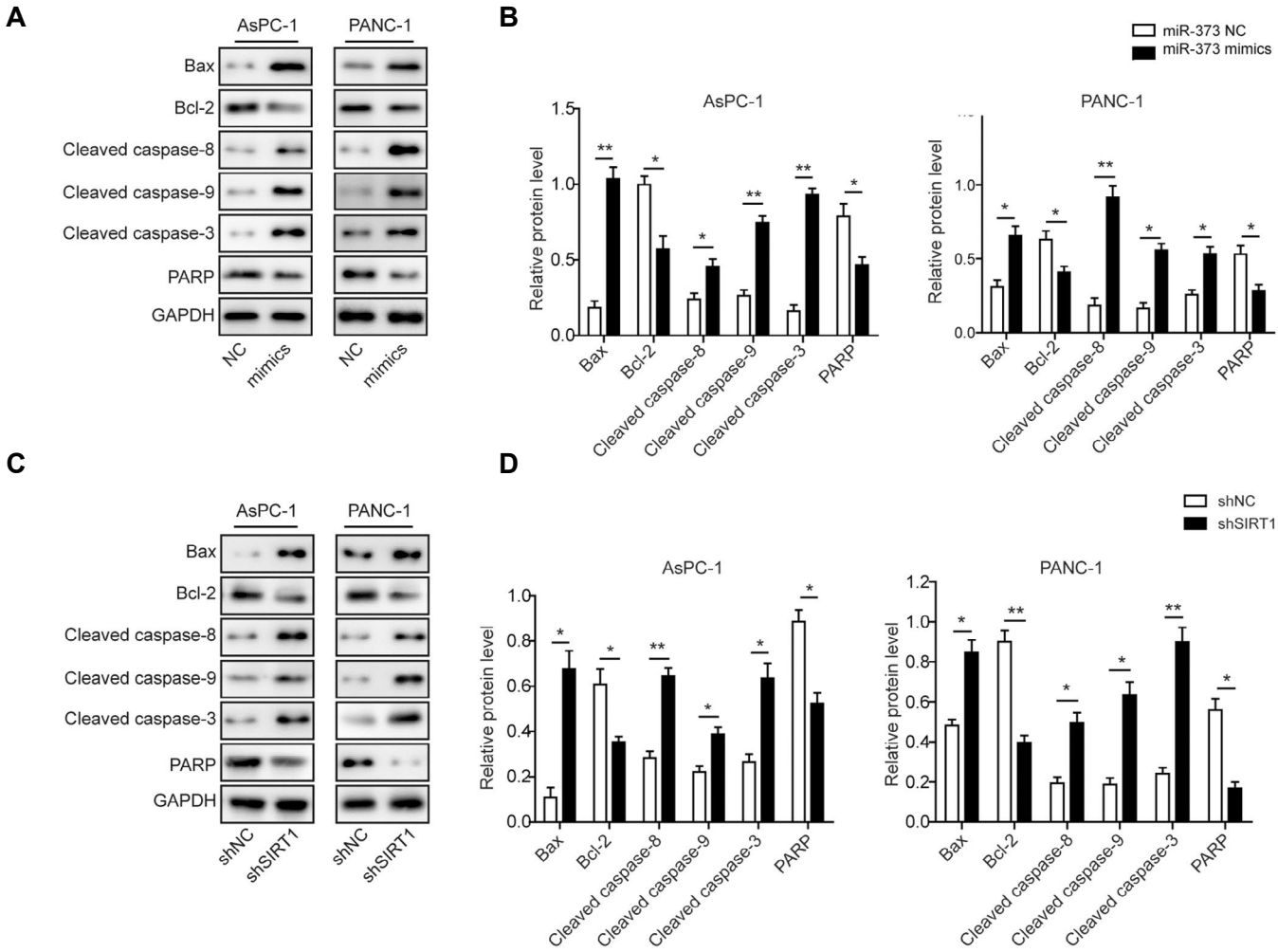

Fig.4: *miR-373* and *SIRT1* regulate apoptosis-associated proteins in PC cells. **A.** Protein expressions of BAX, BCL-2, cleaved CASPASE-8/9/3 and PARP in *miR-373* mimics-transfected PC cells. **B.** Statistical analysis of the relative protein expressions of BAX, BCL-2, cleaved CASPASE-8/9/3 and PARP in the presence of *miR-373* overexpression. **C.** Protein expressions of BAX, BCL-2, cleaved CASPASE-8/9/3 and PARP in sh*SIRT1*-transfected PC cells. **D.** Statistical analysis of the relative protein expressions of BAX, BCL-2, cleaved CASPASE-8/9/3 and PARP in sh*SIRT1*-transfected PC cells. PC; Pancreatic cancer, *; P<0.05, and **; P<0.01.

Restoring *miR-373* or silencing *SIRT1* inhibits PGC-1α/Nrf2 signaling pathway and improves oxidative stress response in pancreatic cancer cells

Since SIRT1 was associated with alteration in the PGC-1α/NRF2 axis, the effects of *miR-373* overexpression or *SIRT1* silencing on PGC-1α/NRF2 signaling pathway were studied. Western blot analysis indicated that the level of PGC-1α, NRF2 and eNOS were dramatically decreased in *miR-373* mimics and sh*SIRT1*-transfected PC cells. In contrast, protein accumulation of iNOS was increased significantly in these *miR-373* mimics and sh*SIRT1*-transfected PC cells (Fig.5A-D).

Since oxidative stress response was an early event in cell apoptosis associated with PGC-1α/ NRF2 signaling pathway, the ROS, MDA and SOD levels involved in *miR-373* and *SIRT1*-mediated regulation were assessed in the PC cells. The contents of ROS and MDA were significantly increased in PC cell lines after transfection with *miR-373* mimics or sh*SIRT1* in comparison with the control groups (Fig.5E, F), whereas, the level of SOD was dramatically decreased by transfection of *miR-373* mimics or sh*SIRT1* in the AsPC-1 and PANC-1 cells (Fig.5G). These results suggested that accumulation of *miR-373* or silence of *SIRT1* could lead to the activation of oxidative stress response via suppressing PGC-1α/NRF2 pathway in both of the PC cells.

miR-373 mediates proliferation and apoptosis of pancreatic cancer cells by SIRT1/PGC-1α/NRF2 signaling pathway

To elucidate whether the SIRT1/PGC-1α/NRF2 signaling pathway participates in the regulatory mechanism of *miR-373* in PC, AsPC-1 cells were treated with *miR-373* mimics followed by pcDNA3.1-*SIRT1*. As shown in Figure 6A and B, MTT and colony formation assays showed no pronounced difference regarding proliferation of PC cells between *miR-373* mimics and *miR-373* mimics+pcDNA3.1-NC groups. We found reduction of proliferative ability of PC cells by *miR-373* mimics was enhanced by overexpression of SIRT1. The results of apoptosis analysis also showed no significant difference of cell apoptosis between *miR-373* mimics and *miR-373* mimics+pcDNA3.1-NC groups, and overexpression of SIRT1 inhibited cell apoptosis induced by *miR-373* (Fig.6C). Western blot analysis displayed increased protein expressions of BAX and cleaved CASPASE-3, while the protein levels of BCL-2 and uncleaved PARP were reduced in PC cells treated with *miR-373* mimics. In

contrast, overexpression of SIRT1 reversed *miR-373* mimics-induced effects (Fig.6D). Subsequently, western blot analysis also showed that transfection of pcDNA3.1-*SIRT1* increased protein levels of PGC-1α, NRF2, eNOS and decreased protein level of iNOS in *miR-373* mimics-treated PC cells, suggesting that overexpression of SIRT1 reversed effects of *miR-373* on PGC-1α/NRF2 signaling and oxidative stress response (Fig.6E). As depicted in Figure 6F, no significant difference concerning the relative levels of ROS, MDA and SOD in *miR-373* mimics as well as *miR-373* mimics+pcDNA3.1-NC groups was observed. We found that reduced levels of ROS and MDA and increased level of SOD in the presence of *miR-373* mimics were rescued by overexpression of SIRT1. Overall, the results suggested that *miR-373* inhibited PC cell proliferation but accelerated apoptosis through modulating oxidative stress response via SIRT1/PGC-1α/NRF2 axis.

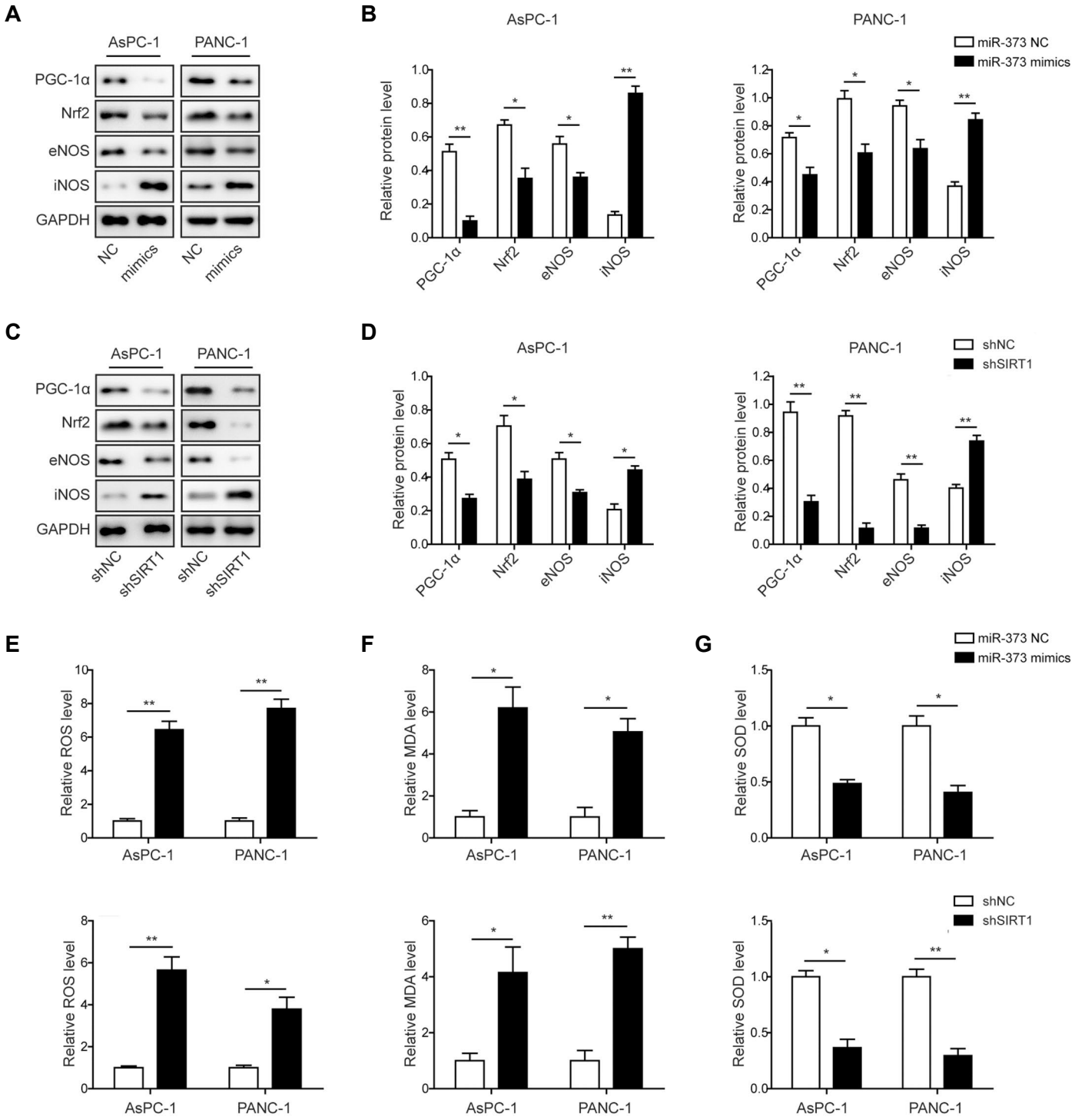

Fig.5: Effects of *miR-373* and *SIRT1* on PGC-1α/NRF2 pathway and oxidative stress response in PC cells. **A.** Levels of PGC-1α, NRF2, eNOS and iNOS in *miR-373* mimics-transfected PC cells. **B.** Statistical analysis of the relative protein levels of PGC-1α, NRF2, eNOS and iNOS in the presence of *miR-373* overexpression. **C.** Expression levels of PGC-1α, NRF2, eNOS and iNOS in sh*SIRT1*-transfected PC cells. **D.** Statistical analysis of the relative protein expression of PGC-1α, NRF2, eNOS and iNOS in the presence of sh*SIRT1*. **E.** Relative ROS level in *miR-373* mimics or sh*SIRT1*-transfected PC cells. **F.** Relative MDA level in *miR-373* mimics or sh*SIRT1*-transfected PC cells. **G.** Relative SOD level in *miR-373* mimics or sh*SIRT1*-transfected PC cells. PC; Pancreatic cancer, *; P<0.05, **; P<0.01, ROS; Reactive oxygen species, MDA; Malondialdehyde, and SOD; Superoxide dismutase.

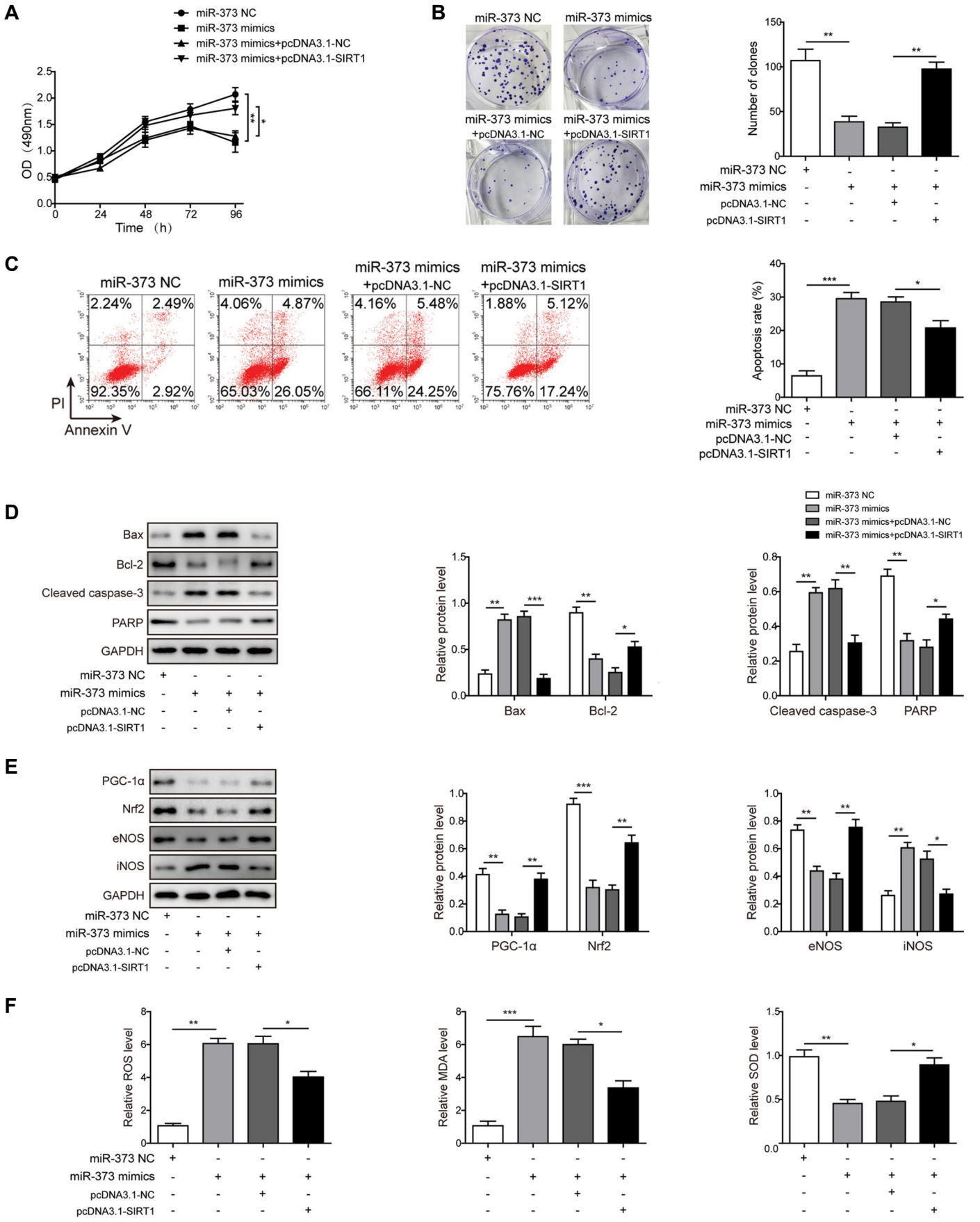

Fig.6: *miR-373* mediates proliferation and apoptosis of PC cells by SIRT1/PGC-1α/NRF2 axis. **A.** Cell proliferation was evaluated by the MTT assays. **B.** Number of cell colonies was tested by colony formation assay. **C.** Cell apoptosis was tested via Annexin-V/PI staining of flow cytometry analysis. **D.** Western blotting of apoptosis-related proteins BCL-2, BAX, cleaved CASPASE-3 and PARP. **E.** Western blotting of PGC-1α, NRF2, eNOS and iNOS proteins. **F.** Relative levels of ROS, MDA and SOD. AsPC-1 cells were treated with *miR-373* NC, *miR-373* mimics, *miR-373* mimics+pcDNA3.1-NC, and *miR-373* mimics+pcDNA3.1-*SIRT1*. PC; Pancreatic cancer, *; P<0.05, **; P<0.01, ***; P<0.001, ROS; Reactive oxygen species, MDA; Malondialdehyde, and SOD; Superoxide dismutase.

Discussion

PC is a lethal malignancy characterized by aggressive biological behaviors with the pronounced potential for invasion and metastasis, as well as resistance to many available anti-cancer agents (25, 26). PC is generally diagnosed in the more advanced stages, with a scarcity of effective therapies available. The present study demonstrated that *SIRT1* was verified as the direct target of *miR-373* in PC cells. Overexpression of *miR-373* decreased cellular accumulation of SIRT1 and resulted in the suppression of SIRT1-mediated PGC-1α/NRF2 signaling pathways. The downstream oxidative response was enhanced by this mechanism, which hindered the progression of PC by impairing PC cells proliferation in one hand and enhancing apoptosis of PC cells on the other hand. The roles of *miR-373*/*SIRT1* axis on regulating proliferation and apoptosis in PC cells were studied for the first time. Our findings provided the possibility that *miR-373* might serve as a potential new therapy for PC.

In our work, we proved that overexpression of *miR-373* in AsPC-1 and PANC-1 cells not only caused suppression of cell proliferation, but also boosted cell apoptosis. These two effects, together, would result in inhibition of PC development. In combination with the reality that *miR-373* level was dramatically declined in PC, we concluded that *miR-373* was indeed a tumor suppressor. Silence of *SIRT1* also had similar effects on proliferation and apoptosis in the examined PC cells. In our study, we also found that application of *miR-373*mimics or sh*SIRT1* in PC cells could stimulate activation of apoptosis through up-regulating expression of BAX and cleaved CASPASE-8/9/3, while down-regulating expression of BCL-2 and uncleaved PARP. Researches proved that *miR-373* had significant regulating functions in breast cancer and seminoma (27, 28). In recent research, the role of a *miR-373* family member (*miR-373-3p*) in cell growth of lung adenocarcinoma was profiled, by targeting amyloid precursor protein (29). However, the function and mechanism of *miR-373* regulating PC progression have not been much clarified. Zhang et al. (30) reported that *miR-373* could down-regulate expression levels of TP53INP1, LATS2 and CD44 to promote PC development. Shao et al. (31) proved that LATS2 reduced antioxidant protein levels which in turn promoted the oxidative stress. These studies suggested that *miR-373* played important roles in promoting development of pancreatic cancer. However, we found that *miR-373* could inhibit cell proliferation and apoptosis via regulation of SIRT1/PGC-1α/NRF2 axis in pancreatic cancer, which was consistent with the report of Nakata et al. (13) indicating that *miR-373* was down-regulated in PC and suppressed invasion of tumor cells. Furthermore, Hua et al. reported that low level of serum *miR-373* predicted poor prognosis in patients with PC (14). This was also consistent with our study. This controversial conclusion needs to be further studied in future. Additionally, interaction of *miR-373* with LATS2 in PC is deeply worthy to explore and investigate, in our lab in future.

Subsequently, we elucidated whether SIRT1/PGC-1α/NRF2 pathway participated in the regulatory mechanism of *miR-373* in PC cells. PC cells were treated with *miR-373* mimics followed by pcDNA3.1-*SIRT1*. Our results suggested overexpression of SIRT1 reversed pro-apoptotic an anti-proliferative effects of *miR-373* on PC cells. At the same time, inhibition of PGC-1α/NRF2 signaling pathway mediated by *miR-373* mimics was weakened in the presence of pcDNA3.1-*SIRT1*. Dual-luciferase reporter assay proved that *miR-373* exerted its regulating functions by direct interaction with *SIRT1*. The present work was a novel report about *miR-373* negatively regulating *SIRT1* interfered in PC progression. Liu and Wilson (32) discovered that *miR-373* was able to target the 3′-UTR of *mTOR* and *SIRT1* mRNA to regulate MMP-9 expression in fibrosarcoma HT1080 cells. In addition, *miR-373* was also found to up-regulate MMP-9 by regulating *SIRT1*, leading to activation of the RAS/RAF/MEK/ERK pathways in fibrosarcoma cells (33). Similarly, *SIRT1* was identified and proved as a direct target of *miR-373* in PC cells for the first time, in the present work. Taken together, this conserved targeting pattern and blocking SIRT1 expression by *miR-373* suggested that regulatory mechanisms of MMP-9, mediated by *miR-373*, may also be existed in PC cells. This could be studied in our future work. In the previous work, *miR-373* was also indicated as a potential "onco-miRNA" in other multiple cancers (34).

SIRT1 plays important roles in diverse cellular processes including oxidative stress alleviation, oncogenesis, aging and cancer progression (35). PGC-1α, as one of downstream targets of SIRT1, is not only a regulator of mitochondrial genesis, but also known to protect from oxidative stress. Previous studies observed that SIRT1/PGC-1α/NRF2 signaling pathway was correlated with various cellular responses to oxidative stress. For instance, overexpression of SIRT1 strongly induced PGC-1α/NRF2 expression levels in human cancer cells (36). In our study, the enhanced oxidative metabolism was found in the *miR-373* mimics or sh*SIRT1*-transfected PC cells. Here, we also found that *miR-373* mimics or sh*SIRT1* could disturb expressions of PGC-1α and NRF2, while up-regulate ROS and MDA levels. These results indicated that overexpression of *miR-373* could interrupt SIRT1-mediated activation of PGC-1α/NRF2 pathway, thus enhancing oxidative stress, preventing PC progression. A large number of studies have also shown that ROS can stimulate tumorigenesis via oxidation of DNA and subsequent mutation of genes promoting carcinogenesis (37). ROS production has been detected in various cancers, which has been proven to have various roles. For example, ROS can activate pro-tumourigenic signaling, promote cell survival and proliferation, in addition to driving DNA damage and genetic instability (38). DeNicola et al. (39) also reported activating a ROS-detoxification program contributed to tumorigenesis. In contrast, Li et al. (40) found that cardamonin suppressed tumor growth by inducing G2/M phase cell cycle arrest and apoptosis via upregulation of ROS. These studies suggested that ROS

could also promote anti-tumourigenic signaling, which were consistent to our study. To summarize, this is a novel research that studied *miR-373*/*SIRT1* axis and PGC-1α/NRF2 pathway-mediated oxidative stress in the PC cell proliferation and apoptosis.

Conclusion

To conclude, our observation demonstrated that *miR-373* was revealed to participate in the modulation of apoptosis and proliferation by directly targeting *SIRT1* in PC cells for the first time. Moreover, the novel correlation of *miR-373*/*SIRT1* axis with PGC-1α/NRF2 pathway to regulate proliferation and apoptosis of PC cells was studied. Our results suggested *miR-373* might be a potential drug target for PC treatment.

Acknowledgements

There is no financial support and conflict of interest in this study.

Authors' Contributions

Z.-Y.L.; Contributed to the conception, design and were responsible for overall supervision. Q.-H.Y., Y.Z.; Contributed to the all experimental work, data and statistical analysis, and interpretation of data. Y.Z.; Drafted the manuscript, which was revised by Q.-H.Y. All authors read and approved the final manuscript.

References

1. Collisson EA, Bailey P, Chang DK, Biankin AV. Molecular subtypes of pancreatic cancer. Nat Rev Gastroenterol Hepatol. 2019; 16(4): 207-220.
2. Golan T, Hammel P, Reni M, Van Cutsem E, Macarulla T, Hall MJ, et al. Maintenance olaparib for germline brca-mutated metastatic pancreatic cancer. N Engl J Med. 2019; 381(4): 317-327.
3. Waddell N, Pajic M, Patch AM, Chang DK, Kassahn KS, Bailey P, et al. Whole genomes redefine the mutational landscape of pancreatic cancer. Nature. 2015; 518(7540): 495-501.
4. Wu HH, Hwangverslues WW, Lee WH, Huang CK, Wei PC, Chen CL, et al. Targeting IL-17B–IL-17RB signaling with an anti–IL-17RB antibody blocks pancreatic cancer metastasis by silencing multiple chemokines. J Exp Med. 2015; 212(3): 333-349.
5. Conroy T, Bachet JB, Ayav A, Huguet F, Lambert A, Caramella C, et al. Current standards and new innovative approaches for treatment of pancreatic cancer. Eur J Cancer. 2016; 57: 10-22.
6. Pan Y, Wang L, Kang SG, Lu Y, Yang Z, Huynh T, et al. Gd-Metallofullerenol nanomaterial suppresses pancreatic cancer metastasis by inhibiting the interaction of histone deacetylase 1 and metastasis-associated protein 1. Acs Nano. 2015; 9(7): 6826-6836.
7. Gebert LFR, MacRae IJ. Regulation of microRNA function in animals. Nat Rev Mol Cell Biol. 2019; 20(1): 21-37.
8. Saliminejad K, Khorram Khorshid HR, Soleymani Fard S, Ghaffari SH. An overview of microRNAs: Biology, functions, therapeutics, and analysis methods. J Cell Physiol. 2019; 234(5): 5451-5465.
9. Wang Y, Xu Z, Wang X. miRNA-373 promotes urinary bladder cancer cell proliferation, migration and invasion through upregulating epidermal growth factor receptor. Exp Ther Med. 2019; 17(2): 1190-1195.
10. Rawat M, Kadian K, Gupta Y, Kumar A, Chain PSG, Kovbasnjuk O, et al. MicroRNA in pancreatic cancer: from biology to therapeutic potential. Genes (Basel). 2019; 10(10). pii: E752.
11. Tian YY, Jia CM, Li Y, Wang Y, Jiang L, Liu AC. Restoration of microRNA-373 suppresses growth of human T-cell lymphoma cells by repressing CCND1. Eur Rev Med Pharm Sci. 2016. 20(21): 4435.
12. Wei F, Wang Q, Su Q, Huang H, Luan J, Xu X, et al. miR-373 inhibits glioma cell U251 migration and invasion by down-regulating CD44 and TGFBR2. Cell Mol Neurobiol. 2016. 36(8): 1389-1397.
13. Nakata K, Ohuchida K, Mizumoto K, Aishima S, Oda Y, Nagai E, et al. Micro RNA-373 is down-regulated in pancreatic cancer and inhibits cancer cell invasion. Ann Surg Oncol. 2014. 21 Suppl 4: 5564-5574.
14. Hua Y, Chen H, Wang L, Wang F, Wang P, Ning Z, et al. Low serum miR-373 predicts poor prognosis in patients with pancreatic cancer. Cancer Biomark. 2017; 20(1): 95-100.
15. Hu W, Liu Q, Pan J, Sui Z. MiR-373-3p enhances the chemosensitivity of gemcitabine through cell cycle pathway by targeting CCND2 in pancreatic carcinoma cells. Biomed Pharmacother. 2018; 105: 887-898.
16. Chen P, Wang M, Wang C. Qingyihuaji formula reverses gemcitabine resistant human pancreatic cancer through regulate lncRNA AB209630/miR-373/EphB2-NANOG signals. Biosci Rep. 2019; 39(6). Pii: BSR20190610.
17. Zhu S, Dong Z, Ke X, Hou J, Zhao E, Zhang K, et al. The roles of sirtuins family in cell metabolism during tumor development. Semin Cancer Biol. 2019; 57: 59-71.
18. Yang H, Liao D, Tong L, Wu L, Wu K. MiR-373 exacerbates renal injury and fibrosis via NF-κB/MatrixMetalloproteinase-9 signaling by targeting Sirtuin1. Genomics. 2019; 111(4): 786-792.
19. Rodgers JT, Lerin C, Haas W, Gygi SP, Spiegelman BM, Puigserver P. Nutrient control of glucose homeostasis through a complex of PGC-1alpha and SIRT1. Nature. 2005; 434(7029): 113-118.
20. Fanibunda SE, Deb S, Maniyadath B, Tiwari P, Ghai U, Gupta S, et al. Serotonin regulates mitochondrial biogenesis and function in rodent cortical neurons via the 5-HT2A receptor and SIRT1-PGC-1alpha axis. Proc Natl Acad Sci USA. 2019; 116(22): 11028-11037.
21. Cloer EW, Goldfarb D, Schrank TP, Weissman BE, Major MB. NRF2 activation in cancer: from dna to protein. Cancer Res. 2019; 79: 889-898.
22. Kubo Y, Wruck CJ, Fragoulis A, Drescher W, Pape HC, Lichte P, et al. Role of Nrf2 in fracture healing: clinical aspects of oxidative stress. Calcif Tissue Int. 2019; 105(4): 341-352.
23. Tu W, Wang H, Li S, Liu Q, Sha H. The anti-inflammatory and anti-oxidant mechanisms of the Keap1/Nrf2/ARE signaling pathway in chronic diseases. Aging Dis. 2019; 10(3): 637-651.
24. Huang K, Huang J, Xie X, Wang S, Chen C, Shen X, et al. Sirt1 resists advanced glycation end products-induced expressions of fibronectin and TGF- β 1 by activating the Nrf2/ARE pathway in glomerular mesangial cells. Free Radic Biol Med. 2013. 65: 528-540.
25. Ono H, Basson MD, Ito H. PTK6 promotes cancer migration and invasion in pancreatic cancer cells dependent on ERK signaling. PLoS One. 2014. 9(5): e96060.
26. Zhou CX, Wang CL, Yu AL, Wang QY, Zhan MN, Tang J, et al. MiR-630 suppresses breast cancer progression by targeting metadherin. Oncotarget. 2016. 7(2): 1288-1299.
27. Keklikoglou I, Koerner C, Schmidt C, Zhang JD, Heckmann D, Shavinskaya A, et al. MicroRNA-520/373 family functions as a tumor suppressor in estrogen receptor negative breast cancer by targeting NF-kappaB and TGF-beta signaling pathways. Oncogene. 2011; 31(37): 4150-4163.
28. Bing Z, Master SR, Tobias JW, Baldwin DA, Xu XW, Tomaszewski JE. MicroRNA expression profiles of seminoma from paraffin-embedded formalin-fixed tissue. Virchows Arch. 2012. 461(6): 663-668.
29. Fan X, Xu S, Yang C. miR-373-3p promotes lung adenocarcinoma cell proliferation via APP. Oncol Lett. 2018; 15(1): 1046-1050.
30. Zhang Y, Yang J, Cui X, Chen Y, Zhu VF, Hagan JP, et al. A novel epigenetic CREB-miR-373 axis mediates ZIP4-induced pancreatic cancer growth. EMBO Mol Med. 2013; 5(9): 1322-1334.
31. Shao D, Zhai P, Del Re DP, Sciarretta S, Yabuta N, Nojima H, et al. A functional interaction between Hippo-YAP signalling and FoxO1 mediates the oxidative stress response. Nat Commun. 2014; 5: 3315.
32. Liu P, Wilson MJ. miR-520c and miR-373 upregulate MMP9 expression by targeting mTOR and SIRT1, and activate the Ras/Raf/MEK/Erk signaling pathway and NF-κB factor in human fi-

brosarcoma cells. J Cell Physiol. 2012; 227(2): 867-876.
33. Lu S, Zhu Q, Zhang Y, Song W, Wilson MJ, Liu P. Dual-functions of miR-373 and miR-520c by differently regulating the activities of MMP2 and MMP9. J Cell Physiol. 2015; 230(8): 1862-1870.
34. Huang Q, Gumireddy K, Schrier M, Sage CL, Nagel R, Nair S, et al. The microRNAs miR-373 and miR-520c promote tumour invasion and metastasis. Nat Cell Biol. 2008. 10(2): 202-210.
35. Alves-Fernandes DK, Jasiulionis MG. The role of SIRT1 on DNA damage response and epigenetic alterations in cancer. Int J Mol Sci. 2019; 20(13): 3153.
36. Kulkarni SR, Donepudi AC, Xu J, Wei W, Cheng QC, Driscoll MV, et al. Fasting induces nuclear factor E2-related factor 2 and ATP-binding Cassette transporters via protein kinase A and Sirtuin-1 in mouse and human. Antioxid Redox Signal. 2014; 20(1): 15-30.
37. Moloney JN, Cotter TG. ROS signalling in the biology of cancer. Semin Cell Dev Biol. 2018; 80: 50-64.
38. Panieri E, Santoro MM. ROS homeostasis and metabolism: a dangerous liason in cancer cells. Cell Death Dis. 2016; 7: e2253.
39. DeNicola GM, Karreth FA, Humpton TJ, Gopinathan A, Wei C, Frese K, et al. Oncogene-induced Nrf2 transcription promotes ROS detoxification and tumorigenesis. Nature. 2011; 475(7354): 106-109.
40. Li Y, Qin Y, Yang C, Zhang H, Li Y, Wu B, et al. Cardamonin induces ROS-mediated G2/M phase arrest and apoptosis through inhibition of NF-kappaB pathway in nasopharyngeal carcinoma. Cell Death Dis. 2017; 8(8): e3024.

Original Article

Identification of Circulating *hsa-miR-324-3p* and *hsa-miR-331-3p* Exchanges in The Serum of Alzheimer's Patients and Insights into The Pathophysiological Pathways

Maryam Heydari, M.Sc., Zohreh Hojati, Ph.D.*, Moein Dehbashi, Ph.D.

Division of Genetics, Department of Cell and Molecular Biology and Microbiology, Faculty of Biological Science and Technology, University of Isfahan, Isfahan, Iran

**Corresponding Address: P.O.Box: 81746-73441, Division of Genetics, Department of Cell and Molecular Biology and Microbiology, Faculty of Biological Science and Technology, University of Isfahan, Isfahan, Iran*
Email: z.hojati@sci.ui.ac.ir

Received: 11/July/2019, Accepted: 8/December/2019

Abstract

Objective: Alzheimer's disease (AD) is a type of dementia. Currently, there are not any existing and reliable methods for the prognosis or diagnosis of AD. Hence, finding a diagnostic/prognostic biomarker for AD helps physicians to prescribe the treatments and methods preventing disease progression. Circulating microRNAs (miRNAs) are the most promising biomarkers due to their non-invasive and easily accessible for diagnosis and prognosis of AD. The aim of current study is to evaluate expression levels of two unwell-known circulating miRNAs including *hsa-miR-324-3p* and *hsa-miR-331-3p* in serums of AD patients and to understand their roles in AD physiopathogenesis by in silico analysis.

Materials and Methods: In this case and control study, to get the gene targets related to these two miRNAs, TargetScan, miRTargetLink Human and mirDIP web servers were applied. In addition, gene networks and gene ontology enrichment analysis were performed by STRING 10.5, KEGG and ShinyGO v0.41. Experimentally, expression levels of these two miRNAs in the serum of 21 patients with AD and 23 healthy individuals were compared using the quantitative reverse transcription polymerase chain reaction (qRT-PCR) method.

Results: The pathophysiological pathways associated with these two miRNAs were nucleotide metabolism and cellular response to stress pathway. Furthermore, the upregulated expression levels of *hsa-miR-324-3p* and *hsa-miR-331-3p* in comparison with the healthy control serums were not statistically significant (P>0.05).

Conclusion: Non-significant results were obtained from the expression levels of AD patients and two significant pathways were obtained by networks and gene enrichment analysis.

Keywords: Alzheimer's Disease, MicroRNAs, Quantitative Reverse Transcription Polymerase Chain Reaction, Serum

Cell Journal(Yakhteh), Vol 23, No 2, July 2021, Pages: 211-217

Citation: Heydari M, Hojati Z, Dehbashi M. Identification of circulating hsa-miR-324-3p and hsa-miR-331-3p exchanges in the serum of alzheimer's patients and insights into the pathophysiological pathways. Cell J. 2021; 23(2): 211-217. doi: 10.22074/cellj.2021.7047.

Introduction

Alzheimer's disease (AD) is a neurodegenerative and age-dependent disease in which the patients suffer loss of memory, cognitive and behavior dysfunctions (1-3). Investigations on postmortem AD brains showed that is mainly relied on intracellular neurofibrillary tangles (NFTs), extracellular (Amyloid β) Aβ plaques, synaptic damage, loss of synapses, loss of synaptic proteins, proliferation of reactive astrocytes and activated microglia, deficiency in cholinergic neurons, an age-dependent imbalance in hormones, as well as structural and functional alterations in mitochondria (4-13). Early manifestations in the pathogenesis and progression of AD include synaptic damage, loss of synapses and mitochondrial oxidative damage (12). Besides, cognitive decline in AD patients are obtained from lack of synapses and synaptic damage, as the most obvious features (14). Aging is a step, making the risk factor for developing AD in the society. However, prognosis and diagnosis of AD can help physicians recognize this neurological disorder to prescribe the drugs delaying or preventing disease progression.

In this way, the molecular biomarkers are under the spotlight for their potential roles. Nowadays, recent achievements demonstrated that circulating and blood-based miRNAs, as small non-coding RNAs (20-24 nucleotides), can be applied as early detectable peripheral biomarkers for aging and AD as well as the other neurological diseases (15, 16). There are some miRNAs that are involved in most of the neurodegenerative diseases (8, 17). Kumar et al. (18) demonstrated the discovery and validation of the unique circulating miRNA signatures including hsa-let-7d-5p, hsa-let-7g-5p, hsa-miR-15b-5p, hsa-miR-142-3p, hsa-miR-191-5p, hsa-miR-301a-3p and hsa-miR-545-3p in plasma, which could identify AD patients from healthy controls.

Some studies also showed miR-324-3p was downregulated in the brain tumor cells and suggested

its hypothetical role as tumor suppressor (19-21). Liu et al. (22) showed that miR-324-3p was downregulated in the brain of an embolic stroke model and its expression may be an indicator of recovery. In addition, Stappert et al. (21) reported that miR-324-3p was upregulated in neural cells compared to human embryonic stem cells and it was further enhanced upon differentiation. However, Vallelunga et al. (23) observed that miR-324-3p, as a circulating miRNA, was upregulated in the serum of Parkinson's disease (PD) and Multiple System Atrophy (MSA) patients in comparison with healthy individuals. Until now, the literature on the role of miR-324-3p in the function and mechanism of AD is undefined. This clue persuaded us to find the miR-324-3p expression level in the serum of AD patients and the signaling pathways in which this miRNA can be computationally involved. On the other hand, Wang et al. (24) reported miR-331-3p was downregulated in the cerebral cortex of Alzheimer's patients (24). Olivieri et al. (25) showed the upregulation of miR-331-3p in the plasma of elderly individuals. Balakathiresan et al. (26) used a rat model of learned helplessness stress to identify significantly modulated miRNAs in serum after traumatic stress and reported miR-331-3p was upregulated. Epis et al. (27) showed HuR and miR-331-3p participate in the overexpression of ERBB-2 observing in some prostate cancers. Saba and Booth (28) analyzed miRNA expression in the mouse brain during prion-induced neurodegeneration and reported that miR-331-3p was up-regulated. Wang et al. (24) showed downregulation of *hsa-miR-331-3p* in the brain white and gray matter of the female AD patients. Zanette et al. (29) showed the upregulation of *hsa-miR-331-3p* in acute lymphoblastic leukemia (ALL) malignancies. This clue motivated us to focus on the role of *hsa-miR-331-3p* in AD patients as a circulating miRNA and to find computationally the disease related pathways. Therefore, two miRNAs in this paper, including hsa-miR-324-3p and hsa-miR-331-3p, were considered by their expression changes and enrichment analyses in serum of AD patients based on pathophysiological approach.

Materials and Methods

Network and enrichment analysis

The publicly available databases including TargetScan (http://www.targetscan.org/vert_71), miRTargetLink Human (https://ccb-web.cs.uni-saarland.de/mirtargetlink) and mirDIP (http://ophid.utoronto.ca/mirDIP/index.jsp) were applied. The targets of hsa-miR-324-3p and hsa-miR-331-3p were obtained using the options including strong evidence, weaker evidence and predicted interactions from miRTargetLink. In addition, the targets of these two miRNAs were achieved according to the score class (very high, high and medium) from mirDIP. Furthermore, STRING 10.5 (https://string-db.org), KEGG biological pathway (https://www.genome.jp) and ShinyGO v0.41 (Gene Ontology Enrichment Analysis + more; http://bioinformatics.sdstate.edu/go) by P value cut off= 0.05 for false discovery rate (FDR) were utilized to determine the gene networks and gene ontology enrichment analysis.

Ethics statements

This research was done in accordance with the Declaration of Helsinki. Informed consents were obtained from all individual participants/their families for this research. In addition, the research was confirmed by the Ethics Committee of the University of Isfahan (Isfahan, Iran), with the approval code of 98/50297.

Serum samples

In this case and control study, the patients included in this survey were people with AD residing at the Sadeghyeh Welfare Organization (Isfahan, Iran) between December 2016 and February 2017. For this aim, 44 blood samples, including 21 patients with AD and 23 healthy individuals were collected. The AD patients were diagnosed following the NINDS-ADRDA criteria (30) and revised criteria from the National Institute on Aging-Alzheimer Association (31). Blood samples were gained by venous puncture, permitted to be clotted for 30 minutes and centrifuged at 2000 rpm for 10 minutes to get the sera sample. The sera were then collected and allocated into the new tubes and stored at -80˚C until.

RNA isolation

All RNAs (including miRNA) were isolated by miRCURY™ RNA Isolation Kit- Biofluids (Exiqon, Denmark) from serum samples according to manufacturer's instruction. The ratio between the 260 nm and 280 nm absorbance (A260/A280) provided us with an estimate of purity of the RNA. The purity of extracted RNAs was analyzed by NanoDrop Spectrophotometer (ND-1000, Thermo Fisher, USA). All purified RNAs had an A260/A280 ratio of 1.8-2.1 in 10 mM Tris-Cl, pH=7.5. *hsa-miR-451* (32, 33) and *UniSp6* (recommended by kit) were used as internal control and the spike-in control, respectively. *UniSp6* spike-in control was added to the RT reaction mix.

cDNA synthesis, quantitative reverse transcription polymerase chain reaction and polyacrylamide gel electrophoresis

cDNAs synthesis for *hsa-miR-324-3p*, *hsa-miR-331-3p* and *hsa-miR-451* (internal control) were performed by miRCURY LNA™ Universal RT microRNA PCR (Exiqon, Denmark), as indicated by the manufacturer, and *UniSp6*, RNA Spike-in template was used as a positive control. cDNA products were incorporated into a master mix composed of 10 pmol/µl of *hsa-miR-324-3p*, *hsa-miR-331-3p* and *hsa-miR-451* DNA primers (Exiqon, Denmark) and 2 U of ExiLEN SYBR® Green master mix (Exiqon, Denmark). 20 µl of RT reaction was diluted

20× and 4 µl of the diluted cDNA was used in 10 µl polymerase chain reaction **(**PCR) amplification reactions. A non-template control (NTC) was added to verify the specificity of the quantitative reverse transcription PCR **(**qRT-PCR). Reactions of qRT-PCR were carried out using Opticon Monitor 3 (Bio-Rad Laboratories Inc., USA). All reactions were carried out in triplicate. Data of qRT-PCR were assessed according to the $2^{-\Delta\Delta CT}$ method. All specific amplicons resulted from qRT-PCR was loaded and electrophoresed on 12% non-denaturing polyacrylamide gel electrophoresis (PAGE) in 1X Tris/Borate/EDTA(TBE) buffer along with 50 bp DNA ladder (Thermo Fisher Scientific, USA) and visualized by silver staining.

Statistical analysis

Statistical tests were executed by SPSS (version 21, IBM Corporation, USA). Student's independent t test was done to analyze the quantitative expression level of *hsa-miR-324-3p* and *hsa-miR-331-3p* between different groups. For all analyses P<0.05 were considered statistically significant.

Results

Enrichment and signaling pathways

In the case of predicted targets of *hsa-miR-324-3p* from mirDIP server, it was notable that integrated scores was ranged between 0.067 and 0.014. In this server, predicted targets of *hsa-miR-331-3p* were qualified between 0.74 and 0.014 by integrated scores. In the case of predicted targets of *hsa-miR-324-3p* from TargetScan 7.1, it was noteworthy that total context++ score was between -1.87 and -0.05. In addition, in this server, predicted targets of *hsa-miR-331-3p* were qualified between -0.87 and -0.26 for total context++ score. Using KEGG server, 12656 predicted target genes were totally pertained to *hsa-miR-324-3p* and *hsa-miR-331-3p* (Table S1, S2) (See Supplementary Online Information at www.celljournal.org), mainly located on the chromosomes 1, 19, 2 and 11 by P=3.1E-136 and P=1.4E-134, respectively (Fig.1A, B). Metabolic pathways for *hsa-miR-324-3p* and *hsa-miR-331-3p* were engaged as the top predicted pathways by P= 2.7E-36 and P= 7.7E-37, respectively [Tables S1, S2 (See Supplementary Online Information at www.celljournal.org), Fig.1C, D]. However, using GO Biological process option, 76552 predicted target genes were totally related to *hsa-miR-324-3p* and *hsa-miR-331-3p* (Tables S3, S4, See Supplementary Online Information at www.celljournal.org) mainly located on the chromosomes 1, 19, 2 and 11 by P=3.1E-136 and P=1.4E-134 (Fig.2A, B). Cellular response to stress pathway for *hsa-miR-324-3p* and *hsa-miR-331-3p* were engaged, as the top predicted pathways by P= 2.6E-162 and P=5.6E-166, respectively [Tables S3, S4 (See Supplementary Online Information at www.celljournal.org), Fig.2C, D).

Expression analysis of *hsa-miR-324-3p* and *hsa-miR-331-3p* in Alzheimer's disease serum samples

Based on the qRT-PCR conclusions, the amplification curve of *hsa-miR-451* with average 21.28 threshold cycle (Ct) and melting curve with 69.8˚Cas temperature (Tm) of primers by single pick and specific amplicon were seen (Table 1). The amplification curve of *hsa-miR-324-3p* and *hsa-miR-331-3p* had 30.92 and 31.77 Ct averages of AD samples in comparison with 32.01 and 34.97 Ct averages of healthy controls, respectively. A 69.9˚Cmelting curve for *hsa-miR-324-3p* and *hsa-miR-331-3p* by single pick and specific amplicon were observed. 12% PAGE system showed one specific amplified product for three miRNAs including *hsa-miR-324-3p*, *hsa-miR-331-3p* and internal control of *hsa-miR-451* (Fig.S1, See Supplementary Online Information at www.celljournal.org). Using GraphPad Prism 7 software, expression level and fold change graph were depicted. Among the studied AD patients, expression level of *hsa-miR-324-3p* and*hsa-miR-331-3p* showed upregulation in comparison with the healthy controls (Fig.3A, B). Statistical analyses revealed that upregulated expression of *hsa-miR-324-3p* and *hsa-miR-331-3p* were not statistically significant, by respectively P=0.61 and P=0.78.

Table 1: Features of Alzheimer's disease (AD) patients and healthy controls entered into the study

AD patients	Sex		Age (Y)			Treatment status	
	Female	Male	50-65	65-80	80-95	Under treatment	Without treatment
Percent (%)	71.42	28.57	28.57	47.61	23.80	14.28	85.71
Healthy controls	Female	Male	50-65	65-80	80-95	Lack of special disease history	With Age-related diseases
Percent (%)	43.47	56.52	65.21	30.43	4.34	86.95	13.04

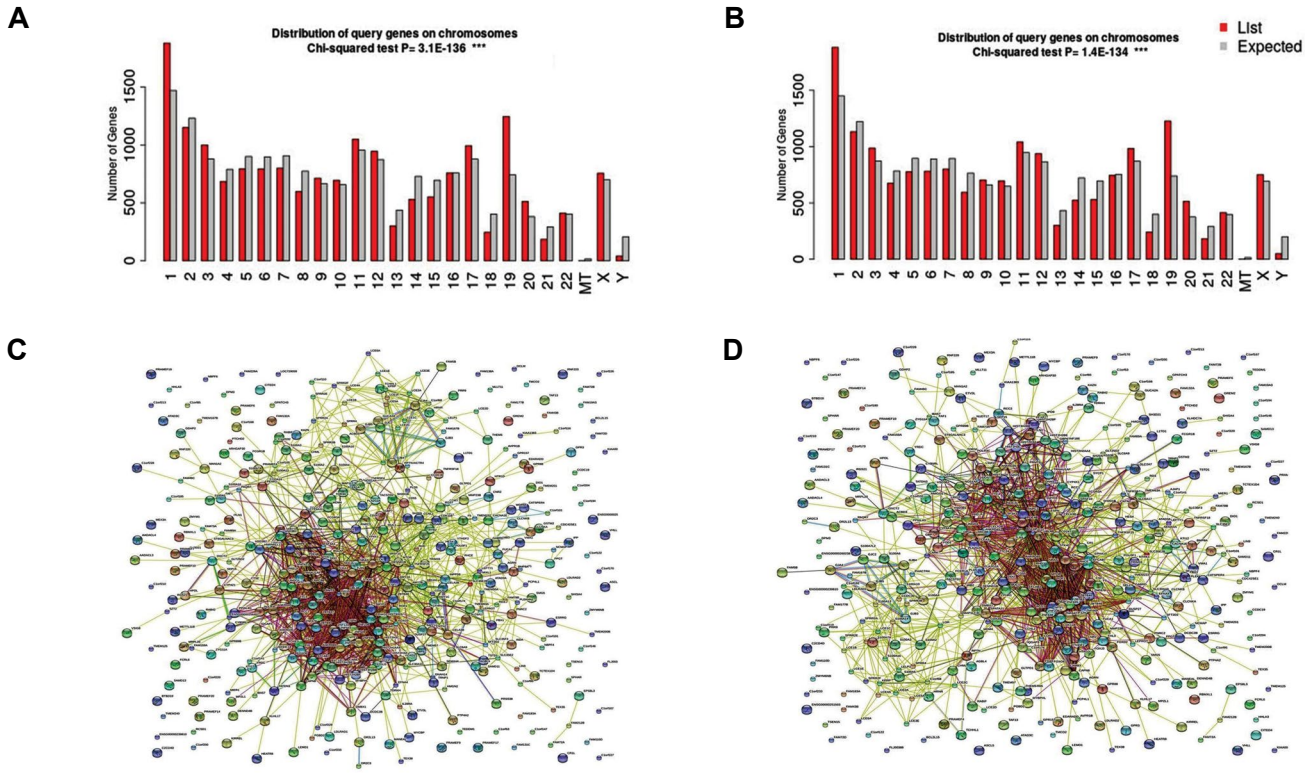

Fig.1: Predicted target genes were totally pertained to *hsa-miR-324-3p* and *hsa-miR-331-3p*, mainly located on the chromosomes 1, 19, 2 and 11 by KEGG server results. **A.** Chromosomal distribution of predicted target genes for *hsa-miR-324-3p*. **B.** Chromosomal distribution of predicted target genes for *hsa-miR-331-3p*. **C.** Network analysis for *hsa-miR-324-3p* by STRING server. **D.** Network analysis for *hsa-miR-331-3p* by STRING server.

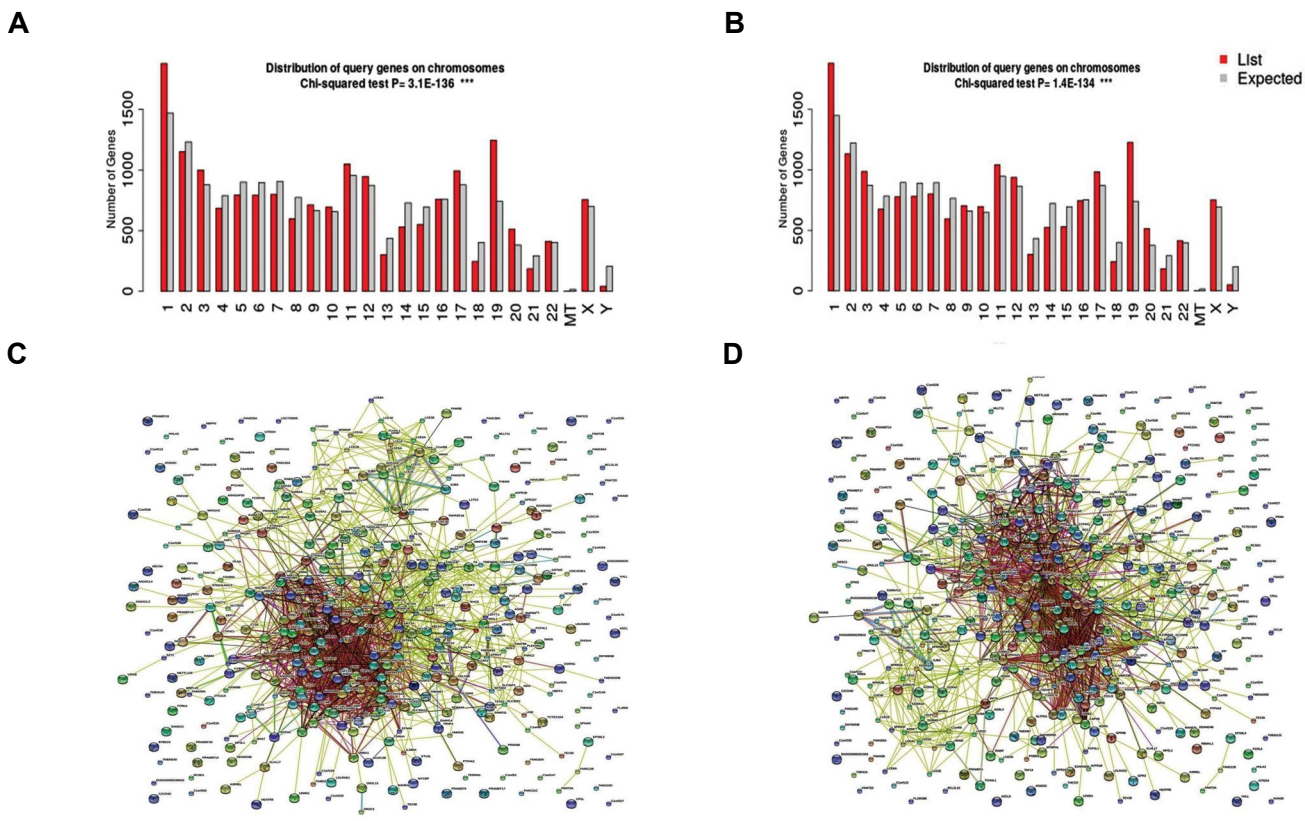

Fig.2: Predicted target genes were totally pertained to *hsa-miR-324-3p* and *hsa-miR-331-3p*, mainly located mainly on the chromosomes 1, 19, 2 and 11 by GO server results. **A.** Chromosomal distribution of predicted target genes for *hsa-miR-324-3p*. **B.** Chromosomal distribution of predicted target genes for *hsa-miR-331-3p*. **C.** Network and protein-protein interaction analysis for *hsa-miR-324-3p* by STRING server. **D.** Network and protein-protein interaction analysis for*hsa-miR-331-3p* by STRING serve.

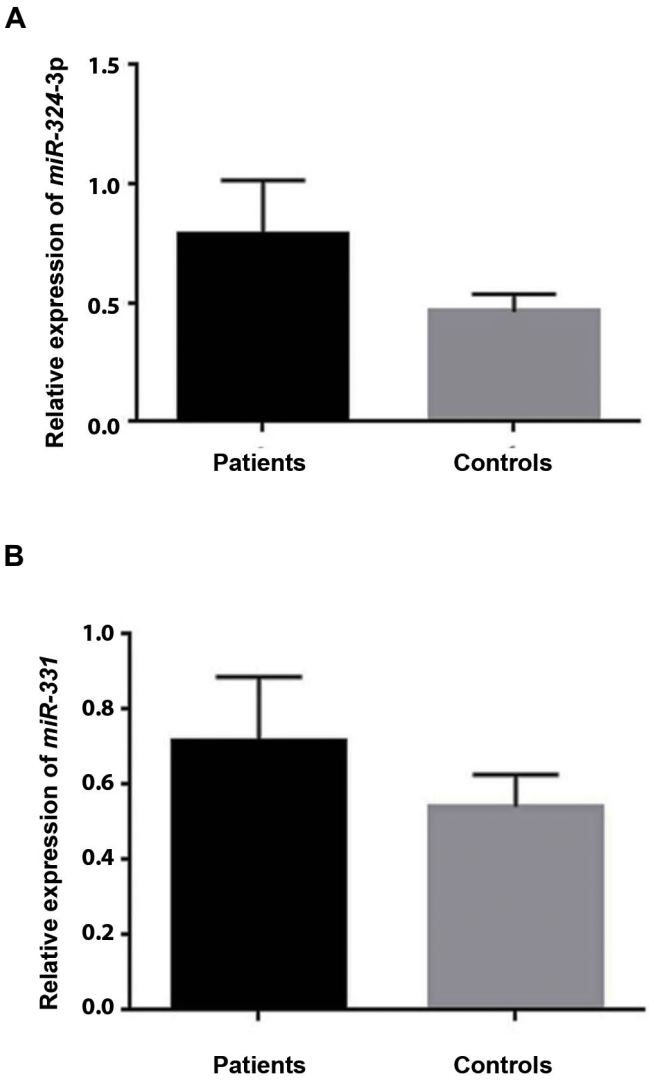

Fig.3: The relative expression graphs of *hsa-miR-324-3p* and *hsa-miR-331-3p*. **A.** *hsa-miR-324-3p* was upregulated in Alzheimer's disease (AD) patients compared to healthy controls (P=0.61). **B.** *hsa-miR-331-3p* was downregulated in AD patients compared to healthy controls (P=0.78).

Discussion

In silico analysis showed *hsa-miR-324-3p* and *hsa-miR-331-3p* are involved in the cellular response to stress and metabolic pathways particularly nucleotide metabolism. It seemed that the functions of these two miRNAs were directly or indirectly associated with AD pathophysiology. Totally, the successful treatment or prevention of AD remains elusive, because the molecular mechanisms driving AD pathology remain poorly understood (34). Different views of mitochondrial dysfunction have been currently characterized as novel components in the aetiology of AD. This is true not only for neuronal mitochondria, but also for astroglial cells which possess strong influence on neuronal function, neuronal development. It has been related to the various neurodegenerative diseases, encompassing AD and other forms of dementia (35, 36). Buffering neurotransmitters and ions (37) and metabolize glucose to lactate, the major fuel for neurons (38), supplying neurons with substrates for oxidative phosphorylation (39, 40) are main mitochondrial functions. On the other hand, damaged mitochondria have been identified in brain tissue, in both familial and sporadic types of AD. In addition, AD is characterized by enhanced numbers of somatic, mitochondrial DNA (mtDNA) mutations, defect of oxidative phosphorylation, imbalance between mitochondrial fission and fusion as well as the alterations in mitochondrial structure, dynamics and motility. Analysis of hippocampal biopsies by microarray have demonstrated a significant reduction of nuclear and one mitochondrial encoded subunits of the mitochondrial electron transport chain in AD patients compared to the age-matched controls. The inverse Warburg hypothesis suggested a bioenergetic model for AD, presuming that AD is an outcome of mitochondrial deregulation, concluding metabolic reprogramming as a beginning attempt to retain neuronal integrity. When this compensatory mechanism is exhausted, bioenergetic deficiencies may result in neuronal death and dementia. Therefore, mitochondrial dysfunction may indicate the missing connection between aging and sporadic AD, andit shows attractive targets against neurodegeneration. Usually, mitochondrial dysfunctions related to AD include direct or indirect prevention of the ability of neuronal and glial mitochondria to carry out oxidative phosphorylation. One direct issue of decreased oxidative phosphorylation is a decline of the ATP production and alterations of mitochondrial bioenergetics crucial for the vitality of cells. An important elevation of oxidized biomolecules has been determined as a sign of AD in brain tissue. Postmortem brains of AD patients showed increased oxidative base damage in both nuclear DNA (nDNA) and mtDNA. In addition, lipid peroxidation of neuronal tissue and oxidative modifications of proteins has been shown in AD. Increased oxidative stress promotes the formation of Aβ plaques and NFTs has been indicated in a mouse model. Oxidative damage is shown to be quantitatively most predominant early event and it is decreased with disease progression in human post-mortem AD brains (7).

The increased levels of reactive oxygen species (ROS) in AD brain has often been proposed by a mitochondrial origin. The high oxygen consumption rate of neurons is used for oxidative phosphorylation and accumulated damaged mitochondria in the AD brain. ROS are endlessly made from up to 4% of the oxygen consumed, during the process of oxidative phosphorylation, by this process. Complex I and especially complex III of the electron transport chain are the initial position for electron leakage to molecular oxygen producing the superoxide anion ($\cdot O_2^-$). Production of ROS is inversely related to the rate of electron transport, elevating exponentially when complex I or III are damaged. Mitochondrial generated ROS as a second messenger molecule suggested to report oxygen available for oxidative phosphorylation, influencing epigenetic marking of nDNA and regulating nuclear transcription factors, kinases and phosphatases. $\cdot O_2^-$ is neutralized by intramitochondrial Manganese (Mn)-dependent superoxide dismutase (SOD_2) catalyzing the formation of H_2O_2, which in turn is inactivated by glutathione

peroxidase. If the amount of generated ROS exceeds the capacity of the mitochondrial antioxidant enzymes, $\cdot O_2^-$ and H_2O_2 levels will be increased. The highly reactive $OH\cdot$ can be generated by Haber-Weiss or Fenton reactions, in the presence of transition metals, such as iron or copper. $OH\cdot$ accumulation can sequentially lead to a plethora of ROS, which has the potential to induce oxidative harm to lipids, proteins, RNA and DNA. Microglia cells are the origin of increased generation of ROS as a part of an inflammatory response in the AD brain. Supporting the idea, NADPH oxidase, the major mediator of microglial ROS, has been shown to be activated in the AD brain, as assessed by translocation of NADPH oxidase subunits. Current studies propose that mitochondrial generated ROS can work as regulators of pro-inflammatory responses of microglia cells. In case of nucleotide metabolism, nucleotide levels in eukaryotes are retained by nucleotide salvage and/or de novo synthesis of ribonucleotide triphosphate (rNTPs) and deoxyribonucleotide triphosphate (dNTPs). Imbalanced dNTP pools have been shown in AD patients and may be an early risk biomarker for AD. Although the underlying detailed mechanism remains unknown, it is conceivable rNTP and/or dNTP pool imbalances carry out a function in AD aetiology. Oxidative phosphorylation is related to the synthesis of rNTP and dNTP indirectly via production of ATP and directly throughout the enzyme dihydroorotate dehydrogenase (DHODHase). ATP is a main source of cellular bioenergetic process. This molecule is utilized as a substrate for rNTP and dNTP synthesis. Furthermore, binding of ATP to the active site of ribonucleotide reductase (RNR) is essential for the key enzyme activation of the dNTP de novo synthesis. DHODHase is an integral protein of the inner mitochondrial membrane encountering the inter membrane space and involving in the conversion of dihydroorotate to orotate. This product is subsequently converted into uridine monophosphates, pyrimidine deoxyribonucleotides. Functionally, DHODHase is linked to the oxidative phosphorylation by a flavinnon-protein group coupling dihydroorotate oxidation to respiratory ubiquinone reduction. Hypoxemia ribonucleotides and pyrimidine, prevention of oxidative phosphorylation, presence of electron transport chain inhibitors or mutations of complex III and IV of the electron transport chain leads to the deficiencies of the de novo UMP synthesis and a subsequent decline in the de novo synthesis of pyrimidines.

dNTP levels are significant substrates for mitochondrial DNA replication and post replicative DNA repair processes in post-mitotic cells such as neurons. rNTP levels serve as the substrates for RNA synthesis, pyrimidine ribonucleotides and the precursors for phospholipids, glycolipids and glycoproteins synthesis of the plasma membrane. Supporting the idea, expression of genes encoding essential proteins for de novo synthesis of pyrimidines and DHODHase have been indicated in neuronal cell bodies of rat brain. High expression levels of DHODHase and other de novo components were recognized in the neocortex and hippocampus which were severely influenced in AD patients. The fundamental functions of generated pyrimidines by mitochondria in neurons can suggest a role for the engagement of imbalanced dNTP levels in the aetiology of AD.

According to the in silico and enrichment analysis, engagement of the nucleotide metabolism and cellular response to stress genes was probably confirmed as the targets of *hsa-miR-324-3p* and *hsa-miR-331-3p*. Experimentally, qRT-PCR results of these two miRNAs were upregulated but not statistically significant. Our result was in accordance with Vallelunga et al. (23) result showing that upregulation of *hsa-miR-324-3p* was occurred in the PD and MSA patient's serums. In addition, our result was in accordance with Olivieri et al. (25) results indicating upregulation of *hsa-miR-331-3p* in AD serum samples. They explained upregulation of the miRNA in age-related disorders by miRNA array method. They also reported the high expression level of *hsa-miR-331-3p* in AD-plasma samples.

Conclusion

Based on the results of present study, *has-miR-324-3p* and *hsa-miR-331-3p* expression levels did not significantly increase in the patients suffering Alzheimer. It may be concluded that these two miRNAs are not involved in the pathogenesis of AD.

Acknowledgments

We greatly acknowledge The Graduate Office of University of Isfahan for providing financial assistance (Grant No. 7262) and Sadeghyeh Welfare Organization (Isfahan, Iran) for their collaborations in collecting blood samples for this study. There is no conflict of interest in this study.

Authors' Contributions

M.H.; Performed the experiments. Z.H.; Supervised the project, designed the experiments, prepared all the requirements and experimental procedures, analyzed the experiments and edited the manuscript. M.D.; Interpreted the data, wrote the manuscript and analyzed the bioinformatic studies. All authors read and approved the final manuscript.

References

1. LaFerla FM, Green KN, Oddo S. Intracellular amyloid-beta in Alzheimer's disease. Nat Rev Neurosci. 2007; 8(7): 499-509.
2. Mattson MP. Pathways towards and away from Alzheimer's disease. Nature. 2004; 430(7000): 631-639.
3. Reddy PH, Manczak M, Mao P, Calkins MJ, Reddy AP, Shirendeb U. Amyloid-beta and mitochondria in aging and Alzheimer's disease: implications for synaptic damage and cognitive decline. J Alzheimers Dis. 2010; 20 Suppl 2: S499-S512.
4. DeKosky ST, Scheff SW, Styren SD. Structural correlates of cognition in dementia: quantification and assessment of synapse change. Neurodegeneration. 1996; 5(4): 417-421.
5. Du H, Guo L, Yan S, Sosunov AA, McKhann GM, Yan SS. Early deficits in synaptic mitochondria in an Alzheimer's disease mouse model. Proc Natl Acad Sci USA. 2010; 107(43): 18670-18675.
6. McGeer PL, McGeer EG. The inflammatory response system of brain: implications for therapy of Alzheimer and other neurodegen-

erative diseases. Brain Res Brain Res Rev. 1995; 21(2): 195-218.
7. Nunomura A, Perry G, Aliev G, Hirai K, Takeda A, Balraj EK, et al. Oxidative damage is the earliest event in Alzheimer disease. J Neuropathol Exp Neurol. 2001; 60(8): 759-767.
8. Reddy PH. Amyloid precursor protein-mediated free radicals and oxidative damage: Implications for the development and progression of Alzheimer's disease. J Neurochem. 2006; 96(1): 1-13.
9. Reddy PH, Beal MF. Amyloid beta, mitochondrial dysfunction and synaptic damage: implications for cognitive decline in aging and Alzheimer's disease. Trends Mol Med. 2008; 14(2): 45-53.
10. Reddy PH, Tripathi R, Troung Q, Tirumala K, Reddy TP, Anekonda V, et al. Abnormal mitochondrial dynamics and synaptic degeneration as early events in Alzheimer's disease: implications to mitochondria-targeted antioxidant therapeutics. Biochim Biophys Acta. 2012; 1822(5): 639-649.
11. Swerdlow RH. Brain aging, Alzheimer's disease, and mitochondria. Biochim Biophys Acta. 2011; 1812(12): 1630-1639.
12. Tampellini D, Gouras GK. Synapses, synaptic activity and intraneuronal abeta in Alzheimer's disease. Front Aging Neurosci. 2010; 2. pii: 13.
13. Terry RD, Masliah E, Salmon DP, Butters N, DeTeresa R, Hill R, et al. Physical basis of cognitive alterations in Alzheimer's disease: synapse loss is the major correlate of cognitive impairment. Ann Neurol. 1991; 30(4): 572-580.
14. Bertoni-Freddari C, Fattoretti P, Casoli T, Caselli U, Meier-Ruge W. Deterioration threshold of synaptic morphology in aging and senile dementia of Alzheimer's type. Anal Quant Cytol Histol. 1996; 18(3): 209-213.
15. Kumar S, Reddy PH. Are circulating microRNAs peripheral biomarkers for Alzheimer's disease? Biochim Biophys Acta. 2016; 1862(9): 1617-1627.
16. Reddy PH, Tonk S, Kumar S, Vijayan M, Kandimalla R, Kuruva CS, et al. A critical evaluation of neuroprotective and neurodegenerative MicroRNAs in Alzheimer's disease. Biochem Biophys Res Commun. 2017; 483(4): 1156-1165.
17. Williams J, Smith F, Kumar S, Vijayan M, Reddy PH. Are microRNAs true sensors of ageing and cellular senescence? Ageing Res Rev. 2017; 35: 350-363.
18. Kumar P, Dezso Z, MacKenzie C, Oestreicher J, Agoulnik S, Byrne M, et al. Circulating miRNA biomarkers for Alzheimer's disease. PLoS One. 2013; 8(7): e69807.
19. Ferretti E, De Smaele E, Miele E, Laneve P, Po A, Pelloni M, et al. Concerted microRNA control of Hedgehog signalling in cerebellar neuronal progenitor and tumour cells. EMBO J. 2008; 27(19): 2616-2627.
20. Smirnova L, Gräfe A, Seiler A, Schumacher S, Nitsch R, Wulczyn FG. Regulation of miRNA expression during neural cell specification. Eur J Neurosci. 2005; 21(6): 1469-1477.
21. Stappert L, Borghese L, Roese-Koerner B, Weinhold S, Koch P, Terstegge S, et al. MicroRNA-based promotion of human neuronal differentiation and subtype specification. PLoS One. 2013; 8(3): e59011.
22. Liu FJ, Lim KY, Kaur P, Sepramaniam S, Armugam A, Wong PTH, et al. microRNAs involved in regulating spontaneous recovery in embolic stroke model. PLoS One. 2013; 8(6): e66393.
23. Vallelunga A, Ragusa M, Di Mauro S, Iannitti T, Pilleri M, Biundo R, et al. Identification of circulating microRNAs for the differential diagnosis of Parkinson's disease and Multiple System Atrophy. Front Cell Neurosci. 2014; 8: 156.
24. Wang WX, Huang Q, Hu Y, Stromberg AJ, Nelson PT. Patterns of microRNA expression in normal and early Alzheimer's disease human temporal cortex: white matter versus gray matter. Acta Neuropathol. 2011; 121(2): 193-205.
25. Olivieri F, Spazzafumo L, Santini G, Lazzarini R, Albertini MC, Rippo MR, et al. Age-related differences in the expression of circulating microRNAs: miR-21 as a new circulating marker of inflammaging. Mech Ageing Dev. 2012; 133(11-12): 675-685.
26. Balakathiresan NS, Chandran R, Bhomia M, Jia M, Li H, Maheshwari RK. Serum and amygdala microRNA signatures of posttraumatic stress: fear correlation and biomarker potential. J Psychiatr Res. 2014; 57: 65-73.
27. Epis MR, Barker A, Giles KM, Beveridge DJ, Leedman PJ. The RNA-binding protein HuR opposes the repression of ERBB-2 expression by miR-331-3p in prostate cancer cells. J Biol Chem. 2011; 286(48): 41442-41454.
28. Saba R, Booth SA. Target labelling for the detection and profiling of microRNAs expressed in CNS tissue using microarrays. BMC Biotechnol. 2006; 6: 47.
29. Zanette DL, Rivadavia F, Molfetta GA, Barbuzano FG, Proto-Siqueira R, Silva WA Jr, et al. miRNA expression profiles in chronic lymphocytic and acute lymphocytic leukemia. Braz J Med Biol Res. 2007; 40(11): 1435-1440.
30. McKhann G, Drachman D, Folstein M, Katzman R, Price D, Stadlan EM. Clinical diagnosis of Alzheimer's disease report of the NINCDS-ADRDA Work Group under the auspices of Department of Health and Human Services Task Force on Alzheimer's Disease. Neurology. 1984; 34(7): 939-944.
31. Jack CR Jr, Albert MS, Knopman DS, McKhann GM, Sperling RA, Carrillo MC, et al. Introduction to the recommendations from the National Institute on Aging-Alzheimer's Association workgroups on diagnostic guidelines for Alzheimer's disease. Alzheimers Dement. 2011; 7(3): 257-262.
32. Zhu C, Ren C, Han J, Ding Y, Du J, Dai N, et al. A five-microRNA panel in plasma was identified as potential biomarker for early detection of gastric cancer. Br J Cancer. 2014; 110(9): 2291-2299.
33. Cheng L, Doecke JD, Sharples R, Villemagne VL, Fowler CJ, Rembach A, et al. Prognostic serum miRNA biomarkers associated with Alzheimer's disease shows concordance with neuropsychological and neuroimaging assessment. Mol Psychiatry. 2015; 20(10): 1188-1196.
34. Cummings JL, Morstorf T, Zhong K. Alzheimer's disease drug-development pipeline: few candidates, frequent failures. Alzheimers Res Ther. 2014; 6(4): 37.
35. Rasmussen LJ, Shiloh Y, Bergersen LH, Sander M, Bohr VA, Tønjum T. DNA damage response, bioenergetics, and neurological disease: the challenge of maintaining brain health in an aging human. Mech Ageing Dev. 2013; 134(10): 427-433.
36. Verkhratsky A, Olabarria M, Noristani HN, Yeh CY, Rodriguez JJ. Astrocytes in Alzheimer's disease. Neurotherapeutics. 2010; 7(4): 399-412.
37. Kubik LL, Philbert MA. The role of astrocyte mitochondria in differential regional susceptibility to environmental neurotoxicants: tools for understanding neurodegeneration. Toxicol Sci. 2015; 144(1): 7-16.
38. Stobart JL, Anderson CM. Multifunctional role of astrocytes as gatekeepers of neuronal energy supply. Front Cell Neurosci. 2013; 7: 38.
39. Pellerin L, Pellegri G, Bittar PG, Charnay Y, Bouras C, Martin JL, et al. Evidence supporting the existence of an activity-dependent astrocyte-neuron lactate shuttle. Dev Neurosci. 1998; 20(4-5): 291-299.
40. Voloboueva LA, Suh SW, Swanson RA, Giffard RG. Inhibition of mitochondrial function in astrocytes: implications for neuroprotection. J Neurochem. 2007; 102(4): 1383-1394.

Original Article

Circ-RNA Expression Pattern and circ-RNA-miRNA-mRNA Network in The Pathogenesis of Human Intervertebral Disc Degeneration

Zhiliang Guo, M.D.[1#*], Yuanyuan Liu, M.D.[2#], Yu Gao, M.M.[3], Xiumei Guan, M.M.[3], Hong Li, M.M.[3], Min Cheng, Ph.D.[3]

1. Department of Orthopedic, No. 89 Hospital of Chinese PLA, Weifang, 261021, China
2. Stomatology Medical College, Weifang Medical University, Weifang 261053, Shandong, China
3. Clinical Medical College, Weifang Medical University, Weifang 261053, Shandong, China

 # The first two authors equally contributed in this study.

Corresponding Address: Department of Orthopedic, No. 89 Hospital of Chinese PLA, Weifang, 261021, China
Email: drzlguo@163.com

Received: 22/February/2019, Accepted: 05/November/2019

Abstract

Objective: The present study aimed to screen the differentially expressed (DE) circular RNAs (circ-RNAs) between lumbar intervertebral disc degeneration (IVDD) and normal tissues.

Material and Methods: In this experimental study, microarray hybridization was performed to evaluate circ-RNA expression, and the DE circ-RNAs were confirmed by quantitative real-time polymerase chain reaction (qRT-PCR). Host genes of DE circ-RNAs were predicted, and their functions were evaluated. Further, a competitive endogenesis (ce) RNA network among 4 DE circ-RNAs-miRNA-mRNA was constructed by Cytoscape.

Results: A total of 2636 circ-RNAs were detected in all samples; among them, 89.23% were exonic circ-RNAs. There were 138 DE circ-RNAs, including 134 up-regulated circ-RNAs and 4 downregulated circ-RNAs in IVDD samples. qRT-PCR validation experiments showed that expression trends of hsa_circ_0003239, hsa_circ_0003162, hsa_circ_0005918, and hsa_circ_0005556 were in line with the microarray analysis results. Functional enrichment analysis showed that host genes of DE circ-RNAs significantly disturbed pathways of regulation of actin cytoskeleton, propanoate metabolism, and ErbB signaling pathway. The four DE circ-RNAs related ceRNA network was constructed.

Conclusions: Our results revealed that circ-RNAs can function as miRNA sponges and regulate parent gene expression to affect IVDD.

Keywords: Biomarkers, Circular, Intervertebral Disc Degeneration, RNA

Cell Journal(Yakhteh), Vol 23, No 2, July 2021, Pages: 218-224

Citation: Guo ZL, Liu YY, Gao Y, Guan XM, li H, Cheng M. Circ-RNA expression pattern and circ-RNA-miRNA-mRNA network in the pathogenesis of human intervertebral disc degeneration. Cell J. 2021; 23(2): 218-224. doi: 10.22074/cellj.2021.6832.

Introduction

Human lumbar intervertebral disc degeneration (IVDD) disease contributes a lot to low back pain (1). Numerous studies have indicated that a variety of cellular events are disrupted in the progression of IVDD, ranging from matrix synthesis to cytokine expression (2). Although increasing evidence has revealed that IVDD is a multifaceted spinal disease, many studies have confirmed that the primary factors contributing to IVDD are genetic factors (3, 4).

Circular RNAs (circ-RNAs) are newly defined non-coding RNAs with special structures (5-7). Unlike linear RNA, which terminates with the 5' cap and 3' tail, circ-RNA forms covalently closed continuous loop structures and are considered as evolutionarily highly conservative and stable (8-10). Increasing evidence suggests that circ-RNAs are present in nearly all types of species and expressed in a tissue- and disease-dependent manner (11, 12). Therefore, circ-RNAs might more appropriate to be used as a molecular diagnostic biomarker for various diseases, including colon cancer, ovarian cancer, and gastric cancer (13-18).

Studies on circ-RNAs are in their early stages. Several studies have shown that circ-RNAs are involved in IVDD diseases and have determined their expression profiles (19, 20). Wang et al. (21) demonstrated that circ-RNAs regulated the viability, degradation, apoptosis, and oxidative stress in nucleus pulposus (NP) cells. However, the role of circ-RNAs in lumbar discs and their overall contribution to IVDD pathogenesis are few investigated. Recent studies found that circ-RNAs can efficiently bind to miRNA and regulate downstream mRNA expression indirectly; these were termed as "competitive endogenesis (ce) RNA" (22). In a recent study, Cheng et al. demonstrated that circ-RNA VMA21 protects against IVDD through targeting miR-200c and X linked inhibitor-of-apoptosis protein (23). Circ-RNA_104670 functions as a ceRNA by binding miR-17-3p to regulate the expression of MMP2 during NP degradation (24). Circ-4099 functions as a

ceRNA by blocking miR-616-5p inhibition of Sox9 in IVDD (25). These studies suggested circ-RNAs can act as ceRNAs to regulate the pathological process of IVDD. Therefore, in this study, we performed acirc-RNA microarray to screen the DE circ-RNAs that might regulate the viability and functions of NP cells. Quantitative reverse transcription-polymerase chain reaction (qRT-PCR) was performed to validate the microarray results. Besides, a ceRNA network of circ-RNA-miRNA-mRNA was constructed. Our study could provide novel data for IVDD diagnosis and pathogenesis.

Material and Methods

Human nucleus pulposus sample collection

In this experimental study, NP tissues from degenerative lumbar and normal lumbar were collected. The patient demographics and IVDD grading were also collected. Lumbar disc tissue (three lumbar disc tissues and three normal tissues) was isolated from surgical operations, immediately put into liquid nitrogen. This study was approved by the Human Ethics Committees Review Board at No. 89 Hospital of Chinese PLA (No.1893), Weifang, China. The written informed consent was obtained from all participants.

Microarray and quantitative analysis

Total RNA of samples was extracted by TRIzol reagent (Invitrogen, Carlsbad, CA, USA) and quantified using a NanoDrop ND-1000 (NanoDrop, Wilmington, DE, USA). Sample preparation and microarray hybridization were performed using Array star standard protocols, as indicated in previous studies (26, 27). Raw microarray data extraction and analysis were performed using the R software package (version 2.15, http://www.r-project.org/). First, the data were normalized and log2-transformed. Then, the DE circ-RNAs between IVDD and normal samples were identified by a t test based on the thresholds of fold-change ≥2.0 and $P<0.05$. Further, heat map, volcano plot, and MA plot were drawn to display circ-RNA expression patterns among samples.

Validation of differentially expressed circ-RNAs using quantitative real-time polymerase chain reaction

The DE circ-RNAs in the microarray experiments were further confirmed by qRT-PCR using the same samples of circ-RNA microarray. Five DE circ-RNAs were selected to verified based on their significant differences and raw signal intensity of expression. β-actin as used as an internal control. Total RNA was isolated and was reverse-transcribed to cDNA using the SuperScript III First-Strand synthesis system (Life Technologies, Carlsbad, CA, USA). Further, the expression of the 5 DE circ-RNAs was determined on the ABI7500 instrument (Thermo Fisher Scientific, Waltham, MA, USA) using the SYBR Green I kit (Thermo Fisher Scientific, Waltham, MA, USA) with primers listed in Table 1. All qRT-PCRs were conducted in triplicate.

Table 1: The primer sequence used in quantitative real-time polymerase chain reaction

Gene	Primer sequences (5′-3′)	Annealing temperature (˚C)	Product sizes (bp)
β-actin (HUMAN)	F: AGCACAGAGCCTCGCCTTTG	60	208
	R: CTTCTGACCCATGCCCACCA		
circ_0003239	F: CCAAGAGACTGCTTTTGAGTGACA	60	124
	R: TTTTAGGAGGTCGGAGGGGATA		
circ_0005556	F: GATGGACTGGTTCGCTTGGT	60	149
	R: TTTCGTGATGATAAAGGATGCA		
circ_0003162	F: CTCAGGAACCTTGGGTAATGTG	60	231
	R: CCACTATTGTCAACATTAGCCAGA		
circ_0075504	F: ATCTTTGGACTGACTGTGGCACT	60	202
	R: GCATCCAGTTATTAGGTAGCCAAA		
circ_0005918	F: GCAAGGAATGATTATCTTCTTACCC	60	187
	R: GAGCCATCTGTTCAGTCTCAAAGT		

GO and KEGG pathway analysis for differentially expressed circ-RNAs related to intervertebral disc degeneration

Co-expression between DE circ-RNAs and mRNAs was calculated, and a gene co-expression network was built using Cytoscape (version 3.0). The co-expressed mRNAs of DE circ-RNAs were regarded as their host genes. The functions of DE circ-RNAs were predicted by gene oncology (GO) enrichment analysis on their host genes in terms of biological processes (BP), cellular components (CC), and molecular functions (MF). Biological pathways involved by the DE circ-RNAs were predicted by the Kyoto Encyclopedia of Genes and Genomes (KEGG) (http://www.genome.jp/kegg/) analysis. Both GO and KEGG enrichment analyses were performed using Database for Annotation, Visualization, and Integrated Discovery (DAVID; http://www.david.abcc.ncifcrf.gov/) (28) based on criteria of $P<0.05$.

Construction of circ-RNAmiRNA-mRNA network

The potential miRNAs binding with DE circ-RNAs were predicted by Array star's in-house miRNA target prediction software based on TargetScan and miRanda (29, 30). A circ-RNA-miRNA-mRNA network was then visualized using Cytoscape v3.0. Five confirmed circ-RNAs, hsa_circ_0003239, hsa_circ_0003162, hsa_circ_0005918, hsa_circ_0075504, and hsa_circ_0005556, were annotated in detail based on the circ-RNA-miRNA-mRNA interaction network.

Statistical analysis

The statistical analysis of microarray data was performed by the R software package (version 2.15, http://www.r-project.org/). The statistical analysis of qRT-PCR was performed using SPSS (version 13.0) software (SPSS, Inc., Chicago, IL, USA). Differences between the two groups were analyzed using the t test, and data were reported as the mean ± standard deviation (SD). P values of less than 0.05 were considered significant.

Results

Screening of differentially expressed circ-RNA in intervertebral disc degeneration

A total of 2636 circ-RNAs were detected by Arraystar Human circ-RNA Array (Fig.1A). The results suggested that the circ-RNAs consisted of 89.23% exonic circ-RNAs (2352 circ-RNAs), 7.28% intronic circ-RNAs (192 circ-RNAs), 1.82% intragenic circ-RNAs (48 circ-RNAs), 1.63% antisense circ-RNAs (43 circ-RNAs) and 0.04% intergenic circ-RNAs (1 circ-RNA) (Fig.1B). There were 134 up- and four down-regulated circ-RNAs in degenerative lumbar NP samples compared with normal control samples with the criteria of fold change ≥2.0 and $P<0.05$ (Fig.1C, D).

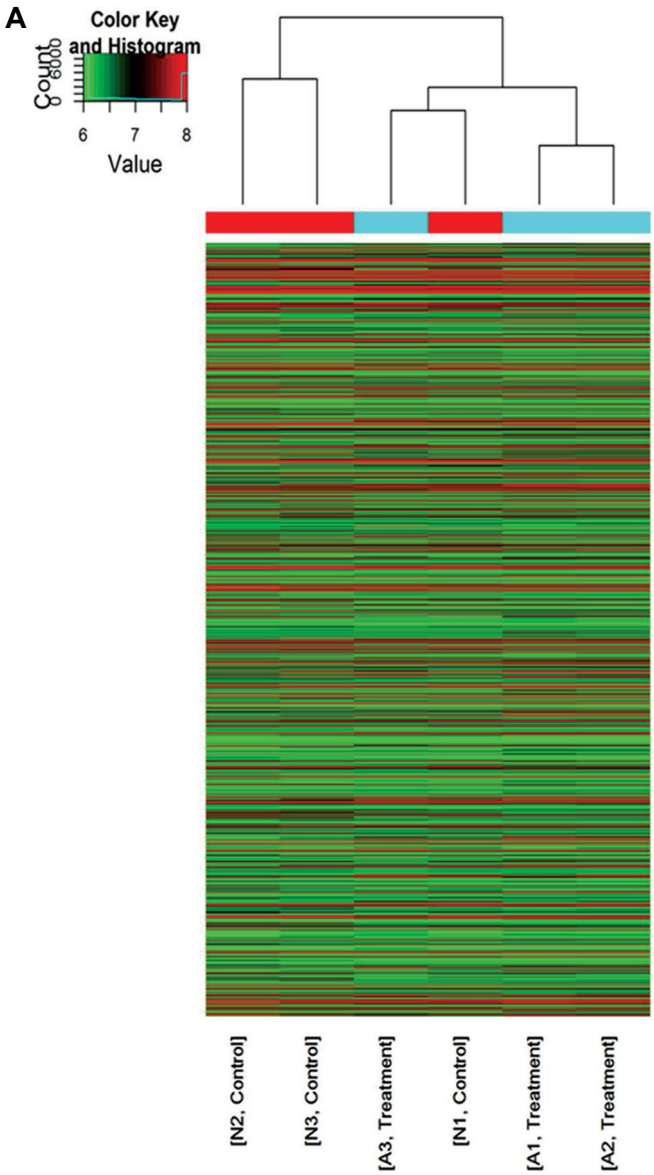

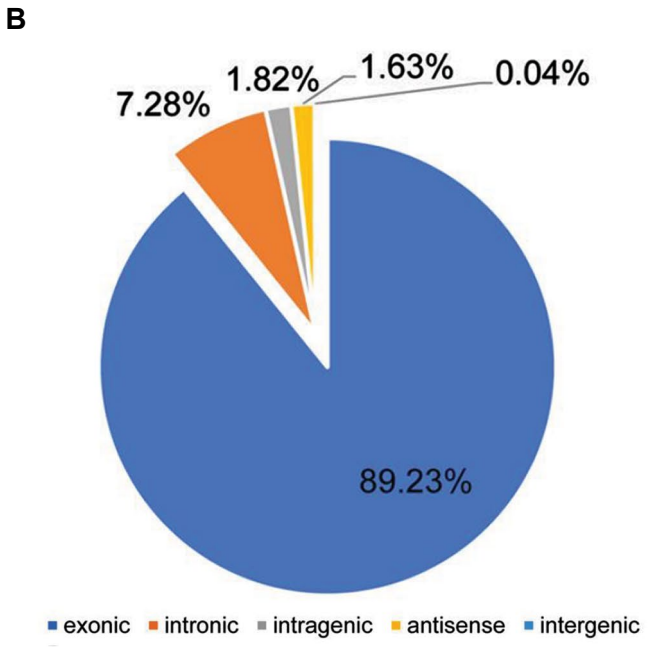

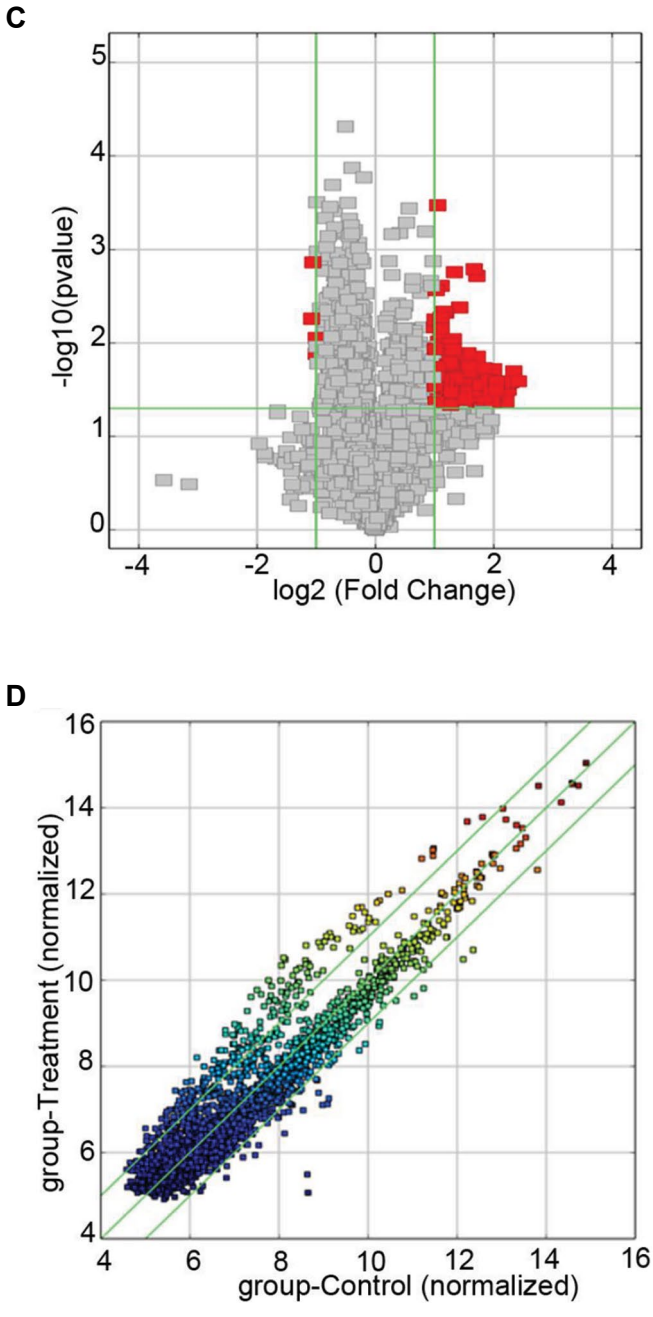

Fig.1: The circ-RNA microarray results. **A.** Exonic circ-RNAs accounted for 89.23%, followed by 7.28% intronic circ-RNAs, and 1.82% intragenic circ-RNAs. **B.** Heat map showed the circ-RNAs detected in all samples. The row of colored boxes indicated circ-RNAs, and the column indicated sample names. **C.** Volcano plot and **D.** Scatter plot showing the DE circ-RNAs. DE; Differentially expressed and circ-RNAs; Circular RNAs.

Validation results of selected circ-RNAs by quantitative real-time polymerase chain reaction

Since the microarray data might generate some false-positive results, we further verified the microarray results by qRT-PCR using the same samples. Exonic circ-RNAs were chosen based on their significant differences and raw signal intensities of expression. Five circ-RNAs (hsa_circ_0003239, hsa_circ_0005556; hsa_circ_0003162; hsa_circ_0075504; and hsa_circ_0005918) that were up-regulated in the IVDD lumbar nucleus by 3.52, 5.05, 5.33, 4.87, and 4.69-fold, respectively in the microarray results were selected for validation. As shown in Figure 2, the relative expression levels of four circ-RNAs (hsa_circ_0003239, hsa_circ_0003162, hsa_circ_0005918, and hsa_circ_0005556) in qRT-PCR results were in line with those in the microarray results. The objective circ-RNA validation rate was 80%, suggesting that the microarray results were reliable.

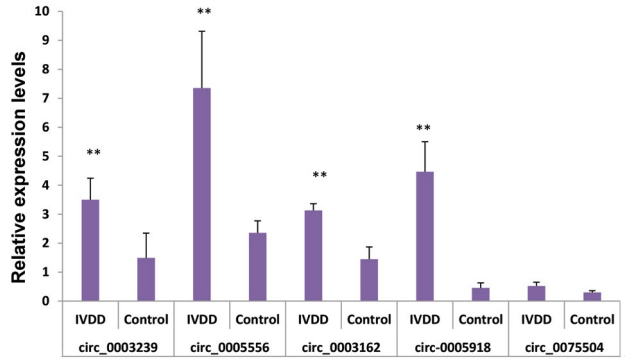

Fig.2: The expression levels of 5 DE circ-RNAs were validated by qRT-PCR. Each qRT-PCR assay was performed in triplicate. **; P<0.01, DE; Differentially expressed, circ-RNAs; Circular RNAs, qRT-PCR; Quantitative real-time polymerase chain reaction, and IVDD; Intervertebral disc degeneration.

Functional annotation of differentially expressed circ-RNAs related to intervertebral disc degeneration

The host genes of DE circ-RNAs were predicted by gene co-expression analysis, and GO and KEGG pathway analyses were performed to investigate the functional annotation of host genes of DE circ-RNAs related to IVDD. At the criteria of P<0.05, 8 GO-CC terms, 6 GO-MF terms, and 22 GO-BP terms were significantly enriched by up-regulated circ-RNAs (Fig.3). The results suggested the circ-RNAs were located in cytosol, cytoplasm, and cell cortex and significantly involved in BP of positive regulation of stress fiber assembly (host genes of circBRAF, circPAK1, circLPAR1 and circARHGEF10L, P=0.02411), biotin metabolic process (host gens of circACACA, circACACB, and circPCCA, P=0.003482), ubiquitin-dependent protein catabolic process (host genes of circCUL3, circNPLOC4, circCUL4A, circUBE2G1, circUSP34, and circFBXO7, P=0.006181) and Fc-gamma receptor signaling pathway involved in phagocytosis (host genes of circACTR2, circMYO10, circPTK2, circDOCK1 and circPAK1, P=0.008847). KEGG pathway enrichment analysis found that the host genes of DE circ-RNAs significantly disturbed pathways of regulation of actin cytoskeleton (host genes of circARHGEF4, circPTK2, circDOCK1, circBRAF, circITGA3 and circPAK1, P=0.01254), propanoate metabolism (host genes of circACACA, circACACB, and circPCCA, P=0.01468) and ErbB signaling pathway [host genes of circPTK2, circBRAF, circSTAT5B, circPAK1, P=0.01982 (Fig.4)].

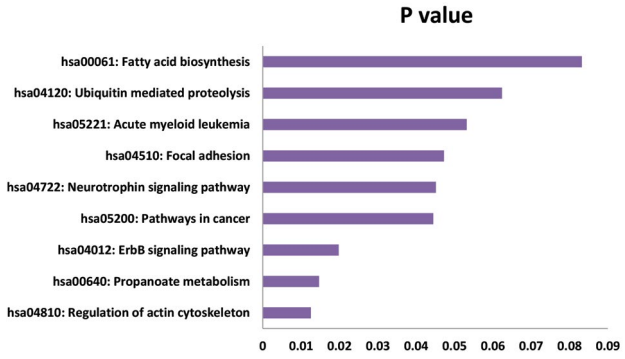

Fig.3: Gene ontology analysis of the host genes that shows the up-regulated circ-RNAs based on the DAVID database.

Construction of circ-RNA-miRNA-mRNA network

The miRNAs and mRNAs related to the four qRT-PCR-verified DE circ-RNAs, including hsa_circ_0003239, hsa_circ_0003162, hsa_circ_0005918, and hsa_circ_0005556, were constructed. The four DE circ-RNAs regulated 31 mRNAs by competitive binding with 17 miRNAs (Fig.5). Notably, hsa_circ_0003162 regulated 18 mRNAs by competitive binding with hsa-miR-6848-5p, hsa-miR-6846-5p, hsa-miR-2392, hsa-miR-664B-5p and hsa-miR-6814-5p.

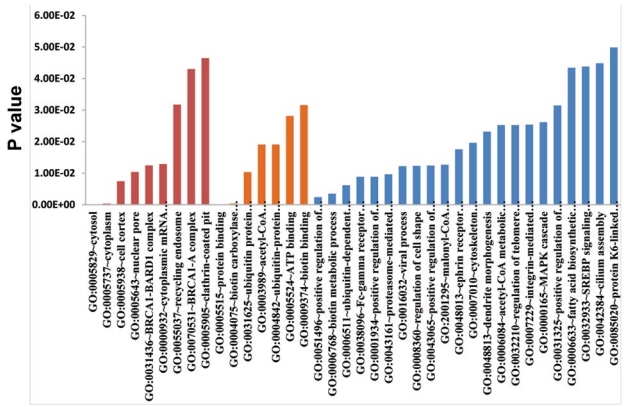

Fig.4: KEGG enrichment analysis of the host genes that demonstrates the up-regulated circ-RNAs according to the DAVID database.

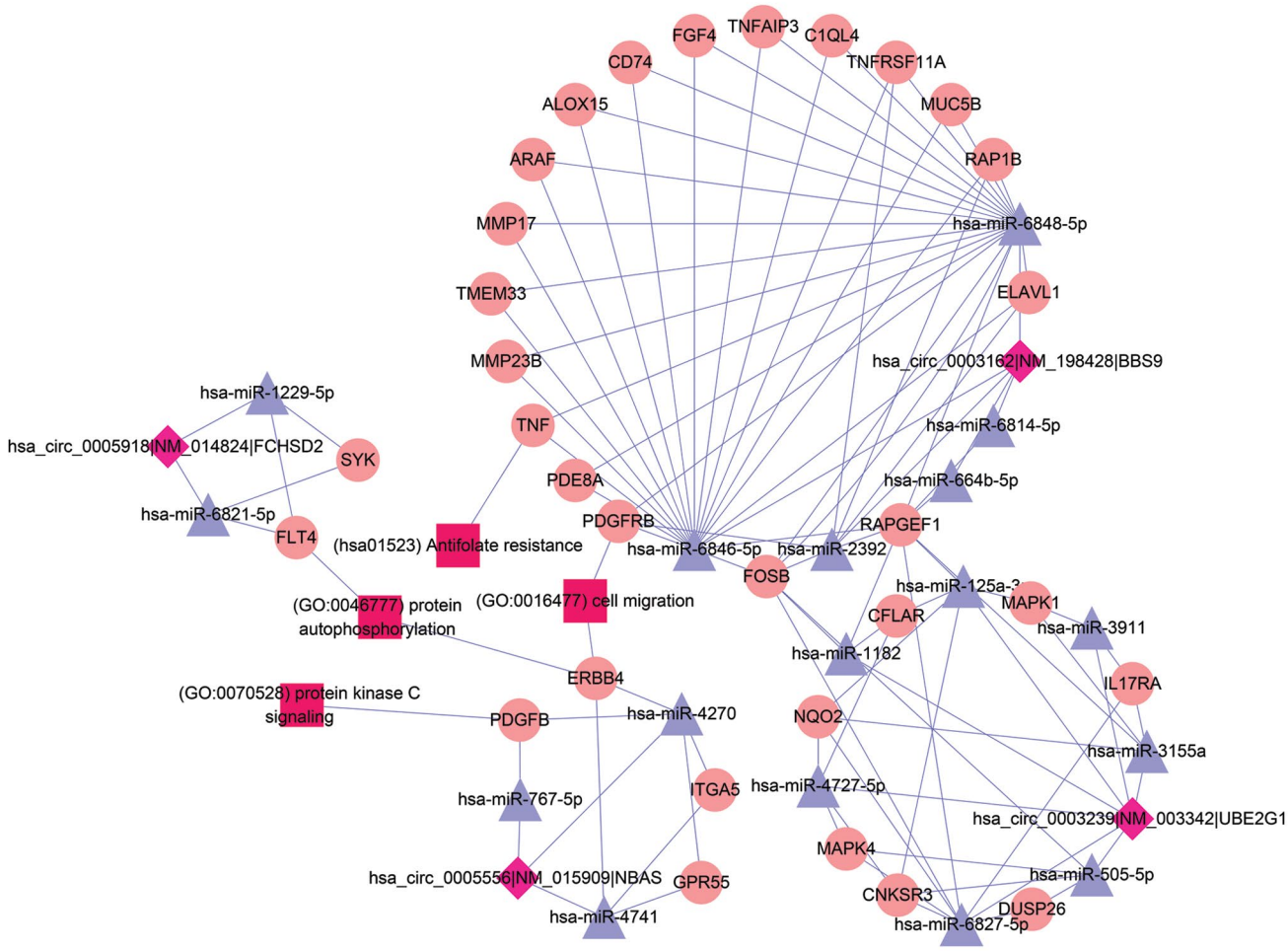

Fig.5: DAVID construction of the circ-RNA-miRNA mRNA network. Diamond nodes represent circ-RNAs, and purple triangle nodes represent miRNAs.

Discussion

Studies have shown that many abnormal cell events occur in the process of IVDD, such as the increase in NP cell apoptosis, various inflammatory factors, and matrix metalloproteinase expression (31, 32). This series of changes suggest that specific molecular gene expression in the intervertebral disc is dysfunctional, and the corresponding regulatory factors are altered, but the etiology and the precise mechanism of disc degeneration remain unclear. In this study, we performed acirc-RNA microarray on human normal and degenerative lumbar NP samples and identified 138 DE circ-RNAs in intervertebral discs from IVDD and normal tissues. Five DE circ-RNAs were selected, and four circ-RNAs (hsa_circ_0003239, hsa_circ_0003162, hsa_circ_0005918, and hsa_circ_0005556) were successfully validated by qRT-PCR, showing consistent results with microarray. The four DEcirc-RNAs regulated 31 mRNAs by competitive binding with 17 miRNAs in the ceRNA network. Notably, hsa_circ_0003162 regulated 18 mRNAs by competitive binding with hsa-miR-6848-5p, hsa-miR-6846-5p, hsa-miR-2392, hsa-miR-664B-5p and hsa-miR-6814-5p. A study of gastric cancer showed that hsa_circ_0005556 and hsa_circ_0003239 attenuate gastric cancer proliferation and metastasis (33). However, the other DE circ-RNAs were not investigated previously. Although the specific functions of most circ-RNAs remain unclear, accumulating evidence has revealed the role of circ-RNAs as miRNA sponges (34, 35). We speculated these ceRNA relationships were important in the occurrence and progression of IVDD. However, further experiments are warranted to validate these relationships.

Functional enrichment analyses suggested that the host genes of the upregulated circ-RNAs were significantly involved in BP of positive regulation of stress fiber assembly, biotin metabolic process, ubiquitin-dependent protein catabolic process and Fc-gamma receptor signaling pathway involved in phagocytosis as well as pathways of regulation of actin cytoskeleton, propanoate metabolism, and ErbB signaling pathway. Stress fibers are contractile actomyosin bundles found in many cultured non-muscle cells, where they have a central role in cell adhesion and morphogenesis (36). The pathologic findings in IVDD include protrusion, spondylolysis, and/or subluxation of vertebrae (spondylolisthesis) and spinal stenosis. We hypothesized that stress fiber assembly might play a role in protrusion. Besides, a previous study suggested the ErbB signaling pathway was disturbed in IVDD, which is consistent with our study.

The strengths of this study are that the circ-RNA microarray of IVDD samples generated hundreds of DE circ-RNAs that might play essential roles in IVDD development. However, there are some limitations to this study. First, the sample size of circ-RNA is relatively small; only three samples in IVDD groups and three samples in the control group were evaluated. Second, though we constructed a ceRNA network for the verified DE circ-RNAs, these ceRNA relationships were not verified by further in vitro or in vivo experiments. In our further studies, we will perform experiments to validate the ceRNA relationship in the DE circ-RNAs-miRNA-mRNA network.

Conclusion

The circ-RNA microarray detected 2636 circ-RNAs expression, with 134 upregulated circ-RNAs and four down-regulated circ-RNAs in IVDD samples. The qRT-PCR validation experiments showed that hsa_circ_0003239, hsa_circ_0003162, hsa_circ_0005918, and hsa_circ_0005556 expression levels were consistent with the microarray analysis results. Our results revealed more circ-RNAs that play important roles in IVDD development.

Acknowledgements

This work was supported by Foundation of Health Commission of Weifang (wfwsjk_2019_025) and Weifang Medical University Doctoral Startup Fund. We thank Shizhe Liu (Kangcheng Corporation, Shanghai, China) for part of bio-informatics analysis. There is no conflict of interest in this study

Authors' Contributions

M.C.; Conception, design of the research, and revision of manuscript for important intellectual content. Y.Y.L., Z.L.G., Y.G., X.M.G., H.L.; Acquisition, analysis and interpretation of data. Y.Y.L., X.M.G., H.L.; Statistical analysis. Z.L.G., Y.Y.L.; Obtaining funding. Y.Y.L., Z.L.G.; Drafting the manuscript. All authors read and approved the final manuscript.

References

1. Gore M, Sadosky A, Stacey BR, Tai KS, Leslie D. The burden of chronic low back pain: clinical comorbidities, treatment patterns, and health care costs in usual care settings. Spine (Phila Pa 1976). 2012; 37(11): E668-E677.
2. Freemont AJ. The cellular pathobiology of the degenerate intervertebral disc and discogenic back pain. Rheumatology (Oxford). 2009; 48(1): 5-10.
3. Battie MC, Videman T, Kaprio J, Gibbons LE, Gill K, Manninen H, et al. The Twin Spine Study: contributions to a changing view of disc degeneration. Spine J. 2009; 9(1): 47-59.
4. Battie MC, Videman T, Levalahti E, Gill K, Kaprio J. Genetic and environmental effects on disc degeneration by phenotype and spinal level: a multivariate twin study. Spine (Phila Pa 1976). 2008; 33(25): 2801-2808.
5. Brosnan CA, Voinnet O. The long and the short of noncoding RNAs. Curr Opin Cell Biol. 2009; 21(3): 416-425.
6. Uchida S, Bolli R. Short and long noncoding RNAs regulate the epigenetic status of cells. Antioxid Redox Signal. 2018; 29(9): 832-845.
7. Twayana S, Legnini I, Cesana M, Cacchiarelli D, Morlando M, Bozzoni I. Biogenesis and function of non-coding RNAs in muscle differentiation and in Duchenne muscular dystrophy. Biochem Soc Trans. 2013; 41(4): 844-849.
8. Salzman J, Gawad C, Wang PL, Lacayo N, Brown PO. Circular RNAs are the predominant transcript isoform from hundreds of human genes in diverse cell types. PLoS One. 2012; 7(2): e30733.
9. Ashwal-Fluss R, Meyer M, Pamudurti NR, Ivanov A, Bartok O, Hanan M, et al. circRNA biogenesis competes with pre-mRNA splicing. Mol Cell. 2014; 56(1): 55-66.
10. Vicens Q, Westhof E. Biogenesis of circular RNAs. Cell. 2014; 159(1): 13-14.

11. Qu S, Yang X, Li X, Wang J, Gao Y, Shang R, et al. Circular RNA: A new star of noncoding RNAs. Cancer Lett. 2015; 365(2): 141-148.
12. Jeck WR, Sorrentino JA, Wang K, Slevin MK, Burd CE, Liu J, et al. Circular RNAs are abundant, conserved, and associated with ALU repeats. RNA. 2013; 19(2): 141-157.
13. Li P, Chen S, Chen H, Mo X, Li T, Shao Y, et al. Using circular RNA as a novel type of biomarker in the screening of gastric cancer. Clin Chim Acta. 2015; 444: 132-136.
14. Chen B, Huang S. Circular RNA: an emerging non-coding RNA as a regulator and biomarker in cancer. Cancer Lett. 2018; 418: 41-50.
15. Yang F, Liu DY, Guo JT, Ge N, Zhu P, Liu X, et al. Circular RNA circ-LDLRAD3 as a biomarker in diagnosis of pancreatic cancer. World J Gastroenterol. 2017; 23(47): 8345-8354.
16. Yin WB, Yan MG, Fang X, Guo JJ, Xiong W, Zhang RP. Circulating circular RNA hsa_circ_0001785 acts as a diagnostic biomarker for breast cancer detection. Clin Chim Acta. 2018; 487: 363-368.
17. Weng W, Wei Q, Toden S, Yoshida K, Nagasaka T, Fujiwara T, et al. Circular RNA ciRS-7-A Promising prognostic biomarker and a potential therapeutic target in colorectal cancer. Clin Cancer Res. 2017; 23(14): 3918-3928.
18. Chen S, Li T, Zhao Q, Xiao B, Guo J. Using circular RNA hsa_circ_0000190 as a new biomarker in the diagnosis of gastric cancer. Clin Chim Acta. 2017; 466: 167-171.
19. Lan PH, Liu ZH, Pei YJ, Wu ZG, Yu Y, Yang YF, et al. Landscape of RNAs in human lumbar disc degeneration. Oncotarget. 2016; 7(39): 63166-63176.
20. Wan ZY, Song F, Sun Z, Chen YF, Zhang WL, Samartzis D, et al. Aberrantly expressed long noncoding RNAs in human intervertebral disc degeneration: a microarray related study. Arthritis Res Ther. 2014; 16(5): 465.
21. Wang S, Sun J, Yang H, Zou W, Zheng B, Chen Y, et al. Profiling and bioinformatics analysis of differentially expressed circular RNAs in human intervertebral disc degeneration. Acta Biochim Biophys Sin (Shanghai). 2019; 51(6): 571-579.
22. Sang M, Meng L, Liu S, Ding P, Chang S, Ju Y, et al. Circular RNA ciRS-7 maintains metastatic phenotypes as a ceRNA of miR-1299 to target MMPs. Mol Cancer Res. 2018; 16(11): 1665-1675.
23. Cheng X, Zhang L, Zhang K, Zhang G, Hu Y, Sun X, et al. Circular RNA VMA21 protects against intervertebral disc degeneration through targeting miR-200c and X linked inhibitor-of-apoptosis protein. Ann Rheum Dis. 2018; 77(5): 770-779.
24. Song J, Wang HL, Song KH, Ding ZW, Wang HL, Ma XS, et al. CircularRNA_104670 plays a critical role in intervertebral disc degeneration by functioning as a ceRNA. Exp Mol Med. 2018; 50(8): 94.
25. Wang H, He P, Pan H, Long J, Wang J, Li Z, et al. Circular RNA circ-4099 is induced by TNF-alpha and regulates ECM synthesis by blocking miR-616-5p inhibition of Sox9 in intervertebral disc degeneration. Exp Mol Med. 2018; 50(4): 27.
26. Sand M, Bechara FG, Gambichler T, Sand D, Bromba M, Hahn SA, et al. Circular RNA expression in cutaneous squamous cell carcinoma. J Dermatol Sci. 2016; 83(3): 210-218.
27. Lv C, Sun L, Guo Z, Li H, Kong D, Xu B, et al. Circular RNA regulatory network reveals cell-cell crosstalk in acute myeloid leukemia extramedullary infiltration. J Transl Med. 2018; 16(1): 361.
28. Huang DW, Sherman BT, Lempicki RA. Systematic and integrative analysis of large gene lists using DAVID bioinformatics resources. Nat Protoc. 2009; 4(1): 44-57.
29. Agarwal V, Bell GW, Nam JW, Bartel DP. Predicting effective microRNA target sites in mammalian mRNA. Elife. 2015; 4: e05005.
30. Nam JW, Rissland OS, Koppstein D, Abreu-Goodger C, Jan CH, Agarwal V, et al. Global analyses of the effect of different cellular contexts on microRNA targeting. Mol Cell. 2014; 53(6): 1031-1043.
31. Wang C, Wang WJ, Yan YG, Xiang YX, Zhang J, Tang ZH, et al. MicroRNAs: New players in intervertebral disc degeneration. Clin Chim Acta. 2015; 450: 333-341.
32. Zhao B, Yu Q, Li H, Guo X, He X. Characterization of microRNA expression profiles in patients with intervertebral disc degeneration. Int J Mol Med. 2014; 33(1): 43-50.
33. Shao Y, Li J, Lu R, Li T, Yang Y, Xiao B, et al. Global circular RNA expression profile of human gastric cancer and its clinical significance. Cancer Med. 2017; 6(6): 1173-1180.
34. Piwecka M, Glazar P, Hernandez-Miranda LR, Memczak S, Wolf SA, Rybak-Wolf A, et al. Loss of a mammalian circular RNA locus causes miRNA deregulation and affects brain function. Science. 2017; 357(6357): eaam8526.
35. Zheng Q, Bao C, Guo W, Li S, Chen J, Chen B, et al. Circular RNA profiling reveals an abundant circHIPK3 that regulates cell growth by sponging multiple miRNAs. Nat Commun. 2016; 7: 11215.
36. Tojkander S, Gateva G, Lappalainen P. Actin stress fibers--assembly, dynamics and biological roles. J Cell Sci. 2012; 125(Pt 8): 1855-1864.

Original Article

Metastasis Inhibition by Cell Type Specific Expression of *BRMS1* Gene under The Regulation of *miR200* Family Response Elements

Samila Farokhimanesh, Ph.D.[1, 2], Mahdi Forouzandeh Moghadam, Ph.D.[1*], Marzieh Ebrahimi, Ph.D.[3], Zahra Sadat Hashemi, Ph.D.[4]

1. Department of Medical Biotechnology, Faculty of Medical Sciences, Tarbiat Modares University, Tehran, Iran
2. Department of Biotechnology, Applied Biophotonics Research Center, Science and Research Branch, Islamic Azad University, Tehran, Iran
3. Department of Stem Cells and Developmental Biology, Cell Science Research Center, Royan Institute for Stem Cell Biology and Technology, ACECR, Tehran, Iran
4. Department of Medical Biotechnology, School of Advanced Technologies in Medicine, Tehran University of Medical Sciences, Tehran, Iran

**Corresponding Address: P.O.Box: 14115-111, Department of Medical Biotechnology, Faculty of Medical Sciences, Tarbiat Modares University, Tehran, Iran*
Email: foroz@modares.ac.ir

Received: 03/June/2019, Accepted: 03/October/2019

Abstract

Objective: Specific expression of therapeutic genes in cancer therapy has been per used for many years. One of the innovative strategies that have recently been introduced is employing miRNA response elements (MREs) of microRNAs (whose expression are reduced or inhibited in cancerous cells) into the 3´UTR of the therapeutic genes for their specific expression. Accordingly, MREs of anti-metastatic miRNA family have been used in 3´UTR of the metastasis suppressor gene in the corresponding cells to evaluate the level of metastatic behavior.

Material and Methods: In this experimental study, 3´UTR of the *ZEB1* gene with 592 bp length, encompassing multiple MREs of *miR-141, miR-429, miR-200b* and *miR-200c*, was employed to replace *BRMS1 3´UTR*. The obtained vector was then assessed in the context of MCF-10A, MDA-MB231 and MCF-7 cells.

Results: It was shown that the employed MREs are able to up-regulate *BRMS* expression in the metastatic MDA-MB231 cells (almost 3.5-fold increase), while it was significantly reduced within tumorigenic/non-metastatic MCF-7 cells. Specific expression of *BRMS1* in metastatic cells led to a significant reduction in their migratory and invasive characteristics (about 65% and 55%, respectively). Two-tailed student's t test was utilized for statistical analysis.

Conclusion: It was demonstrated that a chimeric vector containing *BRMS1* which is regulated by *miR-200* family response element may represent a promising therapeutic tool. This is due to the capability of the chimeric vector for cell type-specific expression of anti-metastatic genes with lowest side-effects. It consequently prohibits the invasive characteristics of metastatic cells.

Keywords: Breast Cancer, *BRMS1, MiR-200*, Neoplasm Metastasis

Cell Journal(Yakhteh), Vol 23, No 2, July 2021, Pages: 225-237

Citation: **Farokhimanesh S, Forouzandeh Moghadam M, Ebrahimi M, Hashemi ZS. Metastasis inhibition by cell type specific expression of BRMS1 gene under the regulation of miR200 family response elements. Cell J. 2021; 23(2): 225-237. doi: 10.22074/cellj.2021.6988.**

Introduction

Despite years of research, metastasis (a multi-steps process through which the primary tumor cells pervade neighbor tissues, while each of these steps requires tight regulation) is still considered as the cause of approximately 90% of the mortalities related to the cancer and for this reason, it has been particularly significant in the cancer treatment investigation. In this regard, up-regulation of the therapeutic genes in metastatic cancer cells have always been a major challenge (1).

Different strategies have been introduced for specific expression of therapeutic genes from which post-transcriptional targeting has attracted enormous interest. This targeting strategy can post-transcriptionally suppress gene expressions via establishing sequence specific interaction with the common miRNA response elements (MREs) over 3´ untranslated regions (3´UTRs) of the associated miRNA targets (2).

Discovery of the abnormal expression of miRNAs (down-regulation or up-regulation) in different steps of malignancy, among the various cancers, have been performed via the genome wide investigation methods, containing distinct micro-array platforms and bead-based flow-cytometry. This finding revealed that 3´UTR of the down-regulated miRNAs (which contain their microRNA target sequences) could be employed for specific expression (3, 4).

For targeting metastasis, miRNAs which are involved in epithelial-mesenchymal transitions (EMT) are thought to

be the best choice, because EMT is one of the early steps to promote malignant tumor progression (5). The above procedure is defined by loss of epithelial features along with the achievement of mesenchymal characteristics. EMT could convert immotile epithelial cells into the motile mesenchymal types (6).

It should be noted that *miR-200* family has been recognized as one of the fundamental regulators of the epithelial phenotype by binding to zinc finger E-box binding homebox1 and 2 (*ZEB1* and *ZEB2,* respectively), two prominent transcriptional repressors of polarity (*CRB3* and *LGL2*) and cell adherence (*E-cadherin*) genes. Their expressions are significantly increased in metastatic cells which have mesenchymal characteristics. In the cells with epithelial characteristics, *miR-200* family members bind to their MREs on the *ZEB1* and *ZEB2* 3´UTR and inhibit their expressions. Using *ZEB1* 3´UTR (that include MREs of *miR-200* family), in the 3´UTR of a therapeutic gene as a post-transcriptional targeting moiety, would be an effective strategy. Using this strategy, specific expression of metastasis suppressor gene in the invasive cells could be occurred (7). This strategy has already been used for on colyticadeno-viruses to possess specific nature to glioma cell by *miR-128*, *miR-124*, *miR-218* and *miR-146b* response elements, as well as for specific expression of *TRAIL* gene in uveal melanoma cells for growth suppression by *miR-34a*, *miR-137* and *miR-182* response elements. The results have been quite satisfactory (8, 9).

In order to select a proper therapeutic gene, pleiotropic anti-metastatic genes are in priority. Due to its ability to regulate multiple steps of metastasis (pleiotropic anti-metastatic function), including metastatic colonization at the secondary tissue site which is believed to be a key vulnerability of metastatic cancer, the metastasis suppressor genes may be the most relevant choice for therapeutic intervention (10). One of the most applicable members of metastasis suppressor family, which has a great potential of metastasis inhibition, is the breast cancer metastasis suppressor 1 (*BRMS1*).

BRMS1 has been first described in 2000 following the observation that entering a typical, neomycin-tagged human chromosome 11 decreased metastatic potential of the MDA-MB435 human breast cancer cells by 70-90% with no prevention of primary tumor growth (11). According to some studies, metastasis is repressed by *BRMS1* via inhibition of several stages throughout the process cascades such as migratory and invasive phenotype, colonization, angiogenesis, programmed cell death, cytoskeleton rearrangement, adhesion, gap junctional intercellular communication and increasing immune recognition by modulating numerous metastasis-related genes along with the metastasis-regulatory microRNA, called metastmiR. Some metastasis-related genes, which are regulated by *BRMS1* include: *urokinase-type plasminogen activator*, *fascin, epidermal growth factor receptor, osteopontin* and *C-X-C chemokine receptor 4* (12).

BRMS1 also over-expresses *miR-146a*, *miR-146b* and *miR-335* which inhibit metastasis. It down-regulates *miR-10b*, *miR-373* and *miR-520c* which promote metastasis. It should be noted that some research found that metastasis suppressor genes have been previously employed for repressing metastasis of invasive cells and their results were promising (13, 14).

Therefore, re-expression of *BRMS1* affects both transcriptome and proteome (15-17). Considering these extensive roles, *BRMS1* could be a rational choice to pave the way for anti-metastatic therapy. In the present study, we exploited the differential profiles of miRNA expression among metastatic breast cancer cells and normal cells to confer specific *BRMS1* expression. Subsequently, we evaluated the possibility and efficiency of *miR-200* family response elements for regulating particular expression level of *BRMS1*.

Materials and Methods

Cell culture

In this experimental study, three cell lines were obtained from ATCC (Manassas, USA) including non-tumuorigenic phenotype of MCF-10A, tumourigenic and non-metastatic phenotype of MCF-7 and metastatic phenotype of MDA-MB231 breast cancer cell lines. It should be noted that the medium selected for culturing MCF-10A cells is Dulbecco's modified Eagle's Medium (DMEM, Life Technologies Inc., USA)/F12 with 0.5 µg/ml hydrocortisone, 20 ng/ml epidermal growth factor (EGF), 100 ng/ml cholera toxin, 10 µg/ml insulin and 5% donor horse serum as supplements. MCF-7 cell line was propagated in DMEM/F12, 1% penicillin/streptomycin (Gibco, USA) and 10% fetal bovine serum (FBS, Gibco, USA). MDA-MB231 cells have been grown in the conventional DMEM with 1% penicillin-streptomycin solution (Life Technologies Inc., USA) and 10% FBS as supplements in a moistened atmosphere of 5% CO_2.

Extraction of RNA and quantitative reverse transcription polymerase chain reaction

Based on the pre-determined plan, total RNA was isolated from the three cell lines via the RNeasy mini kit (Qiagen, Germany). cDNA was primed in a randomized manner from total RNA through the RevertAid First Strand cDNA Synthesis Kit (Thermo Fisher Scientific, USA). Quantitative reverse transcription polymerase chain reaction (qRT-PCR) assay was implemented three times by SybrPremix Ex Taq II (Takara, Japan) on a Rotorgene 3000 series PCR device (Corbett Research, USA) using the following primers for *ZEB1* and *ZEB2,* in addition to the endogenous *BRMS1* gene:

ZEB1-
F: 5′-GAG ATC AAA GAC ATG TGA CGC AG-3′
R: 5′-CTT CTC TCC ACT GTG AAT TCT TAA G-3′

ZEB2-
F: 5′-AGG GAC AGA TCA GCA CCA AAT G-3′
R: 5′-ACT CGT AAG GTT TTT CAC CAC TGT G-3′

BRMS1-
F: 5′-AGC TCT GAA TGG TGG GAT GAC-3′
R: 5′-CAC GAT GTA TGG GCC AGA AAC-3′

After collecting the required information, Rotorgene software was used to analyze the data. Moreover, the comparative quantification feature of the Rotorgene software was used to determine the relative levels of expression. In addition, each mRNA quantification datum was normalized to *β-actin*. All fold changes in the expression were determined by using a comparative Ct (ΔΔCt) technique.

Extraction of miRNA and quantitative reverse transcription polymerase chain reaction

Extraction of the total RNA, with effective recovery of small RNAs, was done in the three cell lines using miRCURY RNA isolation kit (Exiqon, Denmark). Then, cDNA was synthesized using the Universal cDNA Synthesis Kit (Exiqon, Denmark).

With regard to the company's guideline, the mature form of *miR-200* family was detected using LNA microRNA Primer Sets and miRCURY LNA Universal RT microRNA PCR Kit (Exiqon, Denmark). In the next step, relative levels of expression were identified using the relative quantification feature of Rotorgene software. Then, U6 small nuclear RNA was employed as an internal control. Afterwards, comparative Ct (ΔΔCt) technique was applied for determining fold changes of expression. Finally, a melting curve was analyzed for all of the utilized primer collections, all of which exhibited a single peak. They represented specificity of the all experienced primers. All assessments were performed three times.

Construction of plasmids

The 3′UTR sequence of the *ZEB1* was retrieved from UTRdb. According to the results of qRT-PCR for *miR-200* family and bioinformatics analysis, 592 bp (from nucleotide 756 to 1348) region in the central part of *ZEB1* 3′UTR sequence, containing four miRNA binding sites (*miR-141, miR-429*, *miR-200b* and *miR-200c*), was amplified by the following primers:

5′-CGACGCGTCGGATAAGGACAGCAAAATCATC AG-3′

5′-GACTAGTCAAAGTACATATGTCAGTAAGAAG GG-3′

The PCR product was cloned into 3′UTR of luciferase in pmiR-REPORT Luciferase miRNA Expression Reporter (Ambion, USA) by MluI and SpeIrestriction enzymes (Roche Applied Science, Australia; miR-report. *ZEB1)*. Control plasmid of pmiR-REPORT β-gal was employed to normalize the transfection. Fidelity of PCR cloning was confirmed by sequencing. The 592 bp fragment of *ZEB1* 3′UTR was also amplified using the following primers:

5′-CGCGTCGACGATAAGGACAGCAAAATCATC AG-3′

5′-CGGGATCCAAAGTACATATGTCAGTAAGAAG GG-3′

Product of the amplification was cloned into 3′UTR of GFP in the control plasmid of pcDNA 6.2-GW/EmGFPmiR-neg (pc, Invitrogen, USA) through BamHI and SalI restriction enzymes (pc.Z, Roche Applied Science). Verification of PCR cloning was performed by sequencing.

It should be noted that optimization of *BRMS1* gene sequence was performed by GenScript (Genscript Corporation Piscataway, USA) in order to reach the highest probable level of expression. Afterwards, the optimized gene was cloned into both pc and pc.Z plasmids using the restriction enzymes SalI and DraI, which were called pc.BR and pc.BR.Z respectively. The accuracy of cloning was confirmed by sequencing.

Luciferase reporter assay

5×10^4 MCF-7 and MDA-MB231cells were plated in 24-well plates. Then, they were incubated overnight. Both cell lines were co-transfected in a 24-well plates with 0.10 μg of the pmiR-report. *ZEB1* luciferase reporter vector and 0.05 μg of the normalization plasmid pmiR-REPORT β-gal using the Lipofectamine 2000 (Invitrogen, USA). Lysis buffer was used to process the cells. Afterwards, luciferase activities were measured using Dual-Glo Luciferase Assay System (Promega, USA), 24 hours post-transfection. GFP reporter assay was also performed using standard protocol. It should be mentioned that the luciferase activities are presented as the average of three independent tests.

miRNA mimics and inhibitors

miR-200b, miR-200c, miR-141 and *miR-429* mirVana™ mimics and inhibitors (Invitrogen, USA) were completely mixed and added to the cells (5×10^4 MDA-MB231 and MCF-7 cells) with concentration of 40 nM (10 nM for each mimic or inhibitor) using the Lipofectamine™ 2000 based on the company's guidelines. Twenty four hours later, the cells were transfected with pc, pc.BR and pc.BR.Z. Then, expression of *BRMS1* was assessed in these cells by qRT-PCR following the optimized specific primers (exogenous) for *BRMS1* genes:

5′-TACGAACGGAGAAGGAGCGA-3′

5′-CGCTCTGCTCCGACTTCCTCC-3′

All experiments were repeated three times.

Transfections

The 24-well plates were used to plate 5×10^4 cells of all three cell lines. Then, they were incubated overnight. MDA-MB231 and MCF-7 cells were transiently transfected by pc, pc.Z, pc.BR and pc.BR.Z, using lipofectamin 2000 for the subsequent experiments. Each transfection was carried out three times.

Trans well migration assay

In order to assess migration, 2.5×10^4 cells of three cell lines, which were transfected by four constructs (pc, pc.Z, pc.BR and pc.BR.Z) and serum starved cells, were plated into the upper chamber on the non-coated membrane (24-well insert, pore size 8 μm, Millipore Billerica, USA). Then they were allowed to migrate toward medium which contains serum in the lower chamber. When they were incubated at 37˚Cin a 5% CO_2 humidified incubator for 24 hours, the cells on top of the chambers were eliminated via wiping with a cotton swab. Then, the migrated cells to the lower surface of filter were fixed in 4% formaldehyde for 30 minutes. Afterwards, 0.5% crystal violet was used to stain for 10 minutes. Next, cell migration was scored by counting 10 random fields per filter below a light microscope at ×40 magnification. Each assay was repeated three times.

Trans well invasion assay

Matrigel-coated Trans well cell culture chambers (8 μm pore size) were used to analyze cell invasion. Concisely, transfected cells (2.5×10^4 cells/well) were serum starved for 24 hours. Then, they were plated on the top of insert of a 24-well chamber in a medium without serum. Afterwards, the medium with 10% serum was added to the lower wells. Next, incubation of the cells was done for 24 hours. The cells on the upper side of filters were then mechanically removed by scrubbing with a cotton swab. As the last step, 4% formaldehyde was used to fix the membrane for 30 minutes and 0.5% crystal violet was utilized for 10 minutes. Ultimately, counting the invasive cells were performed at ×40 magnification from 10 different fields of each filter. Invasion assays were done in triplicate.

Western blotting

pc.BR construct was used to transfect the MDA-MB231 cells. After 48 hours, the cells were lysed in radio-immunoprecipitation assay (RIPA) buffer (50 mM Tris-HCl pH=7.4, 150 mM NaCl, 1 mM EDTA, 0.1% SDS, 1% sodium deoxycholate and 1% NP-40). The buffer was enriched with cocktail of protease inhibitors (PMSF). Then, a cell scraper was used to scrape the cells. Afterwards, the cells were transferred into the ice cold tube for a brief sonication. Total protein was obtained by centrifuging the extract at 14,000 g at 4˚Cfor 10 minutes. MILLIPORE ultrafiltration column was used to obtain higher concentrations of the protein. It should be noted that Bicinchoninic acid assay (Thermo Fisher Scientific, USA) was used to measure concentration of the protein. The protein sample (40 μg) was isolated on a 12.5% SDS-polyacrylamide gel and transferred electro-phoretically onto Nitrocellulose Transfer membranes (PROTRAN, Schleicher & SchuellBioScience, Germany). Then, 3% skimmed milk in Tris-buffered saline/0.05% Tween-20 was used to block the membrane for one hour. Next, rabbit horseradish peroxidase-conjugated anti-BRMS1antibody (isotype: Ig G, Abcam, UK) was used to blot it for one hour. Ultimately, the augmented chemiluminescence detection kit (Thermo Fisher Scientific, USA) was employed to visualize the protein bands. Western blotting was repeated in triplicate.

Statistical analysis

In order to statistical analyses of the present data, the two-tailed student's t test was utilized. An asterisk means significant that shows $P<0.05$. Prism 6 statistical software (GraphPad Software, Inc.) was used for all graphs and statistical analyses. The results are expressed as mean ± standard deviation. Each experiment was repeated three times.

Ethical considerations

The study does not contain any experimental animals or human participants. It should be noted that each procedure has been implemented based on the Ethical guidelines of Faculty of Medical Sciences, Tarbiat Modares University, Tehran, Iran (code: 52112234).

Results

Differential ZEB factors and *miR-200* family expression profiles between metastatic and normal breast cells

Since *ZEB* 3´UTRs have the *miR-200* family-response elements, their expression profiles were investigated in MDA-MB231 and MCF-7 cells by qRT-PCR assays. The outputs of qRT-PCR assays showed that level of *ZEB1* expression was 7.2 fold higher than *ZEB2* in the metastatic cells compared to the non-metastatic cells (Fig.1A, B). Since the 3´UTR of the *ZEB* gene with higher expression level, is a better choice (due to the less inhibition by *miR-200* family), 3´UTR of *ZEB1* gene was selected. Then, expression profiles of *miR-200*a, *miR-200b*, *miR-200c*, *miR-141* and *miR-429* were investigated by qRT-PCR in the MDA-MB231 and MCF-7 cells relative to the non-tumorigenic MCF-10A. It was demonstrated that the levels of four out of five miRNAs (*miR-200b*, 200c, *miR-141* and *miR-429*) were significantly reduced in the tested metastatic MDA-MB231 cells compared to the cancerous but non-metastatic MCF-7 cells. This was consistent to the previously published data (Fig.1C, D, $P<0.05$) (18). The reduced expression levels of four microRNAs possibly ensure that using their MREs result in expressing the intended exogenous genes in metastatic breast cancer cells instead of non-metastatic and normal cells.

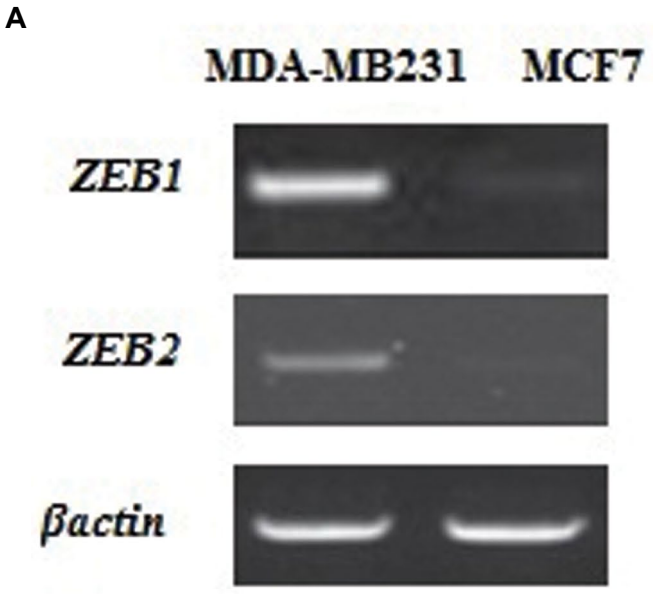

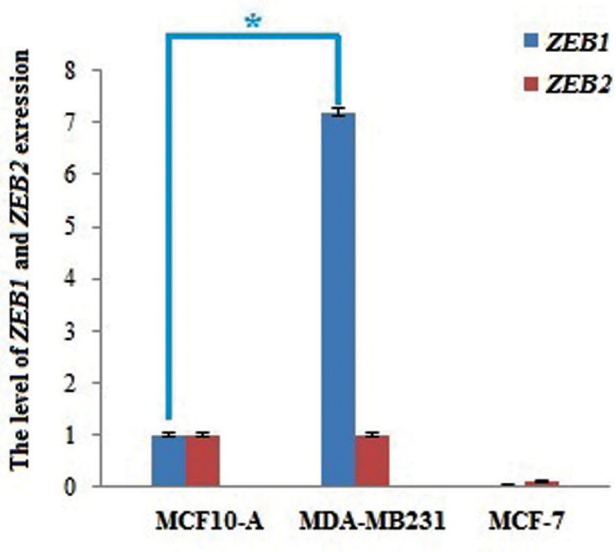

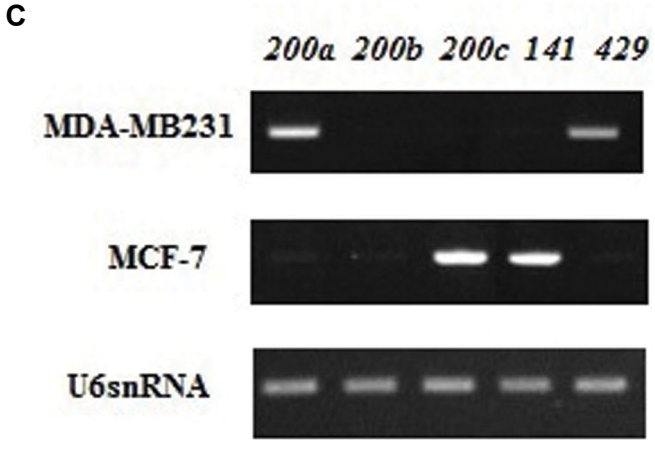

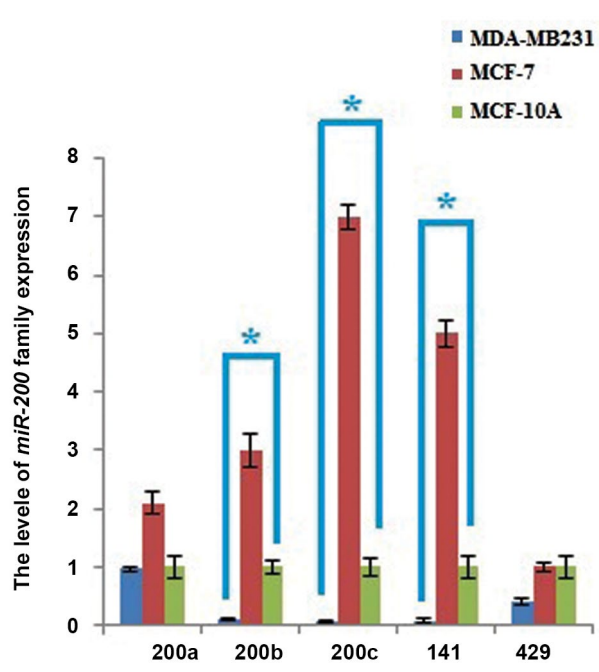

Fig.1: Differential ZEB factors and *miR-200* family expression profiles between metastatic and normal breast cells. **A.** *ZEB1* and *ZEB2* mRNA detections using qRT-PCR method in untreated MDA-MB231 and MCF-7. **B.** *ZEB1* and *ZEB2* expression levels in MDA-MB231 (cancerous, metastatic cell line) and MCF-7 (cancerous, non-metastatic control cell line) relative to MCF-10A (normal cell line). **C.** qRT-PCR of *miR-200* family in MDA-MB231 and MCF-7 cells. **D.** The level of *miR-200* family expression in MDA-MB231 and MCF-7 relative to MCF-10A. Data represent means ± SD of three separate tests. *; P value for each condition was significant in comparison with the normal cells. qRT-PCR; Quantitative reverse transcription polymerase chain reaction.

Application of *miR-200b, miR-200c*, *miR-141* and *miR-429* MREs confined exogenous gene expression within the metastatic cancer cells

For assessing whether MREs could be used for the specific expression of exogenous gene (*BRMS1)* in metastatic breast cancer cells, a reporter plasmid including luciferase regulated by their MREs was successfully constructed (Fig.2A). Results demonstrated that luciferase activity was not significantly changed in the pmiR-report. *ZEB1* transfected MDA-MB231 cells. However, its activity was markedly repressed in the MCF-7 cell line (Fig.2B). To confirm control of *miR-200b*, *miR-200c*, *miR-141* and *miR-429* on the exogenous gene expression under their respective MREs, assaying the luciferase was done in the pmiR-report. *ZEB1*-transfected cells after changing level of the above miRNAs. Expressions of endogenous *miR-200b*, *miR-200c*, *miR-141* and *miR-429* were inhibited by 30-50% in MCF-7 through mixing the above four microRNA inhibitors. Thus, expression of luciferase was considerably up-regulated in pmiR-report. *ZEB1*-transfected cells (Fig.2C, D). Consistently, luciferase expression was almost 50% declined in pmiR-report. *ZEB1*-transfected MDA-MB231 cells, where by *miR-200b*, *miR-200c*, *miR-141* and *miR-429* levels were increased by treating with the mixture of four microRNA mimics (Fig.2E, F). These outputs showed

that MCF-7 cells had higher endogenous expression of *miR-200* family than MDA-MB231 cells. So, using four microRNA inhibitors could inhibit them and luciferase activity was increased. However, in MDA-MB231 endogenous expressions of *miR-200* family were very low, using four microRNA mimics, which could bind to the MREs. This caused reduction of luciferase expression (Fig.2E, F, P<0.05).

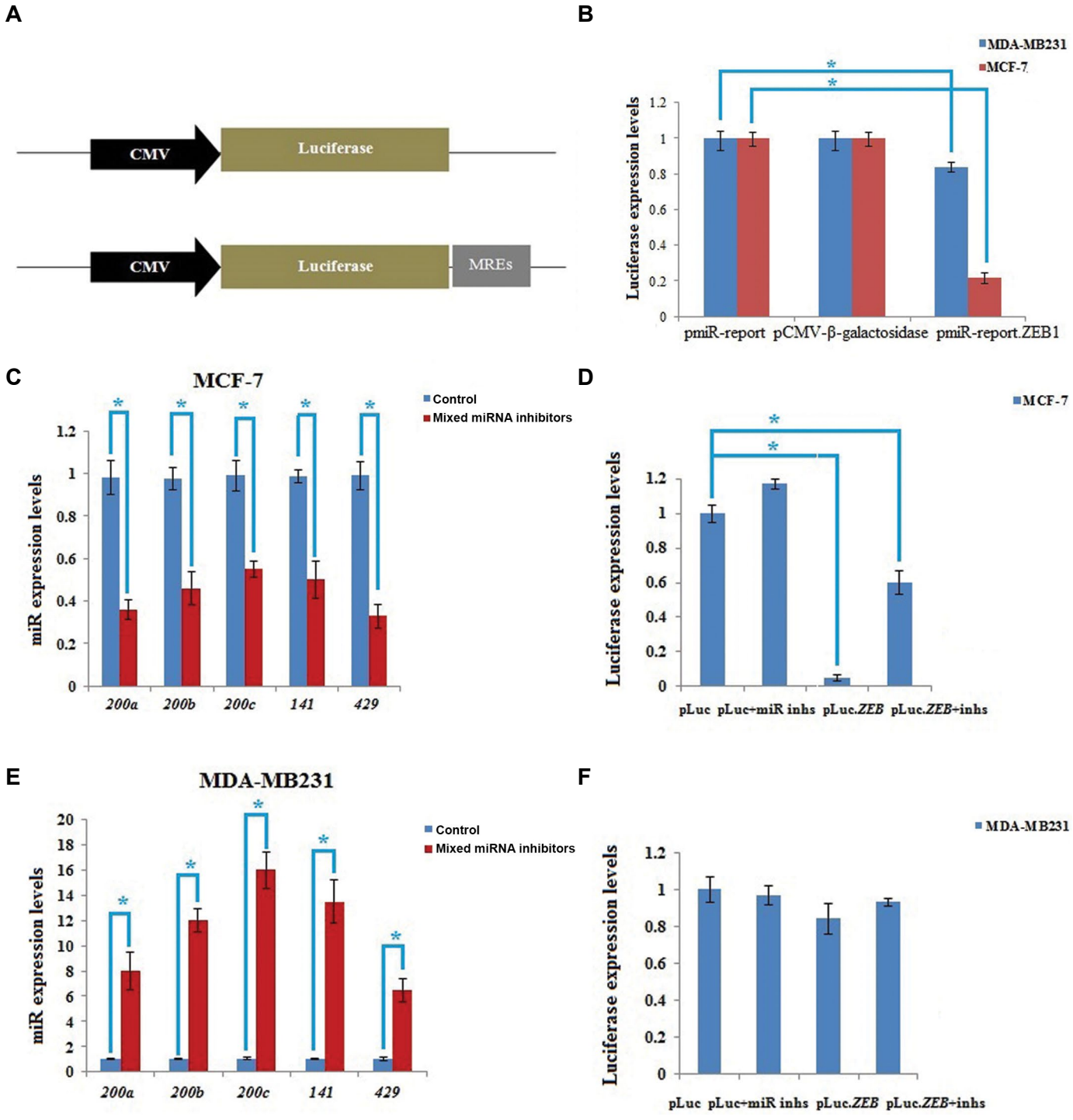

Fig.2: Use of MREs of miR-200 family confined exogenous gene expression within the metastatic cancer cells. **A.** Illustration of the structure of luciferase reporter plasmids. **B.** Evaluation of luciferase expression in MDA-MB231 and MCF-7 cells after the transfection of pmiR-REPORT β-gal control plasmid and pmiR-report ZEB1. **C.** Synthetic inhibitors of *miR-200b*, *miR-200c*, *miR-141* and *miR-429* were mixed and transfected into non-metastatic MCF-7. Expression levels of these miRNAs were assessed by qRT-PCR with U6, as endogenous reference and they were shown as values relative to the control groups. **D.** Co-transfection of MCF-7 cells with the indicated constructs and mixed miRNA inhibitors or controls. Twenty four hours later, luciferase expression was evaluated. Relative luciferase activity in the cells transfected with pmiR-report ZEB and control inhibitors was considered as standard. **E.** Synthetic mimics of *miR-200b*, *miR-200c*, *miR-141* and *miR-429* were mixed and transfected into MDA-MB231. Expression levels of these miRNAs were assessed by qRT-PCR with U6, as the endogenous reference and they were shown as values relative to the control groups. **F.** Co-transfection of MDA-MB231 with the indicated constructs and mixed miRNA mimics or controls. Twenty four hours later, luciferase expression was evaluated. Relative luciferase activity in the cells transfected with pmiR-report ZEB and control inhibitors were considered as standard. Data represent means ± SD of three separate tests. *; P<0.05 and qRT-PCR; Quantitative reverse transcription polymerase chain reaction.

MREs of *miR-200b*, *miR-200c*, *miR-141* and *miR-429* ensured expression of *BRMS1* specifically in MDA-MB231 cells

MREs were subsequently inserted into *BRMS1*expressing pc vector to regulate expression of the aforementioned metastasis suppressor gene. A chimeric plasmid was constructed by inserting 592 bp of *ZEB1* 3´UTR containing MREs of *miR-200b*, *miR-200c*, *miR-141* and *miR-429,* immediately following the *BRMS1* open reading frame coding region (Fig.3A). Expression level of *BRMS1* was assessed in MCF-7 and MDA-MB231 before and after treatment by pc.BR semi-quantitative RT-PCR and qRT-PCR assays. Findings revealed that expression level of *BRMS1* in untreated MCF-7 cells was 10 fold more than MDA-MB231 cells. The results also confirmed increase of in *BRMS1* expression level (more than 3 fold) after transfection by pc.BR construct (Fig.3B, C). qRT-PCR assay showed that chimeric construct of the pc.BR.Z had almost the same levels of *BRMS1* gene expression as pc.BR in MDA-MB231, where as it was considerably inhibited (more than 2 fold decrease of *BRMS1* expression) in pc.BR.Z transfected MCF-7 cells (Fig.3D). These results were compatible to ourexpectation, since MDA-MB231 cells did not have *miR-200* family. So, when they were treated with pc.BR.Z, there was almost no *miR-200* family for binding to *ZEB1* 3´UTR and it could inhibit *BRMS1* expression. However, due to the*miR-200* family expression, expression of *BRMS1* was inhibited in MCF-7 (Fig.3D, $P<0.05$).

Pc.BR.Z mediated *BRMS1* expression depends on the abundance of *miRNA-200b*, *miR-200c, miR-141* and *miR-429*

To test if the *BRMS1* expression by pc.BR.Z was depend on the levels of *miR-200b, miR-200c, miR-141* and *miR-429*, synthetic miRNA inhibitors and mimics were added to the MDA-MB231 and MCF-7 cells. Then, *BRMS1* expression was evaluated in these cells using qRT-PCR assays. In MCF-7, which has higher levels of four microRNAs expression, *BRMS1* expression was significantly inhibited, after transfecting the cells with pc.BR.Z. Nonetheless, treating the pc.BR.Z transfected MCF-7 cells with microRNA inhibitors resulted in partially restoring *BRMS1* expressions (almost more than 2 fold increase in *BRMS1* expression). This increase is owing to the reason that microRNA inhibitors could bind to *miR-200* family and prevent them from attaching to their MREs, so *BRMS1* expression could be performed (Fig.3E). Consistently; transfecting MDA-MB231 cells with microRNA mimics remarkably decreased expression of *BRMS1* (almost 2 fold) in these cells, where by the endogenous levels of *miR-200b*, *miR-200c*, *miR-141* and *miR-429* were low. But, microRNA mimic could bind to MREs and inhibit expression of *BRMS1*. Collectively, pc.BR.Z mediated *BRMS1* expression by the abundance of *miR-200b*, *miR-200c*, *miR-141* and *miR-429* (Fig.3F, $P<0.05$).

pc.BR.Z reduced migration and invasion of the metastatic breast cancers cells without affecting normal cells

To examine whether pc.BR.Z could decrease migration and invasion of metastatic breast cancer cells, we performed *in vitro* analysis specifically expressing *BRMS1* metastasis suppressor gene in the context of a chimeric pc.BR.Z vector in the MCF-7 and MDA-MB231 cells. qRT-PCR analysis demonstrated that *BRMS1* was increased (3.5 fold) in the metastatic cells transfected with pc.BR.Z, compared to the non-metastatic cells (Fig.3D). Then, assaying trans well migration and invasion were done on the untreated cells (Fig.4). The results indicated that migration rate in MDA-MB231 was 2.6 fold more than MCF-7cells (Fig.4A) and the invasion rate was 6.7 fold more than MCF-7 in the non-transfected cells (Fig.4B, C). Subsequently, we tested whether *BRMS1* had effects on the migration and invasion of MDA-MB231 cells, transfected with pc, pc.Z, pc.BR, pc.BR.Z or non-transfected cells. Pc.BR decreased the rate of MDA-MB231 cells migration and invasion of by 68 and 62.3%, respectively. pc.BR.Z also reduced these rates by 65 and 55%, respectively compared to pc and pc.Z transfected cells (Fig.5A-C). Levels of migration and invasion were decreased in the treated cells with pc.BR.Z. This may be due to the little leakage of *miR-429* expression. We also checked migration and invasion rates in MDA-MB231 cells transfected with pc.BR, pc.BR.Z, mixed mimics and inhibitors. It was demonstrated that there is almost more than 10% difference in migration and invasion of pc.BR.Z and pc.BR.Z+mimics, because miR-mimic could bind to MREs and inhibit the expression of *BRMS1*. This caused an increase in migration and invasion of the treated cells. Since the migration and invasion rates of untreated MCF-7 cells were negligible, their transfection with the constructs seemed to be futile (Fig.5D, E, $P<0.05$).

Protein expression level

BRMS1 protein level, encoded by pc.BR construct, was evaluated using western blot method after transfection. Figure 6 shows the western blot result for the total protein sample extracted from pc.BR transfected cell. These results indicated successful expression of the BRMS1 at the protein level (Fig.6, $P<0.05$).

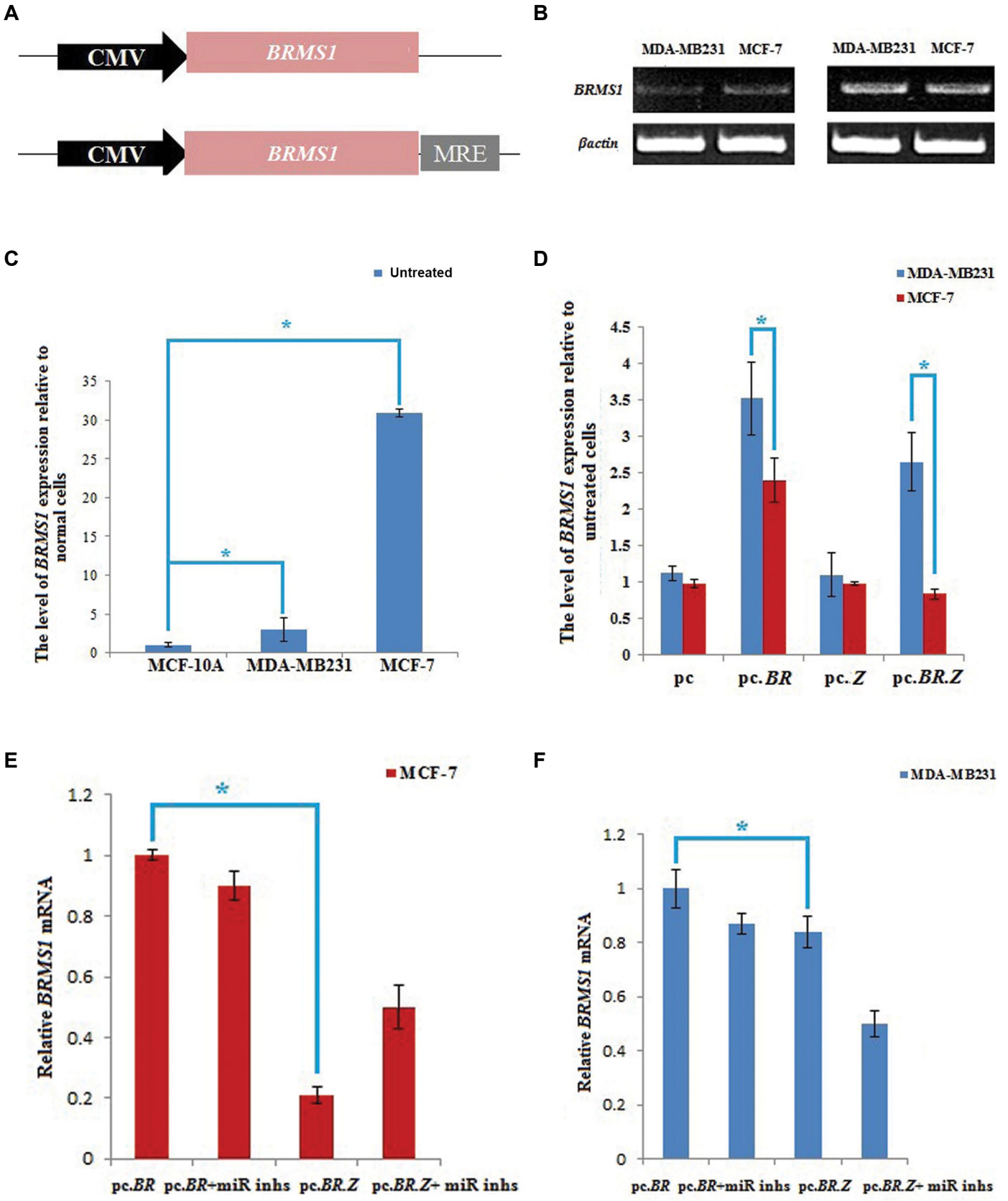

Fig.3: MREs of miR-200 family guaranteed particular expression of BRMS1 in MDA-MB231 cells and Pc.BR.Z mediated *BRMS1* expression depends on the quantity of miR-200 family. **A.** Illustration of the structure of chimeric vectors containing *BRMS1*. **B.** Semi-quantitative RT-PCR of *BRMS1*. *BRMS1* expression level was evaluated in untreated MDA-MB231 and MCF-7 cells (the endogenous level of BRMS1) and after transfection (ectopic level of *BRMS1*). **C.** qRT-PCR assay in untreated MDA-MB231 and MCF-7 cells and *BRMS1* expression level in untreated MDA-MB231 and MCF-7 relative to the normal cells. Data represent means ± SD of three separate tests (*; P<0.05). **D.** *BRMS1* mRNA expression level analysis using qRT-PCR assay in MDA-MB231 and MCF-7 cells transfected with pc, pc.Br, pc.Z and pc.Br.Z. **E.** MCF-7 cells were transfected with pc.Br and pc.Br.Z as well as the mixed inhibitors of miR-200 family. After 24 hours, expression level of *BRMS1* was assessed using qRT-PCR assay. **F.** MDA-MB231 cells were transfected with pc.Br and pc.Br.Z as well as the mixed mimics of miR-200 family. After 24 hours, expression level of *BRMS1* was assessed using qRT-PCR assay. *β-actin* was used as endogenous reference. Data represent means ± SD of three separate tests. P value for each condition was significant, compared to the untreated cells.

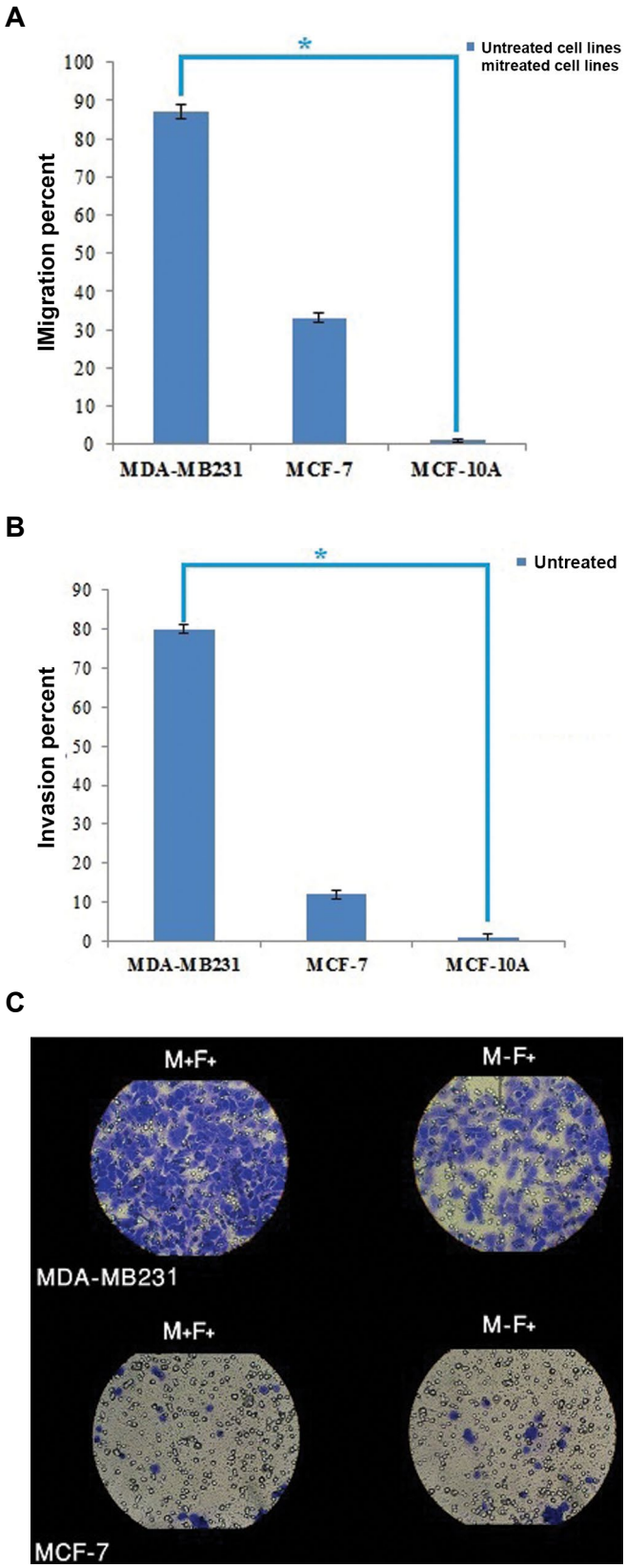

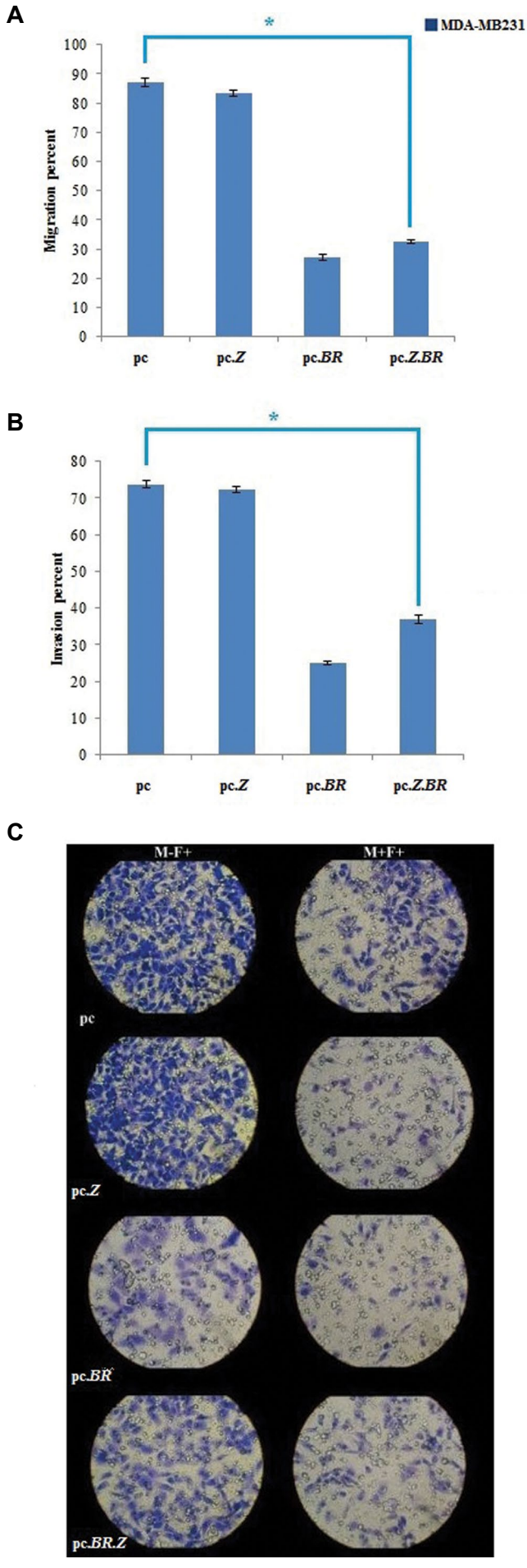

Fig.4: Migration and invasion assays before any treatment. **A.** Migration percent of MDA-MB231 and MCF-7 cells before any treatment. **B.** Invasion percent of MDA-MB231 and MCF-7 cells before any treatment. As it is shown, level of migration and invasion in MDA-MB231 cells are significantly more than MCF-7 without any treatment. **C.** Trans well migration assay and matrigel invasion assay in MDA-MB231 and MCF-7 cells before any treatment. Data represent means ± SD of three separate tests. *; P<0.05, M+F+; Contain matrigel and FBS, M-F+; Without matrigel and contain FBS. One out of 10 field as a sample (M-F+ indicates the level of migration and M+F+ indicates the level of invasion).

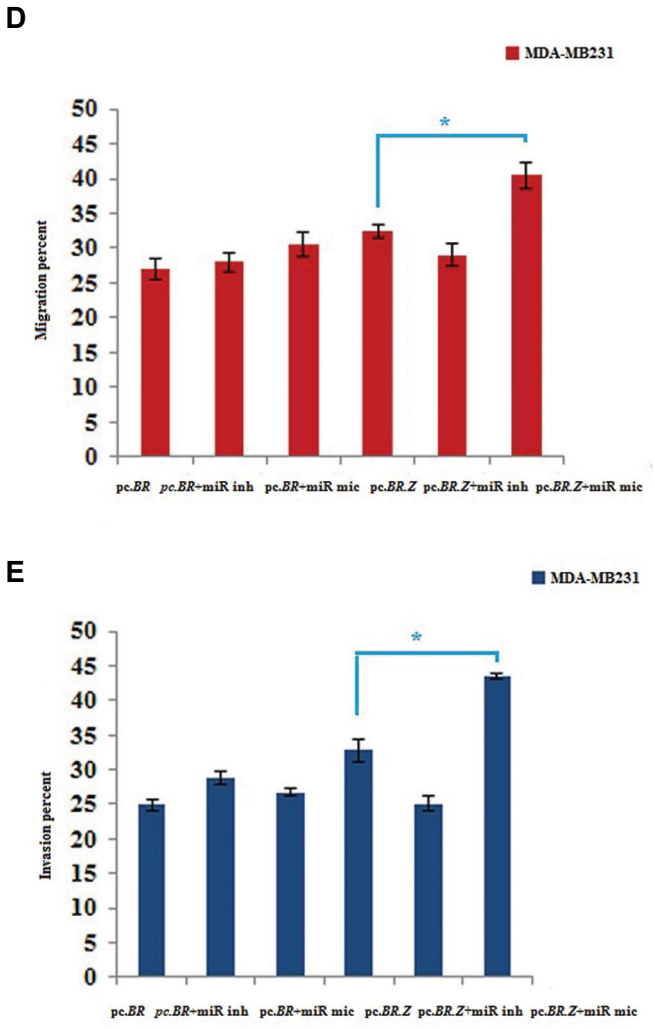

Fig.5: Migration and invasion assays after transfections. **A.** Migration percent after transfection of MDA-MB231 cells by four constructs. **B.** Invasion percent after transfection of MDA-MB231 cells by four constructs. **C.** Matrigel invasion assays in MDA-MB231 cells after transfection by four constructs. M+F+; Containing matrigel and FBS, M-F+; Without matrigel and containing FBS. One out of 10 field as a sample. **D.** Migration percent in MDA-MB231 cells transfected with pc.BR, pc.BR+ miR inhibitor, pc.BR+ miR mimic, pc.BR.Z, pc.BR.Z+ miR inhibitors and pc.BR.Z+ miR mimic. **E.** Invasion percent in MDA-MB231 cells transfected with pc.BR, pc.BR+ miR inhibitor, pc.BR+ miR mimic, pc.BR.Z, pc.BR.Z+ miR inhibitors and pc.BR.Z+ miR mimic. Data represent means ± SD of three separate tests. *; P<0.05.

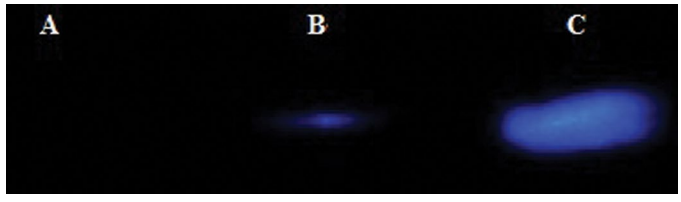

Fig.6: Chemiluminescent western blotting for protein expression levels. **A.** is the MDA-MB231 cell lysis without any *BRMS1* antibody (horseradish peroxidase-conjugated antibody (Abcam Company) treatment as a negative control group. **B.** Is the MDA-MB231 cell lysis with the *BRMS1* antibody treatment. and **C.** Is the MDA-MB231 cell lysis which was transfected by pc.BR construct, with the *BRMS1* antibody treatment.

Discussion

Contemporary, MRE regulated approaches have garnered a lot of attention as an alternative gene therapy strategy for specific targeting of the malignant cells. MREs are more advantageous over the conventional gene therapy approaches (like transcriptional targeting approach or using cancer-specific promoters), offering higher efficacy and specificity for the certain cell types. Specific anti-metastatic microRNAs have been exhibited to be down-regulated in metastatic breast cancer cells (19, 20). Therefore, MREs corresponding to the aforementioned microRNAs might be applied to drive specific expression of well-established anti-metastatic genes in cancer cells and ultimately inhibit their invasiveness. Given these circumstances, we have devised a MRE regulated gene therapy strategy to inhibit invasiveness behavior of metastatic breast cell lines by specific expression of *BRMS1* gene. It has been demonstrated that a MREs-regulated vector containing *BRMS1* gene could be a compelling tool attaining this purpose.

BRMS1 is among the promising anti-metastatic breast cancer genes which selectively suppresses metastasis without suppression of any cancer cell tumorigenicity. Pleiotropically acting *BRMS1* prevents multiple steps of the metastatic cascade. Diversity of *BRMS1* actions, employing a variety of mechanisms, contribute to its robust inhibition of metastasis. The recent reports have shown that *BRMS1* remarkably suppressed migration and invasion of cells in many types of cancer. Analysis of tissue micro-array of the patients revealed that *BRMS1* was considerably down-regulated in glioma cells in comparison with the normal astrocytes. Additionally *BRMS1* over-expression could inhibit migration and invasion of glioma cells via suppressing MMP-2 , NF-κB and uPA (21). In the other work, it was demonstrated that up-regulation of *BRMS1* decreased SDF-induced migration by reducing NF-κB dependent CXCR4 expression in NSCLC cell line (22). Rectal cancer xenograft invasiveness could also be reduced by over-expression of BRMS-1 (23). Besides, investigations on breast cancer showed that there is a reverse association between *BRMS1* over-expression and disease progression. Down-regulation of fascin, which is an actin-bundling protein, by *BRMS1* has been shown in another study. This exerted an inhibitory effect on metastasis of ovarian cancer cells (24, 25). All of the previously found data were in accordance with the present work in terms of reducing level of migration and invasion by up-regulating BRMS-1.

It confers activity of BRMS1 via regulating numerous metastasis-associated genes and microRNAs chiefly due to the altered SIN3: histone deacetylase chromatin remodeling complexes (26). Since *BRMS1* expression could induce various alterations at the molecular (transcriptome and proteome) levels and it is capable of

inducing different phenotypic alterations like changing cyto-architecture (cell topography and ultrastructure), up-regulation of that may have undesirable effects (up-regulation associated cytotoxicity) on some cell types, like mesenchymal cells or endothelial cells. Considering such extensive alterations, specific expression of *BRMS1* in metastatic cells is required (27). We found that re-expression of *BRMS1* in the context of an expeditiously designed gene delivery vehicle may decline the ability of migration and invasion of metastatic adeno-carcinoma cells. This effect could, in turn, be due to the *BRMS1* function as a cellular invasion and migration inhibitory molecule. Stably *BRMS1*-transfected MDA-MB231 cell line had previously been shown to form significantly fewer metastases in all tested organs. Upon direct injection into the vasculature, fewer *BRMS1*-expressing cells attained to lungs or bone compared to the non-expressing *BRMS1* MDA-MB231 cells (17, 28). qRT-PCR analysis revealed that transfected MDA-MB231 expressed higher level of *BRMS1* compared to untreated MDA-MB231 cells. As a result, these metastatic cells have much less migratory and invasive behavior in comparison with parental cells. In concordance with the previous studies, our results revealed that *BRMS1* could significantly prevent *in vitro* migration and invasion of the human breast carcinoma cell lines (29). These unique properties of *BRMS1* gene have convinced us to employ it as an exogenous gene to prevent the invasive behavior of metastatic breast cancer cell lines. Although *BRMS1* gene could exert its anti-metastatic effects within the target cells, designing a gene delivery construct capable of cell-specific expression of this gene remains obscure.

Expression levels of *miR-200* family were evaluated in the non-metastatic and metastatic breast cancer cell lines, to unveil their expression variation in the context of the cells with metastatic behavior. Similar to the research accomplished by Burk et al. (30), we demonstrated remarkable decrease of expressing *miR-200* family members in metastatic cancer cells compared to non-metastatic cells (31), while expression of *ZEB1* and *ZEB2* genes were increased. *miR-200* family members are among the critical regulators of EMT signified by decreased expressions in metastatic cells. They target gene expression of the transcriptional repressor of *E-cadherin* (*ZEB* factors) and prevent their expressions. Since *ZEB1* and *ZEB2* possess *miR-200* family binding sites, the latter recognizes their binding sites in 3′UTR of *ZEB1* and *ZEB2* mRNA and in turn degrades mRNA molecules or prevents their translations. Our results confirmed that low levels of *miR-200* family expression lead to high levels of ZEB expression. These observations could be construed as the presence of a feedback loop between ZEB and *miR-200* family members (32). However, it should be underscored that expression level of *miR-200a* is higher than the other microRNA family members in the metastatic cell line. In agreement with the previous reports, we indicated that expression of *ZEB2* in MDA-MB231 is less increased compared to *ZEB1*. It could be rooted in the fact that *ZEB2* is the functional downstream target of *miR-200a* and higher expression of *miR-200a* caused lower expression of *ZEB2* gene (33, 34). The observed differential expression profiles of *miR-200b*, *miR-200c*, *miR-141 and miR-429* brings about the possibility of using their MREs to restrict the expression of exogenous genes (like *BRMS1*) within the metastatic breast cancer cells and its expression in healthy tissue-derived cells. Therefore, including the MREs of these microRNAs at 3′UTR of an anti-metastatic gene would lead to cell-specific expression of the target gene within the metastatic breast cancer cell lines.

To confer cell type-specific expression of *BRMS1* gene under regulation of *miR-200* family MREs, designing a novel gene delivery construct seems to be vitally important. The saturation effect, spatial hindrance and in appropriate distance between MREs are among the challenges ahead of building efficient MRE regulated gene therapy constructs. In order to circumvent these snags, we used a portion of *ZEB1* 3′UTR which did not harbor any MRE for *miR-200a*. The performed luciferase assays revealed that MREs of *miR-200b*, *miR-200c*, *miR-141* and *miR-429* are capable to suppress expression of accompanying exogenous genes in non-metastatic breast cells without significantly compromising their expressions in the metastatic breast cancer cells. These outcomes verify the efficiency of selected *ZEB1* 3′UTR region to designa MRE regulated expression construct.

This fact suggests that these MREs could be amenable regulators for therapeutic targeting of metastatic breast cells to express *BRMS1*. Our results confirmed the results of other research groups who investigated the MRE-based strategy of gene therapy for several types of malignancies including osteosarcoma (35), bladder cancer (36), uveal melanoma (37), lung (38) and prostate cancers (39). Their results suggested the possibility and effectiveness of using MREs that were down-regulated in cancer cells. It should also be pointed out that we used CMV promoter to construct the gene delivery plasmid. Potency of the cancer-specific promoters (which is used in transcriptional targeting) for driving expression of the exogenous gene is much lower than the CMV promoter. This would lead to the ineffective therapeutic influences of these vectors. Thus, using CMV promoter (potent viral promoter) along with MREs (using post-transcriptional regulation strategy for selective expression) in 3′UTR of the therapeutic gene could simultaneously confer potency and selectivity (38).

Conclusion

It could be proposed that an efficiently designed gene delivery plasmid containing both MREs and *BRMS1* gene could be a hopeful option for gene therapy against metastatic breast cancer and worthy to perform further clinical trials for metastatic cancer therapy. Such construct could provide us with the cell-specific expression of desired exogenous genes, which in turn could minimize the accompanying side-effects of the intended gene therapy.

Acknowledgements

The authors wish to thank Tarbiat Modares University (Tehran, Iran) and the Biotechnology Committee of Tarbiat Modares University for their financial support. The authors declare no conflict of interest.

Authors' Contributions

S.F., M.F.M., M.E., Z.S.H.; Contributed to conception and design. S.F., Z.S.H.; Contributed to all experimental work, data and statistical analysis and interpretation of data. M.F.M., M.E.; Were responsible for overall supervision. S.F.; Drafted the manuscript, which was revised by M.F.M. M.E., Z.S.H. All authors read and approved the final manuscript.

References

1. Catalano V, Turdo A, Di Franco S, Dieli F, Todaro M, Stassi G. Tumor and its microenvironment: a synergistic interplay. Semin Cancer Biol. 2013; 23(6 Pt B): 522-532.
2. Merlin S, Follenzi A. Transcriptional targeting and MicroRNA regulation of lentiviral vectors. Mol Ther Methods Clin Dev. 2019; 12: 223-232.
3. Zhang H, Li Y, Lai M. The microRNA network and tumor metastasis. Oncogene. 2010; 29(7): 937-948.
4. Dhungel B, Ramlogan-Steel CA, Steel JC. MicroRNA-regulated gene delivery systems for research and therapeutic purposes. Molecules. 2018; 23(7). pii: E1500.
5. Tsai JH, Yang J. Epithelial-mesenchymal plasticity in carcinoma metastasis. Genes Dev. 2013; 27(20): 2192-2206.
6. Lamouille S, Xu J, Derynck R. Molecular mechanisms of epithelial-mesenchymal transition. Nat Rev Mol Cell Biol. 2014;15(3):178-196.
7. Bullock MD, Sayan AE, Packham GK, Mirnezami AH. MicroRNAs: critical regulators of epithelial to mesenchymal (EMT) and mesenchymal to epithelial transition (MET) in cancer progression. Biol Cell. 2012; 104(1): 3-12.
8. Yao W, Guo G, Zhang Q, Fan L, Wu N, Bo Y. The application of multiple miRNA response elements enables oncolytic adenoviruses to possess specificity to glioma cells. Virology. 2014; 458-459: 69-82.
9. Liu J, Ma L, Li C, Zhang Z, Yang G, Zhang W. Tumor-targeting TRAIL expression mediated by miRNA response elements suppressed growth of uveal melanoma cells. Mol Oncol. 2013; 7(6): 1043-1055.
10. Smith SC, Theodorescu D. Learning therapeutic lessons from metastasis suppressor proteins. Nat Rev Cancer. 2009; 9(4): 253-264.
11. Kodura MA, Souchelnytskyi S. Breast carcinoma metastasis suppressor gene 1 (BRMS1): update on its role as the suppressor of cancer metastases. Cancer Metastasis Rev. 2015; 34(4): 611-618.
12. Dou J, Zhou Y, Liu X, Qiao X, Yang X, Xie W, et al. BRMS1 participates in regulating cell sensitivity to DNAinterstrand crosslink damage by interacting with FANCI. Oncol Rep. 2019; 41(1): 552-558.
13. Lee JH, Welch DR. Suppression of metastasis in human breast carcinoma MDA-MB-435 cells after transfection with the metastasis suppressor gene, KiSS-1. Cancer Res. 1997; 57(12): 2384-2387.
14. Ozturk S, Papageorgis P, Wong CK, Lambert AW, Abdolmaleky HM, Thiagalingam A, et al. SDPR functions as a metastasis suppressor in breast cancer by promoting apoptosis. Proc Natl Acad Sci USA. 2016; 113(3): 638-643.
15. Edmonds MD, Hurst DR, Welch DR. Linking metastasis suppression with metastamiR regulation. Cell Cycle. 2009; 8(17): 2673-2675.
16. Hurst DR, Welch DR. Unraveling the enigmatic complexities of BRMS1-mediated metastasis suppression. FEBS Lett. 2011; 585(20): 3185-3190.
17. Phadke PA, Vaidya KS, Nash KT, Hurst DR, Welch DR. BRMS1 suppresses breast cancer experimental metastasis to multiple organs by inhibiting several steps of the metastatic process. Am J Pathol. 2008; 172(3): 809-817.
18. Davalos V, Moutinho C, Villanueva A, Boque R, Silva P, Carneiro F, et al. Dynamic epigenetic regulation of the microRNA-200 family mediates epithelial and mesenchymal transitions in human tumorigenesis. Oncogene. 2012; 31(16): 2062-2074.
19. Shi M, Liu D, Duan H, Shen B, Guo N. Metastasis-related miRNAs, active players in breast cancer invasion, and metastasis. Cancer Metastasis Rev. 2010; 29(4): 785-799.
20. Farokhimanesh S, Rahbarizadeh F, Rasaee MJ, Kamali A, Mashkani B. Hybrid promoters directed tBid gene expression to breast cancer cells by transcriptional targeting. Biotechnol Prog. 2010; 26(2): 505-511.
21. Mei P, Bai J, Shi M, Liu Q, Li Z, Fan Y, et al. BRMS1 suppresses glioma progression by regulating invasion, migration and adhesion of glioma cells. PLoS One. 2014; 9(5): e98544.
22. Yang J, Zhang B, Lin Y, Yang Y, Liu X, Lu F. Breast cancer metastasis suppressor 1 inhibits SDF-1α-induced migration of non-small cell lung cancer by decreasing CXCR4 expression. Cancer Lett. 2008; 269(1): 46-56.
23. Zhang Y, Guan J, Sun Y, Chai J, Zou T, Gong W, et al. Effect of BRMS1 on tumorigenicity and metastasis of human rectal cancer. Cell Biochem Biophys. 2014; 70(1): 505-509.
24. Zhang S, LIN QD, Di W. Suppression of human ovarian carcinoma metastasis by the metastasis-suppressor gene, BRMS1. Int J Gynecol Cancer. 2006; 16(2): 522-531.
25. Farokhimanesh S, Forouzandeh Moghadam M, Ebrahimi M. Metastasis inhibition by BRMS1 and miR-31 replacement therapy in claudin-low cell lines. Iran J Basic Med Sci. 2020; 23(2): 264-270.
26. Hurst DR. Metastasis suppression by BRMS1 associated with SIN3 chromatin remodeling complexes. Cancer Metastasis Rev. 2012; 31(3-4): 641-651.
27. Wu Y, McEwen GD, Harihar S, Baker SM, DeWald DB, Zhou A. BRMS1 expression alters the ultrastructural, biomechanical and biochemical properties of MDA-MB-435 human breast carcinoma cells: an AFM and Raman microspectroscopy study. Cancer Lett. 2010; 293(1): 82-91.
28. Marino N, Collins JW, Shen C, Caplen NJ, Merchant AS, Gökmen-Polar Y, et al. Identification and validation of genes with expression patterns inverse to multiple metastasis suppressor genes in breast cancer cell lines. Clin Exp Metastasis. 2014; 31(7): 771-786.
29. Zhang Y, Ye L, Tan Y, Sun P, Ji K, Jiang WG. Expression of breast cancer metastasis suppressor-1, BRMS-1, in human breast cancer and the biological impact of BRMS-1 on the migration of breast cancer cells. Anticancer Res. 2014; 34(3): 1417-1426.
30. Burk U, Schubert J, Wellner U, Schmalhofer O, Vincan E, Spaderna S, et al. A reciprocal repression between ZEB1 and members of the miR-200 family promotes EMT and invasion in cancer cells. EMBO Rep. 2008; 9(6): 582-589.
31. Hill L, Browne G, Tulchinsky E. ZEB/miR-200 feedback loop: at the crossroads of signal transduction in cancer. Int J Cancer. 2013; 132(4): 745-754.
32. Cursons J, Pillman KA, Scheer KG, Gregory PA, Foroutan M, Hediyeh-Zadeh S, et al. Combinatorial targeting by MicroRNAs co-ordinatespost-transcriptional control of EMT. Cell

Syst. 2018; 7(1): 77-91. e7.
33. Korpal M, Lee ES, Hu G, Kang Y. The miR-200 family inhibits epithelial-mesenchymal transition and cancer cell migration by direct targeting of E-cadherin transcriptional repressors ZEB1 and ZEB2. J Biol Chem. 2008; 283(22): 14910-14914.
34. Fardi M, Alivand M, Baradaran B, Farshdousti Hagh M, Solali S. The crucial role of ZEB2: from development to epithelial-to-mesenchymal transition and cancer complexity. J Cell Physio. 2019. (ahead of print).
35. Xiao F, Chen J, Lian C, Han P, Zhang C. Tumor necrosis factor-related apoptosis-inducing ligand induces cytotoxicity specific to osteosarcoma by microRNA response elements. Mol Med Rep. 2015; 11(1): 739-745.
36. Zhao Y, Li Y, Wang L, Yang H, Wang Q, Qi H, et al. microRNA response elements-regulated TRAIL expression shows specific survival-suppressing activity on bladder cancer. J Exp Clin Cancer Res. 2013; 32: 10.
37. Liu J, Ma L, Li C, Zhang Z, Yang G, Zhang W. Tumor-targeting TRAIL expression mediated by miRNA response elements suppressed growth of uveal melanoma cells. Mol Oncol. 2013; 7(6): 1043-1055.
38. Wu G, Ji Z, Li H, Lei Y, Jin X, Yu Y, et al. Selective TRAIL-induced cytotoxicity to lung cancer cells mediated by miRNA response elements. Cell Biochem Funct. 2014; 32(7): 547-556.
39. Huo W, Jin N, Fan L, Wang W. MiRNA regulation of TRAIL expression exerts selective cytotoxicity to prostate carcinoma cells. Mol Cell Biochem. 2014; 388(1-2): 123-133.

Original Article

Bibliometric Analysis of Global Circular RNA Research Trends from 2007 to 2018

Ran Wu, M.D.[1#], Fei Guo, B.M.[2#], Chen Wang, Ph.D.[3#], Baohua Qian, Ph.D.[2], Fuming Shen, Ph.D.[1], Fang Huang, M.D.[1*], Weidong Xu, Ph.D.[3*]

1. Department of Pharmacy, Shanghai Tenth People's Hospital, Tongji University School of Medicine, Shanghai, China
2. Department of Transfusion Medicine, Changhai Hospital, Second Military Medical University, Shanghai, China
3. Department of Orthopaedics, Changhai Hospital, Second Military Medical University, Shanghai, China

 # The first three authors contributed equally to this work.

**Corresponding Addresses: Department of Pharmacy, Shanghai Tenth People's Hospital, Tongji University School of Medicine, Shanghai, China*
Department of Orthopaedics, Changhai Hospital, Second Military Medical University, Shanghai, China
Emails: hazel_huang@126.com, xuwdshanghaichyy@163.com

Received: 06/September/2019, Accepted: 08/February/2020

Abstract

Objective: Circular RNA (circRNA) is of significant interest in genetic research. The aim of this study was to assess global trends in circRNA research production in order to shed new light on future research frontiers.

Materials and Methods: In this retrospective study, we conducted a literature search using the Web of Science Core Collection (WoSCC) database on March 21, 2019 to retrieve publications from 2007 to 2018. Excel 2013, CiteSpace V, and VOSviewer were used to evaluate bibliometric features that included publication output, countries/regions, institutions, journals, citation frequency, H-index, and research hotspots.

Results: Global cumulative publication output on circRNA consisted of 998 papers with a total citation of 28 595 during 2007-2018. China, the US, and Germany were the most prolific countries. China ranked first in H-index (60 times) and citations (13 333 times). The most productive institution was Nanjing Medical University with 73 papers. Biochemical and Biophysical Research Communications (impact factor [IF]2017:2.559) ranked first among journals in the number of publications (64 papers). The keywords shifted from "sequence", "intron", and "splice-site" to "transcriptome", "microRNA sponge", "exon circularization", and "circRNA biogenesis" overtime. The burst keywords "transcriptome", "microRNA sponge", "exon circularization", and "circRNA biogenesis" were the latest frontiers by 2018.

Conclusion: This is a relatively novel bibliometric analysis to inspect research related to circRNA. The results show that publications have continuously increased in the past decade. China, the US, and Germany were the leading countries/regions in terms of quantity. Recent studies on topics related to circRNA biogenesis and function should be closely followed in this field.

Keywords: Bibliometric, Circular RNA, Citation, CiteSpace, VOSviewer

Cell Journal(Yakhteh), Vol 23, No 2, July 2021, Pages: 238-246

Citation: **Wu R, Guo F, Wang Ch, Qian B, Shen F, Huang F, Xu W. Bibliometric analysis of global circular RNA research trends from 2007 to 2018. Cell J. 2021; 23(2): 238-246. doi: 10.22074/cellj.2021.7143.**

Introduction

The concept of "circular RNA (circRNA)" was proposed by Sanger et al. (1) when they reported that viroids are pathogenic to certain higher plants with single-stranded covalently closed circRNA molecules. circRNAs mostly stem from either exons (2, 3) or introns (4, 5). The covalently closed loop is characterized by neither 5′-3′ polarity nor a polyadenylated tail (6), and this distinguishes circRNAs from linear RNAs. Meanwhile, circRNAs are more stable, even when treated with RNase R (7). Researchers initially believed that circRNAs were by-products in the aberrant splicing process, and had little role in biological processes (2). With the rapid advances of high-throughput RNA sequencing (RNA-seq) and bioinformatics, numerous endogenous, diverse, widespread and conserved circRNAs have been identified (8-10). Therefore, these molecules caused a resurgence in interest by researchers. Of particular note, some studies have shown that circRNAs could act as microRNA (miRNA) sponges and regulate line RNA transcription and protein production to modulate gene expression (11-13).

Recent evidences indicated that circRNA plays a role in aging (9, 14) and tissue development (15). circRNAs might be involved in neurological disorders (16), atherosclerotic vascular disease risk (17), Alzheimer's disease (18), and cancer (19). Thus, they might be potentially valuable in disease diagnosis, prognosis, and precise therapy (20, 21). Simultaneously, database setups for circRNA in the last few years include circBase, CIRCpediav2, and CircInteractome (TableS1, See Supplementary Online Information at www.celljournal.org). These databases make it more convenient for researchers to access and study circRNA, and facilitates progress in this field.

Although researches related to circRNA have flourished

in recent years, there have been limited attempts to systematically explore the development of scientific productivity in this area. To our knowledge, there are a few reports on research activity in circRNA that have been published internationally. The focus of bibliometrics is on literature systems and literature metrology characteristics; they statistically and mathematically analyse written publications such as books and periodicals (22). This is a reliable method to analyse literature in the field of science and characterize the tendency of research activity over time. Bibliometrics has contributed to research trends in cardiovascular diseases (23), gastrointestinal diseases (24), and diabetes (25).

The aims of present study were to systematically evaluate the international publication productivity of circRNA research using the Web of Science (WoS) from 2007 to 2018; analyse the most productive countries/institutions/journals; and measure geographic and time distribution of literature that pertained to circRNA.

Materials and Methods

Patient and public involvement

In this retrospective study, no patient or public involvement was available.

Sources of data and the search strategy

We searched literature in the online version of Science Citation Index-Expanded (SCIE), Web of Science Core Collection (WoSCC), and Essential Science Indicator (ESI) databases on March 21, 2019. We downloaded the data from a public database as secondary data, which did not involve ethical considerations. Thus, ethical approval was not applicable in this situation.

We used the following search strategy: (TI=("circRNA*") OR TI=("circular RNA*") OR TI=("circRNA_*") OR TI=("circular noncoding RNA*") OR TI=("circular non coding RNA*") OR TI=("circular untranslated RNA*") OR TI=("circular non translated RNA*") OR TI=("circular non protein coding RNA*") OR TI=("circular ncRNA*")) AND publishing year=(2007-2018) AND Language=(English). Refining for certain document types: the document types were selected as "article" or "review", and we only considered peer-reviewed documents. We chose 2007 as the start check point because it articles in this field began to emerge continuously in 2007.

Data collection

WoSCC was used to analyse the characteristics of the publications, such as annual publications, countries/regions, institutions, journal sources, citation frequency, impact factor (IF), weighted IF (IF^2), H-index, etc. The H-index, citation frequency, IF, and IF^2 were used to qualitatively measure the scientific research performance. IFs were obtained based on the Journal Citation Reports (JCR) 2017 and IF^2 was calculated according to Rasim et al. (26).

The H-index, created by Hirsch (27) in 2005, can more perfectly reveal a country's or individual's achievement. This index takes both the quantity of published papers and the citation frequency into account, which means that H papers published by a researcher/institution/country received at least H citations. A higher H-index shows the larger influential power.

All data were gathered and verified by two authors independently (Ran Wu and Fei Guo). The data in "txt" form were downloaded from WoS and imported into Microsoft Excel 2013, CiteSpace V (64 bits), and VOSviewer (Version1.6.6, Leiden University, Leiden, The Netherlands).

Statistical analysis

A fitting mathematical model that used Microsoft Excel 2013 was employed to analyse the temporal tendency of the publications. The model: $f(x)=ax^4+bx^3+cx^2+dx+e$ was applied to model the cumulative number of publications and present a prediction of the future tendency of circRNA outputs. The symbol x represented the year, and $f(x)$ represented the annual number of publications by year.

The world map of publication distribution was generated by GunnMap 2 (http://www.lert.co.nz/map/). GraphPad Prism version 6.01 (San Diego, CA, USA) was employed to analyse Pearson's correlation between publication number and gross domestic product (GDP) or the population number. $P<0.05$ were considered to be statistically significant. VOSviewer was used for the bibliometric analysis and visualization of the literature (28). In this study, it was used to analyse the collaboration between countries/regions and institutions. Network visualization of journals' citation analysis was also derived through VOSviewer. CiteSpace V was used to construct a knowledge map of journals and keywords, and to obtain burst keywords that had the strongest citation.

Results

Distribution of countries/regions according to circular RNA

A total of 998 studies fulfilled the search criteria (Fig.1A, Fig.S1, See Supplementary Online Information at www.celljournal.org), of which the majority were articles (868, 87.0%), followed by reviews (130, 13%). Figure 1B shows the geographical distribution of publications by individual countries/regions. There were a total of 46 countries/regions. Table 1 lists the top 10 most productive countries/regions; China, with 729 publications ranked first, followed by the US (181), Germany (45), Denmark (23), and Canada (21). After adjustments for GDP and population, we noted that Demark had the most publications per GDP (0.071) and the most publications per million people (3.986). There was an excellent correlation between publication numbers and population ($r=0.996$, $P<0.0001$) (Fig.S2A, See Supplementary Online Information at

www.celljournal.org). No correlation was found between publication numbers and GDP (r=0.606, P=0.063) (Fig. S2B, See Supplementary Online Information at www.celljournal.org). The VOSviewer result showed extensive collaborations between countries/regions (Fig.1C).

Distribution of institutions that published research related to circular RNA

A total of 919 institutions published researches related to circRNA (Table S2, See Supplementary Online Information at www.celljournal.org). The most productive institution was Nanjing Medical University, which published a total of 73 papers. The Chinese Academy of Sciences and Fudan University tied for second with 41 papers. Publications from the top 10 institutions accounted for 34.47% of all literature on circRNA. Figure 1D shows the collaborations between institutions with at least five publications.

Table 1: Top 10 most prolific countries in the field of circRNA research

Rank	Country	Number	Number per GDP* USD (billion)	Number per million population
1	China	729	0.060	0.526
2	USA	181	0.009	0.556
3	Germany	45	0.012	0.544
4	Denmark	23	0.071	3.986
5	Canada	21	0.013	0.572
6	Australia	20	0.015	0.813
7	England	14	0.005	0.212
8	Japan	14	0.003	0.110
9	Italy	13	0.007	0.215
10	France	12	0.005	0.179

*circRNA; Circular RNA and GDP; Gross domestic product.

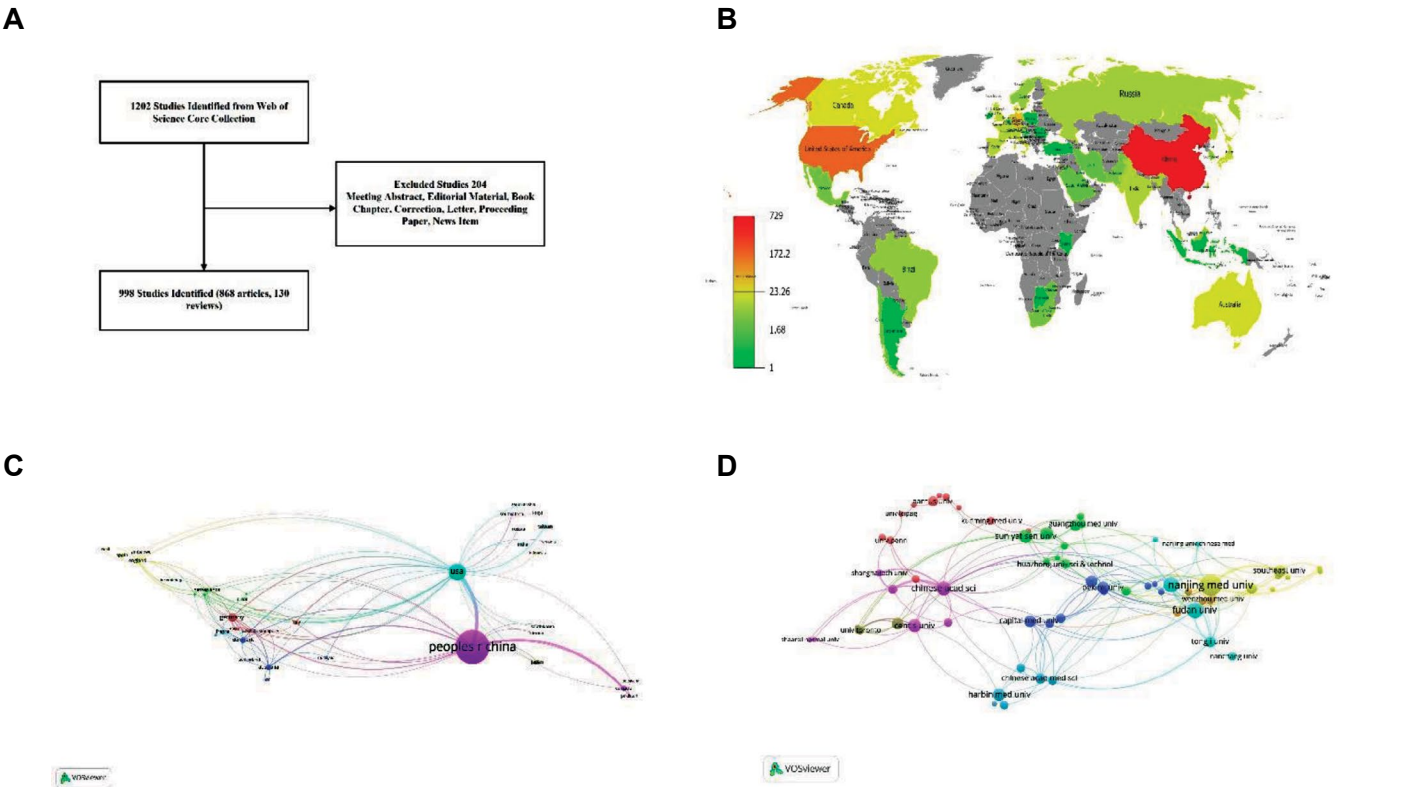

Fig.1: Publication distribution and collaboration analysis. **A.** Flowchart of included circular RNA (circRNA) research, **B.** Geographical distribution of publications related to circRNA research, **C.** Collaboration networks of countries/regions with at least one publication of circRNA research, and **D.** Collaboration networks of institutions with at least five publications of circRNA research.

Publication outputs and growth prediction

The annual publication numbers and accumulated publications are presented in Figure 2A. The annual publications were stably low from 2007 to 2013, and remarkable growth was observed since 2014. In total, the publications related to circRNA consistently increased during the last decade.

As shown in Figure 2B, there was a significant correlation between the publication year and annual number of circRNA publications (R^2=0.997). Worldwide, this was estimated to reach 955 publications in 2019.

Distribution of published journals and funding agencies that focused on circular RNA

The 998 publications on circRNA research appeared in 331 journals (Table S3, See Supplementary Online Information at www.celljournal.org). Table 2 shows the top 20 prolific journals. The Biochemical and Biophysical Research Communications journal (IF 2017: 2.559, IF^2 2017: 7.321) published the most literature related to circRNA research (64 articles, 6.413%), followed by Cellular Physiology and Biochemistry (IF 2017: NA, IF^2 2017: 14.373, 37 articles, 3.707%), Oncotarget (IF 2017: NA, IF^2 2017: 5.503, 36 articles, 3.607%), and Scientific Reports (IF 2017: 4.122, IF^2 2017: 3.706, 35 articles, 3.507%). There was one review in Nature Review Genetics (IF 2017: 41.465), which had the highest IF among the 331 journals. Among the top 20 prolific journals, Molecular Cancer had the highest IF^2 (93.945).

Figure 2C presents the dual-map overlay for the journals. The citing journal map is shown on the left and the cited journal map is displayed on the right. The disciplines covered by journals are marked in the label. Citation links that start from the journals on the left and end with those on the right are presented with lines. The map shows one main citation path, which indicates that most publications appeared in molecular, biology, and immunology journals. These publications were mostly cited from the molecular, biology, and genetics fields.

Table 2: Top 20 journals with most publications related to circRNA research

Rank	Journal	Count	Percent	IF 2017	IF^2 2017
1	Biochemical and Biophysical Research Communications	64	6.413	2.559	7.321
2	Cellular Physiology and Biochemistry	37	3.707	5.5	14.373
3	Oncotarget	36	3.607	NA*	5.503
4	Scientific Reports	35	3.507	4.122	3.706
5	Advances in Experimental Medicine and Biology	28	2.806	1.76	6.024
6	Circular RNAs Biogenesis and Functions	27	2.705	NA*	NA*
7	RNA Biology	23	2.305	5.216	55.590
8	PLOS One	20	2.004	2.766	1.655
9	Nucleic Acids Research	16	1.603	11.561	62.190
10	Biomedicine Pharmacotherapy	15	1.503	3.457	13.020
11	Molecular Cancer	14	1.403	7.776	93.945
12	Cancer Letters	13	1.303	6.491	32.335
13	Gene	13	1.303	2.498	13.970
14	International Journal of Clinical and Experimental Pathology	12	1.202	1.396	4.509
15	BMC Genomics	11	1.102	3.73	17.757
16	Epigenomics	11	1.102	4.979	22.944
17	European Review for Medical and Pharmacological Sciences	11	1.102	2.387	4.569
18	Oncology Letters	11	1.102	1.664	5.372
19	Aging US	10	1.002	5.179	36.308
20	Molecular Therapy Nucleic Acids	10	1.002	5.66	42.156

*circRNA; Circular RNA, NA; Not available, IF; Impact factor, and IF^2; Weighted impact factor.

Totally, 998 publications on circRNA research were funded by 1241 funding agencies (Table S4, See Supplementary Online Information at www.celljournal.org). The National Natural Science Foundation of China supported 455 publications, which accounted for nearly half of all the literature in this case (45.5%). The top 10 funding agencies that supported circRNA research are presented in Figure 2D.

Citation and H-index analysis

Based on our analysis, the citation frequency number of all articles associated with circRNA was 28 595 by 2018. In terms of citations, China ranked first with 13 333 citations, followed by the US with 8460, Germany with 4798, Israel with 1615, and Denmark with 1344. The citation frequency per paper was 28.65 times, and Argentina had the highest frequency per paper (385), followed by Israel (179.44) and Germany (106.62) (Table S5, See Supplementary Online Information at www.celljournal.org). Figure 3A shows the citations and H-index results of the top five productive countries/regions. China, with an H-index value of 60, ranked first.

Citations analysis was conducted within all 331 journals. Our results demonstrated that Molecular Cell had the highest citation frequency (1908), followed by Nature (1519), and Scientific Reports (1464) (Fig.3B).

Hotspots of studies on circular RNA

The total citations of the top 10 most cited publications varied from 386 to 1519 (Table 3). The IF numbers of the listed papers ranged from 2.766 to 41.577. The article that achieved the most citations (1519 times) was published by Memczak et al. (8).

Keywords used in the 998 papers were analysed with CiteSpace V. Totally, we extracted 202 keywords with 648 links, which were defined as the top 50 of the most frequent items from each year with the title, abstract, and keywords field under the condition of the CiteSpace V default setting (Fig. S3, See Supplementary Online Information at www.celljournal.org). The top 20 keywords with strongest citation bursts are shown in Figure 3C. According to the timeline, keywords shifted from "sequence", "intron", and "splice-site" to "transcriptome", "microRNA sponge", "exon circularization", and "circRNA biogenesis. The strongest ones included "exon circularization", "microRNA sponge", "mouse testi", "transcript", and "circRNA biogenesis".

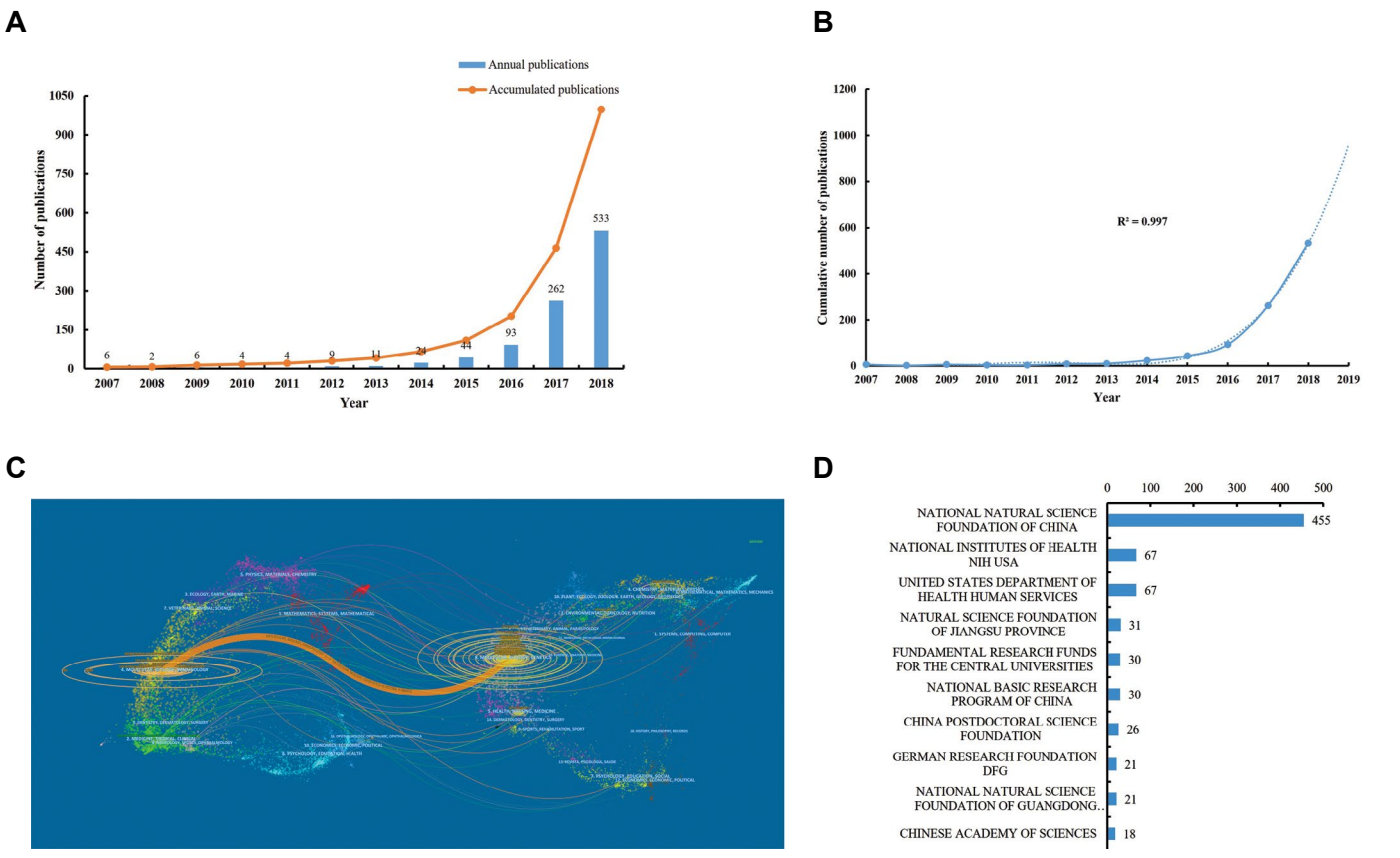

Fig.2: Publication output and growth prediction. **A.** Annual and accumulated publications of circular RNA (circRNA) research from 2007 to 2018, **B.** The model fitting curve of circRNA publication growth, **C.** Dual-map overlay of journals. There was one main citation path coloured with orange. Publications about circRNA research in molecular, biology, and immunology journals mainly cited journals in the molecular, biology, and genetics areas, and **D.** The top 10 funding agencies that supported circRNA research.

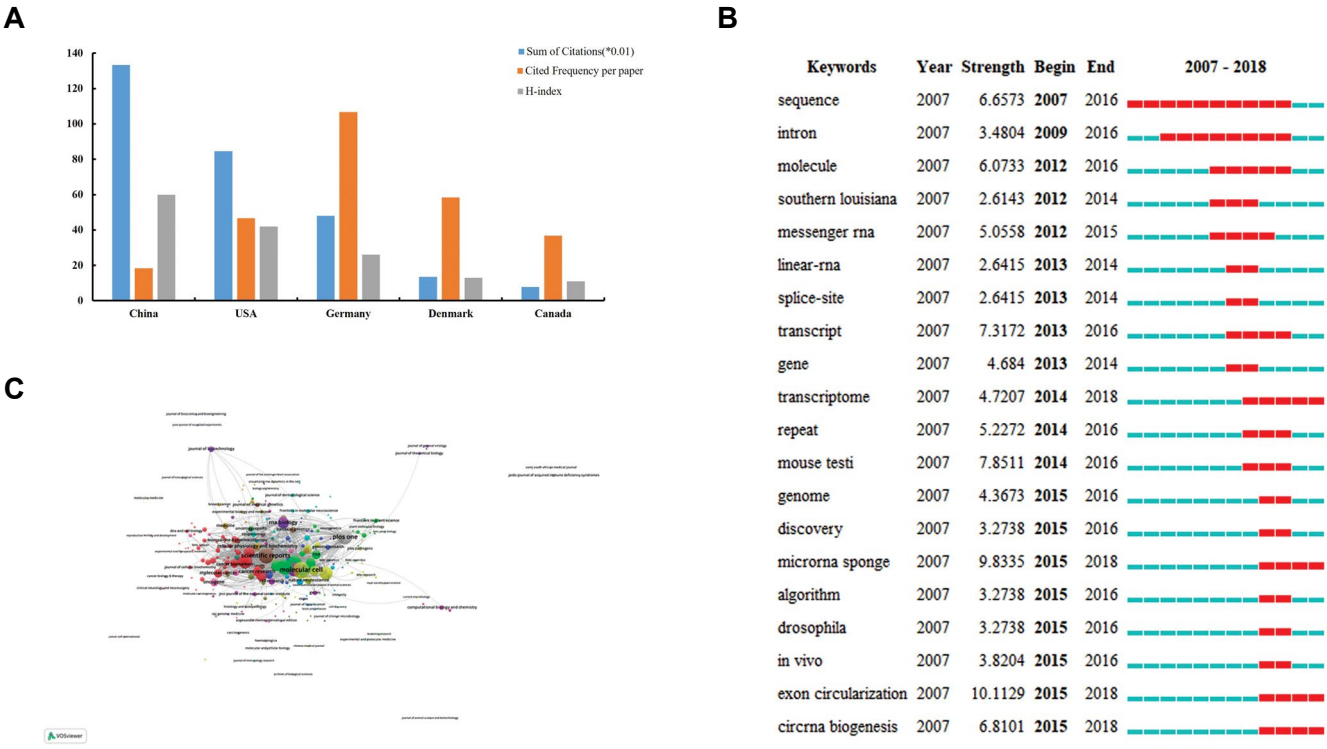

Fig.3: Quality analysis of countries/regions and journals. **A.** The distribution of citation (x0.01), cited frequency per paper, and H-index in the top five countries/regions, **B.** Network visualization of journal citation analysis. The larger spot indicates a higher citation frequency, and **C.** Top 20 keywords with the strongest citation bursts on circular RNA (circRNA) research published during 2007 and 2018.

Table 3: Top 10 studies with the most citation frequencies related to circular RNA research

Title	Journal	First author	Year	Cited by
Circular RNAs are a Large Class of Animal RNAs with Regulatory Potency (8)	Nature	Memczak, Sebastian	2013	1519
Circular RNAs are Abundant, Conserved, and Associated with ALU Repeats (29)	RNA-A Publication of the RNA Society	Jeck, William R.	2013	817
Circular RNAs are the Predominant Transcript Isoform from Hundreds of Human Genes in Diverse Cell Types (12)	PLOS ONE	Salzman, Julia	2012	587
circRNA Biogenesis Competes with Pre-mRNA Splicing (30)	Molecular Cell	Ashwal-Fluss, Reut	2014	522
Detecting and Characterizing Circular RNAs (31)	Nature Biotechnology	Jeck, William R.	2014	484
Exon-intron Circular RNAs Regulate Transcription in the Nucleus (32)	Nature Structural& Molecular Biology	Li, Zhaoyong	2015	465
Circular Intronic Long Noncoding RNAs (33)	Molecular Cell	Zhang, Yang	2013	457
Cell-Type Specific Features of Circular RNA Expression (34)	PLOS Genetics	Salzman, Julia	2013	430
Expanded Identification and Characterization of Mammalian Circular RNAs (35)	Genome Biology	Guo, Junjie U.	2014	396
Expression of Linear and Novel Circular Forms of an INK4/ARF-Associated Noncoding RNA Correlates with Atherosclerosis Risk (36)	PLOS Genetics	Burd, Christin E.	2010	386

Discussion

Researchers previously focused on RNA with protein coding functions derived from DNA. In-depth studies and advanced technology make it clear that there are abundant and widespread noncoding RNAs (ncRNAs), which include miRNA, lncRNA, and circRNA. These RNAs could play significant roles in the life process (11, 21, 22). circRNA is an ncRNA, which was believed to be a by-product and have little function (2, 3). However, recent advances have implied that circRNA might participate in both physiological and pathological processes (9, 14-19). This study aimed to quantitatively and qualitatively evaluate the bibliometric characteristics of circRNA research, and to inspect the future research frontier. Publications, to some extent, could be considered a judgment of development within a certain research field.

Researches related to circRNA have rapidly developed. To the best of our knowledge, this bibliometric analysis is the first attempt in this field. According to the results, the publication year can be separated into two stages. The first stage (2007-2013) had a slow increase in publications and was the initial phase of circRNA research. The second stage (2014-2018) had a sharp growth trend and was the flourishing phase of cicrRNA research. The number of publications in last few years exceeded the accumulative numbers in the early stage. With rapid and substantial progress in this field, the whole world was expected to maintain publishing papers about circRNA in a productive way. According to the prediction curve, more literature will be published in the circRNA research field in the future.

China, the US, and Germany were the leading countries in quantity (total publication number). After standardizing for GDP and population, Denmark ranked first with 0.071 publications per GDP and 3.986 publications per million people. Although Demark ranked fourth with 23 publications, we believed that a highly developed economy and smaller population compared to China and the US placed Denmark first after standardization. GDP and population are relevant to the publication output (37). In the present study, we found no correlation between publication numbers and GDP; however, the population number showed a positive correlation with publication numbers. We employed citations, cited frequency per paper, and H-index to analyse the quality. Among the top five prolific countries/regions, China, with an absolute advantage in publication numbers, scored the highest in both citations and H-index. However, Germany received the largest number of cited frequencies per paper. In terms of collaboration network, far-ranging cooperations were identified worldwide. The strongest cooperation was found between China and the US. Meanwhile, China and the US also had extensive cooperation with other countries/regions, respectively. Generally speaking, international cooperation is a result of cooperation between institutions worldwide (38). However, we found that Chinese institutions tend to collaborate nationally. This may partly explain the large output by China.

Chinese institutions preceded the quantity on circRNA research. The most productive worldwide was Nanjing Medical University. We mentioned that national collaborations were widespread in China. There were over 10 links between the prolific institutions (e.g., Nanjing Medical University, Fudan University, and Shanghai Jiao Tong University) and other institutions. Cooperation facilitates the progress of circRNA research from this perspective. Another interesting finding was that the majority of funding agencies were from China in this field. If one researcher in China successfully applied for major funding, such as the National Natural Science Foundation, and published high-quality articles, he or she might have priority to receive more funding, which becomes a cycle. This could also explain the productivity in China.

In terms of the top 20 prolific journals, Biochemical and Biophysical Research Communications, Cellular Physiology and Biochemistry, Oncotarget, and Scientific Reports were the main journals with over 30 publications. The first one was quantitative (64 publications) but not very qualitative (IF 2017: 2.559). The third one was removed from SCIE in 2018, although there were 36 publications. There were 16 papers in Nucleic Acids Research, of which the IF (11.561) was the highest in the top 20 prolific journal list. IF^2 is a novel and more accurate indicator that assesses journal impact, which considers both the quantity of citations and the quality of cited journals (26). Molecular Cancer, with 14 papers, had the highest IF^2 (93.945) among the top 20 productive journals in circRNA research. In general, future developments that pertain to circRNA would be likely showcased within the top 20 journals.

This study ranked the top 10 cited publications related to circRNA research. The evaluation presented informative insight into the development of popular opinion in the field of circRNA. The number of citations in circRNA varied from 386 to 1519. Undoubtedly, Memczak et al. (8) had a fundamental influence in the circRNA literature. The most influential article, titled "Circular RNAs are a Large Class of Animal RNAs with Regulatory Potency", was published in Nature in 2013 and was cited at least 1519 times. Memcazk et al. (8) provided evidence regarding the regulatory potential of circRNA. The second most frequently cited article by Jeck et al. (29) was published in RNA in 2013. This study reported the involvement of circRNA in control of gene expression.

Keywords assigned in each article or review can make delineation of the topics involved in circRNA research. Burst keywords, which were captured by CiteSpace V in this study, could make a reasonable prediction of research frontiers over time (39). The blue and red lines indicated time intervals and periods of citation bursts, respectively. With advanced technology, the research fields of circRNA transferred from discovery to in-depth mechanism and function, which was in line with the objective law of

research. Below are the top four research frontiers of circRNA research:

i. Transcriptome: To date, circRNA that had been derived from pre-mRNA was primarily identified through high-throughput RNA-seq. It was not until the advanced RNA-seq detecting non-polyadenylated transcriptomes emerged that circRNA was found to be diverse and widespread (8, 10, 12, 29). Thus, transcriptome analysis was of great significance for circRNA identification and research.

ii. miRNA sponge: miRNAs are regulatory RNAs derived from hairpin transcripts. The results of recent studies show that some circRNAs might regulate gene expression at multiple levels (6). Of note, the primary finding was that circRNA could function as a miRNA sponge in the cytoplasm. circRNA competed with mRNA for miRNA biding and then regulated gene expressions (29).

iii. Exon circularization and iv. circRNA biogenesis: The biogenesis of circRNA has been uncovered after in-depth study. For instance, circRNAs are transcribed by RNA polymerase II (30, 40), and this biogenesis is regulated by the *cis*-regulatory elements and trans-acting factors that control splicing (6). Exon circularization is one of the necessary procedures of circRNA formation.

Although this is the first bibliometric study to comprehensively and objectively estimate global trends in circRNA research, there are some limitations. First, the total number of publications differs among the major databases - PubMed, Scopus, and Google Scholar. The use of the WoSCC database could have overlooked relevant publications from analysis. Second, the publications included in this analysis were restricted to the English language. Therefore, non-English papers, which are important, were excluded from the present study. Last but not least, all the searches were conducted over one day (March 21, 2019) to avoid bias; however, the database is constantly updating. Some high-quality publications are still being cited and this information may be omitted. Despite the aforementioned limitations, we believe that the overall results may not have changed.

Conclusion

This study firstly provides a bibliometric analysis on global trends of circRNA research during 2007-2018. Researches in this field have notably increased in recent years and will continue to emerge. Most studies associated with circRNA arose from China, the US, and Germany. China was the leading country with the highest H-index and citations. International cooperation was widely found throughout the world. The most prolific institution, Nanjing Medical University, was from China. Biochemical and Biophysical Research Communications had the most circRNA publications. "Transcriptome", "microRNA sponge", "exon circularization", and "circRNA biogenesis" might be the latest research frontiers that relate to the future for circRNA research.

Acknowledgements

The authors would like to express their particular appreciation to Carl Wang for providing technical support for CiteSpace V and VOSviewer. This study was supported by the National Natural Science Foundation of China (grant numbers: 81672126, 81871751, 81973312, 81971306) and Shanghai Municipal Health and Family Planning Commission Foundation (grant number: 2016ZB0306). The authors declare that they have no conflicts of interest.

Authors' Contributions

W.X., B.Q.; Contributed to the conception of the study. R.W., F.G.; Contributed to the acquisition of the data. R.W., F.G., C.W., F.S.; Contributed to the data analysis. C.W., W.X., F.S., F.H.; Contributed to the data interpretation. All authors read, revised, and approved the final draft.

References

1. Sanger HL, Klotz G, Riesner D, Gross HJ, Kleinschmidt AK. Viroids are single-stranded covalently closed circular RNA molecules existing as highly base-paired rod-like structures. Proc Natl Acad Sci USA. 1976; 73(11): 3852-3856.
2. Nigro JM, Cho KR, Fearon ER, Kern SE, Ruppert JM, Oliner JD, et al. Scrambled exons. Cell. 1991; 64(3): 607-613.
3. Capel B, Swain A, Nicolis S, Hacker A, Walter M, Koopman P, et al. Circular transcripts of the testis-determining gene Sry in adult mouse testis. Cell. 1993; 73(5): 1019-1030.
4. Kopczynski CC, Muskavitch MA. Introns excised from the Delta primary transcript are localized near sites of Delta transcription. J Cell Biol. 1992; 119(3): 503-512.
5. Qian L, Vu MN, Carter M, Wilkinson MF. A spliced intron accumulates as a lariat in the nucleus of T cells. Nucleic Acids Res. 1992; 20(20): 5345-5350.
6. Chen LL. The biogenesis and emerging roles of circular RNAs. Nat Rev Mol Cell Biol. 2016; 17(4): 205-211.
7. Enuka Y, Lauriola M, Feldman ME, Sas-Chen A, Ulitsky I, Yarden Y. Circular RNAs are long-lived and display only minimal early alterations in response to a growth factor. Nucleic Acids Res. 2016; 44(3): 1370-1383.
8. Memczak S, Jens M, Elefsinioti A, Torti F, Krueger J, Rybak A, et al. Circular RNAs are a large class of animal RNAs with regulatory potency. Nature. 2013; 495(7441): 333-338.
9. Westholm JO, Miura P, Olson S, Shenker S, Joseph B, Sanfilippo P, et al. Genome-wide analysis of drosophila circular RNAs reveals their structural and sequence properties and age-dependent neural accumulation. Cell Rep. 2014; 9(5): 1966-1980.
10. Fan X, Zhang X, Wu X, Guo H, Hu Y, Tang F, et al. Single-cell RNA-seq transcriptome analysis of linear and circular RNAs in mouse preimplantation embryos. Genome Biol. 2015; 16(1): 148.
11. Ebert MS, Sharp PA. MicroRNA sponges: progress and possibilities. RNA. 2010; 16(11): 2043-2050.
12. Salzman J, Gawad C, Wang PL, Lacayo N, Brown PO. Circular RNAs are the predominant transcript isoform from hundreds of human genes in diverse cell types. PLoS One. 2012; 7(2): e30733.
13. Chen CY, Sarnow P. Initiation of protein synthesis by the eukaryotic translational apparatus on circular RNAs. Science. 1995; 268(5209): 415-417.
14. Wang YH, Yu XH, Luo SS, Han H. Comprehensive circular RNA profiling reveals that circular RNA100783 is involved in chronic CD28-associated CD8(+)T cell ageing. Immun Ageing. 2015; 12: 17.
15. You X, Vlatkovic I, Babic A, Will T, Epstein I, Tushev G, et al. Neural circular RNAs are derived from synaptic genes and regulated by development and plasticity. Nat Neurosci. 2015; 18(4): 603-610.

16. Floris G, Zhang L, Follesa P, Sun T. Regulatory role of circular RNAs and neurological disorders. Mol Neurobiol. 2017; 54(7): 5156-5165.
17. Holdt LM, Stahringer A, Sass K, Pichler G, Kulak NA, Wilfert W, et al. Circular non-coding RNA ANRIL modulates ribosomal RNA maturation and atherosclerosis in humans. Nat Commun. 2016; 7: 12429.
18. Lukiw WJ. Circular RNA (circRNA) in Alzheimer's disease (AD). Front Genet. 2013; 4: 307.
19. Meng S, Zhou H, Feng Z, Xu Z, Tang Y, Li P, et al. CircRNA: functions and properties of a novel potential biomarker for cancer. Mol Cancer. 2017; 16(1): 94.
20. Zhang Z, Yang T, Xiao J. Circular RNAs: promising biomarkers for human diseases. EBioMedicine. 2018; 34: 267-274.
21. Chen X, Yang T, Wang W, Xi W, Zhang T, Li Q, et al. Circular RNAs in immune responses and immune diseases. Theranostics. 2019; 9(2): 588-607.
22. Miao Y, Xu SY, Chen LS, Liang GY, Pu YP, Yin LH. Trends of long noncoding RNA research from 2007 to 2016: a bibliometric analysis. Oncotarget. 2017; 8(47): 83114-83127.
23. Shuaib W, Khan MS, Shahid H, Valdes EA, Alweis R. Bibliometric analysis of the top 100 cited cardiovascular articles. Am J Cardiol. 2015; 115(7): 972-981.
24. Narotsky D, Green PH, Lebwohl B. Temporal and geographic trends in celiac disease publications: a bibliometric analysis. EurJ Gastroenterol Hepatol. 2012; 24(9): 1071-1077.
25. Geaney F, Scutaru C, Kelly C, Glynn RW, Perry IJ. Type 2 diabetes research yield, 1951-2012: Bibliometrics analysis and density-equalizing mapping. PLoS One. 2015; 10(7): e0133009.
26. Rasim A, Ramiz A, Nigar I. IF2: Impact Factor Weighted by Impact Factor. Emerging Trends and Issues in Scientometrics, Informetrics and Webometrics. 2015. Available from: https://www.researchgate.net/publication/307084605.
27. Hirsch JE. An index to quantify an individual's scientific research output. Proc Natl Acad Sci USA. 2005; 102(46): 16569-16572.
28. van Eck NJ, Waltman L. Software survey: VOSviewer, a computer program for bibliometric mapping. Scientometrics. 2010; 84(2): 523-538.
29. Jeck WR, Sorrentino JA, Wang K, Slevin MK, Burd CE, Liu J, et al. Circular RNAs are abundant, conserved, and associated with ALU repeats. RNA. 2013; 19(2): 141-157.
30. Ashwal-Fluss R, Meyer M, Pamudurti NR, Ivanov A, Bartok O, Hanan M, et al. circRNA biogenesis competes with pre-mRNA splicing. Mol Cell. 2014; 56(1): 55-66.
31. Jeck WR, Sharpless NE. Detecting and characterizing circular RNAs. Nat Biotechnol. 2014; 32(5): 453-461.
32. Li Z, Huang C, Bao C, Chen L, Lin M, Wang X, et al. Exon-intron circular RNAs regulate transcription in the nucleus. Nat Struct Mol Biol. 2015; 22(3): 256-264.
33. Zhang Y, Zhang XO, Chen T, Xiang JF, Yin QF, Xing YH, et al. Circular intronic long noncoding RNAs. Mol Cell. 2013; 51(6): 792-806.
34. Salzman J, Chen RE, Olsen MN, Wang PL, Brown PO. Cell-type specific features of circular RNA expression. PLoS Genet. 2013; 9(9): e1003777.
35. Guo JU, Agarwal V, Guo H, Bartel DP. Expanded identification and characterization of mammalian circular RNAs. Genome Biol. 2014; 15(7): 409.
36. Burd CE, Jeck WR, Liu Y, Sanoff HK, Wang Z, Sharpless NE. Expression of linear and novel circular forms of an INK4/ARF-associated non-coding RNA correlates with atherosclerosis risk. PLoS Genet. 2010; 6(12): e1001233.
37. Meo SA, Usmani AM, Vohra MS, Bukhari IA. Impact of GDP, spending on R&D, number of universities and scientific journals on research publications in pharmacological sciences in Middle East. Eur Rev Med Pharmacol Sci. 2013; 17(20): 2697-2705.
38. Orwat MI, Kempny A, Bauer U, Gatzoulis MA, Baumgartner H, Diller GP. The importance of national and international collaboration in adult congenital heart disease: a network analysis of research output. Int J Cardiol. 2015;195:155-162.
39. Chen C, Dubin R, Kim MC. Emerging trends and new developments in regenerative medicine: a scientometric update (2000 - 2014). Expert Opin Biol Ther. 2014; 14(9): 1295-1317.
40. Starke S, Jost I, Rossbach O, Schneider T, Schreiner S, Hung LH, et al. Exon circularization requires canonical splice signals. Cell Rep. 2015; 10(1): 103-111.

Is There any Alternative Receptor for SARS-CoV-2?

Mahtab Shahriari Felordi, M.Sc.[1], Arash Memarnejadian, Ph.D.[2], Mustapha Najimi, Ph.D.[3]*, Massoud Vosough, M.D., Ph.D.[1]*

1. Department of Regenerative Medicine, Cell Science Research Center, Royan Institute for Stem Cell Biology and Technology, ACECR, Tehran, Iran
2. Sernova Corp., London, Ontario, Canada
3. Laboratory of Pediatric Hepatology and Cell Therapy, Institute of Experimental and Clinical Research (IREC), Université Catholique de Louvain, Brussels, Belgium

Corresponding Addresses: Laboratory of Pediatric Hepatology and Cell Therapy, Institute of Experimental and Clinical Research, Université Catholique de Louvain, B-1200 Brussels, Belgium
Department of Regenerative Medicine, Cell Science Research Center, Royan Institute for Stem Cell Biology and Technology, ACECR, Tehran, Iran
Emails: mustapha.najimi@uclouvain.be, masvos@royaninstitute.org

Received: 13/February/2021, Accepted: 17/April/2021

Abstract

Angiotensin-converting enzyme II (ACE2) in association with type II transmembrane serine protease (TMPRSS2) is considered the main receptor of SARS-CoV-2. However, considering the clinical complications of COVID-19 in different organs, there is no strong association between the abundance of ACE2/TMPRSS2 co-expression and clinical features of the disease and the severity of complications. Since SARS-CoV-2 affects certain organs that lack or have low expression of ACE2/TMPRSS2, it may be possible that the virus employs other receptors for colonization and entry. Based on recent studies, glucose-regulated protein 78 (GRP78) can be a potential alternative receptor for SARS-CoV-2 entry. In this letter, supporting evidence proposed GRP78 as an alternative receptor in SARS-CoV-2 infection.

Keywords: Angiotensin-Converting Enzyme II, COVID-19, Endoplasmic Reticulum Stress, HSPA5, SARS-CoV-2

Cell Journal(Yakhteh), Vol 23, No 2, July 2021, Pages: 247-250

Citation: **Shahriari Felordi M, Memarnejadian A, Najimi M, Vosough M. Is there any alternative receptor for SARS-CoV-2? Cell J. 2021; 23(2): 247-250. doi: 10.22074/cellj.2021.7977.**

Virus clonization and pandemics

World Health Organization declared a global public health emergency of international concern, on 30th January 2020 due to the ongoing pandemic of coronavirus disease 2019 (COVID-19) (1, 2). Clinical features of this disease are extending from an asymptomatic infection to acute respiratory distress syndrome, and multi-organ failure in some cases (2-5). Virus entry and replication relies on a fine interaction between the virus and host cells (6). Studies have shown that the main receptor for SARS-CoV-2 binding is angiotensin-converting enzyme II (ACE2) (7, 8). Successful entry of the virus into host cells depends on two consecutive steps, i. Attachment of the virus to the ACE2 receptor and, ii. Simultaneous activation of type II transmembrane serine protease TMPRSS2 which cleaves and activates the virus spike (S) protein (9-11).

ACE2 expression in different tissues and COVID-19 pathogenesis

According to the Human Protein Atlas, the ACE2 receptor is abundantly expressed in the gut, kidneys, and testis, and at lower levels in the lungs and heart (12). However, the lungs and heart have been documented as important targets for SARS-CoV2 infection. Furthermore, co-expression pattern of ACE2/TMPRSS2 through the tissues does not explain clinical complications or their severity in COVID-19 patients (13, 14). In addition, SARS-CoV-2 infects organs that lack ACE2, probably through interactions with other receptors. Endocrine cells in the prostate gland, astrocytes and pericytes in the central nervous system, and hepatocytes in liver are examples of cells that do not express ACE2 (15). The expression pattern of ACE2 in the mentioned organs are different from higher levels in male gonads to lower levels in heart and CNS. In the other words, SARS-CoV-2 can cause multi-organ failure and there is no strict correlation between the abundancy of ACE2 and clinical complications.

GRP78 as a receptor for different viruses

Glucose-regulated protein 78 (GRP78) is used by different viruses for entry into host cells (16, 17). This receptor (also called BiP and HSPA5) is a member of the heat shock protein 70 (HSP-70) family and a master chaperone protein localized on the endoplasmic reticulum (ER) membrane (18). This protein is broadly expressed in many tissues and composed of two structural domains: i. Nucleotide-binding domain (NBD), or ATP-binding domain (ABD) at the N-terminal and, ii. A substrate binding domain (SBD) at the C-terminal (19). The β region of SBD can play a crucial role in facilitating the interaction between protein ligands and the target cell membrane (20). As a response to ER stress, GRP78 overexpresses and translocates to the cell surface. Cell surface GRP78 (CS-GRP78), along with its SBD domain, can act as a multifunctional receptor and recognize various proteins, ligands, and viruses (16). It was shown that cancer cells overexpress CS-GRP78, which is specifically recognized

by Pep42, a seven-residue cyclic peptide (21). The motif generated by disulfide bonds in Pep42 can interact with CS-GRP78 (20-22). The cyclic structure of Pep42 stabilizes a hydrophobic motif which strenghtens its affinity to CS-GRP78-SBDβ (20). Molecular modeling and docking analyses have revealed 13 regions which are crucial for disulfide bond formation in the SARS-CoV-2 spike (S) protein. The four disulfide bonds located on the outer surface of the S protein can interact with other ligands. The pairwise sequence alignments and hydrophobicity index comparison between S protein regions and Pep42 revealed a remarkable similarity between the region IV of S protein and Pep42. Considering the fact that Pep42 and GRP78 interact strongly, the structural/biochemical similarity between S protein and Pep42 also suggest that GRP78 can bind to the S protein (21, 23); thus, S protein might be a potential ligand for CS-GRP78 (Fig.1) (20). Treatment of cells with AR12, resulted in induction of GRP78 degredation and suppression of production of infectious virions via autophagosome formation. This treatment reduced viral entry through GRP78 (24).

GRP78 vs. ACE2 in SARS-CoV2 clonization

Several studies have highlighted CS-GRP78 as a receptor for different viruses (25-27). Apart from DPP4 (CD26), which was shown to be the main receptor for MERS-CoV infection (28), it has been shown that CS-GRP78 facilitate viral entry into the host cells by sustaining viral attachment (29) and plays a crucial role in this process (30). Based on various sign and symptoms in COVID-19 patients, many researchers have suggested that SARS-CoV-2 predominantly targets endothelial cells, one of the largest populations of cells in the human body (31). GRP78 is broadly expressed in all endothelial cells, but it is upregulated in specific circumstances such as cancer. Owing to the this upregulation, it can be assumed that cancer patients are at higher risk for COVID-19 and severe complications (32).

GRP78 also presents certain properties that can make it a predominant receptor over ACE2 for SARS-CoV-2. Many tissues express only one pairs of ACE2/TMPRSS2 complex (15). While the ACE2 requires association of TMPRSS2 to cleave the S protein (9-11), the ABD domain at the N-terminus of GRP78 can simultanously provide the energy required for the successful entry of SARS-CoV-2 (33). Therefore, researchers assumed that CS-GRP78 could be an alternative receptor for SARS-CoV-2 and suggested natural and synthetic GRP78 inhibitors to block virus entry. For instance, Palmeira and colleagues by in silico analysis identified 409 compounds that can block the binding of the S protein to CS-GRP78 (30). In addition, Sudeep and colleagues reported optimal interaction features of Withaferin A, curcumin and andrographolide, natural ligands for the GRP78 receptor to block virus clonization (34).

All toghether, SBD is necessary for binding to the S protein and ABD provides required energy. Both domains of GRP78 are required for the entry of viruses such as EBOV (35), Borna Disease virus (25), MERS (28), and COVID-19 (30). The cited papers provided details of the function.

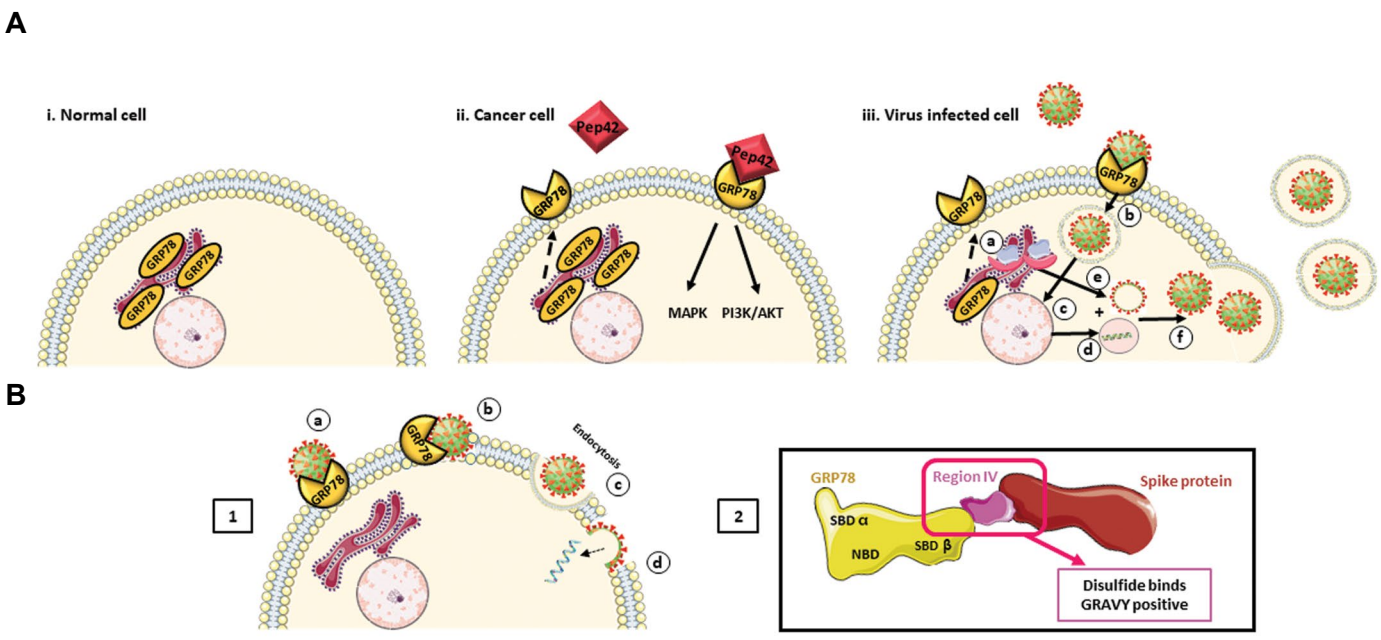

Fig.1: GRP78 in different conditions. **A**. i. Normal cells. GRP78 is an important chaperone in endoplasmic reticulum. ii. Cancer cells. In cancerous cells, GRP78 is translocated to the cell membrane and comprises as a receptor. The main ligand for CS-GRP78 is Pep42 that activates certain pathways at the down-stream and initiate cancerous phenotypes. iii. Virus-infected Cells. GRP78 translocated to the cell surface. CS-GRP78 as a receptor at the cell surface facilitates viral entry into the cell and amplification and release of new viral generations from the host cell. **B.** 1. The proposed mechanism of virus entry through GRP78 receptor. 2. The required energy for virus entry provided by the ABD. CS-GRP78 can interconnect with S protein of SARS-CoV-2 by its SBDβ domain through the constituted disulfide and hydrophobic bonds. ABD; ATP binding domain, CS-GRP78; Cell surface glucose regulated protein 78, NBD; Nucleotide binding domain, SARS-CoV-2; Severe acute respiratory syndrome coronavirus 2, and SBDβ; Substrate binding domain β.

Closing remarks

Although several reports have proposed GRP78 and other receptors as possible receptor for SARS-CoV-2 based on in silico analysis and a few experiments, there is no comprehensive documented paper in which the related data in this subject have been collected, discussed, and the evidences analyzed so far. The concept of existing an alternative receptor for virus entry can explain the involvement of different organs with very low expression of ACE2. This idea will be beneficial for readers to understand that why there is no strong association between the abundance of ACE2/TMPRSS2 co-expression and clinical features of the disease and the severity of complications. However, we provided additional data in terms of the mechanism of entry and function of the receptors. On the other hand, we reviewed other papers that suggested other receptors for SARS-CoV-2 entry and colonization, however our focus in this paper is on GRP78 as an alternative receptor. This protein is very common in different cells and a minor stress can activate this pathway and provide appropriate condition for virus entry.

In summary, the potential role of GRP78 in SARS-CoV-2 entry to the host cells convinced us to suggest that CS-GRP78 can be considered as an alternative receptor for this virus. Further experiments are recommended to confirm this idea.

Acknowledgements

Authors express their gratitude to colleagues in Regenerative Medicine Department, Royan Institute, and Laboratory of Hepatology and Cell Therapy, CU Leuven. There is no financial support and conflict of interest in this study.

Authors' Contributions

M.S.F.; Wrote the first draft. A.M.; Revised the manuscript critically. M.N., M.V.; Were involved in developing concept editing the final draft. All authors read and approved the final manuscript.

References

1. Chan JF, Yuan S, Kok KH, To KK, Chu H, Yang J, et al. A familial cluster of pneumonia associated with the 2019 novel coronavirus indicating person-to-person transmission: a study of a family cluster. Lancet. 2020; 395(10223): 514-523.
2. Chen N, Zhou M, Dong X, Qu J, Gong F, Han Y, et al. Epidemiological and clinical characteristics of 99 cases of 2019 novel coronavirus pneumonia in Wuhan, China: a descriptive study. Lancet. 2020; 395(10223): 507-513.
3. Huang C, Wang Y, Li X, Ren L, Zhao J, Hu Y, et al. Clinical features of patients infected with 2019 novel coronavirus in Wuhan, China. Lancet. 2020; 395(10223): 497-506.
4. Wang D, Hu B, Hu C, Zhu F, Liu X, Zhang J, et al. Clinical Characteristics of 138 hospitalized patients wth 2019 novel coronavirus-infected pneumonia in Wuhan, China. JAMA. 2020; 323(11): 1061-1069.
5. Xu XW, Wu XX, Jiang XG, Xu KJ, Ying LJ, Ma CL, et al. Clinical findings in a group of patients infected with the 2019 novel coronavirus (SARS-Cov-2) outside of Wuhan, China: retrospective case series. BMJ. 2020; 368: m606.
6. Belouzard S, Millet JK, Licitra BN, Whittaker GR. Mechanisms of coronavirus cell entry mediated by the viral spike protein. Viruses. 2012; 4(6): 1011-1033.
7. Enjuanes L, Almazán F, Sola I, Zuñiga S. Biochemical aspects of coronavirus replication and virus-host interaction. Annu Rev Microbiol. 2006; 60: 211-230.
8. Perlman S, Netland J. Coronaviruses post-SARS: update on replication and pathogenesis. Nat Rev Microbiol. 2009; 7(6): 439-450.
9. Glowacka I, Bertram S, Müller MA, Allen P, Soilleux E, Pfefferle S, et al. Evidence that TMPRSS2 activates the severe acute respiratory syndrome coronavirus spike protein for membrane fusion and reduces viral control by the humoral immune response. J Virol. 2011; 85(9): 4122-4134.
10. Matsuyama S, Nagata N, Shirato K, Kawase M, Takeda M, Taguchi F. Efficient activation of the severe acute respiratory syndrome coronavirus spike protein by the transmembrane protease TMPRSS2. J Virol. 2010; 84(24): 12658-12664.
11. Shulla A, Heald-Sargent T, Subramanya G, Zhao J, Perlman S, Gallagher T. A transmembrane serine protease is linked to the severe acute respiratory syndrome coronavirus receptor and activates virus entry. J Virol. 2011; 85(2): 873-882.
12. Hikmet F, Méar L, Edvinsson Å, Micke P, Uhlén M, Lindskog C. The protein expression profile of ACE2 in human tissues. Mol Syst Biol. 2020; 16(7): e9610.
13. Blanco-Melo D, Nilsson-Payant BE, Liu WC, Uhl S, Hoagland D, Møller R, et al. Imbalanced host response to SARS-CoV-2 drives development of COVID-19. Cell. 2020; 181(5): 1036-45. e9.
14. Wyler E, Mösbauer K, Franke V, Diag A, Gottula LT, Arsie R, et al. Bulk and single-cell gene expression profiling of SARS-CoV-2 infected human cell lines identifies molecular targets for therapeutic intervention. bioRxiv. 2020; Available from: https://www.biorxiv.org/content/10.1101/2020.05.05.079194v1 (13 Feb 2021).
15. Singh M, Bansal V, Feschotte C. A single-cell RNA expression map of human coronavirus entry factors. bioRxiv. 2020; https://www.biorxiv.org/content/10.1101/2020.05.08.084806v2 (13 Feb 2021).
16. Ibrahim IM, Abdelmalek DH, Elfiky AA. GRP78: A cell's response to stress. Life Sci. 2019; 226: 156-163.
17. Shu W, Guo Z, Li L, Xiong Z, Wang Z, Yang Y, et al. Regulation of molecular chaperone GRP78 by hepatitis B virus: control of viral replication and cell survival. Mol Cell Biol. 2020; 40(3): e00475-e00419.
18. Brocchieri L, Conway de Macario E, Macario AJ. hsp70 genes in the human genome: Conservation and differentiation patterns predict a wide array of overlapping and specialized functions. BMC Evol Biol. 2008; 8: 19.
19. Lindquist S, Craig EA. The heat-shock proteins. Annu Rev Genet. 1988; 22: 631-677.
20. Ibrahim IM, Abdelmalek DH, Elshahat ME, Elfiky AA. COVID-19 spike-host cell receptor GRP78 binding site prediction. J Infect. 2020; 80(5): 554-562.
21. Kim Y, Lillo AM, Steiniger SC, Liu Y, Ballatore C, Anichini A, et al. Targeting heat shock proteins on cancer cells: selection, characterization, and cell-penetrating properties of a peptidic GRP78 ligand. Biochemistry. 2006; 45(31): 9434-9444.
22. Elfiky AA, Ibrahim IM. Zika virus envelope - heat shock protein A5 (GRP78) binding site prediction. J Biomol Struct Dyn. 2020: 1-13.
23. Pizzo SV. Cell surface GRP78, a new paradigm in signal transduction biology. 1st ed. Academic Press; 2018; 1-7.
24. Rayner JO, Roberts RA, Kim J, Poklepovic A, Roberts JL, Booth L, et al. AR12 (OSU-03012) suppresses GRP78 expression and inhibits SARS-CoV-2 replication. Biochem Pharmacol. 2020; 182: 114227.
25. Honda T, Horie M, Daito T, Ikuta K, Tomonaga K. Molecular chaperone BiP interacts with Borna disease virus glycoprotein at the cell surface. J Virol. 2009; 83(23): 12622-12625.
26. Jindadamrongwech S, Thepparit C, Smith DR. Identification of GRP 78 (BiP) as a liver cell expressed receptor element for dengue virus serotype 2. Arch Virol. 2004; 149(5): 915-927.
27. Triantafilou K, Fradelizi D, Wilson K, Triantafilou M. GRP78, a coreceptor for coxsackievirus A9, interacts with major histocompatibility complex class I molecules which mediate virus internalization. J Virol. 2002; 76(2): 633-643.
28. Vankadari N, Wilce JA. Emerging WuHan (COVID-19) coronavirus: glycan shield and structure prediction of spike glycoprotein and its interaction with human CD26. Emerg Microbes Infect. 2020; 9(1): 601-604.

29. Chu H, Chan CM, Zhang X, Wang Y, Yuan S, Zhou J, et al. Middle East respiratory syndrome coronavirus and bat coronavirus HKU9 both can utilize GRP78 for attachment onto host cells. J Biol Chem. 2018; 293(30): 11709-11726.
30. Palmeira A, Sousa E, Köseler A, Sabirli R, Gören T, Türkçüer İ, et al. Preliminary virtual screening studies to identify GRP78 inhibitors which may interfere with SARS-CoV-2 infection. Pharmaceuticals (Basel). 2020; 13(6): 132.
31. Santulli G, Morelli BM, Gambardella J. Is endothelial dysfunction the concealed cornerstone of COVID-19. BMJ. 2020; 368: m1091.
32. Banerjee A, Begum F, Sricastava AK, Tripathi PP, Ray U. Overexpression of GRP78 receptor and its chemical biology in cancer and autoimmune diseases: high risk for COVID 19? OSF. 2020.
33. Moudi B, Heidari Z, Mahmoudzadeh-Sagheb H, Alavian SM, Lankarani KB, Farrokh P, et al. Concomitant use of heat-shock protein 70, glutamine synthetase and glypican-3 is useful in diagnosis of HBV-related hepatocellular carcinoma with higher specificity and sensitivity. Eur J Histoch. 2018; 62(1): 2859.
34. Sudeep HV, Gouthamchandra K, Shyamprasad K. Molecular docking analysis of Withaferin A from Withania somnifera with the glucose regulated protein 78 (GRP78) receptor and the SARS-CoV-2 main protease. Bioinformation. 2020; 16(5): 411-7.
35. Reid SP, Shurtleff AC, Costantino JA, Tritsch SR, Retterer C, Spurgers KB, et al. HSPA5 is an essential host factor for Ebola virus infection. Antiviral Res. 2014; 109: 171-174.